



Cardiff  
Catalysis Institute  
Sefydliad Catalysis  
Caerdydd

# **Development of Metal Oxide Catalysts for the Removal of Acetaldehyde from Poly(ethylene terephthalate)**

Thesis submitted in accordance with the requirement of Cardiff University for the  
degree of Doctor of Philosophy



**David R. Marchant**

School of Chemistry

Cardiff University

2016-2020



## **Acknowledgements**

Firstly, I would like to thank my supervisors Prof. Stuart Taylor, Prof. Graham Hutchings, and Prof. Stan Golunski of the CCI for all their support and guidance throughout the project. I am also indebted to Dr. Adrian Carmichael and Dr. Chris Starkie of ColorMatrix/PolyOne for helping me with all of the work I conducted in Knowsley and for being such engaged industrial partners. A special thanks to Chris for all of the time and effort he invested in me, and for striving to make the project as successful as it could be.

A massive thanks to Dr. Sam Pattisson without who's help and patience this project would've run far less smoothly. Thank you for putting up with my endless questions and queries and for helping me to think like a researcher. Thank you also to all of the CCI postdocs for all of their help and insight along the way.

Thank you to Dr. Greg Shaw, Dr. Dave Morgan, and Dr. Tom Davies for all their help with running different pieces of laboratory apparatus. Whether it be troubleshooting GC issues, running XPS analysis, or using SEM to look at plastic bottles, thank you very much.

Thank you to my friends and peers who helped to make the whole PhD experience so enjoyable. Thanks to Parag, Luke, Nia, Igor, Joe, Matt, Owen, Kag, Liam, Annie, Louise and others for all the good times we spent in the office and the pub.

Thank you also to my family for all of their love and support and for my wife, Hayley, who was the breadwinner for us while I carried on living the student life for as long as I could. Thanks for putting up with me through everything and supporting me throughout my four years of postgraduate study.

Finally, I would like to thank Jesus Christ, the *Logos*, who spoke order into chaos, and who is the author and sustainer of all things.

## **Abbreviations and Units**

%	Percent
°C	Degrees Celsius
Å	Angstrom ( $1 \times 10^{-10}$ m)
µm	Micrometre ( $1 \times 10^{-6}$ m)
σ	Standard Deviation
AA	Acetaldehyde
acac	Acetylacetone
ATA	Anthranilamide
atm	Standard Atmosphere (101 kPa)
ATR-FTIR	Attenuated Total Reflection–Fourier Transform Infrared Spectroscopy
ATSDR	Agency for Toxic Substances and Disease Registry
BA	Butyraldehyde
bar	100 kPa
BET	Brunauer-Emmett-Teller
BHET	Bis(2-Hydroxyethyl) Terephthalate
CASINO	Monte Carlo Simulation of Electron Trajectory in Solids
cc/g	Cubic Centimetre ( $\text{cm}^3$ ) per Gram
cm <sup>-1</sup>	Wavenumber
CTAB	Cetyltrimethylammonium bromide
dL/g	Decilitres Per Gram
DMT	Dimethyl Terephthalate
DRIFTS	Diffuse Reflectance Infrared Fourier Transform Spectroscopy
EDX	Energy Dispersive X-Ray Spectroscopy

EG	Ethylene Glycol
EM	Electron Microscopy
eV	Electron Volt
FEG-SEM	Field Emission Gun Scanning Electron Microscope
FID	Flame Ionisation Detector
FTIR	Fourier Transform Infrared Spectroscopy
FWHM	Full Width Half Maximum
g	Gram
GC	Gas Chromatography
GC-MS	Gas Chromatography – Mass Spectrometry
GHSV	Gas Hourly Space Velocity
ICDD	International Centre for Diffraction Data
IUPAC	International Union of Pure and Applied Chemistry
IR	Infrared
IV	Intrinsic Viscosity
K	Kelvin
kg	Kilogram
kPa	Kilopascal ( $1 \times 10^3$ Pa)
kV	Kilovolt
mg	Milligram
MPP	Melt-Phase Polymerisation
MPV	Meerwein-Ponndorf-Verley
MS	Mass Spectrometry
nm	Nanometre ( $1 \times 10^{-9}$ m)

NMR	Nuclear Magnetic Resonance
OSC	Oxygen Storage Capacity
P/P <sub>0</sub>	Relative Pressure (Equilibrium Pressure / Saturation Pressure)
PEG	Poly(ethylene glycol)
PEG-DME	Poly(ethylene glycol – dimethyl ether)
PET	Poly(ethylene terephthalate)
PFR	Plug Flow Reactor
POSTC-PET	Post-Consumer Poly(ethylene terephthalate)
ppm	Parts Per Million
PXRD	Powder X-ray Diffraction
QGA	Quantitative Gas Analyser
RF	Response Factor
SCI	Specular Components Included
SEM	Scanning Electron Microscopy
SSP	Solid-State Polymerisation
STP	Standard Temperature and Pressure (273.15 K and 1x10 <sup>5</sup> Pa)
TCD	Thermal Conductivity Detector
TGA	Thermogravimetric Analysis
TPA	Terephthalic Acid
TTAB	Tetradecyltrimethylammonium bromide
VOC	Volatile Organic Compound
XPS	X-Ray Photoelectron Spectroscopy
XRD	X-Ray Diffraction

## **Abstract**

Acetaldehyde (AA) is a degradation product of poly(ethylene terephthalate) (PET). AA can migrate from the walls of a PET bottle into drinking water and cause an off-taste at very low concentrations. Currently anthranilamide (ATA) is added to PET to scavenge the AA and is able to remove up to 80% of the contaminant. However, ATA is a stoichiometric scavenger so there is scope for a more efficient technology to be developed that utilises catalytic scavengers.

ColorMatrix owns a patent for catalytic AA removal technology that uses a hydrous zirconium oxide catalyst. In this study the claims made in that patent were examined and scrutinised, and alternative metal oxide catalysts were prepared and tested to determine if they could be more effective for AA removal.

A laboratory testing protocol for testing the AA conversion activity of the metal oxide catalysts was developed that involved a gas-phase reactor equipped with online Gas Chromatography (GC) analysis. This reactor could be used to determine the suitability of samples for testing in PET at ColorMatrix in Knowsley. ColorMatrix have the capability to test the catalysts under application-like conditions because they have the apparatus to dry, extrude, and analyse the PET. The catalyst samples that were prepared in the laboratory were also subjected to a bevy of characterisation techniques in order to gain understanding regarding which physicochemical properties are most important for an effective AA removal catalyst.

CeO<sub>2</sub> catalysts were found to be the most active of the samples tested in this study. Alternative preparation methods, milling, and doping were among the routes that were explored to attempt to increase the efficiency of the CeO<sub>2</sub> catalysts. The catalyst sample that achieved the greatest AA reduction in PET of 32%, was prepared using urea precipitation with a urea to metal nitrate molar ratio of 3:1.

This project was half-funded by ColorMatrix/PolyOne and half-funded by the EPSRC through the Centre for Doctoral Training in Catalysis.

## **Contents**

1	Introduction .....	1
1.1	Catalysis .....	1
1.1.1	Introduction.....	1
1.1.2	Heterogeneous Catalysis .....	2
1.1.3	Homogeneous Catalysis.....	3
1.1.4	Catalysis in Society.....	4
1.2	Metal Oxide (MO <sub>x</sub> ) Catalysts .....	5
1.3	Ceria (CeO <sub>2</sub> ) in Catalysis .....	6
1.4	Poly(ethylene terephthalate) (PET) .....	8
1.4.1	Introduction.....	8
1.4.2	Synthesis of PET.....	9
1.4.3	Intrinsic Viscosity (IV) .....	11
1.4.4	Recycling .....	12
1.4.4.1	Glycolysis.....	13
1.4.4.2	Hydrolysis .....	13
1.4.4.3	Methanolysis .....	14
1.4.4.4	Ammonolysis and Aminolysis .....	14
1.4.5	Disadvantages of PET.....	14
1.4.6	Processing of PET .....	15
1.4.7	Degradation of PET .....	15
1.4.7.1	Thermal Degradation.....	16
1.4.7.2	Thermal-Oxidative Degradation .....	18
1.4.7.3	Hydrolytic Degradation.....	18
1.5	Acetaldehyde (AA) .....	18
1.5.1	Introduction.....	18
1.5.2	The Problem of AA in PET .....	19
1.5.3	Removal of AA in PET .....	20
1.6	AA Scavengers in PET.....	20
1.6.1	Anthranilamide .....	20
1.6.2	Catalysts for AA Removal .....	21
1.7	Review of AA Chemistry .....	23
1.7.1	Oxidation of AA .....	23
1.7.2	Reduction of AA.....	23
1.7.3	Aldol Condensation .....	23

1.7.4	Oligomerisation.....	23
1.7.5	Reactivity of AA on Metal Oxides.....	24
1.8	Aims of the Project.....	25
1.9	Chapter 1 - References .....	26
2	Experimental.....	34
2.1	Materials .....	34
2.2	Catalyst Preparation .....	35
2.2.1	Urea Precipitation.....	35
2.2.1.1	Experimental Procedure .....	35
2.2.2	TTAB Assisted Preparation .....	36
2.2.2.1	Experimental Procedure .....	36
2.2.3	Pluronic P123 Assisted Preparations .....	36
2.2.3.1	Experimental Procedure .....	36
2.2.4	Wet Milling .....	36
2.2.5	Dry Milling .....	37
2.3	Catalyst Testing.....	37
2.3.1	Gas Phase Reactor.....	37
2.3.1.1	Gas Chromatography (GC) .....	40
2.3.1.2	Mass Spectrometry (MS).....	45
2.3.2	Twin-Screw Extruder .....	45
2.3.3	Headspace GC-FID .....	46
2.3.4	Measurement of Intrinsic Viscosity (IV) .....	47
2.3.5	Injection Moulding.....	48
2.3.6	Blow Moulding .....	48
2.3.7	Colour and Haze Analysis.....	49
2.4	Catalyst Characterisation.....	49
2.4.1	Powder X-Ray Diffraction (PXRD).....	49
2.4.1.1	Background .....	49
2.4.1.2	Experimental Procedure .....	50
2.4.2	Thermogravimetric Analysis (TGA).....	51
2.4.2.1	Background .....	51
2.4.2.2	Experimental Procedure .....	51
2.4.3	Raman Spectroscopy .....	51
2.4.3.1	Background .....	51

2.4.3.2	Experimental Procedure .....	52
2.4.4	BET Surface Area.....	52
2.4.4.1	Background .....	52
2.4.4.2	Experimental Procedure .....	54
2.4.5	Full N <sub>2</sub> Adsorption/Desorption Isotherms .....	54
2.4.5.1	Background .....	54
2.4.5.2	Experimental Procedure .....	55
2.4.6	Attenuated Total Reflection – Fourier Transform Infrared Spectroscopy (ATR-FTIR) .....	56
2.4.6.1	Background .....	56
2.4.6.2	Experimental Procedure .....	57
2.4.7	X-Ray Photoelectron Spectroscopy (XPS) .....	57
2.4.7.1	Background .....	57
2.4.7.2	Experimental Procedure .....	58
2.4.8	Scanning Electron Microscopy (SEM) / Energy Dispersive X-Ray Spectroscopy (EDX).....	59
2.4.8.1	Background .....	59
2.4.8.2	Experimental Procedure .....	60
2.4.9	Monte Carlo Simulations .....	61
2.4.9.1	Background .....	61
2.4.9.2	Experimental Procedure .....	61
2.5	Mechanistic Studies.....	61
2.5.1	Diffuse Reflectance Infrared Fourier Transform Spectroscopy (DRIFTS).....	62
2.5.1.1	Background .....	62
2.5.1.2	Experimental Procedure .....	62
2.6	Chapter 2 - References .....	64
 3	Methodological Development .....	66
3.1	Introduction .....	66
3.2	Testing with AA in Poly(ethylene glycol) (PEG) .....	66
3.3	Testing with Butyraldehyde (BA) in Octane.....	80
3.4	Testing with AA in Gas Phase Reactor.....	83
3.5	Conclusions .....	93
3.6	Chapter 3 - References .....	94

4	Gas Phase Testing of Metal Oxide Catalysts for AA Conversion.....	96
4.1	Introduction .....	96
4.2	Testing with 500 ppm AA .....	97
4.3	Testing with 1000 ppm AA .....	100
4.3.1	Testing of Ceria Catalysts Prepared by Urea Precipitation.....	100
4.3.2	Testing of Ceria Catalysts Prepared with Structure Directing Agents	
	103	
4.4	Effect of Space Velocity on Activity .....	105
4.5	Testing at a GHSV of 300,000 h <sup>-1</sup> .....	108
4.5.1	Testing of Ceria Catalysts Prepared by Urea Precipitation.....	108
4.5.2	Effect of Ball Milling on Activity of Ceria Catalysts .....	110
4.5.3	Effect of Drying on Activity of Ceria Catalysts.....	111
4.5.4	Testing of Doped Ceria Catalysts .....	112
4.6	Structure-Activity Relationship.....	115
4.6.1	Influence of Surface Area .....	115
4.6.2	Influence of Crystallite Size.....	118
4.6.3	Influence of Raman FWHM.....	121
4.6.4	Influence of Oxygen Defects .....	123
4.6.5	Influence of Oxidation State .....	129
4.7	Mechanistic Investigation.....	133
4.7.1	AA DRIFTS Studies .....	133
4.7.2	AA DRIFTS with Nano CeO <sub>2</sub> .....	134
4.7.3	AA DRIFTS with CeO <sub>2</sub> U1.....	136
4.7.4	AA DRIFTS with 5%CuOx-CeO <sub>2</sub> .....	137
4.8	Reaction Mechanism .....	138
4.9	Conclusions .....	141
4.10	Chapter 4 - References .....	144
5	Application Testing of Metal Oxide Catalysts for AA Removal in PET .....	147
5.1	Introduction .....	147
5.2	AA Levels in Blank PET .....	148
5.3	Calculation of Error .....	149
5.4	Testing of Metal Oxide Catalysts using Extruder .....	150
5.5	Colour Testing of PET loaded with metal oxide catalysts .....	155
5.6	Testing of CeO <sub>2</sub> Catalysts using Extruder .....	157

5.7	Intrinsic Viscosity of PET Loaded with Ceria Catalysts.....	164
5.8	Effect of Carrier on Catalyst Activity .....	165
5.9	Testing of milled CeO <sub>2</sub> catalysts.....	168
5.10	Testing of dried CeO <sub>2</sub> catalysts.....	176
5.11	Testing of Doped Ceria Catalysts.....	179
5.12	IV of PET Loaded with Doped Ceria Catalysts .....	180
5.13	SEM of PET loaded with CeO <sub>2</sub> .....	180
5.14	Generation of CeO <sub>2</sub> <i>in-situ</i> .....	187
5.15	Comparison between Testing in Gas Phase and Testing in PET .....	190
5.16	Conclusions .....	191
5.17	Chapter 5 - References .....	193
6	Conclusions and Future Work .....	195
6.1	Chapter 6 – References .....	200

# 1 Introduction

## 1.1 Catalysis

### 1.1.1 Introduction

The term ‘catalysis’ was first coined by Berzelius in 1836, meaning to breakdown, because he observed chemical compounds being broken apart by the action of a catalyst.<sup>1</sup> A catalyst is a chemical additive that increases the rate of a reaction without being consumed, making it available to perform multiple reaction cycles. Industrial catalysts are often active for up to a decade before they need to be replaced or regenerated. For example, a methanol synthesis catalyst can be active for up to 8 years, whilst an ammonia synthesis catalyst can be active for up to 10 years. A catalyst does not affect the thermodynamics of a reaction but offers an alternative lower energy reaction pathway that avoids large kinetic barriers. Another way of saying this is that a catalyst does not alter the equilibrium position of a reaction, but it alters the rate at which the equilibrium is reached. A catalyst can only reduce the kinetic barrier to a reaction that is already thermodynamically feasible. If thermodynamics prevents the feasibility of a reaction then catalysis is unable to overcome this.<sup>2</sup>

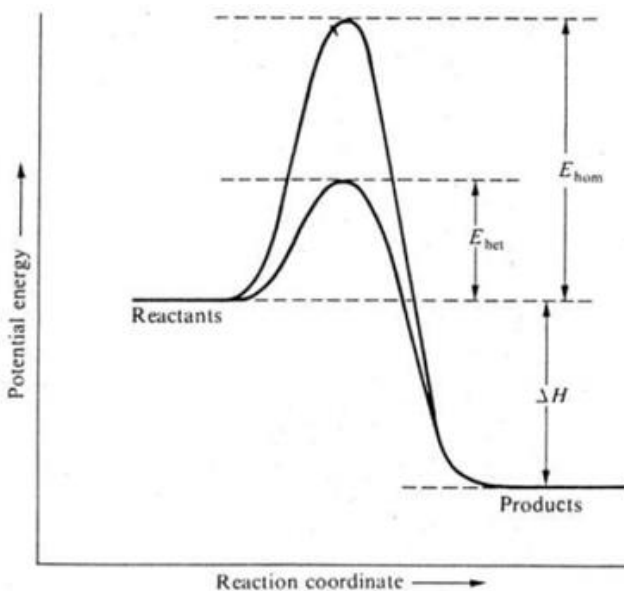


Figure 1.1 Energy profile for a chemical reaction showing alternative lower energy pathway offered by the catalysed reaction. Reproduced from ref 2.

Catalysis is generally categorised into two main areas: heterogeneous or homogeneous. In heterogeneous catalysis, the catalyst and the target molecule are in different physical states (e.g. a solid catalyst and a gaseous target compound), whereas in homogeneous catalysis both the catalyst and the target molecule are in the same physical state (e.g. catalyst and target compound are both dissolved in solution). The research contained within this thesis is concerned with heterogeneous catalysis. Heterogeneous catalysts are often composed of precious metal nanoparticles supported on a metal oxide material. Homogeneous catalysts are generally comprised of a metal centre coordinated to an array of ligand structures.

### 1.1.2 Heterogeneous Catalysis

In the chemical industry, heterogeneous catalysts are more commonly used, especially for bulk chemical production, because it avoids the need to separate the catalyst from the product following a reaction cycle. Catalyst separation can be a very expensive process and so the ability to avoid it can be fiscally beneficial. An example of an industrial process catalysed by a heterogeneous catalyst is the Haber-Bosch process, which utilises a supported iron catalyst to synthesise ammonia from nitrogen and hydrogen.<sup>3</sup> Nitrogen fixation is a well-documented phenomenon within biological systems with cyanobacteria readily taking nitrogen from the air and forming ammonia. However, it has proved fiendishly difficult to mimic this process by man-made means. The Haber-Bosch process was developed over 100 years ago and yet it has still not been surpassed, despite it requiring very energy intensive conditions (200 bar and 500 °C).<sup>4</sup> The process was such a significant breakthrough that Haber and Bosch both won Nobel Prizes for their research contributions in this area. Fritz Haber won the Nobel Prize in Chemistry in 1918 “for the synthesis of ammonia from its elements”, and Carl Bosch won the same prize in 1931 “for his contribution to the invention and development of chemical high-pressure methods”. Haber developed the chemistry, and Bosch made it industrially viable. Ammonia is now made on such a large scale using this methodology that it has been suggested that the Haber-Bosch process consumes up to 2% of the global electricity supply *per annum*. This ammonia synthesis process is also attributed with causing the large increase of global population growth over the last century, due to the increased availability of reactive nitrogen, making the growth of crops for food far more efficient.<sup>5</sup> It is estimated that the world

population would be less than half of its current total if it were not for the Haber-Bosch process (see figure 1.2).

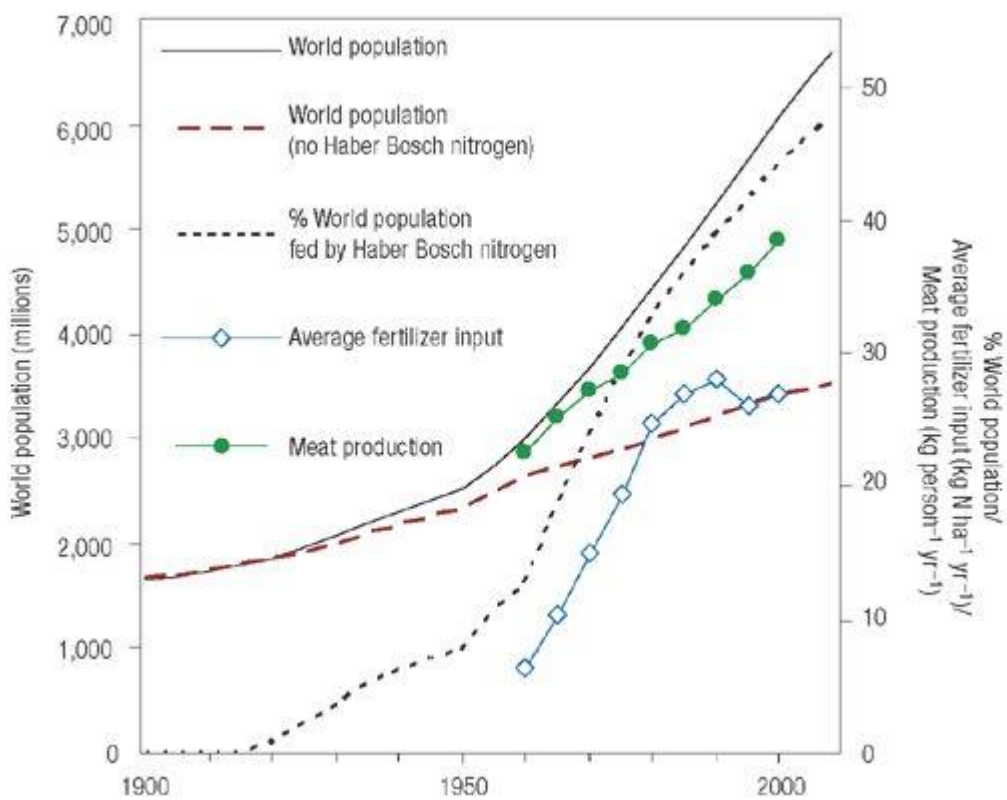


Figure 1.2 Increase in world population due to availability of Haber-Bosch ammonia. Reproduced from ref 5.

### 1.1.3 Homogeneous Catalysis

In certain instances, particularly when the product selectivity of the catalyst is crucial, it can be more suitable to use a homogeneous catalyst. This is generally more of a concern for the production of fine chemicals. An example of a homogeneously catalysed industrial process is the Monsanto process for acetic acid production.<sup>6</sup> This organometallic process uses a rhodium catalyst to facilitate the carbonylation of methanol in order to produce acetic acid. Methanol is converted to methyl iodide using hydrogen iodide because methanol is very difficult to activate. The pre-catalyst species is a *cis*-[Rh(CO)<sub>2</sub>I<sub>2</sub>]<sup>-</sup> complex that is able to catalyse the reaction between methyl iodide and carbon monoxide to form acetic acid.<sup>7</sup> The Monsanto process has been widely replaced by the Cativa process that was developed by BP in the 1990s. The

Cativa process utilises a more active iridium catalyst that makes the process more efficient, economic, and more environmentally friendly.<sup>8</sup>

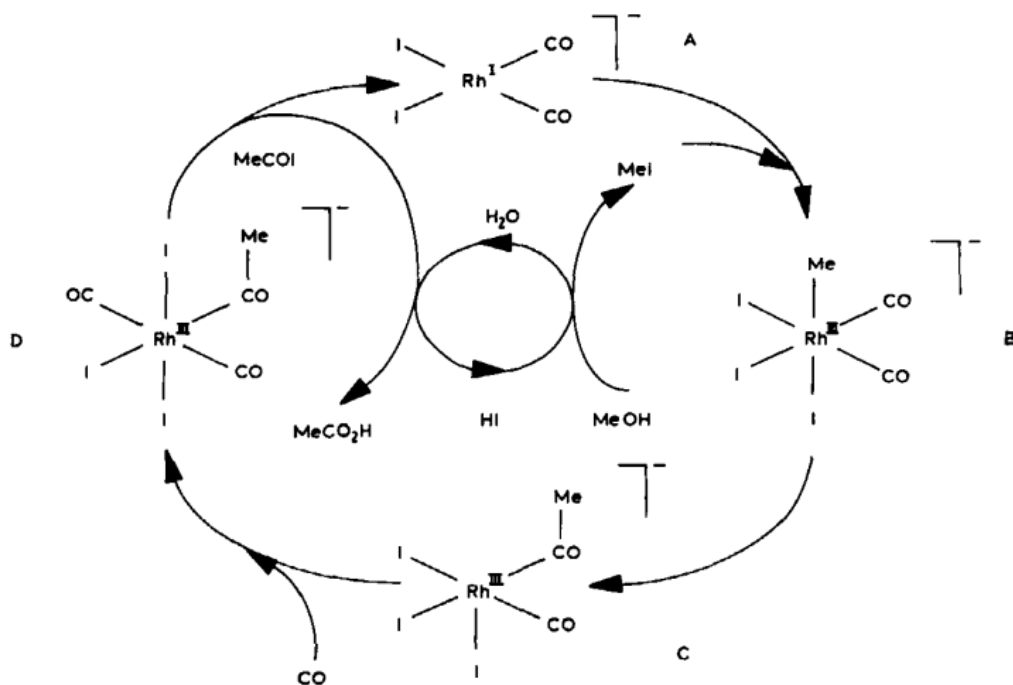


Figure 1.3 Catalytic cycle for the rhodium catalysed Monsanto process for the conversion of methanol to acetic acid. Reproduced from ref 7.

#### 1.1.4 Catalysis in Society

The three-way catalytic converter, which is used to mitigate harmful emissions from petrol engine motorcars, is a fine example of how catalysis can greatly benefit both society and the environment. Since its introduction in the 1970s air quality has been drastically improved in large metropolitan areas across the globe and smog has become a far less common phenomenon. The three-way catalytic converter utilises heterogeneous catalysis whereby a solid catalyst reacts with the harmful gases contained in the effluent stream flowing from the engine. The bimetallic catalyst used in this system is composed of platinum and rhodium nanoparticles supported on a CeO<sub>2</sub>-Al<sub>2</sub>O<sub>3</sub> mixed metal oxide. The catalyst system is coated on to a ceramic monolith that sits downstream of the engine (see figure 1.4).<sup>9</sup> The hot effluent flows through the channels of the monolith where it can interact with the supported bimetallic catalyst. This catalyst is able to control the emissions because the Pt acts

as an oxidation catalyst for the conversion of CO and hydrocarbons to CO<sub>2</sub>, and the Rh acts a reduction catalyst for the conversion of NO<sub>x</sub> to N<sub>2</sub>.<sup>10</sup>

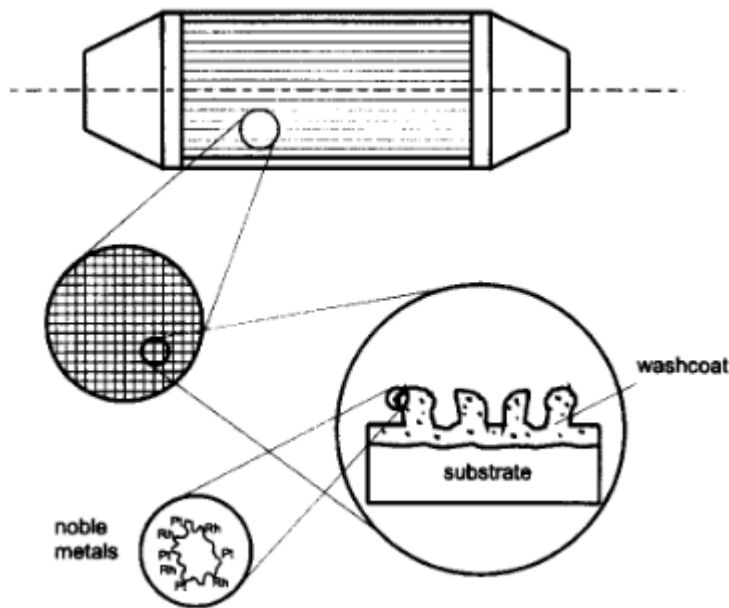


Figure 1.4 Diagram of a monolithic catalytic convertor. Reproduced from ref 9.

## 1.2 Metal Oxide (MO<sub>x</sub>) Catalysts

Metal oxides are often used in heterogeneous catalysis as a support material on which to disperse nanoparticles of precious materials. By using a support, the surface area of a catalyst can be greatly increased and by using a redox active metal oxide like ceria the redox properties of the catalyst can also be enhanced. This was highlighted using ceria in the catalyst support of a three-way catalyst for automotive pollution control.

However, metal oxides can be used as heterogeneous catalysts and are often used in acid/base or redox catalysis. When studying metal oxide catalysts the three most important aspects of the surface chemistry are, as outlined by Barteau, the coordination environment, the redox properties, and the oxidation state of the oxide surface.<sup>11</sup> There are a large variety of metal oxides that find applications in catalysis, and metal oxides can also be combined to form mixed metal oxides with more tuneable properties (as previously seen with CeO<sub>2</sub>-Al<sub>2</sub>O<sub>3</sub> in a three-way catalyst). Metal oxides

are often used as catalysts in pollution control applications because they are a more cost-effective alternative to catalysts based on precious metals.

Titania ( $\text{TiO}_2$ ) is a semiconductor that is famous for its photocatalytic activity using visible light, which can be used for treating wastewater.<sup>12</sup> Uranium oxide ( $\text{U}_3\text{O}_8$ ) catalysts are highly active for the total oxidation of VOCs (volatile organic compounds) for pollution abatement.<sup>13</sup> Nanocrystalline cobalt oxide ( $\text{Co}_3\text{O}_4$ ) is a highly active catalyst for the total oxidation of propane to  $\text{CO}_2$ .<sup>14</sup> Vanadium oxide ( $\text{V}_2\text{O}_5$ ) catalysts are the best known catalysts for the low temperature (250-450 °C) selective catalytic reduction of  $\text{NO}_x$  in the presence of ammonia and oxygen to form nitrogen and water.<sup>15</sup> Zirconia ( $\text{ZrO}_2$ ) can act as a photocatalyst for the decomposition of  $\text{H}_2\text{O}$ , and is also commonly mixed with ceria ( $\text{CeO}_2$ ) to be used as a mixed metal oxide catalyst support.<sup>16,17</sup> Manganese oxide ( $\text{Mn}_3\text{O}_4$ ,  $\text{Mn}_2\text{O}_3$ ,  $\text{MnO}_2$ ) is another metal oxide that can be used to catalyse the combustion of VOCs such as benzene and toluene.<sup>18</sup>

### 1.3 Ceria ( $\text{CeO}_2$ ) in Catalysis

Cerium is a member of a selection of elements found in period six of the periodic table, most commonly referred to as the lanthanides. Lanthanides are alternatively known as rare earth metals due to their low abundance in the Earth's crust. Cerium is the most prevalent of the rare earth elements, with an abundance of about 0.0046 wt% of the Earth's crust.<sup>19</sup>

For the purposes of catalysis, cerium is most commonly used in its oxide form as ceria,  $\text{CeO}_2$ . It has already been noted that ceria is an important component of the catalyst support in the three-way catalyst used for the abatement of polluting emissions from motorcars. Ceria is a very important catalyst support material and has found use in a wide array of catalysts for a broad spectrum of applications. Over the last two decades the number of academic papers published on ceria relating to catalysis has been on the rise, exemplifying the importance of ceria as a material for catalysis.<sup>19</sup> Ceria has some unique physical properties that make it highly desirable for catalysis, of particular significance is its redox behaviour. The ability of ceria to transition between its 3+ and 4+ oxidation states make it an excellent oxygen storage material. The high oxygen storage capacity (OSC) of ceria is what makes it so effective for the

three-way catalyst and other oxidation catalysts.<sup>20</sup> Zirconia ( $\text{ZrO}_2$ ) can be added to ceria to enhance its OSC properties and this mixed metal oxide is of particular interest for use in three-way catalysts.<sup>10,21</sup> Oxygen defects that can form in the ceria lattice are another factor that contributes to the OSC and catalytic activity of ceria.<sup>22,23</sup> These oxygen defects can help to facilitate reaction mechanisms such as the Mars-van Krevelen, whereby a lattice oxygen is used to oxidise a molecule in contact with the metal oxide surface.<sup>24</sup> In many instances the concentration of defect sites in the lattice can be directly correlated to the activity of the sample.<sup>25</sup>

Ceria is most commonly used as a catalyst in oxidation reactions where its oxygen storage properties enable it to oxidise a target substrate very efficiently. It is utilised widely for pollution abatement and general VOC removal applications. Ceria and ceria-based catalysts have been shown to be effective for the total oxidation of a myriad of VOCs including naphthalene, propane, o-xylene, methanol, acetone, toluene, and 1,2-dichloroethane, amongst others.<sup>26–31</sup> Ceria-based materials are also effective for the oxidation of CO to form the less harmful  $\text{CO}_2$ .<sup>32–35</sup> The water-gas shift reaction, which is the oxidation of CO with water vapour to form  $\text{CO}_2$  and hydrogen, is another important industrial reaction that ceria-based catalysts have been utilised within.<sup>36–38</sup>

As already mentioned, ceria is used for pollution abatement in petrol engines through the use of a three-way catalyst, but it is also used in Diesel engines as a soot oxidation catalyst. To clear the soot that accumulates on a Diesel particulate filter an oxidation catalyst can be used to reduce the temperature required to combust the soot, and ceria and ceria-based materials have been found to be effective for this purpose.<sup>39–44</sup> Ceria-based materials can also be used as oxidation catalysts for the construction of desired chemical compounds not just for the destruction of unwanted pollutants. Ceria can oxidise a wide variety of organic moieties for the synthesis of fine chemicals. For example, the oxidation of alcohols to carbonyls, the oxidation of aldehydes to acids, and the oxidation to hydrocarbons, to name but a few.<sup>45–47</sup>

In addition to all the pollution control, combustion, and oxidation catalysis that ceria catalysts are used for, ceria-based materials can also be used to catalyse a variety of organic transformations. Ceria catalysts can be used to dehydrate alcohols such as 4-methyl-2-pentanol and diols such as 1,3-propanediol.<sup>48–50</sup> Ketonisation is another

process that can be catalysed using ceria-based catalysts, whereby a ketone can be generated from the condensation of acids or esters.<sup>51–53</sup> Ceria-based catalysts can also catalyse C-C bond formation *via* aldol condensation reactions which enable the coupling of aldehydes and ketones.<sup>54,55</sup> Due to the redox properties of ceria it can catalyse reductions as well as oxidations, and has been used to hydrogenate alkenes ( $\text{C}=\text{C}$ ), carbonyls ( $\text{C}=\text{O}$ ), and nitriles ( $\text{C}\equiv\text{N}$ ).<sup>56–58</sup>

In a traditional supported catalyst, the metal oxide is used to support the more active and more expensive metal nanoparticles. However, in inverse catalysts this is reversed whereby a metal is used to support metal oxide nanoparticles. Ceria has been investigated for its properties in inverse catalysts and has been studied for its catalytic properties when supported on various metals (e.g. Rh, Cu, Pt).<sup>59–61</sup>

This brief survey of the literature highlights the versatility of ceria within catalysis and the broad array of chemical transformations that can be catalysed using ceria-based materials.

## 1.4 Poly(ethylene terephthalate) (PET)

### 1.4.1 Introduction

Plastics are found all around us and are used for a vast variety of applications from toy soldiers to aeroplanes. The polymer revolution began with the invention of Bakelite, recognised as the world's first synthetic plastic, in 1907 by Leo Baekeland.<sup>62</sup> Bakelite is a thermosetting plastic composed of phenol and formaldehyde, which offered revolutionary electrical insulation and heat-resistant properties. A thermoset is a polymer that is irreversibly hardened once cured, in contrast to a thermoplastic that can be made soft and mouldable at elevated temperatures and so can be remoulded multiple times. The difference between these plastics is caused by the polymer chains in a thermoset forming permanent cross-linking chemical bonds when cured, whereas in a thermoplastic the polymer chains are only bound by intermolecular interactions.<sup>63</sup> Synthetic polymers have developed greatly over the last hundred years and the whole field of polymer science has arisen to grant greater understanding of these materials and their properties. Many new polymeric systems have been invented such as polyesters, polyamides, polycarbonates, and acrylics, just to name a few. The research

in this study is focused on a particular polyester, namely Poly(ethylene terephthalate) (PET).

PET is a thermoplastic that is utilised in a wide range of applications due to its optical, mechanical, and thermal properties (for the chemical structure of PET see figure 1.5). It was first synthesised in 1946 by Whinfield and Dickson and has since become one of the world's most ubiquitous polymers.<sup>64</sup> PET applications can be broken down into two main areas: fibres and packaging. Polyester clothing is very common across the globe and is often used as a cost-effective alternative to cotton. Another large-scale usage of PET is in the manufacture of bottles, especially for mineral water and other soft beverages such as fruit juices and carbonated drinks. PET is particularly desirable for this application due to its glass-like optical clarity, which allows the contained beverage to look most appealing. PET is also lightweight and strong, allowing for the safe and efficient transportation of products without the loss of any valuable commodity due to breakages. These properties are particularly desirable when compared to glass, which is heavy and brittle. Polymers are highly chemically inert making them suitable for food and drink containers, and very malleable to design enabling the production of bottles that are all sorts of shapes and sizes. It is also very easy to add branding or a company logo to polyester bottles, which is crucial for commercial products.

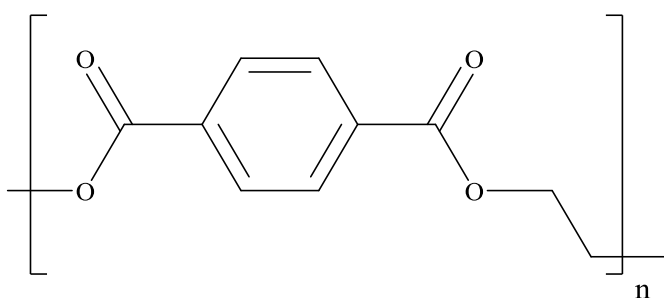


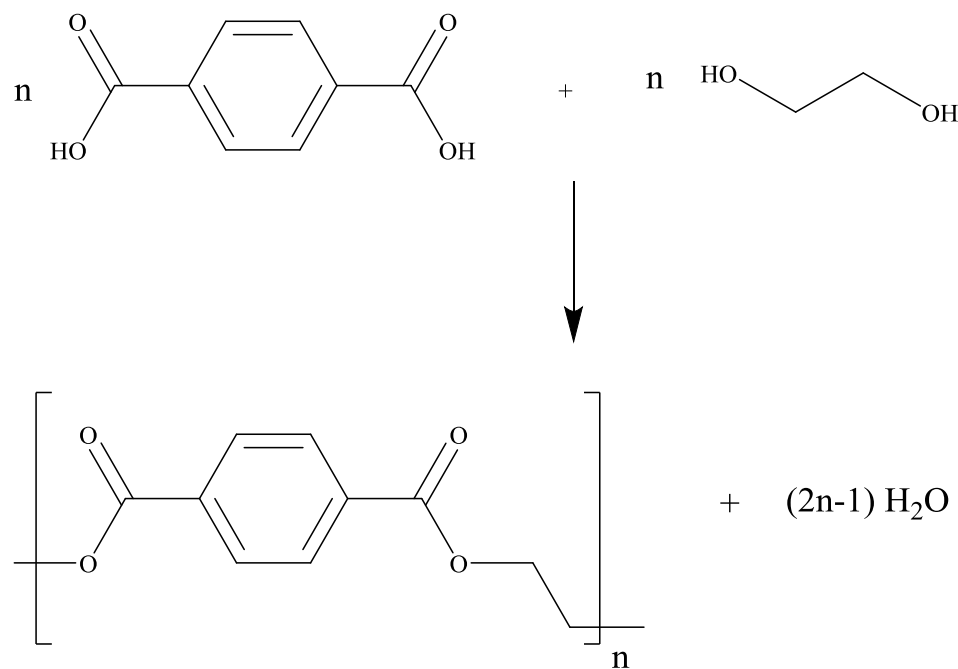
Figure 1.5 Chemical Structure of PET

### 1.4.2 Synthesis of PET

PET is a polyester produced *via* the polycondensation of ethylene glycol (EG) and terephthalic acid (TPA). Not all PET is synthesised directly from EG and TPA, some PET synthesis processes use dimethyl terephthalate (DMT) instead of TPA. In

both cases the di-acids react with EG to form bis-hydroxyethyl terephthalate (BHET), however when TPA is used the only by-product is water, whereas with DMT, acetaldehyde (AA) is also formed. The reaction between EG and TPA is an esterification that is carried out at 240 – 260 °C and pressures of 300 – 500 kPa. Whilst the reaction between EG and DMT is a trans-esterification which is conducted at lower temperatures of 140 – 220 °C and at a reduced pressure of 100 kPa, and is the preferred process because it is easier to purify.<sup>65</sup>

Once BHET has been generated it is then polymerised to produce PET. Traditionally the polymerisation reaction is catalysed by antimony trioxide (Sb<sub>2</sub>O<sub>3</sub>), which is highly active and cost effective. Germanium catalysts are more active for PET production but due to the cost of germanium, antimony catalysts have been preferred in the polymer industry. However, there is a desire to move away from antimony and germanium catalysts towards titanium or aluminium based catalysts. Trace antimony metal can be trapped in the polymer and this can cause grey discolouration, and the formation of insoluble particles within the plastic.<sup>66</sup> Antimony has also been found to leach into mineral water from PET bottles.<sup>67</sup> These issues, alongside environmental concerns, are causing PET manufacturers to consider alternative polycondensation catalysts. These alternatives include catalysts based on titanium, aluminium, molybdenum, cobalt, and zirconium.<sup>68,69</sup> There are three commonly used processes to conduct this polycondensation synthesis which include melt-phase polymerisation (MPP), solid-state polymerisation (SSP), and direct melt-phase polymerisation to high IV material. Melt-phase polymerisation is a high temperature process that is typically conducted at 270-300 °C, whereas SSP is a lower temperature process that is carried out between 200-240 °C. The melting point of PET is 260 °C so as the terms suggest MPP is conducted in the molten phase, whilst SPP is in the solid phase. SSP can be utilised to increase the intrinsic viscosity of the polymer without exposing it to higher temperatures which can cause degradation.<sup>70</sup>



Scheme 1.1 Reaction scheme for the polycondensation reaction between ethylene glycol and terephthalic acid to yield PET.

### 1.4.3 Intrinsic Viscosity (IV)

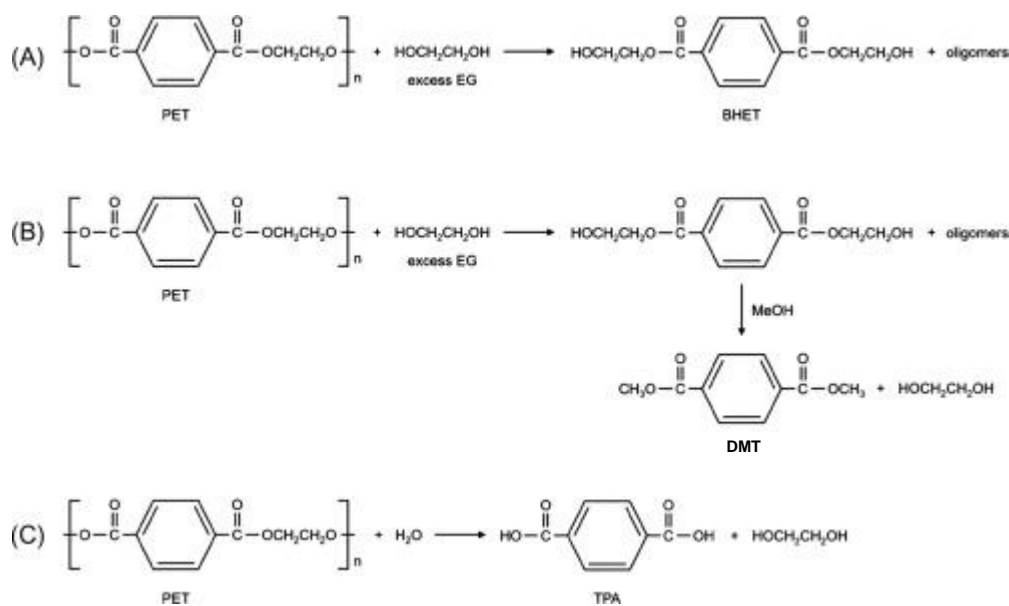
Within the polymer industry it is typical to classify PET by reference to its intrinsic viscosity (IV). Different IV values are desired for different applications of PET, so the IV of the polymer is a good indication of the purpose that it was manufactured for. IV is analogous to molecular weight because as the chain length of the polymer increases so do entanglements between the polymer chains, therefore increasing the viscosity of the material. A greater IV leads to enhanced mechanical strength and rigidity, and bottle grade PET is manufactured to have an IV of 0.70-0.85 dL/g. Bottles manufactured for the storage of carbonated beverages require a higher IV PET than bottles that store still beverages. For fibre applications PET with lower IV is used, whereas for engineering applications higher IV PET is required (see Table 1.1).<sup>71</sup>

Table 1.1 Typical IV value ranges of PET for different applications

Application	Intrinsic Viscosity (dL/g)
Textile fibre	0.40 - 0.70
Technical fibre	0.72 - 0.98
Bottle (still beverage)	0.70 - 0.78
Bottle (carbonated beverage)	0.78 - 0.85
Engineering plastic	1.00 - 2.00

#### 1.4.4 Recycling

A very important factor in the world today, as society becomes increasingly eco-conscious, is recyclability. As the problem of plastic pollution in the oceans becomes more apparent and catastrophic, the recyclability of plastics is becoming a hot-button issue.<sup>72,73</sup> PET is non-biodegradable and therefore, the best way to minimise PET waste is to recycle the polymer. The recycling of post-consumer PET (POSTC-PET) can be classified into two major categories: chemical or mechanical recycling. Chemical recycling involves the depolymerisation of PET into its constituent monomers typically *via* hydrolysis, glycolysis, or methanolysis.<sup>74–76</sup> Ammonolysis or aminolysis can also be used to chemically depolymerise PET.<sup>77</sup> In mechanical recycling the PET is ground down to yield flakes, which can then be reused. Both chemical and mechanical processes require sorting, washing, and drying in order to remove contaminants before the material can be recycled.



Scheme 1.2 Reaction schemes for different PET depolymerisation reactions. A = glycolysis, B = methanolysis, C = hydrolysis. Reproduced from ref 75.

#### 1.4.4.1 Glycolysis

Glycolysis involves using ethylene glycol in the presence of a catalyst to depolymerise PET into the monomer BHET. Zinc and lead acetates are examples of some of the best catalysts for this reaction, and are able to catalyse the reaction at temperatures between 190-200 °C.<sup>78-80</sup> Glycolysis is currently the most cost-effective method for the chemical recycling of PET bottles.

#### 1.4.4.2 Hydrolysis

Hydrolysis is the breaking of bonds using water and it can be used to break down PET into its monomers TPA and EG (it is the reverse of the polycondensation reaction used to make the polymer). The monomers can then be used to produce new PET in a TPA-based process. PET hydrolysis can be conducted under acidic, basic or neutral conditions. Acid hydrolysis can be conducted in sulfuric acid or nitric acid but often at high concentrations (> 10 M).<sup>81</sup> Basic hydrolysis can be carried out in sodium hydroxide solution (up to 20 wt% NaOH). Neutral hydrolysis uses pressurised steam at temperatures greater than 250 °C in the presence of metal acetates to depolymerise PET.<sup>82</sup> The biggest obstacle to PET hydrolysis are difficulties related to the purification of TPA which is not easy to extract from the reaction mixture.

#### 1.4.4.3 Methanolysis

Methanolysis is a more expensive process than glycolysis but it is more tolerant of impurities and so can be used to recycle lower quality plastic, especially if vapor methanolysis is used.<sup>83</sup> Methanolysis uses methanol (MeOH) to break PET down into DMT and EG, these can then be used as a feedstock to produce more PET in a DMT-based process. Liquid methanolysis uses the same catalysts as glycolysis and is typically carried out at temperatures between 180–280 °C and pressures of 20–40 atm.<sup>75</sup>

#### 1.4.4.4 Ammonolysis and Aminolysis

Ammonolysis relates to the decomposition of PET using an ammonia solution in the presence of a catalyst at temperatures of around 100 °C. Whereas, aminolysis refers to the depolymerisation of PET in aqueous solutions of primary amines at elevated temperatures (45–190 °C).<sup>84</sup> Aminolysis is a far faster process than ammonolysis and results in the formation of diamides of TPA and EG. Ammonolysis is a slow process often carried out over weeks and it requires a catalyst (often metal acetates as in glycolysis and methanolysis),<sup>85</sup> but it is of chemical interest because it can be used to convert PET into polyamides. This is because when ammonia reacts with PET it forms terephthalamide which can be used to make monomers for the production of polyamides.

### 1.4.5 Disadvantages of PET

PET is a very useful material with some remarkable properties, but there are certain disadvantages associated with it. For instance, PET does not provide a total gas barrier towards oxygen and carbon dioxide, however, it is still able to provide a good enough barrier to store carbonated soft drinks.<sup>86,87</sup> The O<sub>2</sub> and CO<sub>2</sub> permeability of PET can be reduced by using specifically designed additives. Such additives include Amosorb, which scavenges O<sub>2</sub> through a combination of sodium borohydride (which acts as a hydrogen source) and a palladium catalyst (which catalyses the reaction between hydrogen and oxygen to form water).<sup>88</sup> The transparency of PET to UV light can also be an issue because the radiation can be damaging to the contained product. In certain instances, even the transparency to visible light of PET can be problematic. For

example, UHT milk can sour due to a cascade of reactions triggered by the exposure of riboflavins to light, leading to the milk having what is known as sunlight flavour.<sup>89</sup>

#### 1.4.6 Processing of PET

PET is manufactured in the form of pellets before it is processed to make it suitable for a given application. The processing of PET for bottles consists of five major steps:

1. Pellet → 2. Injection moulding → 3. Preform → 4. Blow moulding → 5. Bottle

Prior to processing is it very important that the pellets are thoroughly dried because PET is hygroscopic, which means that it absorbs moisture from the atmosphere. Moisture in the polymer can lead to increased degradation of the PET due to hydrolysis, and this can result in the production of very low quality PET.<sup>90</sup> PET is dried at around 150 °C to reduce the level of moisture to below 50 ppm.<sup>91</sup> The dried PET is then processed using injection moulding or extrusion. Injection moulding and extrusion are typically carried out at 270–300 °C to convert the solid polymer into the molten phase.<sup>92</sup> Often these apparatuses utilise an Archimedes screw that applies the force to pass the molten polymer through the extruder or moulder. In the case of extrusion, the polymer will adopt the shape of the die through which it passes, and similarly with injection moulding, the PET will adopt the form of the mould into which it is injected. In the case of bottle production, the PET is injection moulded into a preform. The preform is then subjected to blow moulding to produce a bottle, and it is often at this stage that branding motifs are incorporated into the design of the bottle itself.

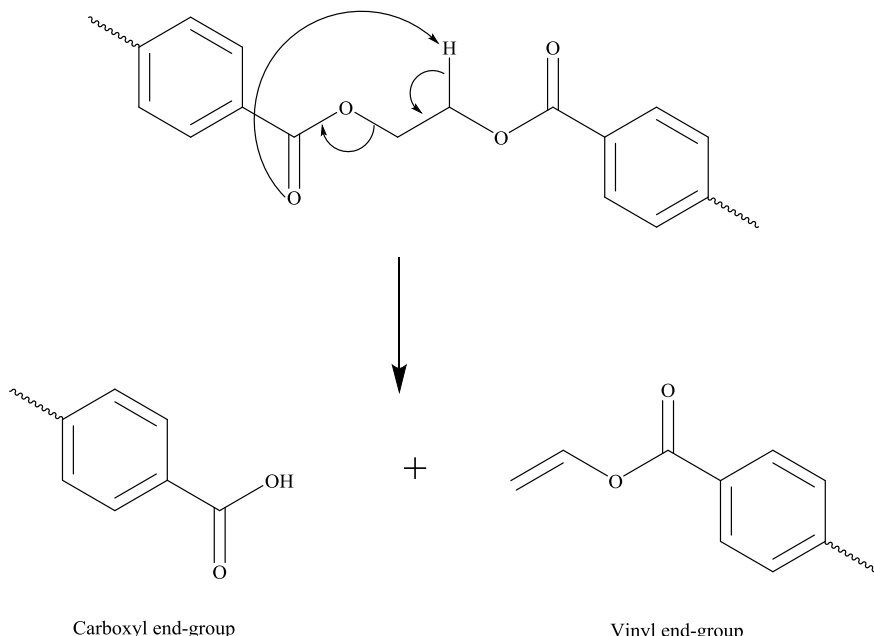
#### 1.4.7 Degradation of PET

PET can degrade *via* various reaction pathways and the conditions exerted upon the polymer during processing can lead to the occurrence of such degradation pathways. These routes include hydrolytic, thermal, and thermal-oxidative degradation and therefore the extent of PET degradation is sensitive to the presence of water and/or oxygen. Polymer degradation is also made more likely by increased temperatures, shear, and pressure, which are all utilised in the processing of PET. PET

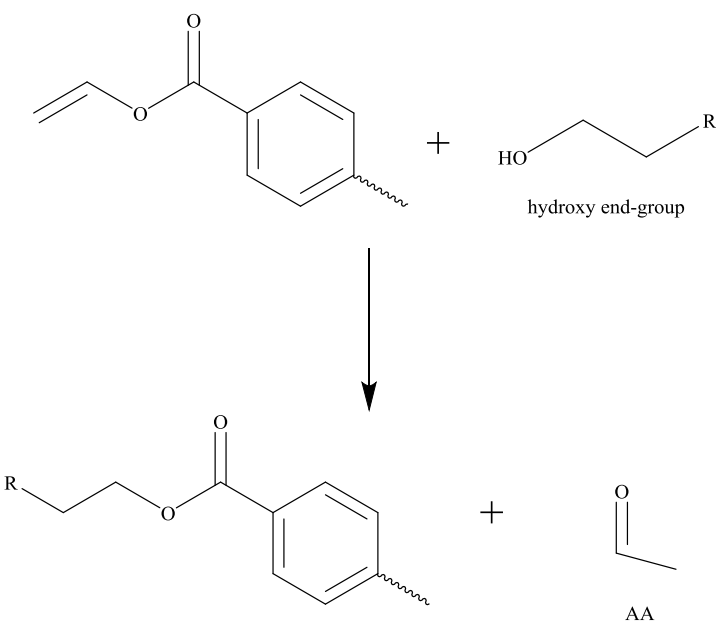
degradation can often lead to a reduction in IV, discolouration, formation of oligomers, or the formation low molecular weight organic products. One of the most common degradation products of PET is acetaldehyde (AA)<sup>93,94</sup>, and this will be the focus of the research conducted in the study.

#### 1.4.7.1 Thermal Degradation

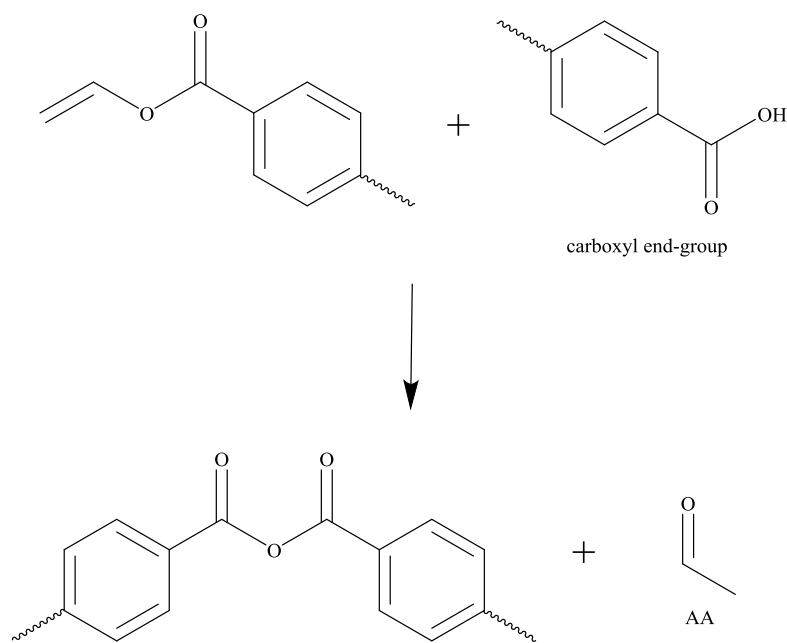
During extrusion or injection moulding PET is exposed to high temperatures (270–300 °C), shear stress, and elevated pressure. These conditions cause degradation of the PET, which leads to the formation of AA that can become trapped within the polymer matrix. CO and CO<sub>2</sub> can also be formed due to thermal degradation of PET.<sup>95</sup> In schemes 1.3, 1.4, and 1.5 the reaction mechanisms for how PET chains can degrade to produce AA due to thermal degradation are outlined. Initially β-scission can cleave a PET chain to yield two shorter chains, one with a carboxyl end-group and the other with a vinyl end-group (see scheme 1.3). A vinyl end-group can interact with hydroxy or carboxyl end-groups to generate new polymer chains along with a molecule of AA as a by-product (see schemes 1.4 and 1.5).



Scheme 1.3 β-scission of PET chain to yield two shorter polymer chains; one with a carboxyl end-group, and the other with a vinyl end-group.



Scheme 1.4 Route for formation of AA from a vinyl end-group whereby the vinyl end-group interacts with a hydroxy end-group.



Scheme 1.5 Alternative route for AA formation from a vinyl end-group whereby the vinyl end-group interacts with a carboxyl end-group.

These reaction mechanisms highlight why vinyl end-group concentration is considered the most important factor leading to AA generation from PET degradation.<sup>96,97</sup> A high vinyl end-group concentration is generally considered to be

indicative of poor quality PET, and it will lead to PET containing higher concentrations of AA.

#### 1.4.7.2 Thermal-Oxidative Degradation

Thermal-oxidative degradation of PET can occur when the polymer is exposed to elevated temperatures in the presence of oxygen. To minimise the effect of this degradation measures should be taken to ensure that PET is processed in an inert atmosphere. For instance, an extruder can be purged with a nitrogen flow to remove any oxygen in the headspace.

#### 1.4.7.3 Hydrolytic Degradation

As aforementioned, hydrolysis can be used to depolymerise PET for the recycling of the polymer (see section 1.4.4.2). Therefore, it is unsurprising that moisture can also cause degradation of PET during processing. This is why the drying of PET prior to processing is so crucial to ensure that the polymer reaches the required quality standards.

### 1.5 Acetaldehyde (AA)

#### 1.5.1 Introduction

AA is a C<sub>2</sub> organic compound with a boiling point of 21 °C and is highly volatile with a vapour pressure of 98.7 kPa at 20 °c. AA is naturally occurring in citrus fruits, beer, and milk, amongst other foodstuffs that we commonly consume.<sup>98</sup> It has a sweet odour that is characteristic of aldehydes and esters, and has a fruity taste. However, even at ppm levels the smell of AA is highly irritant and nauseating. AA is the primary product of ethanol metabolism in the liver, and it causes many of the symptoms associated with a hangover.<sup>99</sup> The facial flush of the alcohol flush reaction is caused by the accumulation of AA due to aldehyde dehydrogenase 2 deficiency.<sup>100</sup> AA is also considered to be carcinogenic and mutagenic, which means that people who suffer from alcohol flush reaction have an increased cancer risk from alcohol consumption. However, at the very low levels that are found in PET, AA is not considered to be a health concern.<sup>101</sup>

### 1.5.2 The Problem of AA in PET

The levels of AA in PET throughout the bottle manufacturing process are indicated in figure 1.6, and this helps to show how each step contributes to the generation of the AA. The AA is at its highest concentration following the MPP due to the high temperatures that are used (270-300 °C). The crystallisation, SSP, and drying steps then help to reduce the levels of AA to below 1 ppm. Before injection moulding again causes the concentration increase due to the high temperatures and shear forces that are required in the moulding process. The degradation of the polymer during injection moulding leads to the preform having a typical AA concentration of 7-10 ppm.

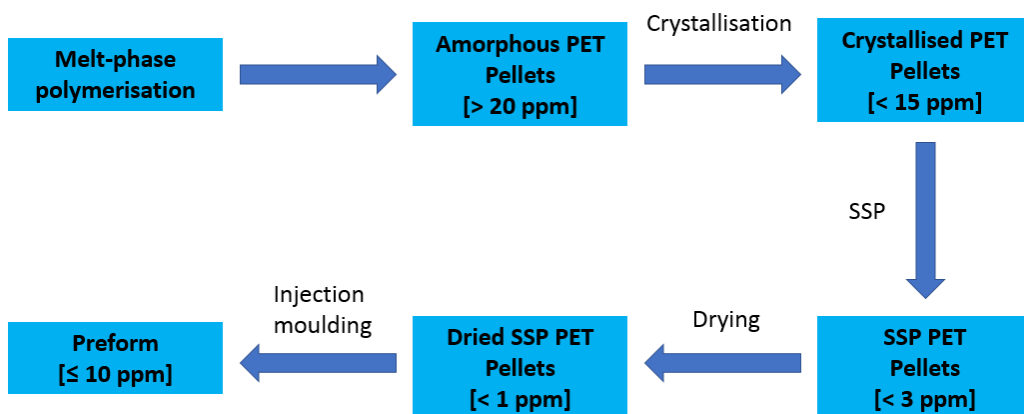


Figure 1.6 The level of AA typically present at each stage in the manufacture and processing of PET bottles (SSP = solid-state polymerisation)<sup>102</sup>

The sweet and fruity flavour of AA is inconsequential in orange juice or cola, however it is highly undesirable in mineral water. AA has a taste threshold of < 40 ppb in water, so even very low concentrations can affect the potability of bottled mineral water.<sup>103,104</sup> The volatility of AA makes it far more problematic as it enables the AA to migrate from the plastic into the beverage more readily. This issue is amplified once the PET has been blow moulded into a bottle because the surface area of the plastic is greatly increased. Combine this with the fact that an average PET bottle contains around 7-10 ppm AA, and the need to reduce the AA content of PET for water bottles becomes apparent. This is further elucidated by the suggestion that

for a bottle containing 600 ml of beverage, a preform AA content of 8 ppm can lead to > 40 ppb AA in the beverage within a month.<sup>105</sup> In order to ensure that bottled mineral water is of optimum quality, and to achieve a prolonged shelf-life of up to two years, AA must be removed from PET. Moreover, the primary quality indicator of bottle-grade PET for food and drink packaging is AA concentration. Regulations have been introduced to ensure that PET is suitable for contact with food or drink. For example, in China regulations require that bottle-grade PET contains less than 1 ppm AA.<sup>106</sup>

### 1.5.3 Removal of AA in PET

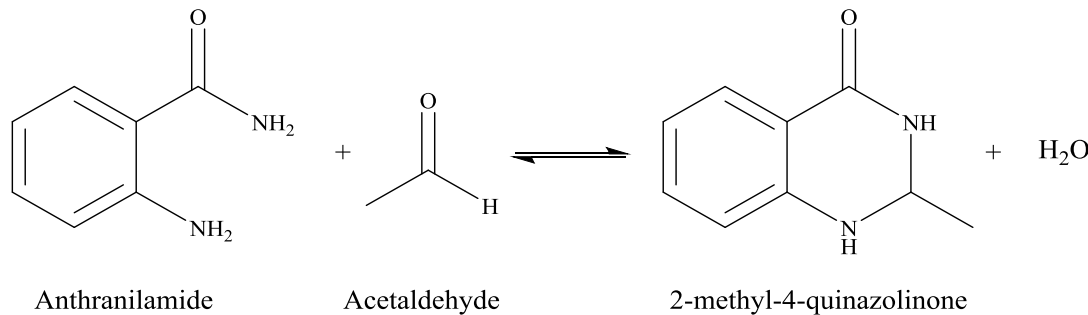
To remove AA from PET it is common to utilise additives that can scavenge the AA once it has been generated within the polymer matrix. Chemical solutions are often preferable to engineering solutions because they allow for the use of current apparatus which has often been bought at great expense. Therefore, instead of having to buy new and improved extruders or injection moulders or relying upon improvements in the quality of the synthesis of PET; a chemical additive can be used to minimise the issue at lower monetary cost and less dead time. The goal of this research project is to develop a catalytic AA scavenger that could improve upon the current state of the art.

## 1.6 AA Scavengers in PET

### 1.6.1 Anthranilamide

The most common AA scavengers in the polymer industry are currently based on anthranilamide, which is composed of a benzene ring functionalised by an amide group and an amine moiety at the ortho position. The anthranilamide removes the AA *via* a ring-closing mechanism that causes the formation of bicyclic adduct and water (see scheme 1.6).<sup>107</sup> Anthranilamide is a highly effective scavenger of AA however it acts *via* a stoichiometric reaction and is added in excess (500 ppm). A catalytic scavenger could operate at lower loadings and would possibly be active throughout multiple recyclings of the PET. Amine based AA scavengers are an alternative, but they produce a Schiff base as a by-product, which can cause a yellowing of the plastic. The anthranilamide reaction only produces water as a by-product, which is preferable,

however a yellowing of the PET also occurs with anthranilamide. This discolouration is corrected using toners and dyes, which restores the colourless appearance of the polymer. There has also been research into the AA scavenging properties of biological compounds such as  $\alpha$ -cyclodextrin.<sup>108</sup>



Scheme 1.6 Reaction scheme for AA scavenging mechanism of anthranilamide.

### 1.6.2 Catalysts for AA Removal

In a previous PhD study it was suggested that an area of future research should focus on catalysts that sequester AA.<sup>102</sup> Oxidation and hydrogenation catalysts were highlighted as potential candidates for effective removal of AA from PET. Therefore, there is precedent for an in-depth study into the efficacy and viability of catalysts for AA scavenging in PET.

For more than a decade, catalytic solutions have been proposed for removing AA from PET, but none have been taken up on a large scale by industry, and anthranilamide remains the benchmark scavenger (up to 80% AA removal). Patents have been filed for oxidation catalysts based on Mn or Co salts, and hydrogenation catalysts based on group VIII metals or metal hydrides.<sup>103,105</sup> An oxidation catalyst has the advantage of being able to consume some of the O<sub>2</sub> that can permeate through the PET, and so enhance the O<sub>2</sub> barrier properties of the polymer whilst also oxidising AA into acetic acid. Acetic acid may not seem like a particularly desirable compound to have in mineral water, however the taste threshold of acetic acid is far greater than AA and so is less easily detected. Rule *et al* claim that levels of acetic acid of up to 40 ppm are acceptable, which is 1000 times greater than the 40 ppb limit for AA.<sup>103</sup> The oxidation catalyst system was able to achieve up to 32% AA removal, but was also found to be active for the generation of AA under melt-processing conditions. This is

counter-productive for a catalyst designed to remove AA from PET, but is unsurprising considering such catalysts are also used to recycle PET which involves depolymerising the structure.<sup>109</sup> Using a hydrogenation catalyst involves the added complication of requiring a hydrogen source, which Rule *et al* suggest could be achieved by adding gaseous H<sub>2</sub> to the polymer melt or *via* the introduction of a silicon hydride (e.g. poly(methylhydro)siloxane (PMHSO)).<sup>105</sup> The hydrogenation catalyst system was demonstrated to achieve a 31% decrease in AA content, and therefore both of these systems have been found to be far less effective than anthranilamide.

ColorMatrix owns a patent for catalytic AA scavenging technology which is based on a hydrous zirconium oxide catalyst.<sup>110</sup> The patent suggests that the hydrous metal oxide is able to catalyse hydride transfer reactions between AA and an organic donor molecule (e.g. AA, aldehyde, alcohol, glycol, etc.). Different reaction products were observed based on the reaction conditions. At elevated temperatures (150 °C for 30 mins) three reaction products were identified; ethanol, acetic acid, and ethyl acetate. These products could be the result of the disproportionation of AA *via* a Cannizzaro or Tishchenko reaction to form ethanol and acetic acid. The acid and alcohol could then combine to form ethyl acetate. A decrease in AA concentration of 80% was achieved with a 1000 ppm catalyst loading. At room temperature (22-24 °C), ethanol was observed to be the only reaction product. This could be caused by a Meerwein-Ponndorf-Verley (MPV) reduction of the AA to yield an alcohol. Ethanol was not formed in the absence of the catalyst, so this suggests that there is activity at room temperature and that the catalyst can reduce AA levels even under ambient conditions over a 17-day period.

The presence of AA in POSTC-PET is an important factor for the recyclability of the polymer. This is especially the case if the recycled PET is to be used in food or beverage packaging, due to the volatility of AA and its ability to migrate out of the polymer.<sup>74</sup> Therefore, if the levels of AA in PET can be reduced by the use of a catalytic additive, the recyclability of the polymer could be increased, and plastic waste associated with PET could be minimised.

## 1.7 Review of AA Chemistry

### 1.7.1 Oxidation of AA

AA is used within the chemical industry as a precursor to acetic acid. This offers an alternative route to the Monsanto and Cativa processes that use methanol as a feedstock for acetic acid production. The industrial oxidation of AA is carried out at 150 °C and 55 atm of pressure in the presence of cobalt(II) or manganese(II) acetate catalysts.<sup>6</sup>

### 1.7.2 Reduction of AA

AA can also be reduced to ethanol and this can be achieved using gold catalysts.<sup>111</sup> However, this reaction is most often conducted in reverse, particularly industrially, as ethanol can be used as source of AA. AA can be produced by oxidising ethanol in the presence of a silver catalyst at temperatures above 500 °C.<sup>112</sup> Although, it is more common for AA to be produced *via* the Wacker process which involves the oxidation of ethylene in the presence of homogeneous palladium and copper catalysts.<sup>113</sup>

### 1.7.3 Aldol Condensation

A reaction that is well known within organic chemistry is the aldol condensation of AA to form longer chain aldehydes. Aldol condensation reactions can be used to convert two AA molecules into crotonaldehyde. These reactions are most often catalysed using solid base heterogeneous catalysts (e.g. MoO<sub>3</sub>, WO<sub>3</sub>).<sup>114</sup> Different aldehydes can also be condensed with each other in order to form different reaction products. For example, condensing AA with formaldehyde generates acrolein as a product.<sup>115</sup>

### 1.7.4 Oligomerisation

AA can oligomerise to form cyclic trimers or tetramers. The cyclic trimer is known as paraldehyde, whilst the cyclic tetramer is referred to as metaldehyde. Both oligomers can be obtained by treating acetaldehyde with catalytic amounts of acid.<sup>116</sup> Paraldehyde has a variety of medical applications and is used as an anti-seizure

medication, whereas metaldehyde is most commonly used as a pesticide. Both paraldehyde and metaldehyde can be used as sources of AA because at 80-100 °C in the presence of acid they readily decompose back to AA.<sup>117</sup>

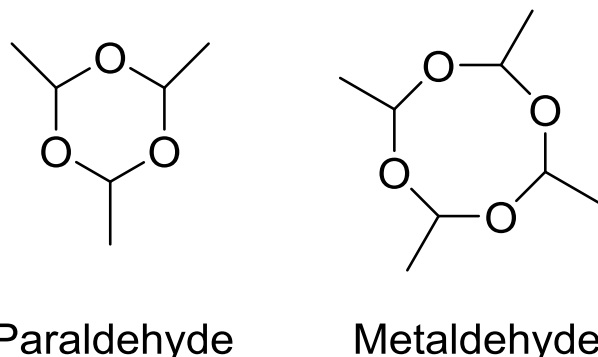


Figure 1.7 The chemical structures of paraldehyde and metaldehyde

### 1.7.5 Reactivity of AA on Metal Oxides

AA is a highly reactive species that readily undergoes a variety of transformations in the presence of a ceria catalyst (for examples see figure 1.8).<sup>118</sup> AA can undergo redox reactions, and can be reduced to form ethanol or oxidised to form acetic acid. Acetates often act as intermediates on a catalyst surface in these systems, as they can couple together to form acetone along with the evolution of CO<sub>2</sub>, in a process known as ketonisation. AA can also undergo aldol condensation reactions in the presence of ceria, that lead to the formation of reaction products such as crotonaldehyde. Crotonaldehyde is highly toxic and would be a very undesirable product to form within the packaging intended for contact with food or beverages. Therefore, this is not a viable route for removing AA within PET and aldol condensation reactions must be avoided. Another reaction pathway that can convert AA in the presence of a ceria catalyst, is that of reductive coupling which leads to the formation of but-2-ene.

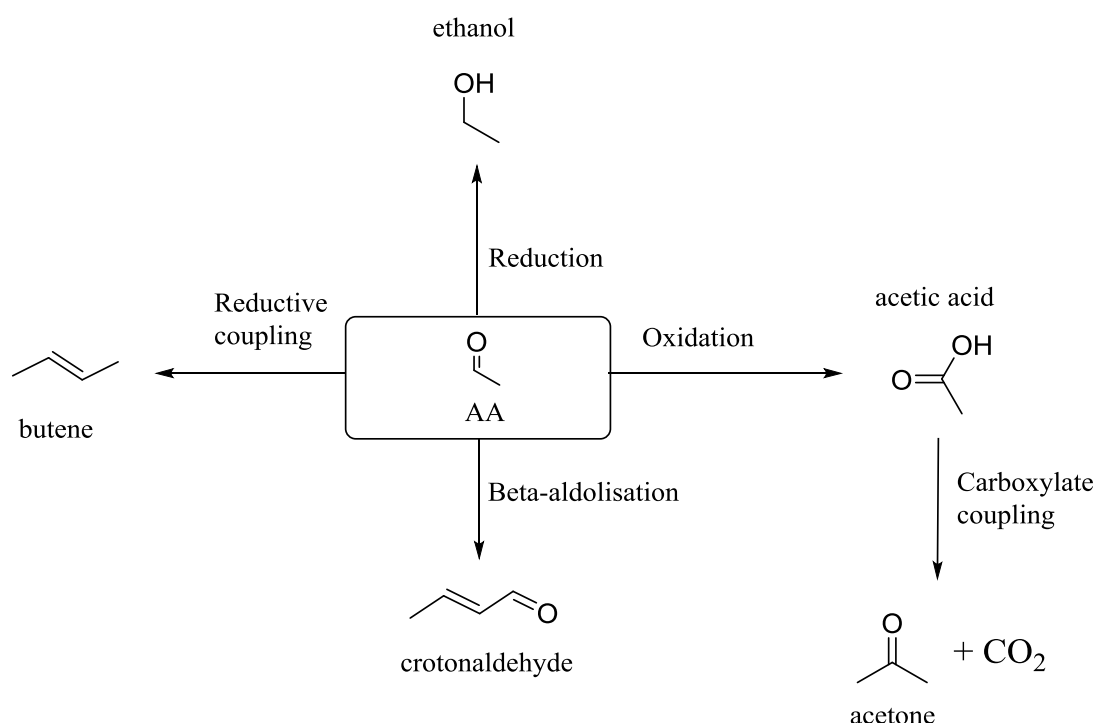


Figure 1.8 Various reactions that AA can undergo in the presence of a ceria catalyst<sup>118</sup>

## 1.8 Aims of the Project

The main objectives of this project include investigating the claims made in the ColorMatrix patent. To verify whether a hydrous zirconium oxide catalyst can be an effective catalytic AA scavenger and to further probe the reaction mechanism. Also, alternative metal oxide catalysts will be prepared and tested for their efficacy in converting AA to determine whether zirconia is the best candidate for this technology. The catalysts will be characterised using various techniques to determine which physicochemical properties are most important for an effective AA conversion catalyst. A laboratory testing protocol will need to be developed in order to screen catalysts before they are examined in PET at ColorMatrix, and this will allow for greater investigation into the chemistry of the reactions between AA and metal oxide catalysts.

The ultimate goal of this research project is to develop a catalytic AA scavenger that is more effective than Anthranilamide and that remains active through multiple recyclings of the polymer.

## 1.9 Chapter 1 - References

1. J. J. Berzelius, *Edinb. New Philos. J.*, 1836, **21**, 223–228.
2. G. C. Bond, *Heterogeneous Catalysis: Principles and Applications*, Clarendon Press, 1987.
3. F. Haber and G. van Oordt, *Z. Für Anorg. Chem.*, 1905, **44**, 341–378.
4. T. Kandemir, M. E. Schuster, A. Senyshyn, M. Behrens and R. Schlögl, *Angew. Chem. Int. Ed.*, 2013, **52**, 12723–12726.
5. J. W. Erisman, M. A. Sutton, J. Galloway, Z. Klimont and W. Winiwarter, *Nat. Geosci.*, 2008, **1**, 636.
6. P. Pal and J. Nayak, *Sep. Purif. Rev.*, 2017, **46**, 44–61.
7. J. H. Jones, *Platin. Met. Rev.*, 2000, **44**, 94–105.
8. N. Yoneda, S. Kusano, M. Yasui, P. Pujado and S. Wilcher, *Appl. Catal. Gen.*, 2001, **221**, 253–265.
9. G. C. Koltsakis and A. M. Stamatelos, *Prog. Energy Combust. Sci.*, 1997, **23**, 1–39.
10. J. Kašpar, P. Fornasiero and N. Hickey, *Catal. Today*, 2003, **77**, 419–449.
11. M. A. Barreau, *Chem. Rev.*, 1996, **96**, 1413–1430.
12. S.-Y. Lee and S.-J. Park, *J. Ind. Eng. Chem.*, 2013, **19**, 1761–1769.
13. S. H. Taylor, C. S. Heneghan, G. J. Hutchings and I. D. Hudson, *Catal. Today*, 2000, **59**, 249–259.
14. B. Solsona, I. Vázquez, T. Garcia, T. E. Davies and S. H. Taylor, *Catal. Lett.*, 2007, **116**, 116–121.
15. H. Bosch, F. J. J. G. Janssen, F. M. G. van den Kerkhof, J. Oldenziel, J. G. van Ommen and J. R. H. Ross, *Appl. Catal.*, 1986, **25**, 239–248.
16. K. Sayama and H. Arakawa, *J. Photochem. Photobiol. Chem.*, 1996, **94**, 67–76.
17. M. Fernández-García, A. Martínez-Arias, A. Iglesias-Juez, C. Belver, A. B. Hungría, J. C. Conesa and J. Soria, *J. Catal.*, 2000, **194**, 385–392.
18. S. C. Kim and W. G. Shim, *Appl. Catal. B Environ.*, 2010, **98**, 180–185.

19. T. Montini, M. Melchionna, M. Monai and P. Fornasiero, *Chem. Rev.*, 2016, **116**, 5987–6041.
20. H. C. Yao and Y. F. Y. Yao, *J. Catal.*, 1984, **86**, 254–265.
21. E. Mamontov, T. Egami, R. Brezny, M. Koranne and S. Tyagi, *J. Phys. Chem. B*, 2000, **104**, 11110–11116.
22. J. Paier, C. Penschke and J. Sauer, *Chem. Rev.*, 2013, **113**, 3949–3985.
23. J. C. Conesa, *Surf. Sci.*, 1995, **339**, 337–352.
24. C. T. Campbell and C. H. F. Peden, *Science*, 2005, **309**, 713–714.
25. A. Aranda, S. Agouram, J. M. López, A. M. Mastral, D. R. Sellick, B. Solsona, S. H. Taylor and T. García, *Appl. Catal. B Environ.*, 2012, **127**, 77–88.
26. P. M. Shah, A. N. Day, T. E. Davies, D. J. Morgan and S. H. Taylor, *Appl. Catal. B Environ.*, 2019, **253**, 331–340.
27. D. R. Sellick, A. Aranda, T. García, J. M. López, B. Solsona, A. M. Mastral, D. J. Morgan, A. F. Carley and S. H. Taylor, *Appl. Catal. B Environ.*, 2013, **132–133**, 98–106.
28. L. Wang, Y. Wang, Y. Zhang, Y. Yu, H. He, X. Qin and B. Wang, *Catal. Sci. Technol.*, 2016, **6**, 4840–4848.
29. S. Scirè, P. M. Riccobene and C. Crisafulli, *Appl. Catal. B Environ.*, 2010, **101**, 109–117.
30. L. Torrente-Murciano, A. Gilbank, B. Puertolas, T. Garcia, B. Solsona and D. Chadwick, *Appl. Catal. B Environ.*, 2013, **132–133**, 116–122.
31. Q. Dai, H. Huang, Y. Zhu, W. Deng, S. Bai, X. Wang and G. Lu, *Appl. Catal. B Environ.*, 2012, **117–118**, 360–368.
32. E. Aneggi, J. Llorca, M. Boaro and A. Trovarelli, *J. Catal.*, 2005, **234**, 88–95.
33. S. Carrettin, P. Concepción, A. Corma, J. M. L. Nieto and V. F. Puntes, *Angew. Chem. Int. Ed.*, 2004, **43**, 2538–2540.
34. H. Y. Kim, H. M. Lee and G. Henkelman, *J. Am. Chem. Soc.*, 2012, **134**, 1560–1570.

35. G. Avgouropoulos and T. Ioannides, *Appl. Catal. Gen.*, 2003, **244**, 155–167.
36. D. Andreeva, V. Idakiev, T. Tabakova, L. Ilieva, P. Falaras, A. Bourlinos and A. Travlos, *Catal. Today*, 2002, **72**, 51–57.
37. X. Wang, J. A. Rodriguez, J. C. Hanson, D. Gamarra, A. Martínez-Arias and M. Fernández-García, *J. Phys. Chem. B*, 2006, **110**, 428–434.
38. A. Luengnaruemitchai, S. Osuwan and E. Gulari, *Catal. Commun.*, 2003, **4**, 215–221.
39. R. Ramdas, E. Nowicka, R. Jenkins, D. Sellick, C. Davies and S. Golunski, *Appl. Catal. B Environ.*, 2015, **176–177**, 436–443.
40. K. Krishna, A. Bueno-López, M. Makkee and J. A. Moulijn, *Appl. Catal. B Environ.*, 2007, **75**, 189–200.
41. Q. Liang, X. Wu, D. Weng and H. Xu, *Catal. Today*, 2008, **139**, 113–118.
42. D. Mukherjee and B. M. Reddy, *Catal. Today*, 2018, **309**, 227–235.
43. C.-B. Lim, H. Kusaba, H. Einaga and Y. Teraoka, *Catal. Today*, 2011, **175**, 106–111.
44. A. Cooper, T. E. Davies, D. J. Morgan, S. Golunski and S. H. Taylor, *Catalysts*, 2020, **10**, 294.
45. M. I. Zaki and N. Sheppard, *J. Catal.*, 1983, **80**, 114–122.
46. A. Corma and M. E. Domine, *Chem. Commun.*, 2005, 4042–4044.
47. T. Rajiah, K. V. R. Chary, K. S. R. Rao, R. N. Rao and R. Prasad, *Green Chem.*, 2002, **4**, 210–212.
48. V. Solinas, E. Rombi, I. Ferino, M. G. Cutrufello, G. Colón and J. A. Navío, *J. Mol. Catal. Chem.*, 2003, **204–205**, 629–635.
49. M. G. Cutrufello, I. Ferino, V. Solinas, A. Primavera, A. Trovarelli, A. Auroux and C. Picciau, *Phys. Chem. Chem. Phys.*, 1999, **1**, 3369–3375.
50. S. Sato, R. Takahashi, T. Sodesawa, N. Honda and H. Shimizu, *Catal. Commun.*, 2003, **4**, 77–81.

51. M. Gliński and M. Kaszubski, *React. Kinet. Catal. Lett.*, 2004, **82**, 157–163.
52. M. Gliński, J. Kijeński and A. Jakubowski, *Appl. Catal. Gen.*, 1995, **128**, 209–217.
53. M. Gliński, G. Zalewski, E. Burno and A. Jerzak, *Appl. Catal. Gen.*, 2014, **470**, 278–284.
54. E. L. Kunkes, E. I. Gürbüz and J. A. Dumesic, *J. Catal.*, 2009, **266**, 236–249.
55. E. I. Gürbüz, E. L. Kunkes and J. A. Dumesic, *Appl. Catal. B Environ.*, 2010, **94**, 134–141.
56. R. de S. Monteiro, F. B. Noronha, L. C. Dieguez and M. Schmal, *Appl. Catal. Gen.*, 1995, **131**, 89–106.
57. D. Haffad, U. Kameswari, M. M. Bettahar, A. Chambellan and J. C. Lavalle, *J. Catal.*, 1997, **172**, 85–92.
58. J. B. Branco, D. Ballivet-Tkatchenko and A. P. de Matos, *J. Mol. Catal. Chem.*, 2009, **307**, 37–42.
59. S. Eck, C. Castellarin-Cudia, S. Surnev, K. C. Prince, M. G. Ramsey and F. P. Netzer, *Surf. Sci.*, 2003, **536**, 166–176.
60. J. A. Rodriguez, J. Graciani, J. Evans, J. B. Park, F. Yang, D. Stacchiola, S. D. Senanayake, S. Ma, M. Pérez, P. Liu, J. F. Sanz and J. Hrbek, *Angew. Chem. Int. Ed.*, 2009, **48**, 8047–8050.
61. A. Ostroverkh, V. Johánek, P. Kúš, R. Šedivá and V. Matolín, *Langmuir*, 2016, **32**, 6297–6309.
62. Bakelite First Synthetic Plastic - National Historic Chemical Landmark, <https://www.acs.org/content/acs/en/education/whatischemistry/landmarks/bakelite.html>, (accessed 22 June 2020).
63. M. Alauddin, I. A. Choudhury, M. A. El Baradie and M. S. J. Hashmi, *J. Mater. Process. Technol.*, 1995, **54**, 40–46.
64. GB578079A, 1946.

65. O. Olabisi, K. Adewale and K. Adewale, *Handbook of Thermoplastics*, CRC Press, 2016.
66. J. Yang, Z. Xia, F. Kong and X. Ma, *Polym. Degrad. Stab.*, 2010, **95**, 53–58.
67. S. Keresztes, E. Tatár, V. G. Mihucz, I. Virág, C. Majdik and G. Záray, *Sci. Total Environ.*, 2009, **407**, 4731–4735.
68. US8710128 B2, 2014.
69. U. K. Thiele, *Int. J. Polym. Mater. Polym. Biomater.*, 2001, **50**, 387–394.
70. Qiu Gao, Huang Nan-Xun, Tang Zhi-Lian and L. Gerking, *Chem. Eng. Sci.*, 1997, **52**, 371–376.
71. V. B. Gupta and Z. Bashir, in *Handbook of Thermoplastic Polyesters*, John Wiley & Sons, Ltd, 2005, pp. 317–361.
72. L. C. M. Lebreton, J. van der Zwet, J.-W. Damsteeg, B. Slat, A. Andrade and J. Reisser, *Nat. Commun.*, 2017, **8**, 15611.
73. J. R. Jambeck, R. Geyer, C. Wilcox, T. R. Siegler, M. Perryman, A. Andrade, R. Narayan and K. L. Law, *Science*, 2015, **347**, 768–771.
74. F. Awaja and D. Pavel, *Eur. Polym. J.*, 2005, **41**, 1453–1477.
75. M. Han, in *Recycling of Polyethylene Terephthalate Bottles*, eds. S. Thomas, A. Rane, K. Kanny, A. V.k. and M. G. Thomas, William Andrew Publishing, 2019, pp. 85–108.
76. A. Sheel and D. Pant, in *Recycling of Polyethylene Terephthalate Bottles*, eds. S. Thomas, A. Rane, K. Kanny, A. V.k. and M. G. Thomas, William Andrew Publishing, 2019, pp. 61–84.
77. P. Gupta and S. Bhandari, in *Recycling of Polyethylene Terephthalate Bottles*, eds. S. Thomas, A. Rane, K. Kanny, A. V.k. and M. G. Thomas, William Andrew Publishing, 2019, pp. 109–134.
78. G. Xi, M. Lu and C. Sun, *Polym. Degrad. Stab.*, 2005, **87**, 117–120.
79. K. Troev, G. Grancharov, R. Tsevi and I. Gitsov, *J. Appl. Polym. Sci.*, 2003, **90**, 1148–1152.

80. S. R. Shukla and K. S. Kulkarni, *J. Appl. Polym. Sci.*, 2002, **85**, 1765–1770.
81. T. Yoshioka, T. Sato and A. Okuwaki, *J. Appl. Polym. Sci.*, 1994, **52**, 1353–1355.
82. J. R. Campanelli, D. G. Cooper and M. R. Kamal, *J. Appl. Polym. Sci.*, 1994, **53**, 985–991.
83. J. Scheirs, *Polymer recycling: science, technology, and applications*, Wiley, 1998.
84. K. Fukushima, J. M. Lecuyer, D. S. Wei, H. W. Horn, G. O. Jones, H. A. Al-Megren, A. M. Alabdulrahman, F. D. Alsewailem, M. A. McNeil, J. E. Rice and J. L. Hedrick, *Polym. Chem.*, 2013, **4**, 1610–1616.
85. A. Jain and R. K. Soni, *J. Polym. Res.*, 2007, **14**, 475–481.
86. R. Di Felice, D. Cazzola, S. Cobrro and L. Oriani, *Packag. Technol. Sci.*, 2008, **21**, 405–415.
87. M. Frounchi and A. Dourbash, *Macromol. Mater. Eng.*, 2009, **294**, 68–74.
88. US20140295028A1, 2014.
89. J. B. Webster, S. E. Duncan, J. E. Marcy and S. F. O’Keefe, *J. Food Sci.*, 2009, **74**, S390–S398.
90. E. Pirzadeh, A. Zadhoush and M. Haghigat, *J. Appl. Polym. Sci.*, 2007, **106**, 1544–1549.
91. S. S. Hosseini, S. Taheri, A. Zadhoush and A. Mehrabani-Zeinabad, *J. Appl. Polym. Sci.*, 2007, **103**, 2304–2309.
92. S. R. Shukla, E. A. Lofgren and S. A. Jabarin, *Polym. Int.*, 2005, **54**, 946–955.
93. F. Samperi, C. Puglisi, R. Alicata and G. Montaudo, *Polym. Degrad. Stab.*, 2004, **83**, 3–10.
94. G. Montaudo, C. Puglisi and F. Samperi, *Polym. Degrad. Stab.*, 1993, **42**, 13–28.
95. I. Marshall and A. Todd, *Trans. Faraday Soc.*, 1953, **49**, 67–78.
96. T. Y. Kim and S. A. Jabarin, *J. Appl. Polym. Sci.*, 2003, **89**, 228–237.
97. K. C. Khemani, *Polym. Degrad. Stab.*, 2000, **67**, 91–99.

98. E. D. Lund, C. L. Kirkland and P. E. Shaw, *J. Agric. Food Chem.*, 1981, **29**, 361–366.
99. R. D. Hawkins and H. Kalant, *Pharmacol. Rev.*, 1972, **24**, 67–157.
100. P. J. Brooks, M.-A. Enoch, D. Goldman, T.-K. Li and A. Yokoyama, *PLoS Med.*, 2009, **6**, 258–263.
101. P. J. Brooks and J. A. Theruvathu, *Alcohol*, 2005, **35**, 187–193.
102. B. A. Mrozinski, PhD Thesis, University of Toledo, 2010.
103. US20020136808 A1, 2002.
104. B. Nijssen, T. Kamperman and J. Jetten, *Packag. Technol. Sci.*, 1996, **9**, 175–185.
105. US7041350 B1, 2006.
106. Z. Xi, T. Liu, W. Si, F. Bi, Z. Xu and L. Zhao, *Chin. J. Chem. Eng.*, , DOI:10.1016/j.cjche.2018.03.007.
107. US6274212 B1, 2001.
108. B. A. Mrozinski, Y.-W. Kim, E. A. Lofgren and S. A. Jabarin, *J. Appl. Polym. Sci.*, 2013, **130**, 4191–4200.
109. M. Imran, D. H. Kim, W. A. Al-Masry, A. Mahmood, A. Hassan, S. Haider and S. M. Ramay, *Polym. Degrad. Stab.*, 2013, **98**, 904–915.
110. WO2005010088 A1, 2005.
111. M. Pan, D. W. Flaherty and C. B. Mullins, *J. Phys. Chem. Lett.*, 2011, **2**, 1363–1367.
112. J. Xu, X.-C. Xu, X.-J. Yang and Y.-F. Han, *Catal. Today*, 2016, **276**, 19–27.
113. J. A. Keith and P. M. Henry, *Angew. Chem. Int. Ed.*, 2009, **48**, 9038–9049.
114. W. Ji, Y. Chen and H. H. Kung, *Appl. Catal. Gen.*, 1997, **161**, 93–104.
115. E. Dumitriu, V. Hulea, C. Chelaru, C. Catrinescu, D. Tichit and R. Durand, *Appl. Catal. Gen.*, 1999, **178**, 145–157.
116. E. C. Craven, H. Jowitt and W. R. Ward, *J. Appl. Chem.*, 1962, **12**, 526–535.

117. W. Kenneth Busfield, R. Martin Lee and D. Merigold, *J. Chem. Soc. Faraday Trans. 1 Phys. Chem. Condens. Phases*, 1973, **69**, 936–940.

118. H. Idriss, C. Diagne, J. P. Hindermann, A. Kiennemann and M. A. Barteau, *J. Catal.*, 1995, **155**, 219–237.

## 2 Experimental

### 2.1 Materials

- Ammonium cerium(IV) nitrate was purchased from Acros Organics.
- Urea was purchased from Sigma-Aldrich.
- Zirconium(IV) hydroxide was purchased from Sigma-Aldrich.
- Zirconium(IV) oxynitrate hydrate was purchased from Sigma-Aldrich.
- Manganese(II) nitrate tetrahydrate was purchased from Sigma-Aldrich.
- Copper(II) nitrate trihydrate was purchased from Fluka.
- Cerium(III) nitrate hexahydrate was purchased from Sigma-Aldrich.
- TTAB (Tetradecyltrimethylammonium bromide) was purchased from Alfa Aesar.
- Pluronic P123 was purchased from Sigma-Aldrich.
- Cerium(III) chloride heptahydrate was purchased from Sigma-Aldrich.
- Cylinders containing AA/He and AA/acetone/CO<sub>2</sub>/He were purchased from BOC.
- Cerium(IV) oxide nanopowder was purchased from Sigma-Aldrich.
- Cerium(IV) hydroxide was purchased from Sigma-Aldrich.
- Cerium(III) carbonate hydrate was purchased from Sigma-Aldrich.
- Cerium(III) acetate hydrate was purchased from Sigma-Aldrich.
- Cerium(III) acac hydrate was purchased from Sigma-Aldrich.
- Cerium(III) oxalate hydrate was purchased from Sigma-Aldrich.

## 2.2 Catalyst Preparation

### 2.2.1 Urea Precipitation

#### 2.2.1.1 Experimental Procedure

Ceria samples were prepared by precipitating a cerium nitrate precursor with urea in deionised water at reflux.<sup>1-3</sup> Ammonium cerium nitrate (20 g, 0.0365 mol) and urea (6.58 g, 0.110 mol) (3:1 urea to nitrate precursor molar ratio) were added to deionised water (100 ml) and stirred until dissolved. The solution was heated to 110 °C and left to age under reflux for 24 hours in a round bottom flask equipped with a reflux condenser. The mixture was vacuum filtered using a Buchner funnel and the filter cake was washed with three portions of hot deionised water. The solid product was dried overnight in an oven at 110 °C, and then calcined at 400 °C for 5 hours in static air. All static air calcinations in this project were conducted in a fume cupboard with extraction. Both ends of the tubular furnace were open so there would have been a degree of airflow through the furnace during the calcination.

- CeO<sub>2</sub> U1, U2, U3 were prepared using this method.
- CeO<sub>2</sub> U4 was prepared using 200 ml water.
- CeO<sub>2</sub> U5, U6 was prepared using this method on a 2x scale.
- CeO<sub>2</sub> U7 was prepared using a 1:1 urea to nitrate precursor molar ratio.
- CeO<sub>2</sub> U8 was prepared using a 1:2 urea to nitrate precursor molar ratio.
- CeO<sub>2</sub> U9 was prepared using a 5:1 urea to nitrate precursor molar ratio.

Zirconia and manganesia samples were prepared using the urea precipitation method with a 3:1 urea to nitrate precursor molar ratio. To prepare ZrO<sub>2</sub>, zirconyl oxynitrate hexahydrate (12.38 g, 0.0365 mol) was used, for Mn<sub>2</sub>O<sub>3</sub>, manganese nitrate tetrahydrate (6.53 g, 0.0365 mol) was used. Tetragonal ZrO<sub>2</sub> (t-ZrO<sub>2</sub>) and Mn<sub>2</sub>O<sub>3</sub> were both prepared using this method. Monoclinic ZrO<sub>2</sub> (m-ZrO<sub>2</sub>) was prepared by calcining Zr(OH)<sub>4</sub> at 400 °C for 5 hours in static air.

Doped catalysts were prepared by adding the desired molar ratio of the dopant to the ceria urea precipitation preparation with a 3:1 urea ratio. To prepare 5%ZrO<sub>x</sub>-CeO<sub>2</sub> zirconyl oxynitrate hexahydrate (0.62 g, 0.0018 mol) was added to ammonium cerium nitrate (19 g, 0.0347 mol). To prepare 5%MnO<sub>x</sub>-CeO<sub>2</sub> manganese nitrate

tetrahydrate (0.45 g, 0.0018 mol) was added to ammonium cerium nitrate (19 g, 0.0347 mol). To prepare 5% $\text{CuO}_x\text{-CeO}_2$  copper nitrate trihydrate was (0.44 g, 0.0018 mol) was added to ammonium cerium nitrate (19 g, 0.0347 mol).

## 2.2.2 TTAB Assisted Preparation

### 2.2.2.1 Experimental Procedure

This preparation method was adapted from a study by Yuejuan *et al.*<sup>4</sup> A solution of NaOH (1g, 0.0250 mol) in distilled water (150 ml) was added to a stirred solution of Ce(NO<sub>3</sub>)<sub>3</sub>.6H<sub>2</sub>O (2.17 g, 0.00500 mol) and TTAB (1.09 g, 0.00324 mol) in distilled water (100 ml). The mixture was stirred overnight at 90 °C, then filtered and washed with hot deionised water. The solid product was dried overnight at 110 °C before being calcined at 400 °C for 4 hours under static air.

- CeO<sub>2</sub> T1, T2 was prepared using TTAB.

## 2.2.3 Pluronic P123 Assisted Preparations

### 2.2.3.1 Experimental Procedure

This preparation method was adapted from a study by Yoshikawa *et al.*<sup>5</sup> Added Pluronic P123 (1 g) to ethanol (10 g) and stirred until solution turned clear. Added CeCl<sub>3</sub>.7H<sub>2</sub>O (2.98 g, 0.00800 mol) and stirred for 30 mins until solution turned clear. The resultant gel was then aged before being calcined at 500 °C for 5 hours under flowing air.

- CeO<sub>2</sub> P1 was aged overnight at 60 °C.
- CeO<sub>2</sub> P2 was aged for 7 days at 40 °C.

## 2.2.4 Wet Milling

Wet milling was conducted in the laboratory at ColorMatrix using an Eiger Torrance 250 ml Mill. Ceria (50 g) was added to triglyceride oil (350 g) (this is used as a carrier material to add powder additives to PET) and circulated through the mill

for varying durations of time (2, 10, and 20 minutes). 4 g of the milled catalyst dispersion was added to PET (1 kg) to yield a 500 ppm loading for the extruder test.

### 2.2.5 Dry Milling

Dry milling was conducted in a planetary ball mill in the CCI using a Retsch PM 100 ball mill equipped with a ZrO<sub>2</sub> grinding jar and ZrO<sub>2</sub> grinding balls. At least 10 ml of solid material was added to the grinding vessel and was milled at 300 rpm for 3 hours.

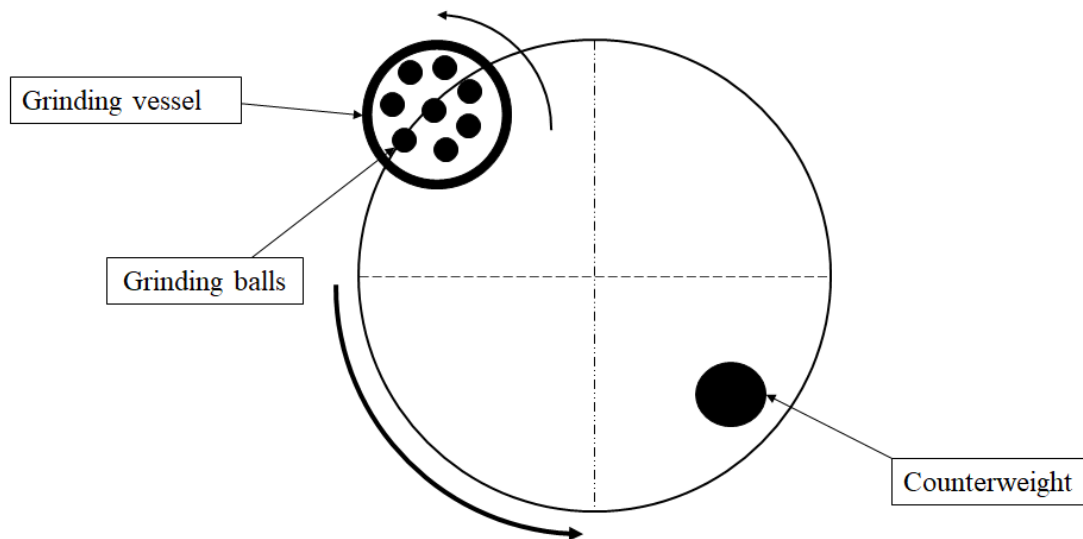


Figure 2.1 Schematic of planetary ball mill

## 2.3 Catalyst Testing

### 2.3.1 Gas Phase Reactor

A continuous flow fixed-bed gas phase reactor (for schematic see figure 2.2) was used to measure the catalytic activity of metal oxide catalysts for the conversion of AA at 300 °C in an inert atmosphere at atmospheric pressure. This reactor utilises a continuous flow regime within a tubular geometry, so it can also be described as a plug flow reactor (PFR).<sup>6</sup> Quartz reactor tubes (outer diameter = 9 mm, internal diameter = 7 mm, length = 350 mm) were packed with a catalyst bed sat between two quartz wool plugs. The depth of the catalyst bed was dependent upon the density of the catalyst material, but the bed depth was generally around 1 cm. The reactor tube

was oriented vertically within the furnace and the gas flowed down through the catalyst bed. A thermocouple was fixed in place just above the catalyst bed, which was able to accurately control the temperature within the reactor. MKS mass flow controllers were used to control the flow of AA/He and a Carbolite furnace was used to heat the catalyst bed to 300 °C. Initial testing was conducted using a 50 mg catalyst bed in a flow of AA/He of 50 ml/min. For testing at a gas hourly space velocity (GHSV) of 300,000 h<sup>-1</sup>, AA/He was flowed at 200 ml/min over a catalyst bed of the desired volume that is dependent upon the density of the material.

$$GHSV (h^{-1}) = \frac{\text{Total flow (ml/min)} * 60}{\frac{\text{Catalyst mass (g)}}{\text{Catalyst denisty (g/ml)}}}$$

Equation 2.1 Equation for calculating the GHSV of a gas phase reaction

The gaseous product stream was analysed by online gas chromatography (GC) analysis using an Agilent 7890B GC equipped with a thermal conductivity detector (TCD) and flame ionisation detector (FID). The columns fitted in the GC included HayeSep Q (80-100 mesh, 1.8m) and MolSieve 5A (80-100 mesh, 2m). For the analysis of the reactions in this project the FID results were more relevant than the TCD results.

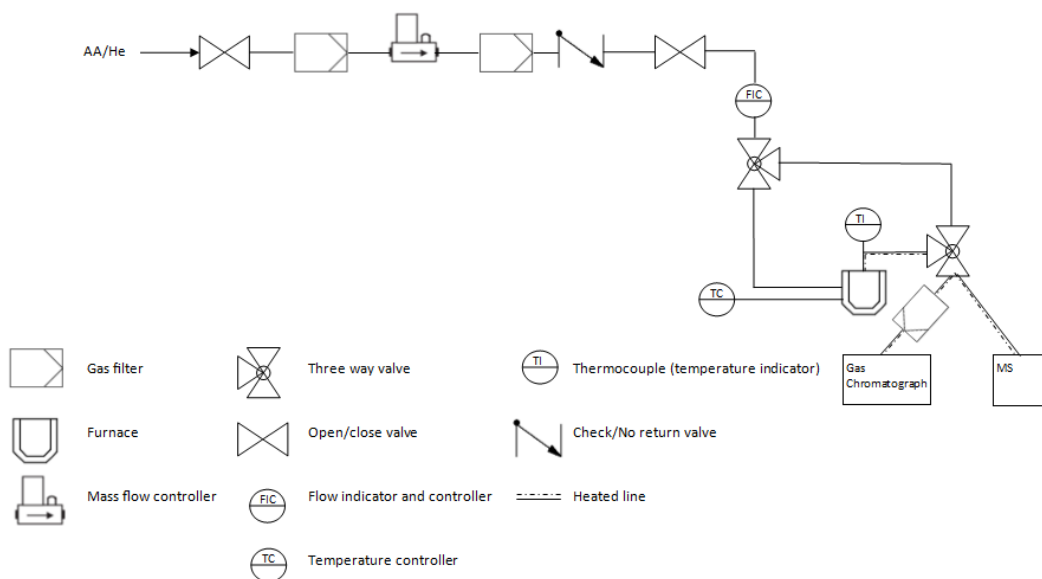


Figure 2.2 Schematic of continuous flow fixed-bed gas phase reactor for the testing of AA removal catalysts



Figure 2.3 Photograph of ceria catalyst bed between quartz wool plugs within quartz reactor tube

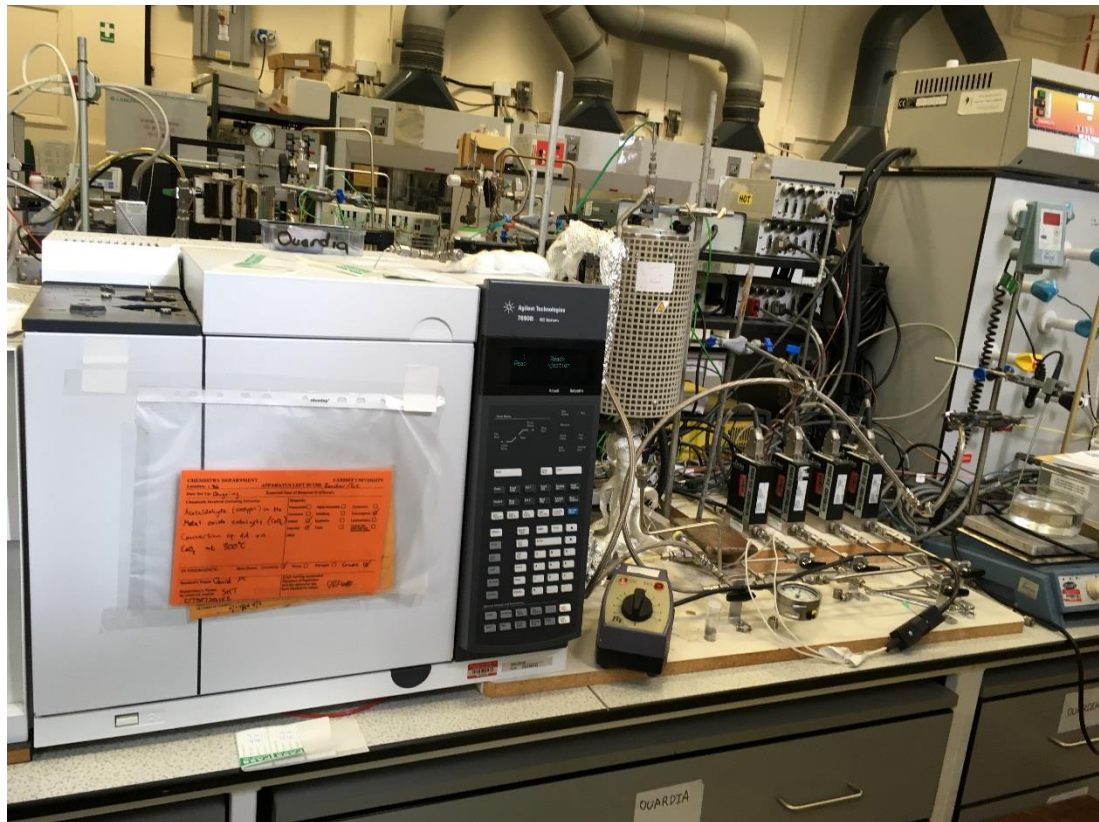


Figure 2.4 Photograph of continuous flow fixed-bed gas phase reactor with tubular furnace containing vertical reactor tube and online GC analysis

### 2.3.1.1 Gas Chromatography (GC)

The gaseous product stream flowed from the catalyst bed to the GC injector where it is injected using a six-port valve with He as a carrier gas and at a temperature of 150 °C. CO<sub>2</sub> and organic products were separated using the HayeSep Q column, whilst the other light gaseous products such as CO and CH<sub>4</sub> were separated using the MolSieve 5A column.

In this GC configuration there are three six-port valves (V1, V2, V3), V1 controls the use of the methaniser, V2 controls the use of the MolSieve 5A column, and V3 controls the use of the HayeSep Q column. Valves allow for the isolation of products onto specific columns which allows for greater optimisation and ensures that columns can be protected from compounds they are incompatible with. For example, CO<sub>2</sub> binds irreversibly to the MolSieve 5A so the GC method needs to be designed in such a way that CO<sub>2</sub> elutes on the HayeSep Q column. Otherwise CO<sub>2</sub> will not reach the detectors and will not appear in any of the analysis and will also cause damage to the column. Therefore, a valve change was used to elute the CO<sub>2</sub> on the HayeSep Q column between 2 and 3 mins, before it was switched back to the molecular sieve column between 3 and 10 mins to elute the CO and CH<sub>4</sub>. Finally, the HayeSep Q was switched back into the series and the molecular sieve switched out for the rest of the sequence (10-20 mins) in order to elute the AA and acetone. The valve sequence is presented in table 2.1 and shows the status of each six-port valve for the different steps within the method.

Table 2.1 Valve sequence for GC-FID analysis of reactions between AA and metal oxide catalyst in gas phase. ON = in series, OFF = bypassed.

Time mins	V1 (methaniser)	V2 (molecular sieve)	V3 (HayeSep Q)
0.5	OFF	ON	ON
2	ON	OFF	ON
3	ON	ON	OFF
10	ON	OFF	ON

The catalyst that is found before the FID in the GC schematic (figure 2.3) is a methaniser that is composed of a Raney nickel catalyst that converts CO and CO<sub>2</sub> to CH<sub>4</sub> before being processed by the FID.<sup>7</sup> The nickel catalyst is fed with H<sub>2</sub> and is heated to 350 °C to enable it to act as an effective reduction catalyst. This allows for non-combustible products, like CO and CO<sub>2</sub>, to be analysed by FID. These products can be analysed using the TCD, but FID analysis is preferred because it is a more sensitive detection method.

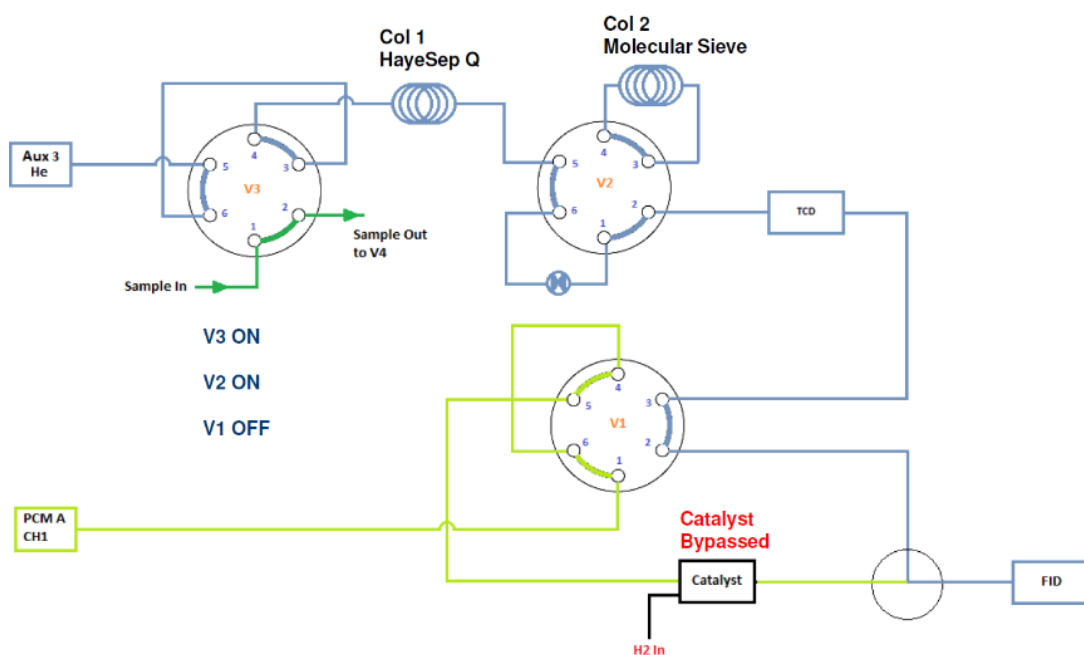


Figure 2.5 Sample injection in GC during analysis of AA conversion products.

In figure 2.3 the valve configuration for 0.5-2 mins of the GC sequence can be seen, which is used to inject the gas samples onto the two columns. In this case V3 is set to the inject position for the start of the GC method, for the rest of the method it is switched on for the analysis of the gases. It can also be seen from this figure that the TCD is earlier in the sequence than the FID. It is important that the FID follow the TCD in the sequence because the FID destroys the analyte and so TCD analysis would not be able follow FID analysis, whereas TCD analysis is non-destructive.

The temperature profile of the GC method also needed to be programmed in order to ensure effective separation and to keep the length of each sequence to a

minimum. Therefore, for the first 10 mins of the sequence the temperature was held at 120 °C, because this allowed for efficient separation of the light gaseous products CO and CH<sub>4</sub> on the molecular sieve column. Between 10 and 12 mins the temperature was increased from 120 to 200 °C, at a rate of 40 °C per min, and this achieves separation of the AA and acetone on the HayeSep Q column. The final 8 mins of the sequence are carried out at 200 °C to ensure no organic compounds remain on the column and to prevent any contamination with following injections from the reactor.

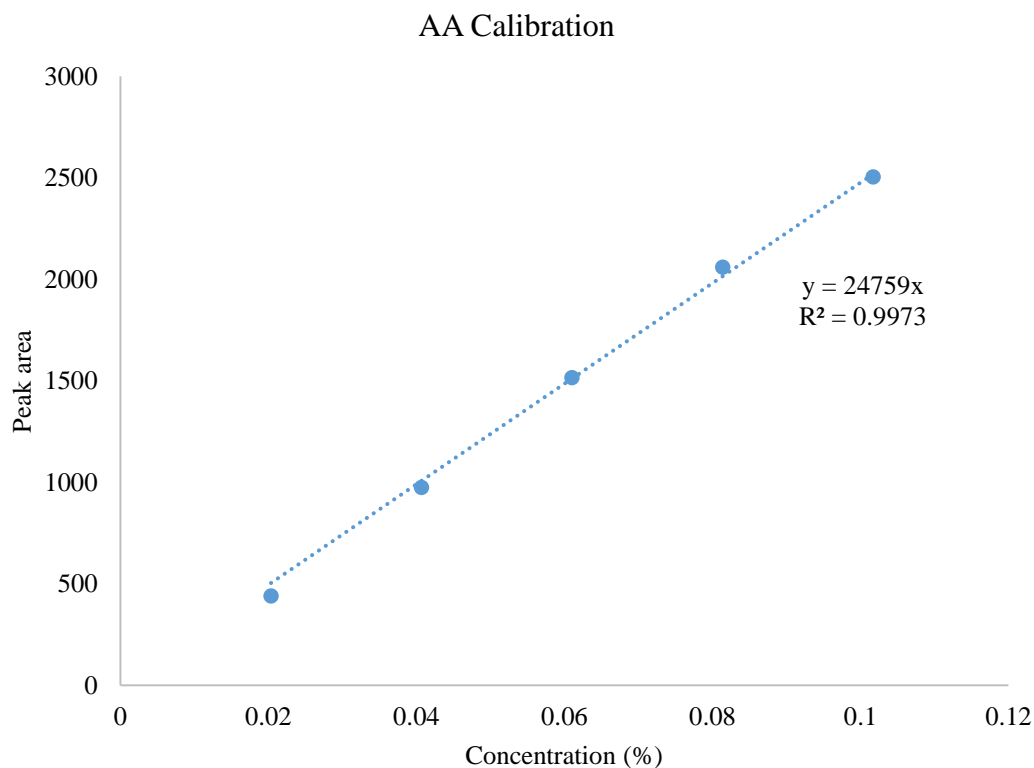


Figure 2.6 Calibration for AA in gas phase reactor (100% AA/He (AA ≈ 0.1%), 80% AA/He : 20% N<sub>2</sub> (AA ≈ 0.08%), 60% AA/He : 40% N<sub>2</sub> (AA ≈ 0.06%), 40% AA/He : 60% N<sub>2</sub> (AA ≈ 0.04%), 20% AA/He : 80% N<sub>2</sub> (AA ≈ 0.02%)

The response factor (RF) obtained from calibrations can be used to convert the peak area to the analyte concentration. The RF is equal to the peak area divided by the concentration, which is also equal to the slope of the calibration plot. From the calibration in figure 2.4 the peak area of the AA signal can be converted to the concentration as a percentage by dividing it by the RF which is equal to 24759.

$$\text{Analyte concentration (\%)} = \frac{\text{Peak area}}{\text{RF}}$$

Equation 2.2 Equation for the conversion of peak area in a GC trace to analyte concentration

$$\text{AA conversion (\%)} = \left( \left( \frac{C_2H_4O_{in} - C_2H_4O_{out}}{C_2H_4O_{in}} \right) * 100 \right)$$

Equation 2.3 Equation for the calculation of AA conversion in the gas phase reactor

$\text{CO}_2$  and acetone are the major products observed in the gas phase reactions between metal oxide catalysts and AA at 300 °C. These products were calibrated for using a cylinder containing AA(500 ppm)/ $\text{CO}_2$ (500 ppm)/acetone(500 ppm)/He (balance) (see figures 2.5 and 2.6). Due to the GC being equipped with a methaniser the RF for other  $\text{C}_1$  products such as CO and  $\text{CH}_4$  was assumed to be the same as that for  $\text{CO}_2$ .

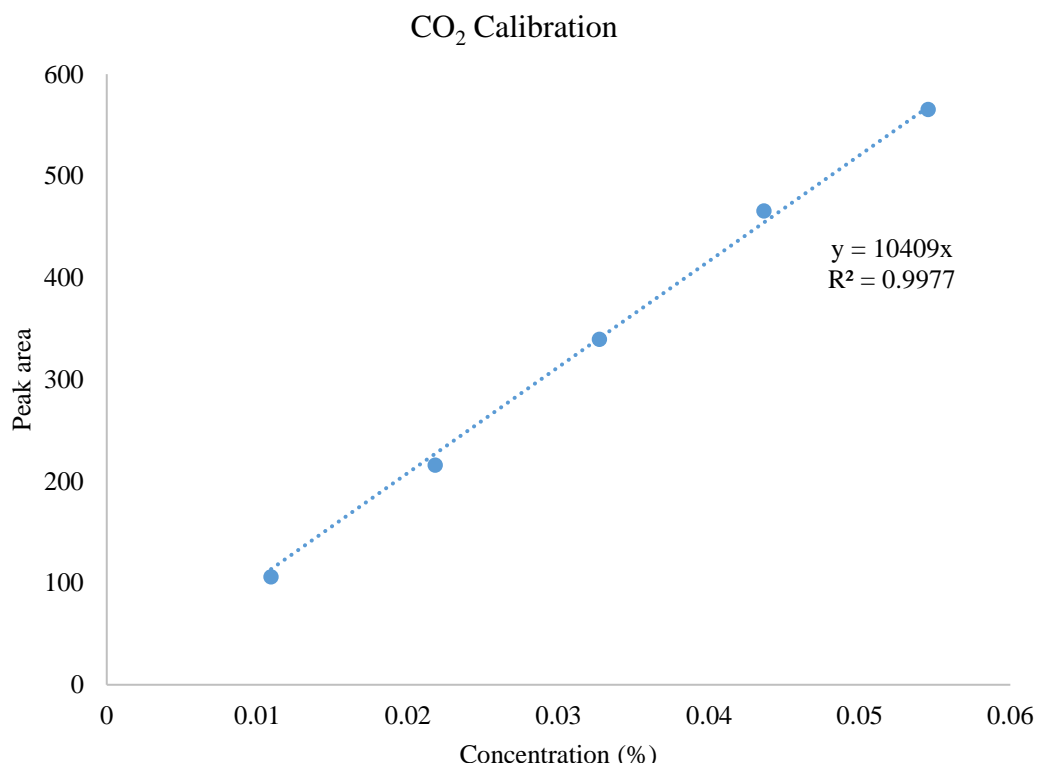


Figure 2.7 Calibration for  $\text{CO}_2$  in gas phase reactor (100%  $\text{CO}_2/\text{He}$  ( $\text{CO}_2 \approx 0.05\%$ )), 80%  $\text{CO}_2/\text{He} : 20\% \text{N}_2$  ( $\text{CO}_2 \approx 0.04\%$ )), 60%  $\text{CO}_2/\text{He} : 40\% \text{N}_2$  ( $\text{CO}_2 \approx 0.03\%$ )), 40%  $\text{CO}_2/\text{He} : 60\% \text{N}_2$  ( $\text{CO}_2 \approx 0.02\%$ )), 20%  $\text{CO}_2/\text{He} : 80\% \text{N}_2$  ( $\text{CO}_2 \approx 0.01\%$ ))

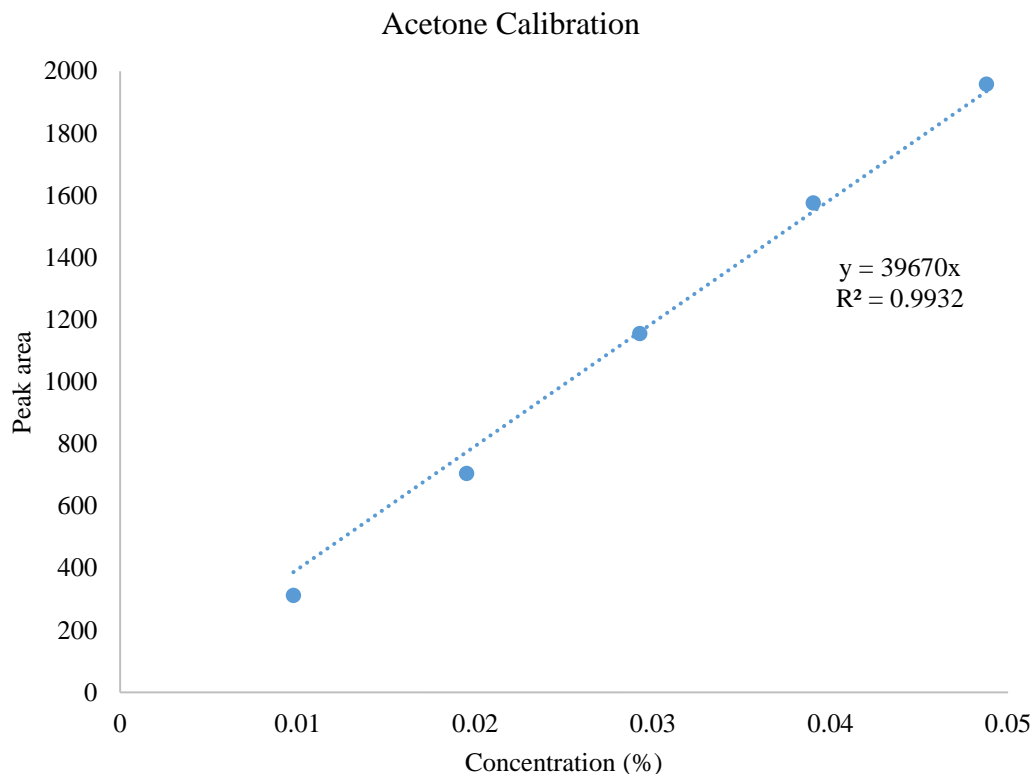


Figure 2.8 Calibration for acetone in gas phase reactor (100% acetone/He (acetone  $\approx$  0.05%), 80% acetone/He : 20% N<sub>2</sub> (acetone  $\approx$  0.04%), 60% acetone/He : 40% N<sub>2</sub> (acetone  $\approx$  0.03%), 40% acetone/He : 60% N<sub>2</sub> (acetone  $\approx$  0.02%), 20% acetone/He : 80% N<sub>2</sub> (acetone  $\approx$  0.01%))

To calculate the carbon balance of the reaction the amount of carbon in the reactant stream is divided by the amount of carbon in the product stream. Each compound is weighted based upon the number of carbon atoms they contain. The equation for the calculation used to measure the carbon balance is found in equation 2.4.

$$\begin{aligned}
 & \text{Carbon balance (\%)} \\
 &= 100 \\
 &\times \left( \frac{(C_2H_4O_{out}(\%) \times 2) + CO_2(\%) + CH_4(\%) + CO(\%) + (C_3H_6O(\%) \times 3)}{(C_2H_4O_{in}(\%) \times 2)} \right)
 \end{aligned}$$

Equation 2.4 Equation for calculating carbon balance from GC data

### 2.3.1.2 Mass Spectrometry (MS)

For online MS analysis in the gas phase reactor a Hiden Analytical Quantitative Gas Analyser (QGA) Mass Spectrometer was placed downstream of the catalyst bed in place of the GC. A pump was used to pull the reaction stream into the MS. The MS analysis was used to identify the reaction products because it is difficult to identify unknown products using GC-FID. An MS program was designed using QGA Professional software that scanned for a selection of organic compounds to identify the reaction products.

### 2.3.2 Twin-Screw Extruder

To test the activity of metal oxide catalysts for their ability to convert AA within PET, extrusion was used to add the catalysts to the polymer. During extrusion a polymer is melted down into its molten state before being forced through a die and then cooled and cut into pellets. Extrusion offers the opportunity to add chemical additives to a polymer, and polymers can also be reacted together using this technique.

A Rondol Technology 21 mm Lab Twin Screw Extruder, cooling table and pelletiser was used. The extruder was fitted with a 3 mm two slot strand die. Prior to extrusion the PET was dried using a Motan Drier at 160 °C to achieve a moisture level of < 50 ppm.

Prior to testing the catalyst samples were sieved using Fisherbrand Test Sieves (200 mm diameter) with mesh sizes of 75 and 25 µm. The 25-75 µm particle size sieve fraction was used for the catalyst testing. To add catalyst to PET, dried PET (1 kg) was placed into a bucket and catalyst (500 mg for 500 ppm loading) and carrier (900 ppm if required) were added. The lid was fixed into place on the bucket and was shaken vigorously by hand to ensure good mixing. The catalyst/PET mixture was then poured into the hopper that feeds the extruder, which was set using the following parameters:

- Zone 1 = 265 °C (this is the feed throat section of the instrument where the polymer is added)
- Zone 2 = 285 °C
- Zone 3 = 285 °C

- Zone 4 = 285 °C
- Zone 5 = 285 °C
- Die = 280 °C
- Screw speed = 150 rpm

The extruded PET was fed onto a conveyor belt fitted with fans for cooling the polymer. By the time the PET reached the end of the conveyor it had solidified and was passed into a pelletiser where the polymer strands were cut down into pellets. The strand cut length was 5 mm. Samples of the pellets were collected to be used for analysis. The pellets were stored in a freezer to prevent the loss of AA due to evaporation out of the PET.

### 2.3.3 Headspace GC-FID

Headspace GC is a vapour-phase extraction technique that can be used to measure the concentration of volatile compound bound within a substrate.<sup>8</sup> It is a technique that is commonly used for the measurement of AA trapped within PET.<sup>9,10</sup>

To measure the concentration of AA in PET an Agilent 6890N GC-FID equipped with an Agilent 7694 Headspace Sampler is used. Between 1.2-1.3 g of PET was added to a 22 ml headspace vial and was heated to 150 °C for 1 hour by the sampler. Heating the PET liberates any volatile compounds that may be contained within the sample. The gas from the headspace vial was transferred to the GC via a transfer line that was heated to 175 °C. The headspace gas was injected into the GC and it was separated into its constituents using an Agilent J&W DB-1 column. The GC response to AA must be calibrated in order to measure the concentration of AA based on the trace generated by the GC-FID analysis. This is achieved by measuring a set of standard solutions containing a known concentration of AA across the concentration of interest. A straight line can be drawn between concentration and peak area to give the data found in tables 2.2-2.4 below. The GC-FID used for measuring AA concentration was calibrated every few months as follows:

Table 2.2 Calibration of headspace GC-FID for AA

<b>Regression Linear Curve July 2018</b>			
	<b>y = mx + c</b>	<b>m</b>	<b>c</b>
<b>Acetaldehyde</b>	$y = 0.7253x + 0.1089$	0.7253	0.1089

Table 2.3 Calibration of headspace GC-FID for AA

<b>Regression Linear Curve May 2019</b>			
	<b>y = mx + c</b>	<b>m</b>	<b>c</b>
<b>Acetaldehyde</b>	$y = 0.7350x + 0.0254$	0.7350	0.0254

Table 2.4 Calibration of headspace GC-FID for AA

<b>Regression Linear Curve August 2019</b>			
	<b>y = mx + c</b>	<b>m</b>	<b>c</b>
<b>Acetaldehyde</b>	$y = 0.365x + 0.0487$	0.365	0.0487

These calibrations are used to convert the peak area of the AA peak in the chromatogram to a concentration of AA. This conversion is calculated using the following equation:

$$\frac{(Peak\ area\ (a.u.) - c)}{m}$$

$$\frac{}{Mass\ of\ PET\ sample\ (g)}$$

Equation 2.5 Conversion of GC peak area to concentration for headspace GC-FID. c = intercept of y axis, m = gradient of slope

### 2.3.4 Measurement of Intrinsic Viscosity (IV)

Intrinsic viscosity (IV) can indicate the molecular weight and chain lengths of polymers. The higher the IV the greater the chain lengths found within the polymer, due to the way in which longer chains become more entangled with each other, which causes the viscosity of the material to increase. The IV was measured using a Viscotek 430 Dilution Solution Intrinsic Viscometer. The PET was dissolved in a phenol and 1,1,2,2-tetrachloroethane solvent mixture at a 60:40 ratio, for 2 hours at 110 °C. Equipolymers C93 PET was used as a reference sample.

### 2.3.5 Injection Moulding

To make plaques or preforms, injection moulding was carried out using a Husky Injection Moulder 160T. For the preparation of preforms a two-cavity mould was used to make two 33 g preforms per injection. Prior to moulding the PET was dried using a Motan Drier at 160 °C to achieve a moisture level of < 50 ppm. The injection moulder was set up using the following parameters:

- Zone 5 = 280 °C (this is the feed throat section of the instrument where the polymer is added)
- Zone 4 = 290 °C
- Zone 3 = 290 °C
- Zone 2 = 290 °C
- Zone 1 = 290 °C
- Nozzle = 290 °C
- Mould = 290 °C

### 2.3.6 Blow Moulding

The 33 g preforms prepared using injection moulding can be converted into 1 L bottles using blow moulding. A Sidel SBO Lab Armoire Electrique stretch blow moulder was utilised for this process. The preforms are softened as they pass along a rotating carousal surrounded by Infrared (IR) lamps. The polymer needs to be made soft and malleable so that it can be blown into the desired form. The target temperature for the preform was 115 °C and the following profile was used for the IR radiation (the IR zones are stacked on top of each other and the preforms are loaded neck side down, therefore, Zone 1 heats the neck of the preform, whilst zone 10 heats the bottom of the preform):

- Zone 1 = 44%
- Zone 2 = 65%
- Zone 3 = 72%

- Zone 4 = 54%
- Zone 5 = 42%
- Zone 6 = 55%
- Zone 7 = 75%
- Zone 8 = OFF
- Zone 9 = OFF
- Zone 10 = OFF

### 2.3.7 Colour and Haze Analysis

A Konica Minolta cm3600A spectrophotometer was used to measure the haze and colour of the PET. For colour analysis the spectrophotometer was set to transmission mode and was run with the specular components included (SCI). CIELAB was used as a colour system in order to convert the colour of the polymer into numerical data where L\* = lightness (0 = black, 100 = white), a\* = green/red (- = green, + = red), and b\* = blue/yellow (- = blue, + = yellow).

For haze analysis the spectrophotometer was set to haze mode and Equipolymers C93 PET was used as a reference sample.

## 2.4 Catalyst Characterisation

Metal oxide catalyst samples were characterised using a variety of techniques. A brief background summary of the theory that underpins each technique and the procedure used to carry out the different measurements is given.

### 2.4.1 Powder X-Ray Diffraction (PXRD)

#### 2.4.1.1 Background

XRD is a commonly used method for the characterisation of the bulk crystalline phases of powder samples. Within the field of catalysis, XRD is used to identify the phases of metal oxide catalysts or supports, and to calculate average

crystallite sizes.<sup>11</sup> A material must be crystalline and have long-range in order to be suitable for XRD analysis. When X-rays interact with a crystalline solid, the radiation can interfere in either a constructive or deconstructive manner. It is the constructive interference that is identified by the detector in the XRD apparatus. Bragg's law (see equation 2.6) allows for the diffraction pattern of the X-rays to be related to lattice spacing.<sup>12</sup> The solid material is able to be identified due to its characteristic lattice spacings and diffraction angles.

$$n\lambda = 2dsin\theta$$

Equation 2.6 Bragg's law; n = order of reflection,  $\lambda$  = wavelength of the x-rays, d = lattice spacing,  $\theta$  = angle of diffraction.<sup>12</sup>

Average crystallite sizes can be calculated from diffraction patterns using the Scherrer equation (see equation 2.7).<sup>13</sup> The foundation of the Scherrer equation is that the width of a reflection in a PXRD pattern is inversely related to the mean crystallite size of a material.<sup>14</sup> Therefore, as the crystallite size becomes smaller the width of the reflection in the XRD pattern becomes broader. However, this method for calculating crystallite sizes does have its limitations. PXRD is a bulk technique and therefore the crystallite size that is calculated is a mean value for the entire sample, and also errors can be introduced due to line broadening effects and inaccuracies related to using Gaussian functions.<sup>15</sup>

$$\tau = \frac{K\lambda}{\beta cos\theta}$$

Equation 2.7 Scherrer equation;  $\tau$  = mean crystallite size, K = shape factor,  $\lambda$  = wavelength of the x-rays,  $\beta$  = FWHM,  $\theta$  = Bragg angle.<sup>13</sup>

#### 2.4.1.2 Experimental Procedure

Catalyst samples were packed into a metal sample holder and XRD analysis was carried out using a Panalytical X'Pert diffractometer equipped with a Cu X-ray source operated at 40 kV and 40 mA. 40-minute scans were performed over a range of 5–80° 2θ angles to attain diffraction patterns. Identification of the diffraction patterns was achieved *via* comparison with patterns stored in the International Centre for Diffraction Data (ICDD) database. A silicon standard was also analysed before

each experiment to act as a control sample and help minimise errors associated with the Scherrer equation.

## 2.4.2 Thermogravimetric Analysis (TGA)

### 2.4.2.1 Background

TGA allows for the measurement of the mass of sample as it is exposed to increasing temperatures at a controlled rate. The apparatus is composed of a highly sensitive balance suspended in a furnace, and a gas inlet that can be used to control the flow of a gas into the apparatus. Different atmospheres can be used to carry out TGA depending on what information is required (e.g. if the calcination temperature of a sample in air is required then air would be flowed into the TGA). TGA can be used to determine the decomposition of catalyst precursors and to indicate the moisture content in metal oxide samples.

### 2.4.2.2 Experimental Procedure

Analysis was conducted using a Perkin Elmer TGA 4000 and a 20-30 mg sample was heated to 800 °C at a rate of 5 °C/min. The analysis was either carried out in air or an inert atmosphere of nitrogen, and the gases were introduced at a flow rate of 50 ml/min.

## 2.4.3 Raman Spectroscopy

### 2.4.3.1 Background

Raman spectroscopy is a vibrational spectroscopy technique that focuses on the inelastic scattering of radiation as it interacts with a material, as demonstrated by Sir C.V. Raman in 1928.<sup>16</sup> When photons interact with a sample they can be scattered elastically or inelastically. Elastic scattering occurs when an excited photon returns to its original energy level (where  $\Delta\nu = 0$ ), and this is known as Rayleigh scattering (this is the basis for infrared spectroscopies). Inelastic scattering occurs when the excited photon returns to an energy level that is higher or lower in energy than its original state (where  $\Delta\nu \neq 0$ ). If the photon gains energy this is known as a Stokes shift, and if the photon loses energy this is referred to as an anti-Stokes shift (see figure 2.7).<sup>17</sup> Raman

scattering is characterised by a difference in energy between the incident and scattered radiation, therefore both forms of Stokes scattering are observed in Raman spectroscopy. Many molecules are not Raman active, and in order to have Raman activity a molecule must have changeable polarizability and must not have any centres of symmetry. A disadvantage of Raman spectroscopy is that Raman scattering is of very low intensity in comparison to Rayleigh scattering, so intense lasers are required to increase the strength of the signal.

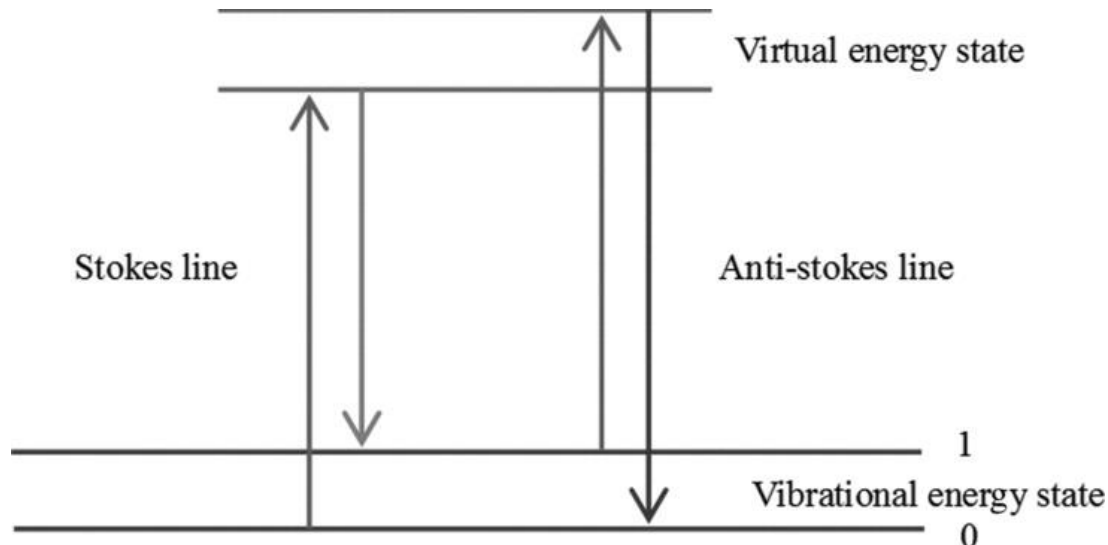


Figure 2.9 Energy level diagram showing Stokes and Anti-stokes lines caused by the inelastic scattering of a photon. Reproduced from ref 13.

#### 2.4.3.2 Experimental Procedure

Raman spectroscopy measurements were conducted using a Renishaw inVia confocal Raman microscope with a Stellar-REN 3B green Ar<sup>+</sup> laser at an emission of 514 nm. An Olympus BH2-UMA microscope was used to focus on the catalyst samples which were placed on a metal plate, and the surface of the sample was flattened using a glass slide.

#### 2.4.4 BET Surface Area

##### 2.4.4.1 Background

Brunauer-Emmett-Teller (BET) theory was first developed in 1938 by the researchers whom the theory is named after, Stephen Brunauer, Paul Hugh Emmett,

and Edward Teller.<sup>18</sup> The theory offers a way to model the physisorption of a gas onto a solid surface using the following equation:

$$\frac{P}{V(P_0 - P)} = \frac{C - 1}{CV_m} \frac{P}{P_0} + \frac{1}{CV_m}$$

Equation 2.8 BET equation.  $P$  = equilibrium pressure,  $P_0$  = saturation pressure,  $V$  = adsorbed volume at STP (standard temperature and pressure),  $V_m$  = monolayer volume at STP,  $C$  = BET constant (see equation 2.9)

$$C = e^{(E_1 - E_L/RT)}$$

Equation 2.9 BET constant.  $E_1$  = heat of adsorption for first monolayer,  $E_L$  = heat of adsorption for layers  $2 \rightarrow \infty$

The BET constant,  $C$ , offers an indication as to the shape of the isotherm associated with the physisorption. There are eight standard physisorption isotherms as recognised by IUPAC (International Union of Pure and Applied Chemistry), and BET theory is only applicable with type II and IV isotherms (see figure 2.8).<sup>19</sup> If  $C$  is greater than 80 the knee of the isotherm (also known as point B, labelled on isotherm II in figure 2.8) is sharp, and therefore monolayer adsorption is easily defined. If  $C$  is less than 50 the knee of the isotherm cannot be identified as a single point. If  $C$  is below 2 then BET theory is non-applicable and the isotherm will either be type III or V. For BET theory to be reliable  $C$  should be at least around 100 so that the monolayer and multilayer adsorptions can be clearly distinguished. A  $C$  value of 20 or less makes the application of BET theory dubious.<sup>20</sup>

$$S = \frac{V_m}{22414} \cdot N_A \sigma$$

Equation 2.10 Surface area calculation;  $S$  = surface area,  $V_m$  = monolayer volume at STP, 22414 ml = volume of one mole of  $N_2$  at STP,  $N_A$  = Avogadro's constant,  $\sigma$  = cross sectional area of  $N_2$  ( $0.162\text{ nm}^2$ )

The surface area of a catalyst can be calculated using BET theory *via* equation 2.10. A standard BET measurement uses 5 points from the linear region of an isotherm between 0.05-0.35  $P/P_0$ . If the BET equation is plotted as a straight line then the intercept and gradient of that line can be used to calculate  $V_m$ , which is then inserted into equation 2.10 to calculate the surface area of the material under investigation.

Due to assumptions made by the BET theory the error in the surface area measurements can be as high as 20%, therefore for a material with a BET surface area of  $140 \text{ m}^2/\text{g}$  the actual surface area could be anywhere between  $126\text{--}154 \text{ m}^2/\text{g}$ .<sup>21</sup> This level of error can be minimised by using data where the C constant is  $> 80$ .

#### 2.4.4.2 Experimental Procedure

BET surface area measurements were carried out using a Quantachrome NOVA 2200e surface area and pore size analyser. Firstly, a sample of catalyst ( $\sim 10 \text{ m}^2$ ) was degassed overnight at  $120^\circ\text{C}$ , before undergoing  $\text{N}_2$  physisorption at  $77 \text{ K}$  ( $-196^\circ\text{C}$ ). BET theory was then used to calculate the surface area of the material from 5 data points within the linear region between  $0.05\text{--}0.35 \text{ P/P}_0$ .

### 2.4.5 Full $\text{N}_2$ Adsorption/Desorption Isotherms

#### 2.4.5.1 Background

Porous materials are generally categorised into three major classes. Microporous materials have a pore diameter  $< 2 \text{ nm}$ , mesoporous materials have a pore diameter between  $2\text{--}50 \text{ nm}$ , and macroporous materials have a pore diameter  $> 50 \text{ nm}$ .<sup>20</sup>

Type I isotherms are characteristic of microporous solids that have small external surfaces, such as activated carbons, molecular sieve zeolites, and porous oxides. Type II isotherms occur with nonporous or macroporous materials, while type III isotherms have no point B so monolayer formation is not identifiable. Type IV isotherms are generated by mesoporous materials, with IV(a) isotherms including the feature of a hysteresis loop. If  $\text{N}_2$  is used as the adsorbate, hysteresis begins to occur at pore widths of greater than  $4 \text{ nm}$ . Type V isotherms are similar to type III at low  $\text{P/P}_0$ , but as the pressure increases molecular clustering is followed by pore filling. Hysteresis loops, as seen in the Type IV(a) and Type V isotherms in figure 2.8, are indicative of mesoporous materials. Type VI isotherms represent layered adsorption on a uniform nonporous surface.<sup>19</sup>

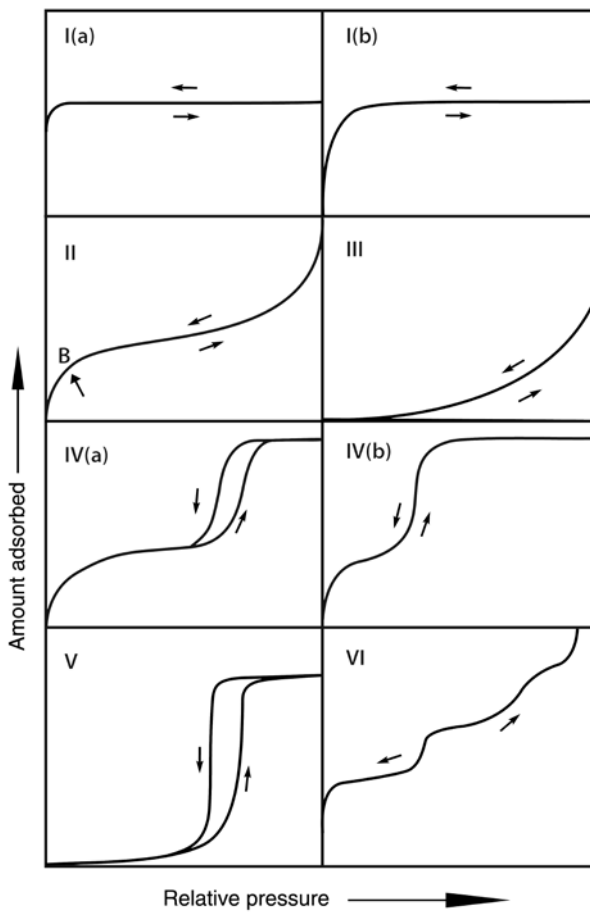


Figure 2.10 IUPAC classification of physisorption isotherms. Reproduced from ref. 18.

#### 2.4.5.2 Experimental Procedure

A Micromeritics 3Flex was used to carry out full adsorption/desorption isotherms. A sample of catalyst ( $\sim 50 \text{ m}^2$ ) was degassed *in-situ* at 200 °C (temperature was increased at a rate of 10 °C/min) for 6 hours, before it was dosed with N<sub>2</sub> at 77 K to carry out N<sub>2</sub> physisorption. The method involves both adsorption and desorption to construct a full isotherm. The N<sub>2</sub> was dosed onto the catalyst as follows:

- P/P<sub>0</sub> 0 – 0.005: dose 0.04461 mmol/g at 20 s intervals (adsorption)
- P/P<sub>0</sub> 0.005 – 0.99: increase pressure by 0.025 P/P<sub>0</sub> at 5 s intervals (adsorption)
- P/P<sub>0</sub> 0.99 – 0.005: decrease pressure by 0.025 P/P<sub>0</sub> at 10 s intervals (desorption)

Points from these isotherms could also be used to calculate BET surface areas and so could be used to compare with data collected using the Quantachrome NOVA 2200e.

## 2.4.6 Attenuated Total Reflection – Fourier Transform Infrared Spectroscopy (ATR-FTIR)

### 2.4.6.1 Background

Fourier Transform Infrared spectroscopy (FTIR) is one of the most commonly utilised analytical techniques in the field of chemistry and is particularly useful for identification of organic functional groups. When a molecule is irradiated with infrared (IR) radiation (2.5–25  $\mu\text{m}$  wavelength) it is absorbed by the chemical bonds and causes them to vibrate or bend. These bends and vibrations are characteristic of the bonds because different bonds absorb different energies of radiation. Therefore, the bond can be identified by measuring the wavenumbers ( $\text{cm}^{-1}$ ) of the absorbed radiation. The Fourier Transformation is a mathematical function that converts an interferogram (the raw data generated by interactions between IR radiation and a molecule) into a spectrum that can be interpreted and analysed. Using the Fourier Transform allows for the use of multiple wavelengths of light in one analysis which, according to Fellgett's advantage, means that the signal to noise ratio is increased, and the analysis time is also reduced.<sup>22</sup>

In order to be IR active a molecule must undergo a change in dipole moment, however a permanent dipole is not necessary. For example, symmetrical diatomic molecules like  $\text{N}_2$  are not IR active because there can be no change in its dipole moment, whereas asymmetrical diatomics like CO are IR active. A linear molecule with  $N$  atoms has  $3N-6$  vibrational modes, whilst a non-linear molecule with  $N$  atoms has  $3N-5$  vibrational modes. The vibrational modes of a non-linear molecule can be classified as stretching (symmetric or asymmetric), scissoring, rocking, wagging, or twisting.

An FTIR spectrometer can be fitted with an Attenuated Total Reflectance (ATR) attachment. ATR makes the FTIR analysis of liquid or solid samples simpler by removing the need for any sample preparation. A liquid sample can be directly placed upon the ATR crystal and analysed, whereas a solid sample must be clamped down upon the ATR crystal. Powder samples must be clamped to provide good contact with the crystal and to remove any air contained within the sample that may cause the signal to noise ratio to decrease. ATR works by using total internal reflection to generate an evanescent wave that travels through the crystal and it is this wave that interacts with the sample (see figure 2.10).<sup>23,24</sup> The evanescent wave is able to interact

with the sample sitting on the surface of the crystal because it protrudes slightly from the crystal surface and into the sample. Therefore, good contact between the sample and the ATR crystal is crucial.

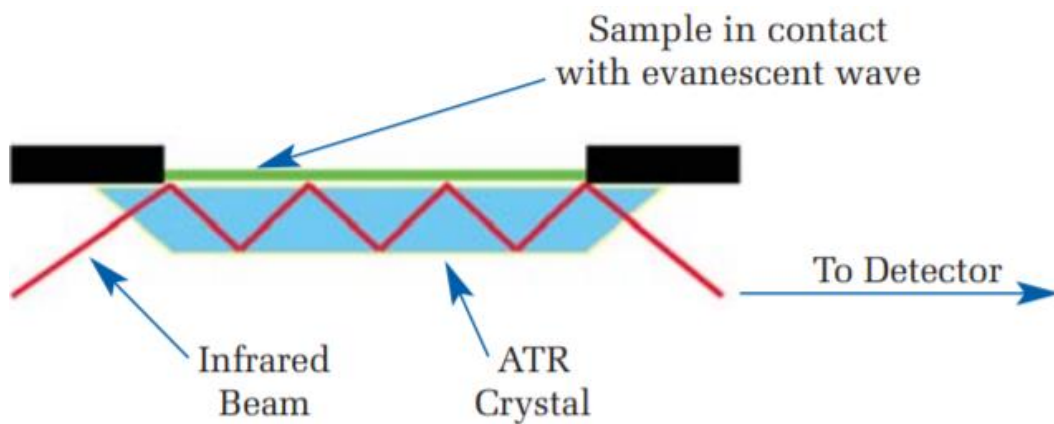


Figure 2.11 Diagram showing the reflections of an IR beam in an ATR crystal. Reproduced from ref 22.

#### 2.4.6.2 Experimental Procedure

ATR-FTIR was carried out using a Bruker Vertex 70 FT-IR Spectrometer fitted with a A225/Q PLATINUM ATR accessory. The spectrometer was equipped with two detectors: a mercury cadmium telluride (MCT) detector, and a deuterated triglycine sulphate (DTGS) detector. For the analysis in this study the MCT detector was used because it gives higher resolution spectra in the region where organic functional groups are analysed. The MCT detector was cooled with liquid N<sub>2</sub> and 16 background scans were measured. For the sample analysis 32 scans were measured at a resolution of 2 cm<sup>-1</sup> in absorbance mode across the range of 500–4000 cm<sup>-1</sup>.

#### 2.4.7 X-Ray Photoelectron Spectroscopy (XPS)

##### 2.4.7.1 Background

XPS is a surface sensitive technique that is based on the photoelectric effect as theorised by Einstein for which he went on to win the Nobel Prize in Physics in 1921.<sup>25</sup> The photoelectric effect (see equation 2.11) outlines how a core electron can be ejected from an atom because that atom has absorbed a photon. The kinetic energy of the photoelectron ( $E_k$ ) is measured by the XPS detector and it is related to the binding

energy of the electron ( $E_b$ ). The binding energy of a core photoelectron is characteristic of the atom from which it has been ejected and so can be used to identify the molecules at the surface of the material. These binding energies can also be used to indicate the oxidation state of a compound, which makes XPS a very powerful tool for analysing metal oxides.

$$E_k = h\nu - E_b - \phi$$

Equation 2.11 The photoelectric effect;  $E_k$  = kinetic energy of a photoelectron,  $h$  = Planck's constant,  $\nu$  = frequency of radiation,  $E_b$  = binding energy of a photoelectron,  $\phi$  = work function of the spectrometer.<sup>26</sup>

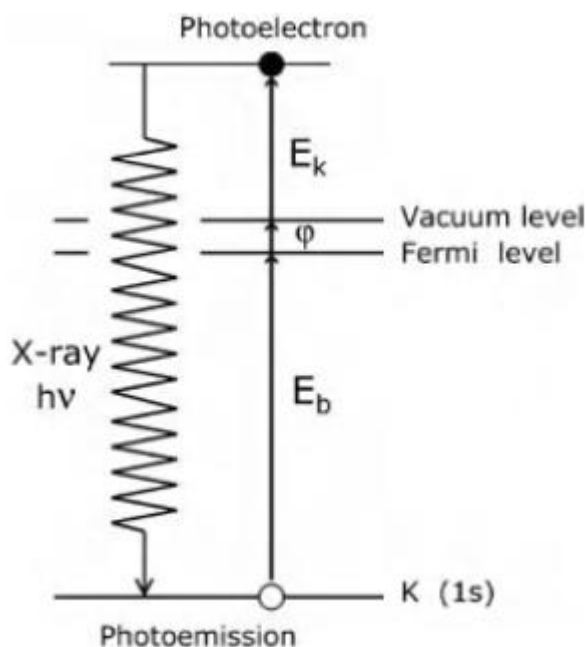


Figure 2.12 Energy level diagram showing the photoemission of a core electron due to X-ray irradiation. Each aspect of the photoelectric effect is labelled to illustrate the role of each term within the equation. Reproduced from Ref. 25.

#### 2.4.7.2 Experimental Procedure

XPS experiments were conducted using a Thermo Scientific K-Alpha<sup>+</sup> spectrometer. A monochromatic Al K $\alpha$  X-ray source analysed the samples across an area of 600 x 400  $\mu\text{m}$ . Survey scans were recorded at an energy of 150 eV, whilst high resolution scans were measured at an energy of 40 eV with a step size of 0.1 eV. Low energy electrons and Ar ions were used in combination to neutralise the charge of the

sample. XPS analysis and peak fittings were carried out by Cardiff University's Surface Analysis Manager, Dr. David Morgan.

## 2.4.8 Scanning Electron Microscopy (SEM) / Energy Dispersive X-Ray Spectroscopy (EDX)

### 2.4.8.1 Background

Electron microscopy (EM) uses a high-energy electron beam to image catalyst samples at far greater resolution and magnification than optical microscopy can achieve. This allows for the morphology and topology of a sample to be investigated and provides a very accurate method for measuring the size and shape of nanoparticles. Electrons have a wavelength of  $< 1 \text{ \AA}$  which is comparable to the size of an atomic radius, and this enables EM to generate images with atomic detail.

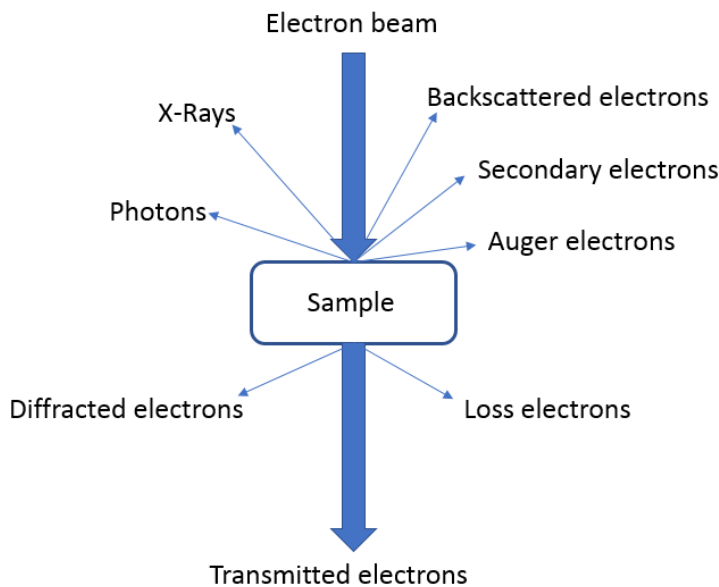


Figure 2.13 Diagram showing the different ways in which an electron beam interacts with a sample in EM.<sup>27</sup>

The interaction between an electron beam and a chemical sample is very complex and can activate a variety of different processes (see figure 2.11). Some electrons just pass through the sample, but other electrons can interact with the sample and through these interactions EM can be used to gather information on the sample

under investigation. SEM uses detectors to monitor either backscattered or secondary electrons in order to image the chemical sample.

Backscattered electrons are good for differentiating between heavier and lighter atoms, as an element with greater atomic mass will cause a larger number of electrons to be backscattered. This is particularly useful for analysing supported metal catalysts as the heavier metal atoms will give a stronger and brighter signal than the lighter atoms in the support. This depends on the composition of the catalyst, but generally the metal nanoparticles will have a greater atomic mass than the support material (e.g. Pt/Al<sub>2</sub>O<sub>3</sub>). Backscattering of electrons can also be enhanced by increasing the intensity of the electron beam.

Secondary electrons are generated by inelastic scattering processes as the electron is emitted from the atom. Secondary electrons provide more information about the surface of the sample because most often an emitted secondary electron will have undergone its last loss process near to the surface of the material.

When a core electron is removed from an atom, a valence or higher energy electron can replace the core electron that has been lost. As this electron moves into the core orbitals of the atom an X-ray is emitted due to the conservation of energy. These X-rays can be utilised in EDX spectroscopy to provide elemental information about the sample. This can help to identify the elemental composition of specific regions of the sample and can also identify surface poisons that may affect catalyst performance. EDX involves high energy electrons that can emit core electrons, making this technique analogous to XPS as discussed previously.

#### 2.4.8.2 Experimental Procedure

SEM experiments were carried out using a Tescan Maia3 Field Emission Gun Scanning Electron Microscope (FEG-SEM) equipped with an Oxford Instruments XMAX<sup>N</sup> 80 Energy Dispersive X-ray (EDX) detector. Sections of PET bottles loaded with catalyst were cut and cleaned in ethanol in a sonic bath for 10 mins to remove any surface debris. Once the sample had dried it was mounted onto an aluminium SEM sample stub using carbon tape and silver DAG paint. The silver DAG paint was used because of PET's lack of conductivity. The sample was then sputter coated with Au/Pd (80:20 ratio) to a thickness of 10 µm. Images of the samples were obtained using

backscattered and secondary electron detectors at various magnifications, field views, and beam intensities. SEM and EDX spectroscopy analysis were conducted by Dr. Thomas Davies, the Electron Microscopy Experimental Officer for the CCI.

### 2.4.9 Monte Carlo Simulations

#### 2.4.9.1 Background

Monte Carlo methods use large numbers of simulations to find the most probabilistic outcome. The computer algorithms randomly sample a large number of scenarios within given parameters to provide the most statistically likely solution. Therefore, Monte Carlo simulations have a vast array of applications within computational chemistry. Monte Carlo methods can be used to determine the most stable configuration of a chemical compound in molecular modelling, and to predict the behaviour of reaction equilibria.<sup>28,29</sup> Such simulations can also be used to model the trajectory of an electron beam through a solid matrix.<sup>30</sup> This can be helpful for interpreting observations made when using electron microscopy, and for indicating how deep into the sample the electron beam is able to penetrate.

#### 2.4.9.2 Experimental Procedure

A software package called Monte Carlo Simulation of Electron Trajectory in Solids (CASINO)<sup>31</sup> was used to model the penetration of electrons into a PET matrix. The composition ((C<sub>10</sub>H<sub>8</sub>O<sub>4</sub>)<sub>n</sub>) and density (1.38 g/ml) of PET and the accelerated voltage of the electron beam were input into the software. CASINO uses various physical models to simulate the different factors that influence the path of an electron as it travels through a solid material. The Monte Carlo simulations then generate a large set of electron trajectories based on the parameters that were input. From this set of trajectories one can estimate the average depth of penetration of the electron beam into the sample at a particular accelerated voltage.

## 2.5 Mechanistic Studies

In heterogeneous catalysis research various *in-situ* techniques can be utilised to gain insight into the reaction mechanisms by which the catalyst transforms a target

substrate. In this study Diffuse Reflectance Infrared Fourier Transform Spectroscopy (DRIFTS) was used to analyse the interactions between AA and a metal oxide catalyst surface.

### 2.5.1 Diffuse Reflectance Infrared Fourier Transform Spectroscopy (DRIFTS)

#### 2.5.1.1 Background

DRIFTS is an infrared-based technique that uses diffuse reflectance to analyse a solid sample. Diffuse reflectance is caused by the uneven nature of the sample surface which means that the IR radiation is reflected off at many angles. A DRIFTS cell surrounds the sample with mirrors in order to collect and focus the diffusely reflected light and guide it to the IR detector. DRIFTS is a technique that can be used to analyse the nature of surface-bound intermediates that are generated during a reaction taking place on the surface of a solid catalyst. As previously mentioned, AA is a carbonyl compound and so gives rise to a strong IR signal ( $\sim 1700 \text{ cm}^{-1}$ ) and this make an IR-based technique a good tool for analysing such a compound.

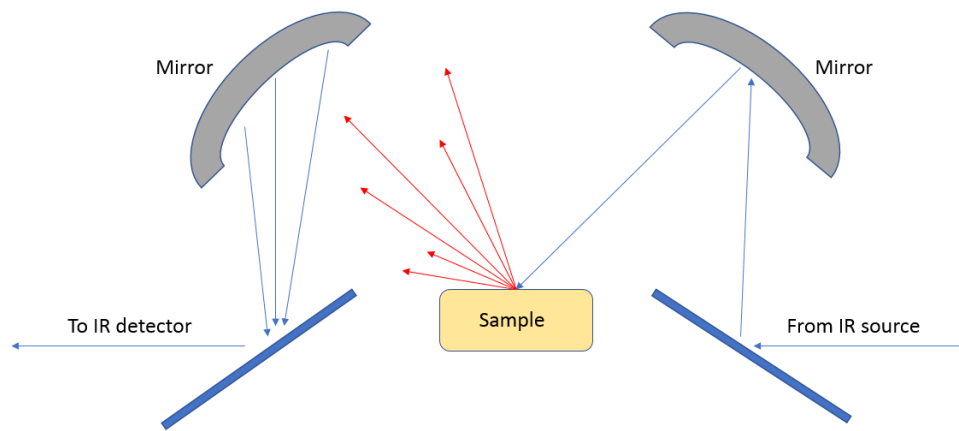


Figure 2.14 Schematic of a DRIFTS cell showing how the diffusely reflected light (red arrows) is focussed and guided towards the detector using mirrors.<sup>32</sup>

#### 2.5.1.2 Experimental Procedure

DRIFTS experiments were conducted using a Bruker Tensor 27 spectrometer equipped with a Harrick *in-situ* cell fitted with 2 mm CaF<sub>2</sub> windows. The DRIFTS cell was connected to a heating unit and Swagelok lines enabled gases to be flown through

the system. A BOC cylinder containing 2000 ppm AA in He (balance) was used to introduce AA into the cell at a flow rate of 30 ml/min. The IR detector was cooled with liquid N<sub>2</sub> before 32 background scans were acquired. For sample analysis, 32 scans were conducted in absorbance mode over the range of 1000-4000 cm<sup>-1</sup>.

## 2.6 Chapter 2 - References

1. E. Ntайнюа N., T. Garcia, B. Solsona and S. H. Taylor, *Catal. Today*, 2008, **137**, 373–378.
2. T. Garcia, B. Solsona and S. H. Taylor, *Catal. Lett.*, 2005, **105**, 183–189.
3. Y. Li, Q. Fu and M. Flytzani-Stephanopoulos, *Appl. Catal. B Environ.*, 2000, **27**, 179–191.
4. W. Yuejuan, M. Jingmeng, L. Mengfei, F. Ping and H. Mai, *J. Rare Earths*, 2007, **25**, 58–62.
5. K. Yoshikawa, H. Sato, M. Kaneeda and J. N. Kondo, *J. CO<sub>2</sub> Util.*, 2014, **8**, 34–38.
6. I. S. Metcalfe, *Chemical Reaction Engineering: A First Course*, Oxford University Press, Oxford, 1997.
7. M. Kamiński, R. Kartanowicz, D. Jastrzębski and M. M. Kamiński, *J. Chromatogr. A*, 2003, **989**, 277–283.
8. N. H. Snow and G. C. Slack, *TrAC Trends Anal. Chem.*, 2002, **21**, 608–617.
9. M. Dong, A. H. DiEdwardo and F. Zitomer, *J. Chromatogr. Sci.*, 1980, **18**, 242–246.
10. J. Linssen, H. Reitsma and J. Cozijnsen, *Z. Für Lebensm.-Unters. Forsch.*, 1995, **201**, 253–255.
11. S. Wang, L. Zhao, W. Wang, Y. Zhao, G. Zhang, X. Ma and J. Gong, *Nanoscale*, 2013, **5**, 5582–5588.
12. W. H. Bragg and W. L. Bragg, *Proc. R. Soc. Lond. Ser. Contain. Pap. Math. Phys. Character*, 1913, **88**, 428–438.
13. P. Scherrer, *Math.-Phys. Kl. 2*, 1918, 98–100.
14. J. S. J. Hargreaves, *Catal. Struct. React.*, 2016, **2**, 33–37.
15. A. Monshi, M. R. Foroughi and M. R. Monshi, *World J. Nano Sci. Eng.*, 2012, **2**, 720–726.
16. C. V. Raman and K. S. Krishnan, *Nature*, 1928, **121**, 501–502.

17. D. Yang and Y. Ying, *Appl. Spectrosc. Rev.*, 2011, **46**, 539–560.
18. S. Brunauer, P. H. Emmett and E. Teller, *J. Am. Chem. Soc.*, 1938, **60**, 309–319.
19. M. Thommes, K. Kaneko, A. V. Neimark, J. P. Olivier, F. Rodriguez-Reinoso, J. Rouquerol and K. S. W. Sing, *Pure Appl. Chem.*, 2015, **87**, 1051–1069.
20. J. Rouquerol, D. Avnir, C. W. Fairbridge, D. H. Everett, J. M. Haynes, N. Pernicone, J. D. F. Ramsay, K. S. W. Sing and K. K. Unger, *Pure Appl. Chem.*, 1994, **66**, 1739–1758.
21. K. S. W. Sing, in *Adsorption by Powders and Porous Solids*, Elsevier, 2nd edn., 2013, pp. 237–268.
22. P. B. Fellgett, *JOSA*, 1949, **39**, 970–976.
23. Perkin Elmer, *Attenuated Total Reflectance (ATR) Technical Note*, 2005.
24. B. C. Smith, *Fundamentals of Fourier Transform Infrared Spectroscopy, Second Edition*, CRC Press, 2011.
25. A. Einstein, *Ann. Phys.*, 1905, **322**, 132–148.
26. J. W. Niemantsverdriet, in *Spectroscopy in Catalysis*, John Wiley & Sons, Ltd, 2007, pp. 39–83.
27. J. W. Niemantsverdriet, in *Spectroscopy in Catalysis*, John Wiley & Sons, Ltd, 2007, pp. 179–216.
28. A. Lüchow and J. B. Anderson, *Annu. Rev. Phys. Chem.*, 2000, **51**, 501–526.
29. C. H. Turner, J. K. Brennan, M. Lísal, and W. R. Smith, J. K. Johnson and K. E. Gubbins, *Mol. Simul.*, 2008, **34**, 119–146.
30. D. C. Joy, *Scanning Microsc.*, 1991, **5**, 329–337.
31. Casino, <https://www.gel.usherbrooke.ca/casino/What.html>, (accessed 26 June 2020).
32. G. Renner, T. C. Schmidt and J. Schram, in *Comprehensive Analytical Chemistry*, eds. T. A. P. Rocha-Santos and A. C. Duarte, Elsevier, 2017, vol. 75, pp. 67–118.

## 3 Methodological Development

### 3.1 Introduction

At the outset of this project it was necessary to develop a testing methodology that could be used within the labs of the CCI. The CCI does not have the capabilities to test using PET, so a mimic test was required that would give an indication to the activity of a catalyst for AA removal within PET. To handle and process PET specialist apparatus is needed such as extruders, injection moulders, and maybe most importantly, PET driers. Due to the hygroscopicity of PET, thorough drying is essential for effective and reproducible processing. ColorMatrix, as polymer specialists, have access to all of the equipment that is needed to handle PET and to test AA removal catalysts under application conditions within the polymer itself. Therefore, it was decided that all catalyst testing in PET would be carried out at the ColorMatrix site in Knowsley, whilst the testing in the CCI would be carried out using a model reaction. This chapter details the development of the testing protocol used in the CCI and provides the basis for the data that is discussed in chapter 4.

### 3.2 Testing with AA in Poly(ethylene glycol) (PEG)

As mentioned in Chapter 1 (section 1.4.3), bottle grade PET is a highly viscous material with an IV of 0.7-0.85 dL/g. For the catalytic removal of AA from PET a catalyst needs to be active within a highly viscous molten polymer matrix, so it seemed reasonable to test catalysts in the lab within a viscous polymer matrix. Poly(ethylene glycol) (PEG) was chosen to act as a mimic for molten PET to use as a reaction matrix for the testing of catalysts prepared in the CCI. Ethylene glycol is a constituent of PET and PEG so there are chemical similarities between the two. However, due to the absence of a terephthalic acid unit, the two polymers have very different physical properties. PET has a melting point of 260 °C whereas PEG is a liquid at room temperature, and PET is far more viscous than PEG.

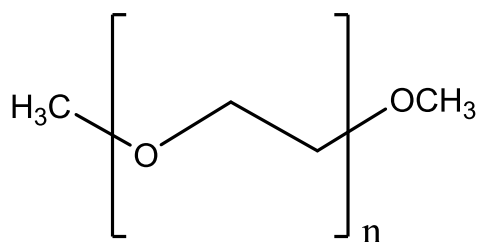


Figure 3.1 Chemical structure of Poly(ethylene glycol) dimethyl ether (PEG-DME)

Poly(ethylene glycol) dimethyl ether (PEG-DME) with an average  $M_n$  of 250 was purchased to act as a mimic for molten PET. Acetaldehyde was added to give the desired concentration and the mixture was heated on a stirrer plate in a round-bottom flask equipped with a reflux condenser. Metal oxide catalysts were added to the mixture to determine whether they had any influence on the concentration of AA. These mixtures were analysed using Attenuated Total Reflectance – Fourier Transform Infrared Spectroscopy (ATR-FTIR) due to the carbonyl group of AA which is IR active and gives rise to a distinct signal at about  $1720\text{ cm}^{-1}$ . A reduction in intensity of this IR signal can be used to calculate the reduction in AA concentration when compared to calibration solutions. FTIR can also give indications of the nature of reaction products as different organic functional groups have distinct stretching frequencies that give rise to signals at different wavenumbers in the IR spectrum. Therefore, if the catalysts were able to convert the aldehyde to a different functional group, for example to an alcohol, this would be identifiable using FTIR analysis.

In figure 3.2 the IR spectra of PEG-DME containing different concentrations of AA is presented. From these spectra the carbonyl vibrational frequency at  $1723\text{ cm}^{-1}$  that is indicative of AA is only observable at an AA concentration of greater than 1%. Therefore, using this methodology the concentrations of AA that will need to be used are far higher than the 7-10 ppm present in PET preforms. To test at concentrations below 10 ppm a far more sensitive analytical technique would be required. However, the techniques that can be used to analyse PEG-DME solutions are limited due to compatibility issues with using such a solvent. For example, GC and LC could not be utilised because the PEG-DME is incompatible with the columns.

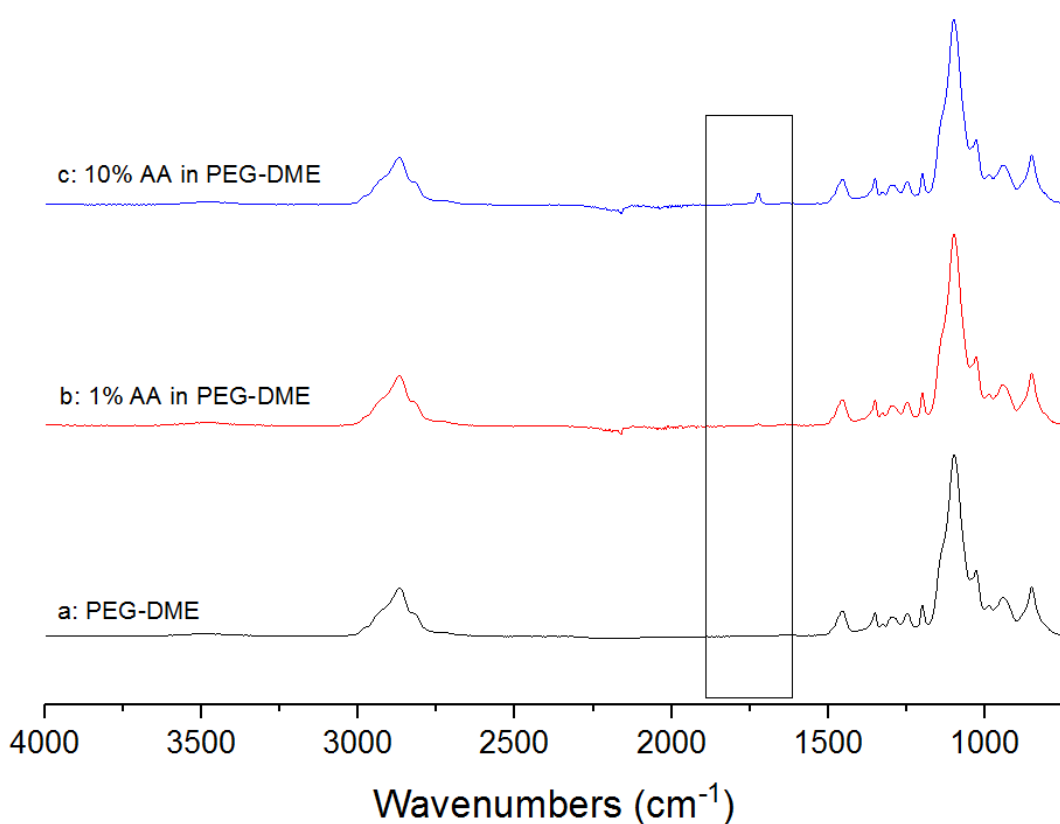


Figure 3.2 ATR-IR spectra of a = PEG-DME, b = 1% AA in PEG-DME, c = 10% AA in PEG-DME. Area containing AA signal ( $1723\text{ cm}^{-1}$ ) highlighted by black box.

Reactions were therefore conducted with a starting concentration of 10% AA in PEG-DME using a commercial  $\text{Zr(OH)}_4$  as a catalyst. This was chosen for initial testing due to the ColorMatrix patent referring to the use of a hydrous zirconium oxide catalyst.<sup>1</sup> The chemical similarities to a hydrated metal oxide suggested this would be a good candidate, although there are slight differences between the materials.<sup>2</sup> Therefore, the  $\text{Zr(OH)}_4$  was used as an initial benchmarking material for the development of an AA removal testing methodology. In figure 3.3 various IR spectra are presented for reactions with  $\text{Zr(OH)}_4$  under different conditions. These experiments were conducted in a round bottom flask equipped with a reflux condenser. High loadings of catalyst were used initially to test the process, to see if this was a feasible method for testing the AA removal activity of metal oxide catalysts. From these experiments it can be seen that at room temperature and  $50\text{ }^\circ\text{C}$  the  $\text{Zr(OH)}_4$  has very little effect upon the AA signal in the IR spectrum. However, once the temperature is increased to  $105\text{ }^\circ\text{C}$  the AA signal is removed from the IR spectra at a catalyst loading of 0.5 g and 1 g in a 10 ml sample of 10% AA in PEG-DME. This

suggests that once the temperature is increased the  $\text{Zr}(\text{OH})_4$  is able to catalyse the reaction of AA. Although, even with the use of a reflux condenser, the possibility of evaporation of the AA cannot be discounted, especially when working at temperatures of 105 °C when the boiling point of AA is 20 °C. Apparatus involving a sealed autoclave reactor, in which the headspace could be sampled for evaporated AA, could help to resolve this issue. The data obtained from the condenser setup may indicate catalyst activity at elevated temperatures, however it is difficult to know how much influence evaporation of AA may have on the results if one is only able to measure the reduction in substrate signal. The appearance of a reaction product signal would help to confirm that the catalyst is converting the AA into another compound.

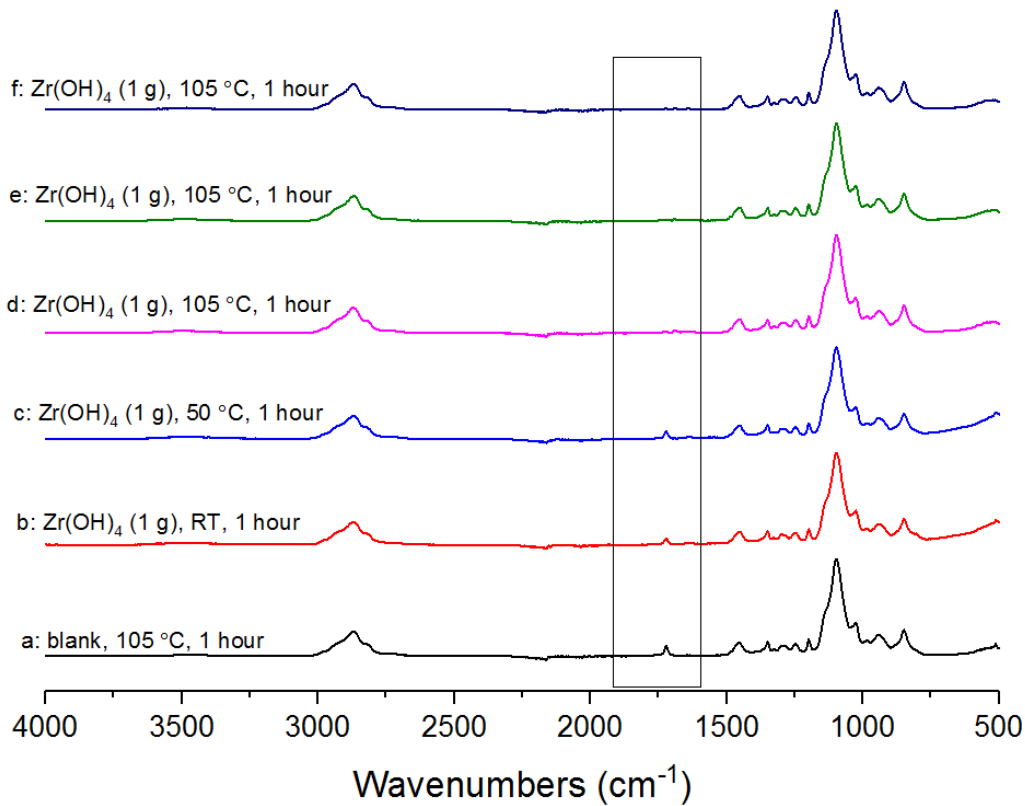


Figure 3.3 ATR-IR spectra of aliquots taken from reactions in 10 ml samples of 10% AA in PEG-DME solution conducted in a round bottom flask equipped with condenser; a = blank heated to 105 °C for 1 hour under stirring, b =  $\text{Zr}(\text{OH})_4$  (1 g) at room temperature for 1 hour under stirring, c =  $\text{Zr}(\text{OH})_4$  (1 g) at 50 °C for 1 hour under stirring, d =  $\text{Zr}(\text{OH})_4$  (1 g) at 105 °C for 1 hour under stirring, e =  $\text{Zr}(\text{OH})_4$  (1 g) at 105 °C for 1 hour under stirring, f =  $\text{Zr}(\text{OH})_4$  (0.5 g) at 105 °C for 1 hour under stirring

In figure 3.4 spectra d,e,f are the same spectra as d,e,f in figure 3.3 but they are focussed in on the 1500-2000 cm<sup>-1</sup> range to make the AA peak at 1723 cm<sup>-1</sup> easier to study. From the magnified spectra in figure 3.4 it can be observed that not only has the AA signal diminished but also a signal at 1690 cm<sup>-1</sup> has emerged. This is likely due to the formation of a reaction product as a result of interactions between AA and the metal hydroxide. To attempt to determine the product, the AA in PEG mixture was spiked with acetic acid (figure 3.4 spectrum c), however the acid gave rise to a signal at 1752 cm<sup>-1</sup> which does not match the signal observed for the reaction product. This suggests that the AA has not undergone oxidation to acetic acid in the presence of Zr(OH)<sub>4</sub>, and therefore an alternative reaction must have taken place.

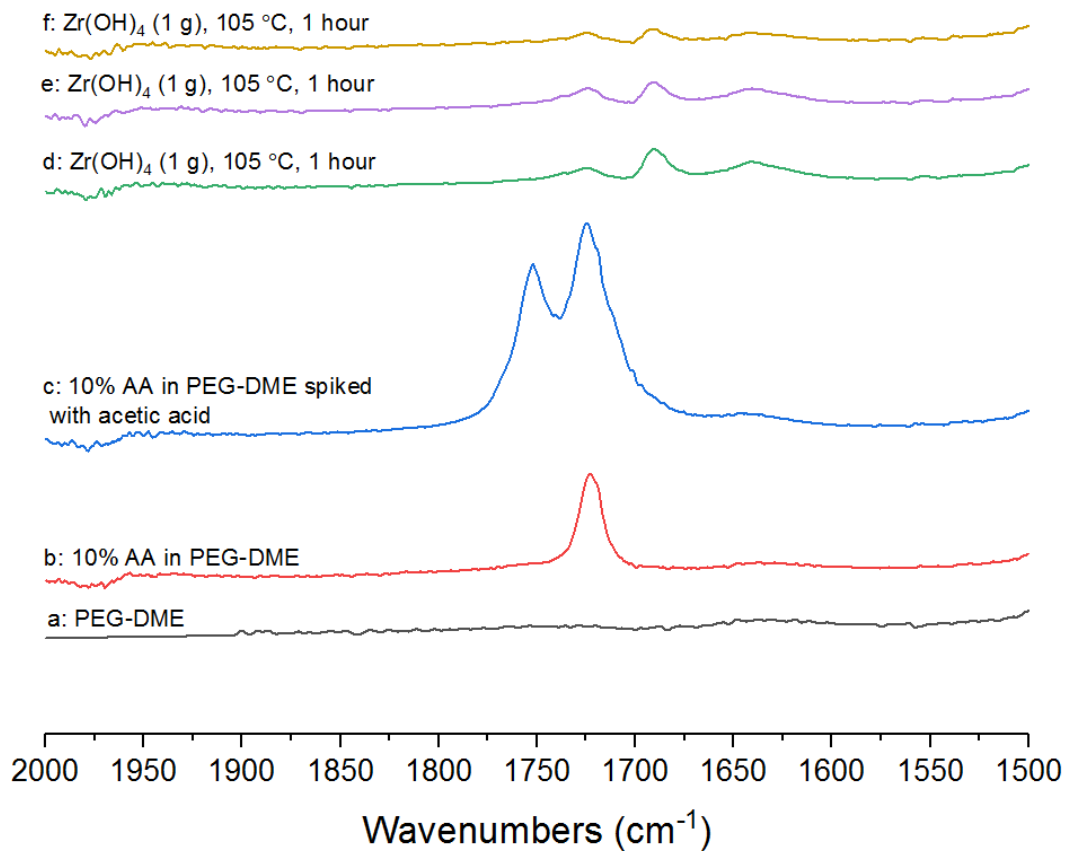


Figure 3.4. ATR-IR spectra of aliquots taken from reactions in 10% AA in PEG solution conducted in a round bottom flask equipped with condenser; a = PEG-DME only, b = 10% AA in PEG-DME blank, c = 10% AA in PEG-DME spiked with acetic acid (1 ml), d = Zr(OH)<sub>4</sub> (1 g) at 105 °C for 1 hour under stirring, e = Zr(OH)<sub>4</sub> (1 g) at 105 °C for 1 hour under stirring, f = Zr(OH)<sub>4</sub> (0.5 g) at 105 °C for 1 hour under stirring

It has been established that AA conversion was observed, therefore calibration solutions were prepared to enable quantification of the AA conversion. In order to measure catalytic performance and compare the activities of different catalytic materials a quantitative screening method is required. Solutions of AA (5%, 2.5%, 1.25%) in PEG were measured in duplicate to construct the calibration curve in figure 3.5.

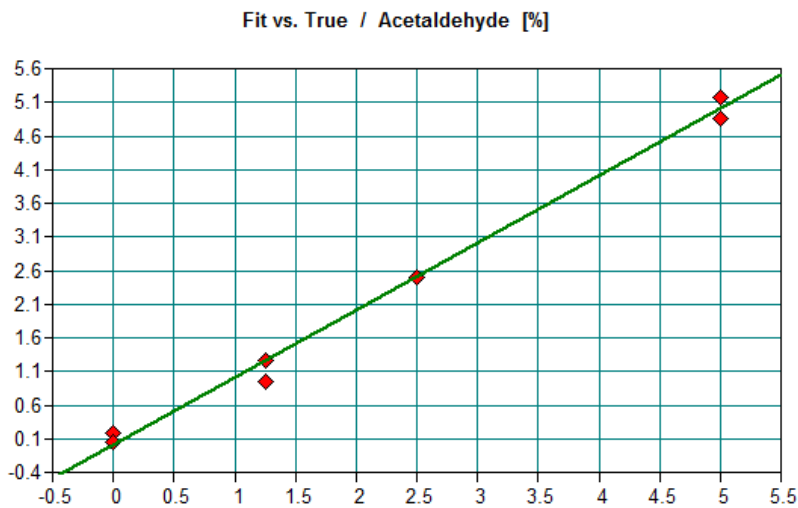


Figure 3.5 Calibration of AA signal in ATR-IR using calibration solutions of 5% AA in PEG, 2.5% AA in PEG, 1.25% AA in PEG and PEG

Using the IR calibration, the reaction spectra in figure 3.6 were quantified for their AA concentrations. Spectrum a is for the pre-reaction 5% AA in PEG solution, and this was quantified as having a concentration of 4.8%. Spectrum b is of the same solution following 1 hour of stirring at 105 °C in the presence of 500 mg of Zr(OH)<sub>4</sub>. The AA concentration in the post-reaction solution was measured to be 1.2%, which is a reduction in AA of 75%. The product peak at 1690 cm<sup>-1</sup> which was observed previously is present in spectrum b.

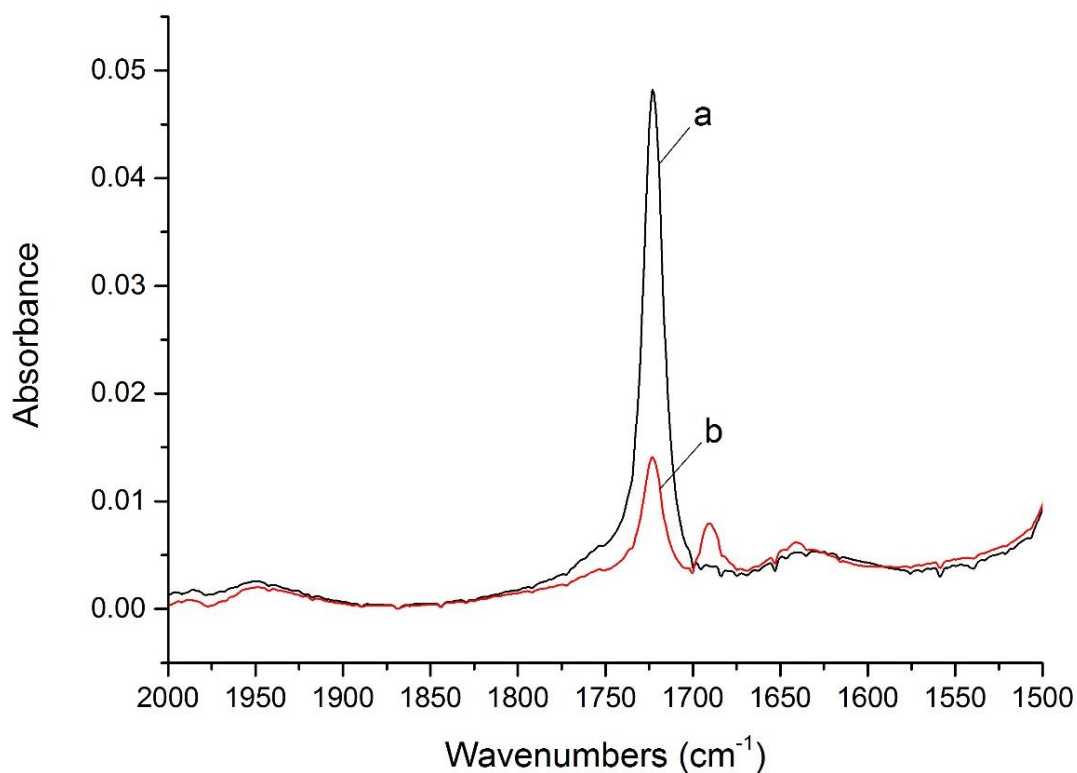


Figure 3.6 ATR-IR spectra of aliquots taken from reaction between Zr(OH)<sub>4</sub> and AA; a = 5% AA in PEG, b = added Zr(OH)<sub>4</sub> (0.5 g) to 5% AA in PEG solution and heated to 105 °C for 1 hour under stirring in round bottom flask equipped with a reflux condenser

In figure 3.7 the same reaction was conducted but in the absence of catalyst to obtain a blank measurement. In this case the AA concentration was still found to significantly decrease. The pre-reaction solution was found to have 5.2% AA which after 1 hour at 105 °C was decreased to 1.3% and following a further hour at 105 °C was decreased again to 1.0%. The blank reduction of AA after 1 hour was 75% and so was equal to the conversion of AA in the presence of Zr(OH)<sub>4</sub>. Therefore, the conversion in AA is likely to just be evaporation of the aldehyde due to its low boiling point and high volatility. This means that this method cannot be used as a rigorous and reliable method for testing catalysts, as without a reproducible blank measurement no certainty can be had regarding the validity of the testing. However, in the blank tests no product peak was observed, which suggests that the appearance of the signal at 1690 cm<sup>-1</sup> is due to a reaction of AA catalysed by the zirconium hydroxide.

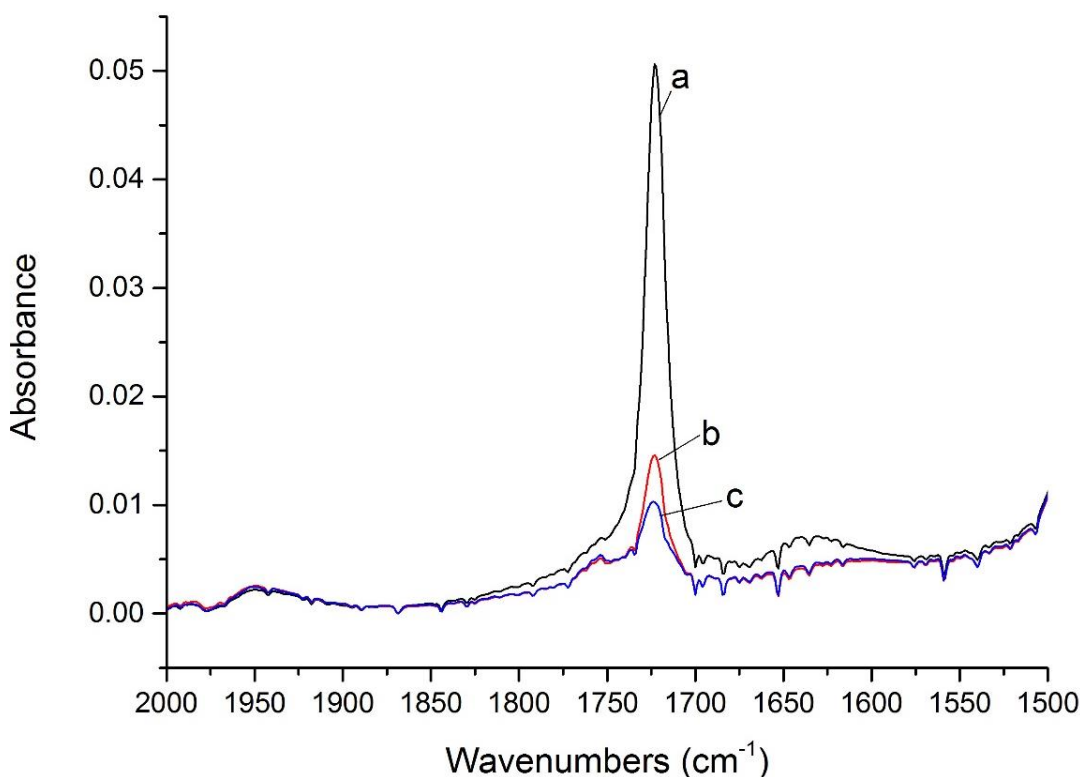


Figure 3.7 ATR-IR spectra of a = 5% AA in PEG solution, b = heated 5% AA in PEG solution to 105 °C for 1 hour under stirring in round bottom flask equipped with reflux condenser, c = heated 5% AA in PEG solution to 105 °C for 2 hours under stirring in round bottom flask equipped with reflux condenser

To identify the peak at 1690 cm<sup>-1</sup> further product candidates were spiked into PEG-DME and analysed with FTIR. These product candidates included acetic acid, ethyl acetate, acetone, formic acid, and formaldehyde. Acetic acid has been previously shown not to give rise to a signal at 1690 cm<sup>-1</sup> and all of the other compounds that were tested were found not to produce that IR signal either. This provided confirmation that the reaction was not the result of an oxidation or reduction of the AA.

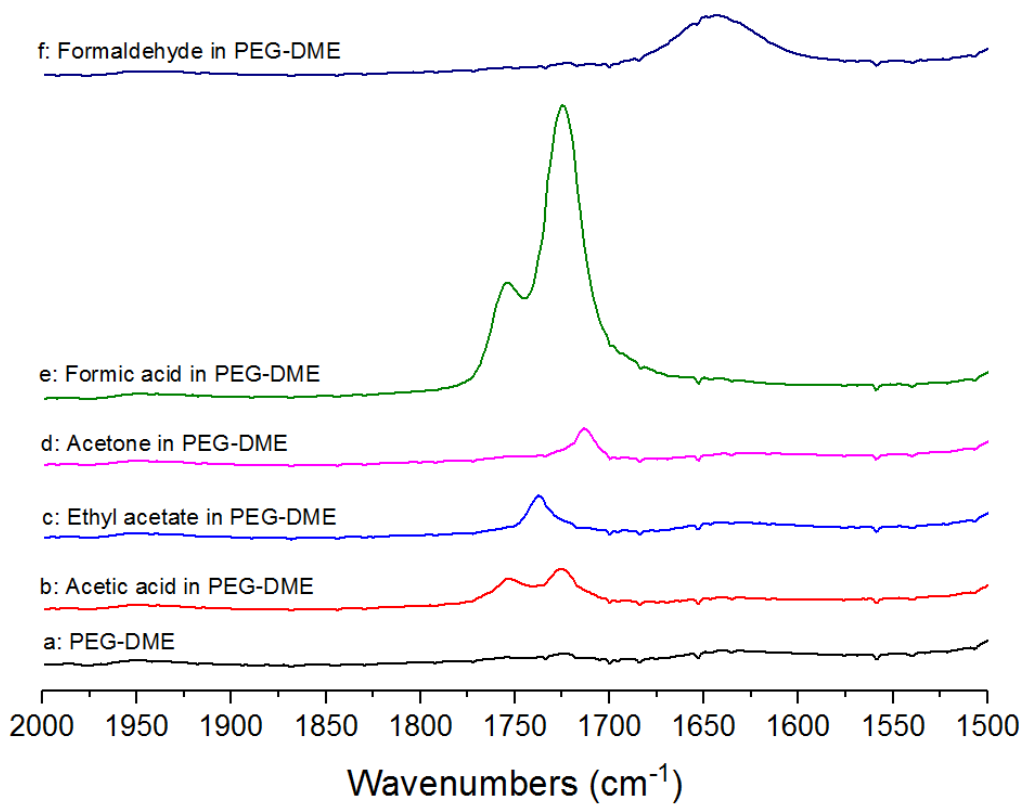


Figure 3.8 ATR IR spectra of 5 ml samples of PEG-DME spiked with potential reaction product candidates (formaldehyde = 37 wt% solution in water). a = PEG-DME only, b = PEG- DME spiked with acetic acid, c = PEG- DME spiked with ethyl acetate, d = PEG-DME spiked with acetone, e = PEG-DME spiked with formic acid, f = PEG-DME spiked with formaldehyde solution.

A chemical reaction that aldehydes are known to commonly undergo on solid catalyst surfaces is that of an aldol condensation.<sup>3–11</sup> Generally, in the literature, these reactions are carried out in the gas-phase using microreactors. A variety of metal oxide catalysts have been studied including MgO, ZrO<sub>2</sub>, CeO<sub>2</sub>, TiO<sub>2</sub>, MoO<sub>3</sub>, WO<sub>3</sub>, mixed metal oxides, and zeolites. Although the studies reported in the literature use quite different reaction setups, they are generally in agreement with the finding that at temperatures of around 100 °C AA is observed to undergo aldol condensation reactions in the presence of a metal oxide catalyst. In an aldol condensation reaction two aldehyde molecules are coupled together to form a longer chain β-unsaturated aldehyde. Examples of such β-unsaturated aldehydes include acrolein and crotonaldehyde. Therefore, PEG-DME was spiked with acrolein and crotonaldehyde and analysed using ATR-IR to see if either compound would give rise to a signal at 1690  $\text{cm}^{-1}$  (see figures 3.9 and 3.10). It is suggested that these reactions are catalysed by Lewis acid-base pairs on the ZrOH<sub>4</sub> surface.<sup>4</sup>

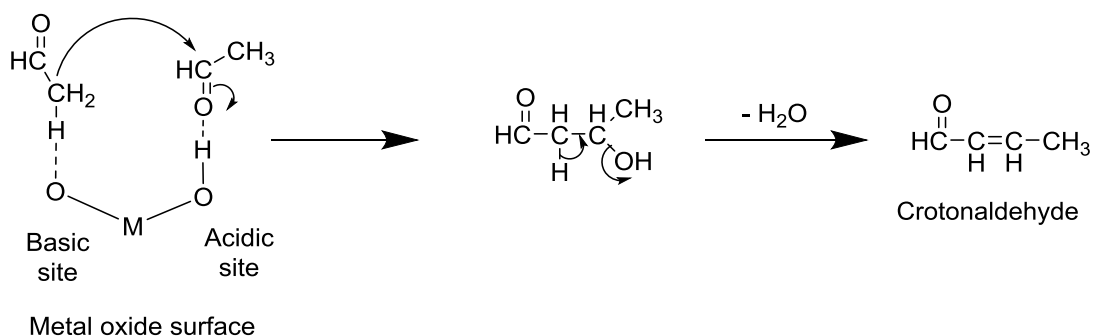


Figure 3.9 Possible aldol condensation mechanism for the self-condensation of AA on a metal oxide surface to form crotonaldehyde<sup>3</sup>

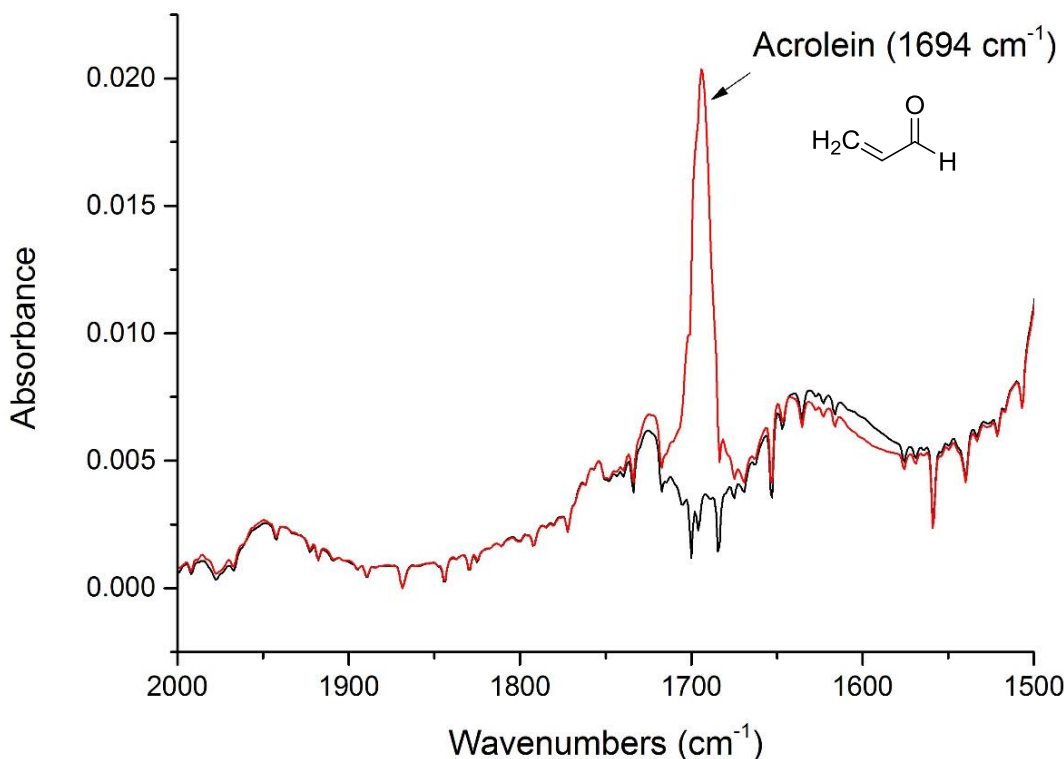


Figure 3.10 Black spectrum = PEG-DME, Red spectrum = PEG-DME spiked with acrolein (observed product peak =  $1690 \text{ cm}^{-1}$ )

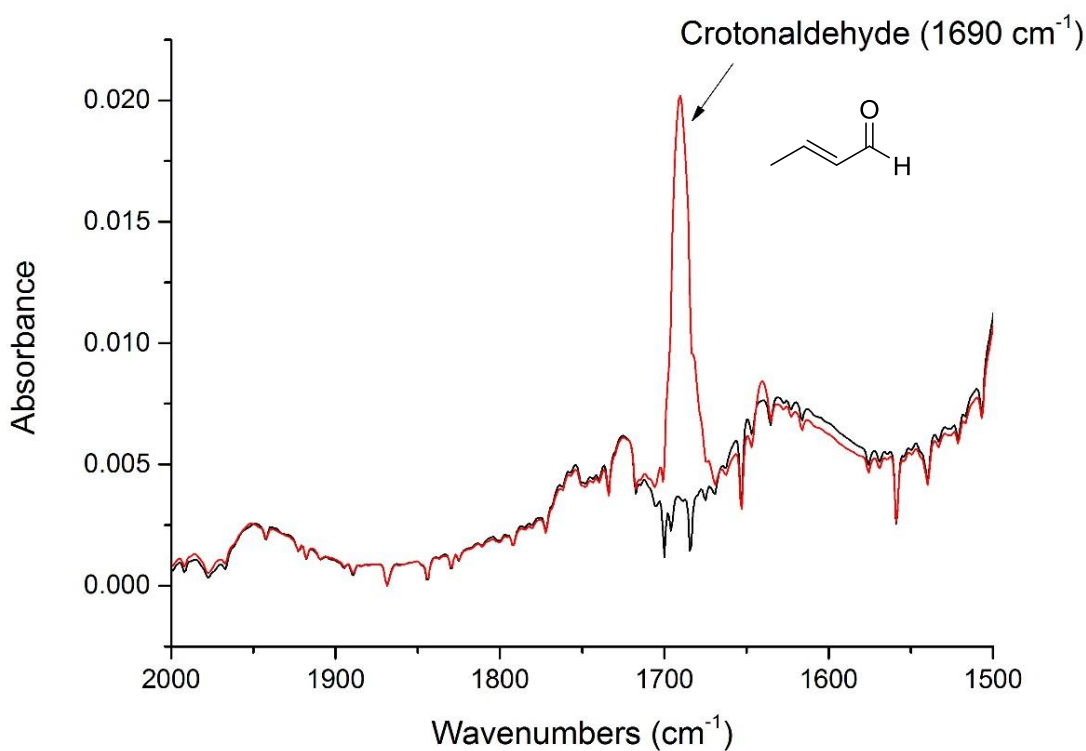


Figure 3.11 Black spectrum = PEG-DME, Red spectrum = PEG-DME spiked with crotonaldehyde (observed product peak = 1690 cm<sup>-1</sup>)

From the IR spectra of PEG-DME spiked with acrolein and crotonaldehyde it can be seen that crotonaldehyde does give rise to a signal at 1690 cm<sup>-1</sup> which matches with the product peak observed in reactions between AA and Zr(OH)<sub>4</sub>. Also, from the perspective of the reaction it is more likely that the product is crotonaldehyde rather than acrolein. Acrolein is formed by a condensation reaction between AA and formaldehyde which results in a C<sub>3</sub> product, whereas crotonaldehyde is the product of a self-condensation reaction between two AA molecules.<sup>3</sup> In the reactions conducted in this study there is no formaldehyde present, and therefore, the most likely condensation reaction would occur between AA molecules. This self-condensation reaction is made more likely due to the high AA concentrations being used in the reaction solution. Hence, crotonaldehyde is most likely the product observed in the IR spectra of the reaction mixtures. Crotonaldehyde is an extremely hazardous substance and is highly toxic by all routes of exposure according to the Agency for Toxic Substances and Disease Registry (ATSDR).<sup>12</sup> Due to the health concerns associated with crotonaldehyde it would be highly undesirable to convert AA *via* aldol condensation reactions within a PET bottle manufactured for the storage of mineral water for human consumption. Therefore, if a metal oxide catalyst is ever to be

implemented for scavenging AA in PET, the mechanism for converting AA under melt-processing conditions of PET must be something other than aldol condensation reactions. However, it must also be noted that under the real conditions in PET the AA concentration is far lower than those used in these experiments (< 10 ppm), which makes a self-condensation reaction much less likely.

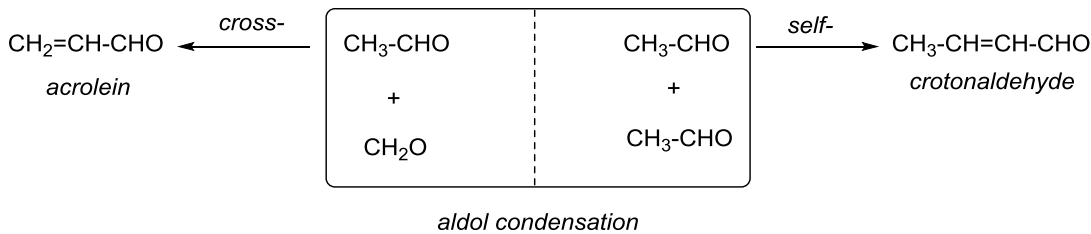


Figure 3.12 Scheme for condensation reactions between AA and formaldehyde.<sup>3</sup>

Due to issues with evaporation of AA from reactions conducted in a round-bottom flask equipped with a reflux condenser, reactions were instead conducted in a glass Colaver reactor (see photograph in figure 3.12). These reactors can be sealed and can withstand pressures up to 5 bar. Gases can be added to the reactor *via* the inlet so that reactions can be conducted in a particular atmosphere. For example, if an inert atmosphere is required the reactor could be charged with N<sub>2</sub> before sealing the reactor to provide the desired reaction atmosphere. This also makes these reactors suitable for carrying out oxidation or hydrogenation reactions where gases need to be added to the reaction.<sup>13,14</sup>

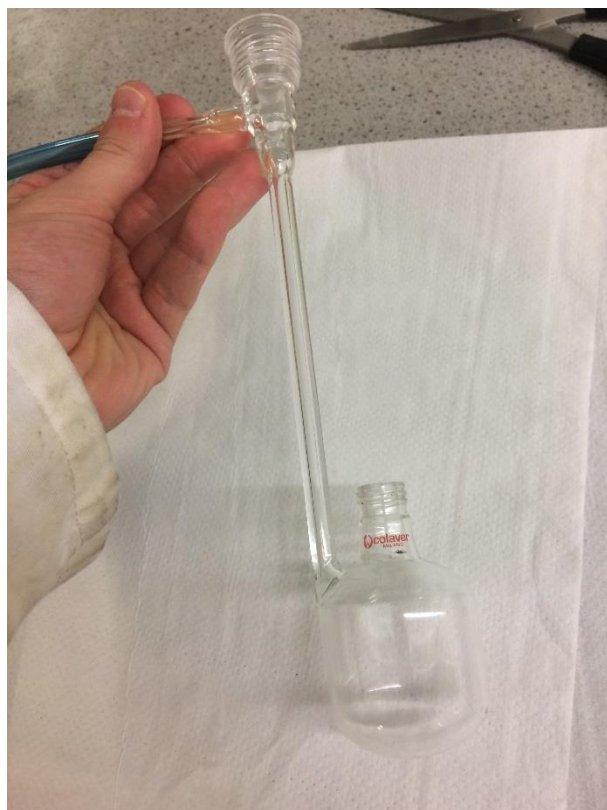


Figure 3.13 Photograph of glass Colaver reactor

In figure 3.13 IR spectra for reactions between AA and Zr(OH)<sub>4</sub> in PEG-DME are presented and the data that is obtained is very similar to that of the reactions previously conducted in a round bottom flask. As the AA is exposed to the catalyst for longer periods of time at 105 °C, more of the AA is converted and more crotonaldehyde is produced.

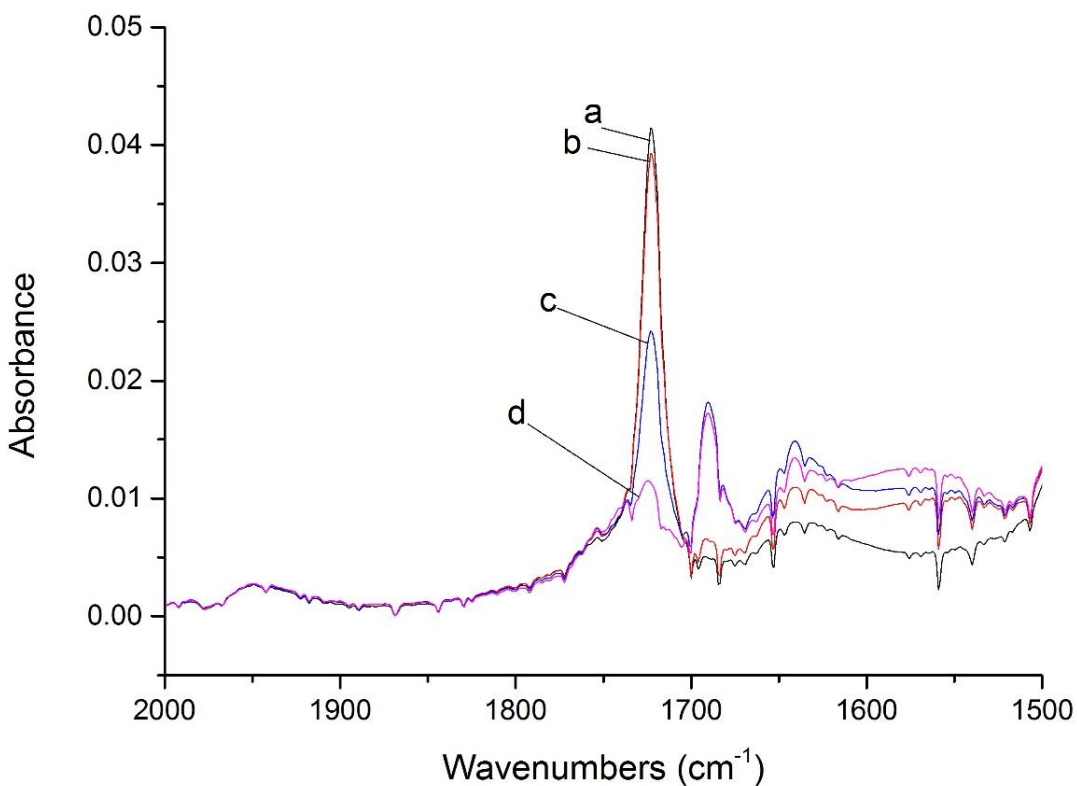


Figure 3.14 Reaction with  $\text{Zr}(\text{OH})_4$ . a) AA in PEG-DME solution, b) AA in PEG-DME solution following addition of  $\text{Zr}(\text{OH})_4$  (0.5 g) and heated to 105 °C for 20 mins under stirring in a Colaver, c) AA in PEG-DME solution following addition of  $\text{Zr}(\text{OH})_4$  (0.5 g) and heated to 105 °C for another 16 hours under stirring in a Colaver, d) AA in PEG-DME solution following addition of  $\text{Zr}(\text{OH})_4$  (0.5 g) and heated to 105 °C for another 96 hours under stirring in a Colaver.

However, when a blank reaction was left for 96 hours it was found that the AA concentration decreased by 57% in the Colaver reactor (see figure 3.14). This suggests that even with a sealed glass reactor the AA was still able to evaporate out of the PEG-DME and lead to a reduction in the AA concentration. It is also very difficult to ensure that no AA evaporates when the sample is being transferred from the reaction to the IR spectrometer for analysis. Certain precautions can be taken such as freezing the glass pipette tips, however due to the volatility of AA it is difficult to prevent any loss due to evaporation. Therefore, this setup was deemed unsuitable for further catalyst testing also.

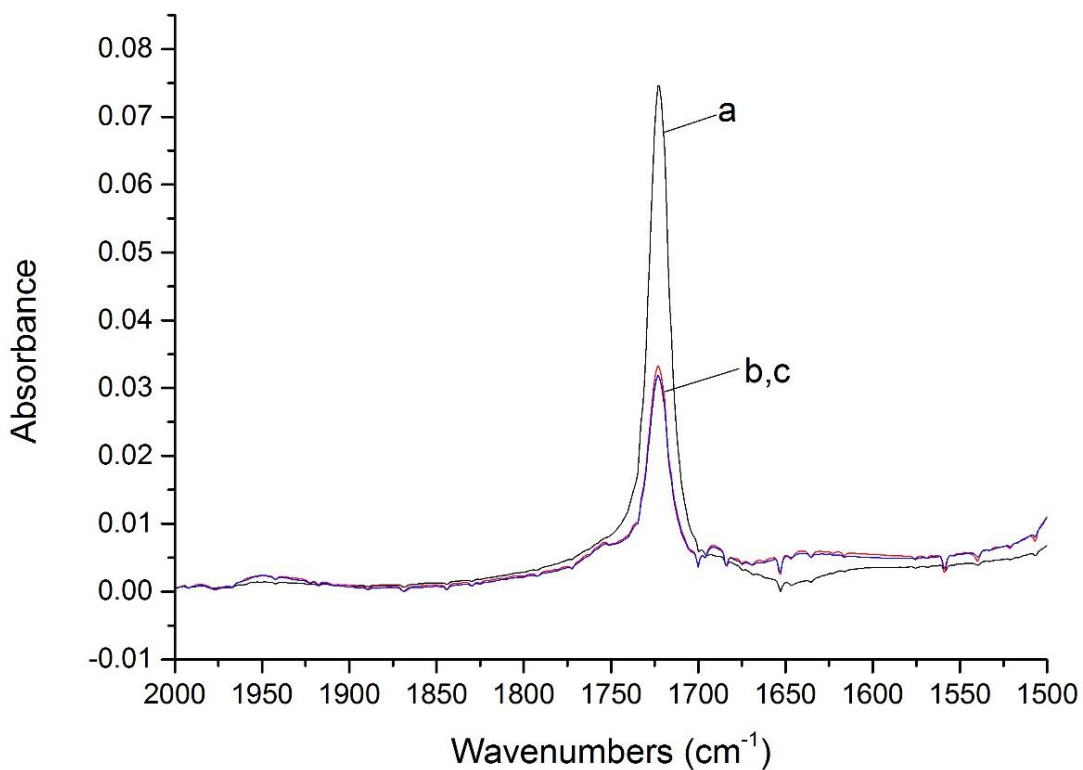


Figure 3.15 Blank reaction. a) AA in PEG solution, b,c) AA in PEG solution heated to 105 °C for 96 hours under stirring in a Colaver.

### 3.3 Testing with Butyraldehyde (BA) in Octane

In light of the issues encountered while testing the catalysts with AA in PEG-DME and conducting the analysis using ATR-FTIR, a new reaction protocol was adopted. Reactions were instead carried out using butyraldehyde (BA), a longer chain aldehyde that has a four-carbon chain as opposed to the two-carbon chain of AA, as the model substrate. This increased carbon chain length causes BA to have a higher boiling point of 75 °C and is far less volatile than AA. The choice of solvent was also changed to enable the use of GC analysis to monitor the conversion achieved in the reactions. PEG-DME is incompatible with the GCs in the CCI, so octane was chosen as an inert hydrocarbon reaction media. This represented a move further away from the PET mimic conditions, however this BA in octane model system offered the possibility of a more stable and robust testing protocol. Due to the greater stability of BA there should be less issues with blank reactions, and GC is able to be more accurately calibrated than IR and so should provide more reliable data. Also, when conducting reactions with AA in PEG-DME with IR starting concentrations of 5-10% AA were required to give a strong enough signal in the IR spectrum. Such

concentrations are far higher than the 7-10 ppm AA that is present in processed PET, so for the BA in octane reactions much lower starting aldehyde concentrations were used. A starting BA concentration of 1000 ppm was used for the reactions conducted using this model.

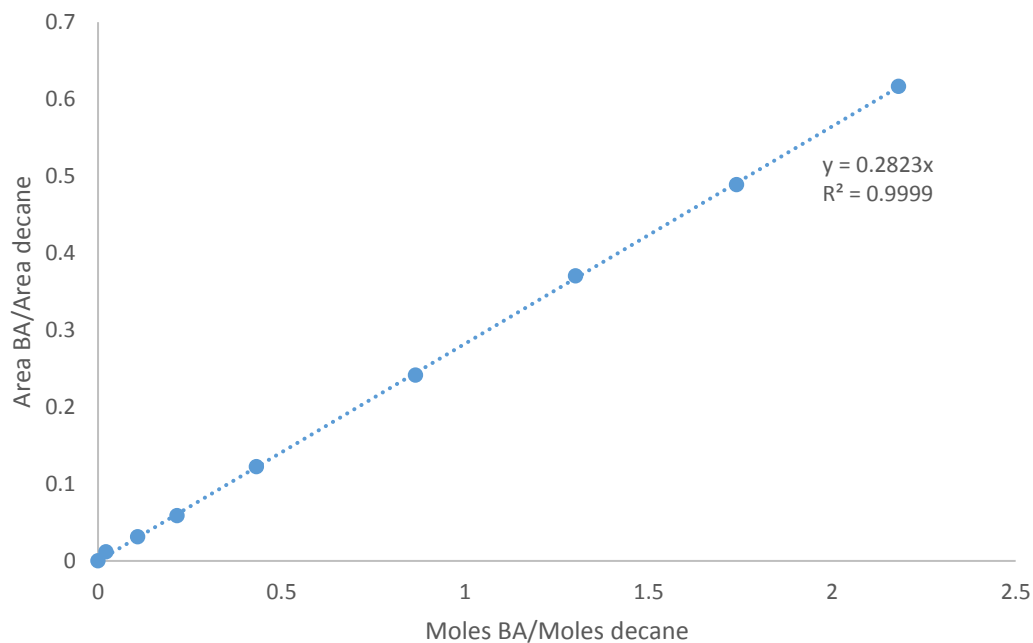


Figure 3.16 Calibration for BA in octane (1000 ppm, 800 ppm, 600 ppm, 400 ppm, 200 ppm, 100 ppm, 50 ppm, 10 ppm) in the presence of an internal standard, decane (1000 ppm).

Before catalyst testing could be conducted using this reaction system the BA signal in the GC needed to be calibrated. Decane was added to the solution of BA and octane to act as internal standard, to ensure the veracity of the data that was generated. The calibration of the BA in the presence of the internal standard can be found in figure 3.15 and was found to give an  $R^2$  value very close to 1. The BA signal was calibrated in relation to the signal of the internal standard. The detection of BA at concentrations as low as 10 ppm meant that lower aldehyde concentrations, more similar to the levels of AA in PET, could be used with this method.

Different loadings of  $Zr(OH)_4$  were tested for their ability to convert BA in octane (see figure 3.16). To minimise the effect of evaporation these reactions were run at a lower temperature than previous reactions ( $40\text{ }^\circ\text{C}$  instead of  $105\text{ }^\circ\text{C}$ ). It was

found that the BA conversion increased as the loading of the catalyst increased. Although GC analysis is preferable for quantification than IR, in this case it was far more difficult to identify the occurrence of any chemical reactions in the GC than in the IR. Due to the presence of the large solvent peak and a low starting concentration of aldehyde of 1000 ppm, it was very difficult to identify the formation of any reaction products. This meant it was difficult to determine whether the BA was reacting with the catalyst or just being absorbed by it.

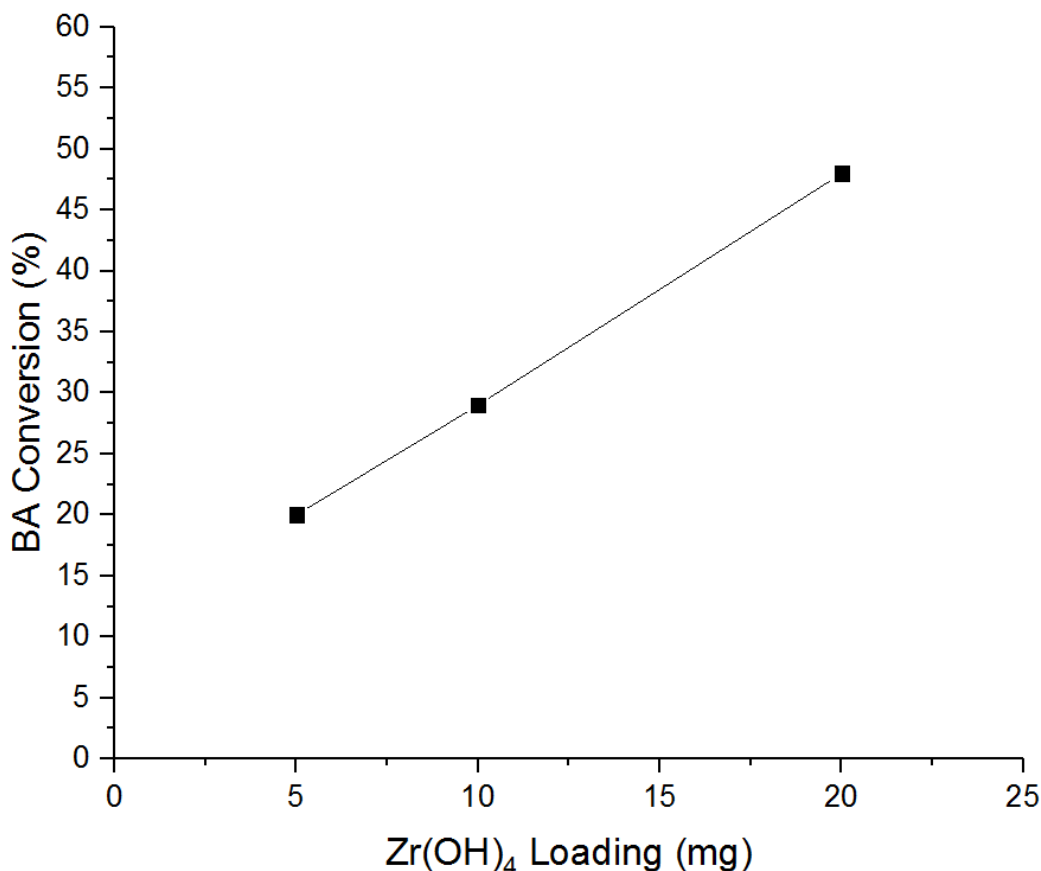


Figure 3.17 Testing data with different loadings of Zr(OH)<sub>4</sub> for the conversion of BA at 40 °C for 22 hours (Reaction medium = BA (1000 ppm), decane (1000 ppm) in octane (10 ml)).

Blank reactions were conducted to ensure that no BA was being lost due to any other factors beside the activity of the catalyst upon the aldehyde. From figure 3.17, reactions A and C at 40 °C show that the concentration of BA only changed by ±1%. However, in reactions B and D at 40 and 60 °C respectively the BA concentration was reduced by 5% or more and show that there is still quite a significant degree of error

associated with this testing protocol. Despite charging the reactor with N<sub>2</sub> to try to prevent evaporation of the aldehyde, it seems as though the BA is still able to move from the reaction solution and into the headspace of the reactor which then causes a lower concentration of BA to be measured in the testing. Therefore, due to a lack of reproducibility between tests, accompanied with the difficulty in observing the formation of reaction products, this method could not be used to reliably test the AA conversion of catalysts.

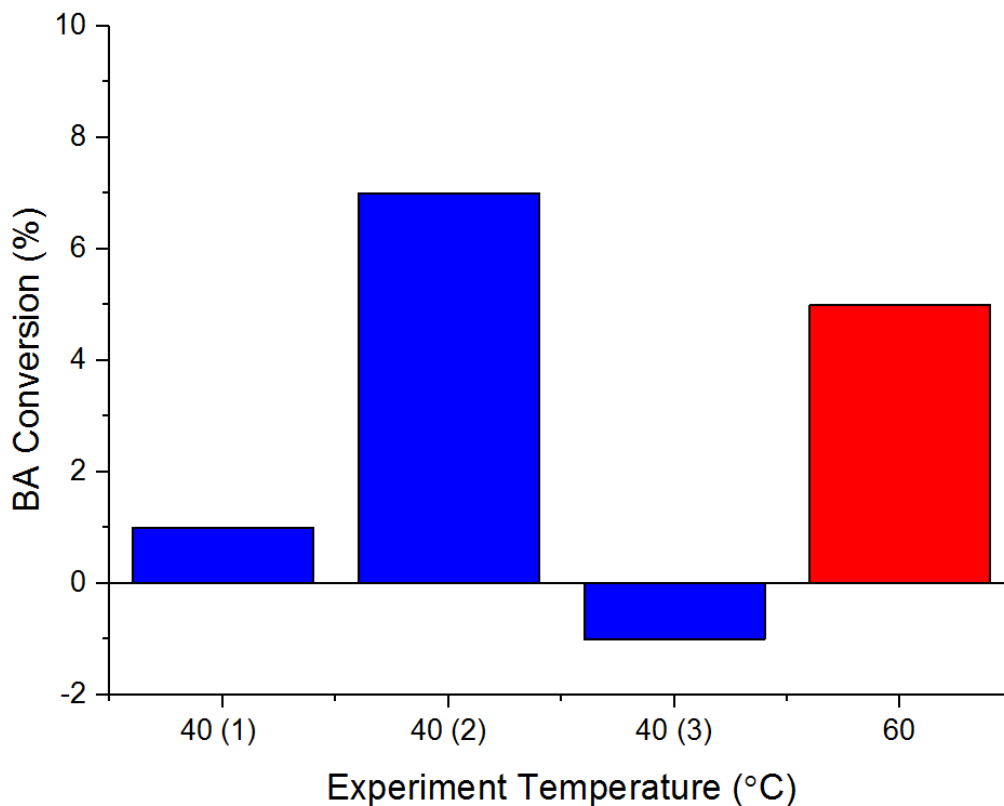


Figure 3.18 BA conversion for blank reactions at temperatures of 40 °C or 60 °C for 22 hours. (Reaction medium = BA (1000 ppm), decane (1000 ppm) in octane (10 ml)).

### 3.4 Testing with AA in Gas Phase Reactor

It was decided that working with AA or BA in the liquid phase was not providing data of sufficient quality and would not be suitable for this research project. Therefore, development began on a test that would use AA in the gas phase which would avoid any issues associated with the volatility of AA during liquid phase testing. Initially, experiments were trialled using DRIFTS analysis, whereby a flow of N<sub>2</sub> was

fed through a chilled Dreschel bottle containing AA to generate a flow of AA through the system. However, it was difficult to accurately control the concentration of AA within the gas flow and so gas cylinders were used to provide the source of gas phase AA. A cylinder was purchased from BOC containing 500 ppm AA in helium balance for conducting experiments in a gas phase reactor (for details see section 2.3.1), and optimisation of a GC method for analysing reactions with AA was conducted using CeO<sub>2</sub> as a catalyst. Based on a study by Kydd *et al.* where CeO<sub>2</sub> was found to be a much more effective AA oxidation catalyst than ZrO<sub>2</sub>.<sup>15</sup> They examined the activities of CeO<sub>2</sub>, TiO<sub>2</sub>, ZrO<sub>2</sub>, Al<sub>2</sub>O<sub>3</sub>, and SiO<sub>2</sub> catalysts for the conversion of AA (200 ppm in air) in a gas-phase reactor at temperatures between 175-275 °C. CeO<sub>2</sub> was the only metal oxide catalyst able to achieve 100% AA conversion within that temperature range, and was also found to be the best support material for 4% Cu supported catalysts. Therefore, a ceria catalyst was prepared by urea precipitation adapted from research by Sellick *et al.*<sup>16</sup> This ceria catalyst was used for the optimisation of the GC method for gas phase testing of the AA removal catalysts.

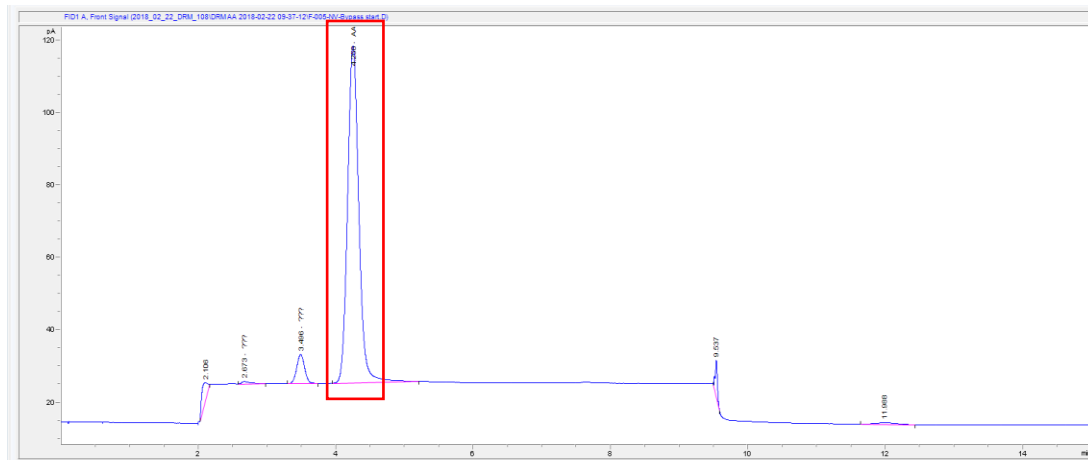


Figure 3.19 Gas chromatogram of AA(500ppm)/He on bypass at room temperature. AA signal at 4.2 mins (x axis = time in minutes, y axis = detector response in picoamps)

In figure 3.18 the GC trace of 500 ppm AA flowed through the bypass of the reactor is displayed. This trace shows a signal at 4.2 minutes which can be identified as the AA. The other small peaks in the trace are associated with valve changes or with impurities on the column. Due to the low concentration of AA that is being used, any impurities are more visible than they would be were higher starting concentrations

being used. Higher reactant concentrations help to disguise any small deviations in the baseline of a trace. More thorough conditioning of the column would help to remove any impurities residing on the column that may be causing the signal at 3.5 mins.

When the AA is exposed to a ceria catalyst at 175 °C the trace in figure 3.19 is observed and a new peak is introduced at 5.4 minutes indicating the formation of a reaction product. When the temperature of the reaction is increased to 300 °C the peak at 5.4 minutes is no longer observed, and a new signal can be seen at 7.6 mins (see figure 3.20). This indicates that different reaction mechanisms are occurring under the different temperature regimes, which lead to the formation of different reaction products. One limitation of GC analysis is that it does not identify reaction products. A molecule will have a particular retention time depending on the design of the method and the way that it interacts with the column. Standards can be used to identify the molecules that give rise to the peaks found in the GC trace. In order to know which standards to use one must have a good idea as to what the products of the reaction could be. In the case where one has a large pool of possible reaction products, it may not be feasible to identify the relevant products using standards in a GC. Some compounds may have the same or very similar retention times that cause the signals to overlap, and therefore other analytical techniques are often required in conjunction with GC to differentiate between molecules with very similar retention times (e.g. GC-MS).

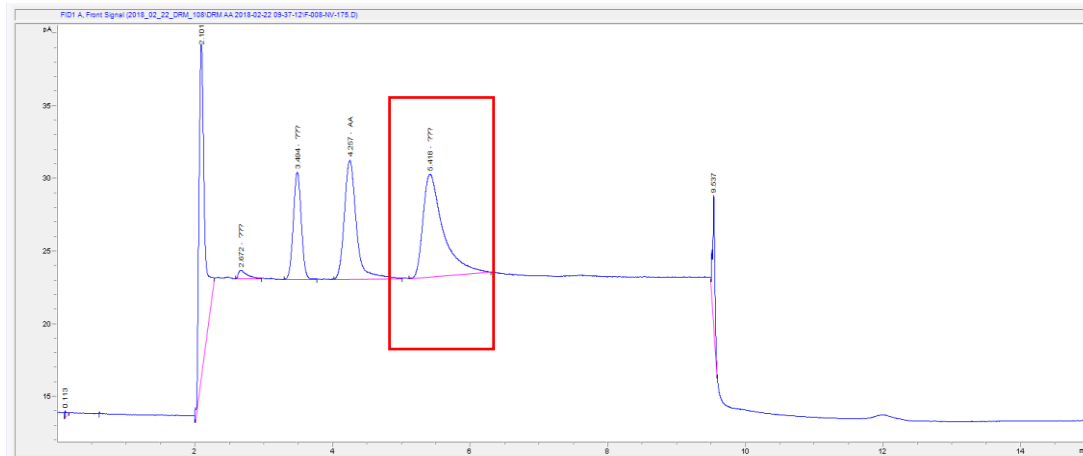


Figure 3.20 Gas chromatogram of AA flowed over CeO<sub>2</sub> at 175 °C. Unidentified product at 5.4 mins (highlighted by red box). (x axis = time in minutes, y axis = detector response in picoamps)

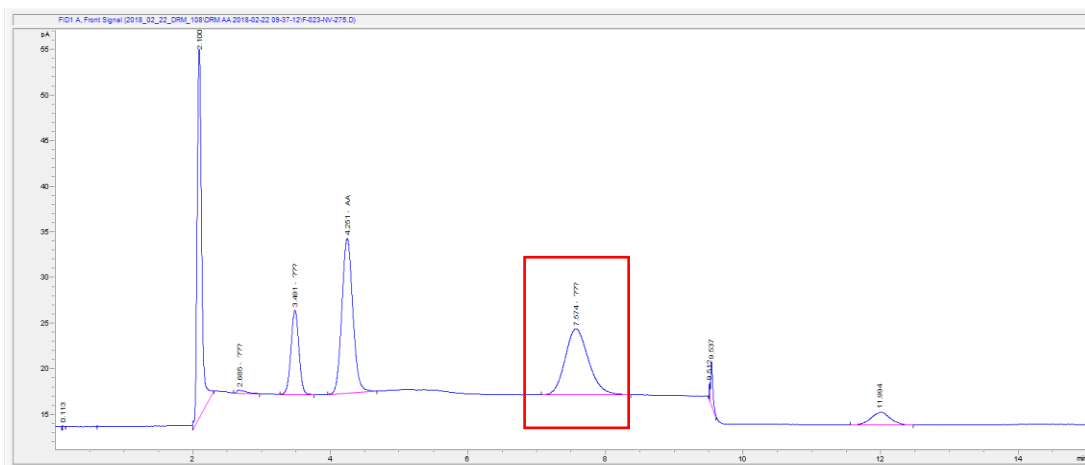


Figure 3.21 Gas chromatogram of AA flowed over CeO<sub>2</sub> at 275 °C. Unidentified product at 7.6 mins (highlighted by red box). (x axis = time in minutes, y axis = detector response in picoamps)

A selection of reaction product candidates were bubbled through the reactor in an attempt to identify the products being formed in the reactions between AA and ceria. Crotonaldehyde was chosen based on what had been observed using the ATR-FTIR analysis with the liquid phase reactions (see figure 3.10). Some of the candidates were tested based on the ColorMatrix patent where the products were identified as ethanol, acetic acid, and ethyl acetate.<sup>1</sup> Other candidates (furan and acetone) were tested based on reports in the literature where reactions between AA and metal oxides had been investigated.<sup>15,17</sup> The retention times for these compounds can be found in table 3.1. From this data the low temperature product is most likely to be ethanol with a retention time of 5.3 minutes. However, for the high temperature product both acetone and furan gave retention times of 7.3 minutes, so these were the most likely products based on this limited survey. Different reaction products have been observed for reactions between AA and metal oxides in different temperature regimes. For example, in a study by Idriss *et al.* reduction of AA to ethanol in the presence of a CeO<sub>2</sub> at temperatures between 117-127 °C was observed, and when the temperature was increased to 357 °C conversion of AA to acetone was observed.<sup>18</sup> This provides a strong precedent for the observations that have been made in the GC-FID analysis of reactions between AA and ceria at varying temperatures.

Table 3.1 GC retention times for potential reaction products

Compound	Retention time / minutes
Crotonaldehyde	4.9 (very broad)
Ethanol	5.3
Acetone	7.3
Acetic acid	8.7
Ethyl acetate	2.4
Furan	7.3

In order to conduct a more extensive survey of possible product candidates Mass Spectrometry (MS) was utilised, as it is able to identify species based on the m/z ratio of characteristic fragment ions. The m/z ratio is essentially equivalent to molecular weight of the fragment ion provided that the ion has a +1 charge. Based on a survey of the academic literature relating to MS analysis of reactions between AA and metal oxide catalysts, an MS program (as seen in figure 3.21) was designed that probed for the following gases: AA, crotonaldehyde, crotyl alcohol, furan, acetic acid, acetone, 1,3-butadiene, but-2-ene, ethyl acetate, ethanol.<sup>15,17</sup> Using this method would help to identify the reaction products that were observed in both the low temperature and high temperature regimes.

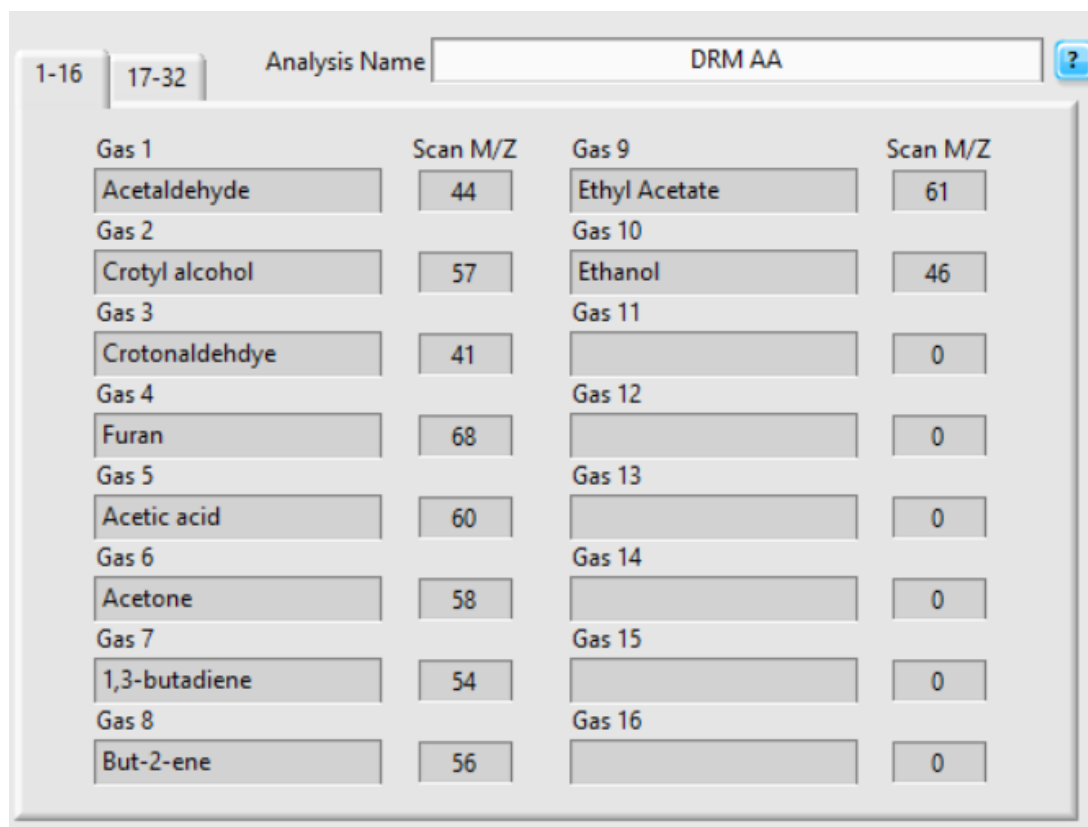


Figure 3.22. MS program for analysis of reaction between AA and metal oxide catalyst, including gaseous product candidates and the m/z value of their most characteristic fragment ion

In order to carry out a blank experiment AA (500 ppm AA/He) was flowed at 50 ml/min through an empty reactor tube as the temperature of the furnace was increased up to 400 °C at 1 °C/min. The data for the blank reaction can be found in figure 3.22, and shows no conversion of AA up to 400 °C. This indicates that AA is thermally stable up to these temperatures and that a catalyst is required if the AA is to be converted within this temperature range. The MS appeared to detect a certain level of crotonaldehyde throughout the experiment. However, the concentration of crotonaldehyde does not change from room temperature up to 400 °C and so is most likely part of the background noise of the analysis.

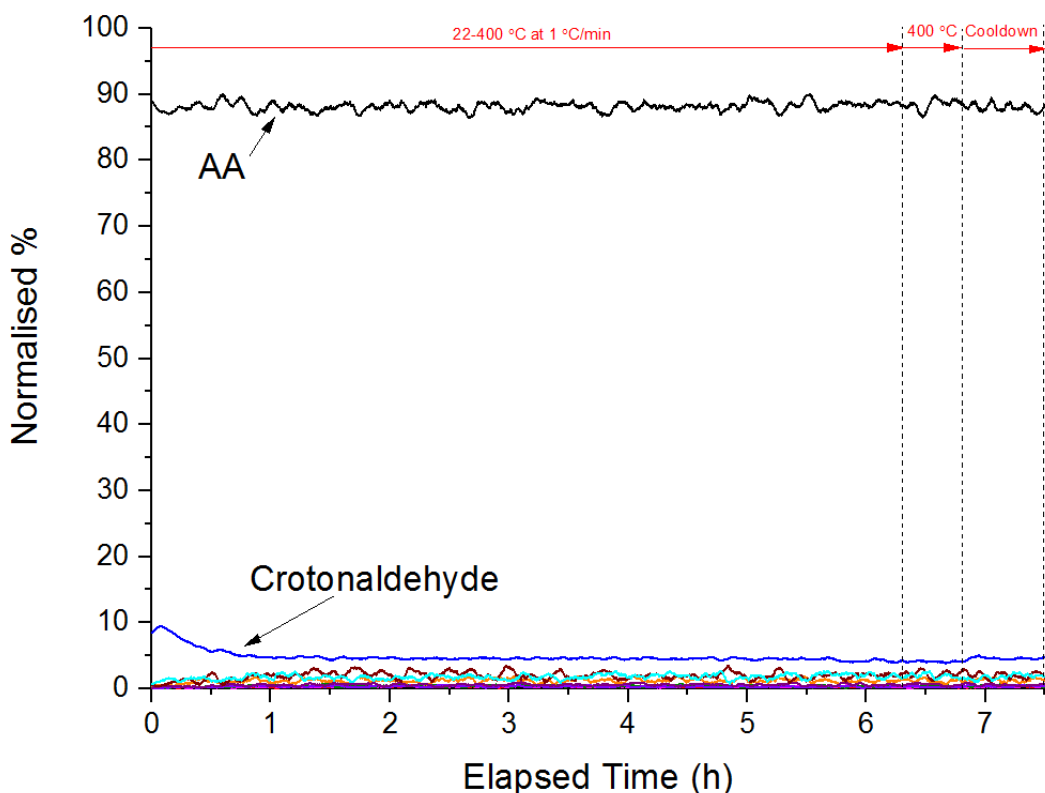


Figure 3.23 Mass Spectrometry data for blank reaction. 0-6.3 hrs increased temperature from 22–400 °C at 1 °C/min, 6.3-6.8 hrs held temperature at 400 °C, 6.8-7.5 hrs reactor cooldown. (Conditions: 500 ppm AA/He flowed at 50 ml/min)

To analyse the interaction between AA and a ceria catalyst, a 50 mg catalyst bed was loaded into the reactor (see figure 3.23). For the initial 30 minutes the gas was flowed through the bypass of the reactor in order to obtain a blank reading, after which the gas was switched to flow over the catalyst for the next hour at room temperature. No reaction was observed during this time, showing the catalyst to be inactive for conversion of AA at room temperature. The reactor was then heated to 175 °C and held at that temperature for the next hour and a half where the formation of ethanol was identified by the MS. The catalyst was able to convert AA to ethanol initially under these conditions and then quickly deactivated with very little ethanol formation observed at the end of the 1.5 hour period at 175 °C. In the subsequent 3.75 hours, the reactor was heated from 175 to 400 °C at 1 °C/min. During this temperature ramp the formation of acetone was observed, and the temperature at which the highest the acetone concentration was achieved was found to be 326 °C. This analysis confirmed that the product observed in the GC at lower temperatures was ethanol and the high

temperature product was acetone. These findings are in agreement with a report by Idriss *et al.* that was previously discussed.<sup>18</sup>

The same analysis was conducted using commercial Zr(OH)<sub>4</sub> and ZrO<sub>2</sub> made *via* urea precipitation. The Zr(OH)<sub>4</sub> catalyst achieved its maximum acetone concentration at 353 °C, whilst the prepared ZrO<sub>2</sub> catalyst reached its maximum acetone concentration at 383 °C. This indicates that the ceria catalyst is more active for converting AA to acetone than either of the Zr-based samples. This activity trend is in line with observations made by Kydd *et al.*<sup>15</sup>

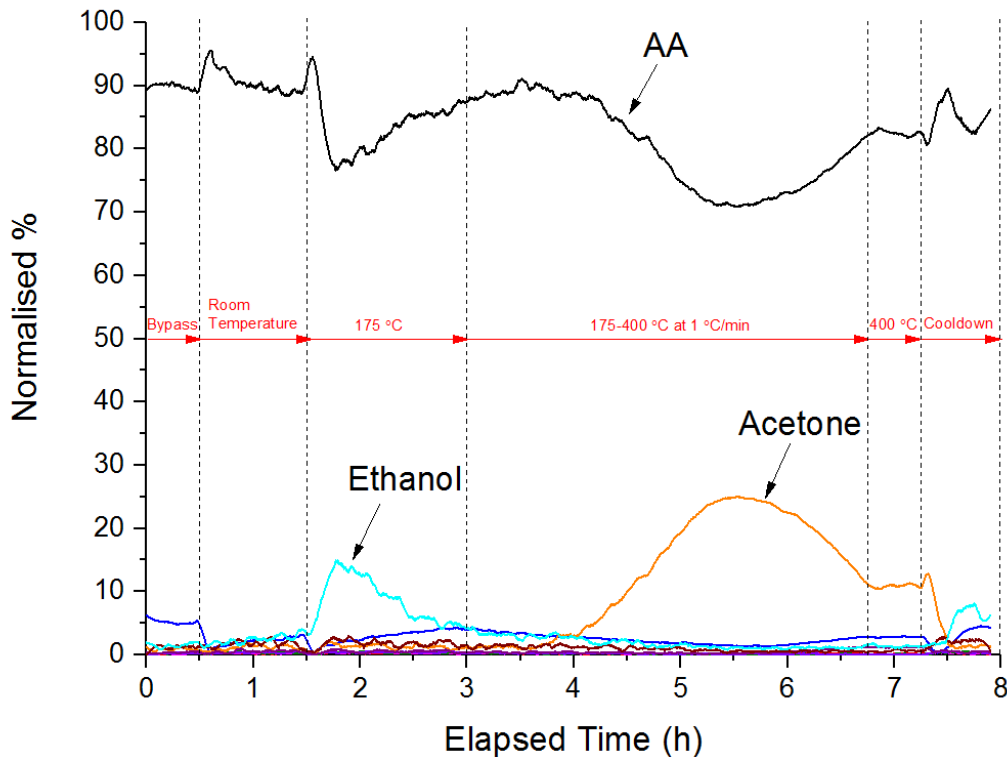


Figure 3.24 Mass spectrometry data for reaction between AA and CeO<sub>2</sub> catalyst. 0-0.5 hrs flowed AA through bypass, 0.5-1.5 hrs flowed AA through catalyst bed at room temperature, 1.5-3 hrs flowed AA through catalyst bed at 175 °C, 3-6.75 hrs increased temperature from 175-400 °C at 1 °C/min, 6.75-7.25 hrs held temperature at 400 °C, 7.25-8 hrs reactor cooldown (Conditions: 500 ppm AA/He flowed at 50 ml/min over a 50 mg CeO<sub>2</sub> catalyst bed)

Based on the results of the MS analysis the product peaks in the GC trace were labelled correctly and a new GC method was developed to separate all of the observed products (for further details see section 2.3.1.1) This method involved having suitable valve changes and temperature ramps. The GC used in this reactor is equipped with

two different columns and these columns are used to elute different types of compounds, and valve changes are required to ensure that the product gases are eluted with the appropriate column. The two columns used in this apparatus are a MolSieve 5A and a HayeSep Q. The MolSieve 5A is used for the separation of light gases, whereas the HayeSep Q is used for the separation of organic moieties. Therefore, the MolSieve 5A column is required to elute CO and CH<sub>4</sub>, and the HayeSep Q column is more suitable for eluting CO<sub>2</sub>, AA, and acetone. CO<sub>2</sub> is a light gaseous product, however it binds irreversibly to the MolSieve column so the HayeSep Q column is utilised for the elution of carbon dioxide.

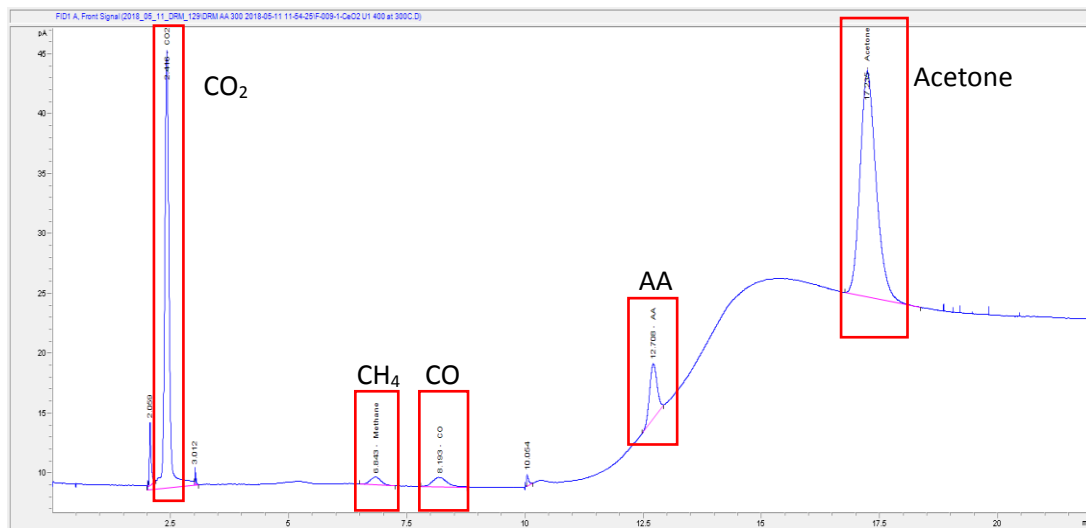


Figure 3.25 GC trace for reaction between AA and a CeO<sub>2</sub> catalyst at 300 °C using optimised GC method with labelled reaction products (highlighted by red boxes, CO<sub>2</sub> at 2.4 mins, CH<sub>4</sub> at 6.8 mins, CO at 8.2 mins, acetone at 17.2 mins). (x axis = time in minutes, y axis = detector response in picoamps)

In figure 3.24 the GC trace for a reaction between AA and ceria is displayed using the optimised GC method for separation of the observed products. The timeline for the column activity in this GC method is as follows:

- 0.5-2 mins HayeSep Q and MolSieve 5A (fill columns)
- 2-3 mins HayeSep Q (elute CO<sub>2</sub>)
- 3-10 mins MolSieve 5A (elute CO and CH<sub>4</sub>)
- 10-20 mins HayeSep Q (elute AA and acetone)

The first valve change occurs at 2 minutes to allow for the elution of CO<sub>2</sub> which is observed at 2.4 minutes. The second valve change occurs at 3 minutes to facilitate the elution CH<sub>4</sub> and CO at 6.8 and 8.2 minutes respectively. The final valve change occurs at 10 minutes to enable the elution of AA and acetone at 12.7 and 17.2 minutes respectively.

The temperature of the GC oven also needs to be optimised in order to separate the reaction products effectively. The temperature conditions for this GC method are as follows:

- 0-10 mins at 120 °C (separate CO<sub>2</sub>, CO, and CH<sub>4</sub>)
- 10-12 mins temperature ramp of 40 °C/min (separate AA and acetone)
- 12-20 mins at 200 °C

The first 10 minutes of the sequence are isothermal at 120 °C to separate and elute the light gaseous products of CO, CO<sub>2</sub>, and CH<sub>4</sub>. The temperature of the column then needs to be increased to elute and separate the organic products of AA and acetone. The use of a temperature ramp also helps to shorten the analysis time for each injection, which allows for more data to be collected during a reaction to yield more effective reaction monitoring.

Table 3.2 FID retention times for observed compounds using optimised GC method

Compound	FID Retention Time (mins)
Carbon dioxide (via methaniser)	2.4
Methane	6.8
Carbon monoxide (via methaniser)	8.2
AA	12.7
Acetone	17.2

Now that an effective GC method had been developed, catalyst activities could be measured and product selectivities could be monitored. This would enable the screening of catalyst samples for performance in AA conversion catalysis (see chapter 4) before testing in application conditions at ColorMatrix (see chapter 5).

### 3.5 Conclusions

In conclusion, various testing methodologies were examined for providing a catalyst screening protocol for assessing the performance of metal oxide catalysts for converting AA. Experiments involving PEG or octane as a reaction medium using AA or BA as reactants with FTIR or liquid phase GC analysis were trialled, before gas phase AA testing with online GC analysis was deemed most suitable. Each test method has its own advantages and disadvantages and reflect different aspects of the industrial conditions. For example, testing in PEG-DME allowed for testing within a liquid polymer matrix analogous to the molten PET in which the catalysts need to convert AA. However, gas phase testing allows for low, ppm range concentrations of AA, that are analogous to the concentrations of AA found in PET and allows for testing at PET processing temperatures.

Ultimately, gas phase testing provides a much more reliable protocol for handling AA in the laboratory and provides data of far greater quality and reproducibility than any of the liquid phase testing that was trialled. Reaction products were identified using MS, and an optimised GC method was developed specifically for the reaction system under investigation. Therefore, catalyst screening could be conducted in the CCI laboratories before samples were tested in PET under application conditions at the ColorMatrix site in Knowsley.

Different reaction mechanisms have been observed under different testing regimes. At 105 °C in the liquid phase AA was converted to crotonaldehyde *via* an aldol condensation reaction. In the gas phase reactions AA was converted to ethanol at 175 °C and acetone at 300 °C. All of these reactions have been reported in the scientific literature in studies of interactions between AA and metal oxides, so there is a strong precedent for the observations that have been made here. Further investigation will be conducted to gain greater understanding of the mechanisms involved in these reactions.

### 3.6 Chapter 3 - References

1. WO2005010088 A1, 2005.
2. C. Huang, Z. Tang and Z. Zhang, *J. Am. Ceram. Soc.*, 2001, **84**, 1637–1638.
3. E. Dumitriu, V. Hulea, C. Chelaru, C. Catrinescu, D. Tichit and R. Durand, *Appl. Catal. Gen.*, 1999, **178**, 145–157.
4. V. V. Ordomsky, V. L. Sushkevich and I. I. Ivanova, *J. Mol. Catal. Chem.*, 2010, **333**, 85–93.
5. W. Ji, Y. Chen and H. H. Kung, *Appl. Catal. Gen.*, 1997, **161**, 93–104.
6. E. Dumitriu, V. Hulea, N. Bilba, G. Carja and A. Azzouz, *J. Mol. Catal.*, 1993, **79**, 175–185.
7. S. Luo and J. L. Falconer, *Catal. Lett.*, 1999, **57**, 89–93.
8. D. Tichit, D. Lutic, B. Coq, R. Durand and R. Teissier, *J. Catal.*, 2003, **219**, 167–175.
9. Z. D. Young, S. Hanspal and R. J. Davis, *ACS Catal.*, 2016, **6**, 3193–3202.
10. C. Zhao, C. Watt, P. R. Kent, S. H. Overbury, D. R. Mullins, F. C. Calaza, A. Savara and Y. Xu, *J. Phys. Chem. C*, 2019, **123**, 8273–8286.
11. M. Singh, N. Zhou, D. K. Paul and K. J. Klabunde, *J. Catal.*, 2008, **260**, 371–379.
12. ATSDR - Medical Management Guidelines (MMGs), <https://www.atsdr.cdc.gov/MMG/MMG.asp?id=947&tid=197>, (accessed 23 September 2019).
13. R. Qu, M. Macino, S. Iqbal, X. Gao, Q. He, G. J. Hutchings and M. Sankar, *Nanomaterials*, 2018, **8**, 690.
14. S. Pattisson, O. Rogers, K. Whiston, S. H. Taylor and G. J. Hutchings, *Catal. Today*, 2020, **357**, 3-7.
15. R. Kydd, W. Y. Teoh, J. Scott, D. Ferri and R. Amal, *ChemCatChem*, 2009, **1**, 286–294.

16. D. R. Sellick, A. Aranda, T. García, J. M. López, B. Solsona, A. M. Mastral, D. J. Morgan, A. F. Carley and S. H. Taylor, *Appl. Catal. B Environ.*, 2013, **132–133**, 98–106.
17. A. K. P. Mann, Z. Wu, F. C. Calaza and S. H. Overbury, *ACS Catal.*, 2014, **4**, 2437–2448.
18. H. Idriss, C. Diagne, J. P. Hindermann, A. Kiennemann and M. A. Barteau, *J. Catal.*, 1995, **155**, 219–237.

## 4 Gas Phase Testing of Metal Oxide Catalysts for AA Conversion

### 4.1 Introduction

In the previous chapter the development of a testing protocol for the screening of metal oxide catalysts for the conversion of AA was outlined. The methodology that provided the most rigorous and reliable testing involved a gas phase test where gaseous AA in He was flowed through a catalyst bed and product analysis was conducted using online GC-FID. A GC method was developed that ensured the separation of the gases observed in the product stream (AA, CO, CO<sub>2</sub>, methane, ethanol, and acetone). The catalysts were examined for their activity for AA conversion at 300 °C due to the processing of PET generally being carried out at temperatures between 270-300 °C.<sup>1</sup> This gas phase testing method was used to compare the activities of different catalysts prepared in the laboratory using various preparation techniques to determine which catalyst would most likely be effective for removing AA from PET. The catalysts were characterised using a variety of techniques to determine which physicochemical properties are most important for an AA conversion catalyst. The reaction was also analysed using DRIFTS to give greater mechanistic understanding of the conversion of AA on a metal oxide surface.

Table 4.1 Summary of the preparation and properties of a selection of catalysts tested in this chapter

Catalyst	Preparation Method	BET surface Area (m <sup>2</sup> /g)	Catalyst Density (g/ml)	Average Crystallite Size (Å)
CeO <sub>2</sub> U1	Urea precipitation (3:1 urea to metal nitrate ratio)	140	1.52	62
CeO <sub>2</sub> U2	Urea precipitation (3:1 urea to metal nitrate ratio)	130	1.43	67

Table 4.1 continued

CeO <sub>2</sub> U3	Urea precipitation (3:1 urea to metal nitrate ratio)	95	1.56	105
CeO <sub>2</sub> U4	Urea precipitation (3:1 urea to metal nitrate ratio)	130	1.27	76
CeO <sub>2</sub> U6	Urea precipitation (3:1 urea to metal nitrate ratio)	115	1.70	81
CeO <sub>2</sub> U6 ball milled	Urea precipitation (3:1 urea to metal nitrate ratio), ball milled at 300 rpm for 3 hours	100	2.28	79
CeO <sub>2</sub> T2	TTAB assisted	230	1.03	36
CeO <sub>2</sub> P2	Pluronic P123 assisted (aged for 7 days)	30	0.73	507
Nano CeO <sub>2</sub>	Commercial material	50	0.22	315
Nano CeO <sub>2</sub> ball milled	Commercial material, ball milled at 300 rpm for 3 hours	40	2.25	270
5%ZrO <sub>x</sub> -CeO <sub>2</sub>	Urea precipitation (3:1 urea to metal nitrate ratio)	170	1.40	51
5%MnO <sub>x</sub> -CeO <sub>2</sub>	Urea precipitation (3:1 urea to metal nitrate ratio)	95	1.49	84
5%CuO <sub>x</sub> -CeO <sub>2</sub>	Urea precipitation (3:1 urea to metal nitrate ratio)	105	1.48	85

## 4.2 Testing with 500 ppm AA

Initial testing was conducted using a gas mixture of AA(500 ppm)/He at a flow of 50 ml/min and a catalyst loading of 50 mg. Due to the very low concentrations of AA in PET (< 10 ppm) it was considered important that the gas phase testing also be conducted using low concentrations of AA. Therefore, 500 ppm of AA in He (balance) was used to ensure that this test was more representative of the application conditions. The decision to carry out these reactions within an inert atmosphere of He was also made to attempt to more accurately replicate the reaction conditions within PET. PET

does not provide a total barrier to oxygen, however oxygen ingress is minimal and very difficult to measure.<sup>2,3</sup> Also, the concentration of oxygen in PET is likely to be so low that it would be very difficult to add such small quantities to the gas phase tests. Due to these considerations, the reactions were carried out under anaerobic conditions. This is one aspect in which the gas phase reactions conditions are possibly less favourable than in the PET application, and so could increase the likelihood that if the catalysts are active in the gas phase reaction that they would also be active for converting AA within PET.

Under these conditions a selection of metal oxide catalysts were tested for their ability to convert AA (see table 4.1). These catalysts were chosen based on the ColorMatrix patent and results from testing in liquid phase systems (see sections 3.2 and 3.3).<sup>4</sup> The results of the tests show that the ceria catalyst is far more active for this reaction than either of the zirconia catalysts or the manganese oxide material. The greater activity of the ceria is likely due to its superior redox properties. Ceria is more reducible than oxides of zirconium and manganese and can more easily switch between oxidation states.<sup>5</sup>

Table 4.2 Catalyst testing data in gas phase reactor. Average values are averaged over 3 hours of testing. Initial result is taken from first injection, after 20 mins exposure to catalyst. Conditions: 500 ppm AA in He at 50 ml/min, catalyst loading of 50 mg, 300 °C for 3 hours.

Sample	Initial AA Conversion (%)	Average AA Conversion (%)	CO <sub>2</sub> Selectivity (%)	Acetone Selectivity (%)	CO + CH <sub>4</sub> Selectivity (%)	Carbon Balance (%)
CeO <sub>2</sub> U1	99	98	56	40	4	65
t-ZrO <sub>2</sub>	78	58	54	23	23	50
Mn <sub>2</sub> O <sub>3</sub>	87	36	80	18	2	86
m-ZrO <sub>2</sub>	77	54	56	29	15	58

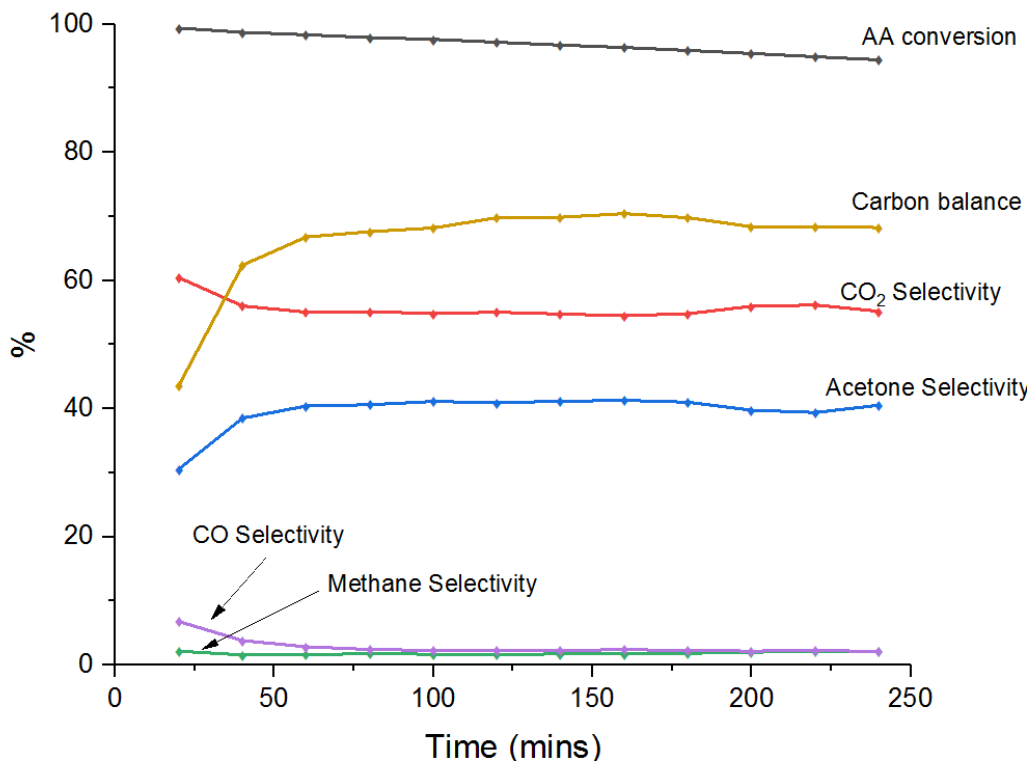


Figure 4.1 Time on stream conversion and selectivity data for the reaction between CeO<sub>2</sub> U1 and AA. Black line = AA conversion, yellow line = carbon balance, red line = CO<sub>2</sub> selectivity, blue line = acetone selectivity, purple line = CO selectivity, green line = methane selectivity. Conditions: 500 ppm AA in He at 50 ml/min, catalyst loading of 50 mg, 300 °C for 3 hours.

The ceria catalyst was able to achieve almost total conversion of the AA and was also found to deactivate less quickly than the other catalysts. This is most likely due to the oxygen storage capacity (OSC) of the ceria catalyst being greater than the other catalysts.<sup>6</sup> During the experiments the activity of the zirconia and manganesia catalysts decreased significantly, whereas the ceria activity was stable throughout the three-hour experiment. It has been shown in previous studies that ZrO<sub>2</sub> catalysts can react readily with AA, but then quickly deactivate.<sup>7</sup> The selectivities were also found to vary between the different catalyst samples for the reaction with AA at 300 °C. The ceria was found to have the greatest selectivity towards acetone, while the manganesia was found to generate the most CO<sub>2</sub> and the least acetone. The zirconia catalysts had the highest selectivity for CO and methane, and also had the lowest carbon balance which suggests that some of the carbon could have been left on the catalyst surface. Alternatively, higher molecular weight structures could be formed due to competing

reaction mechanisms (e.g. aldol condensation or polymerisation), and these larger molecules are more difficult to observe during analysis.<sup>8</sup>

The initial activity is quoted for these reactions (conversion measured from first GC injection) because in PET processing the reaction window, at 270-300 °C in molten PET, is approximately 1 minute. Therefore, the activity after short reaction times is far more relevant to the potential application of these catalysts than the activity after prolonged exposure. The average conversion is measured over a three-hour period and given to indicate the stability of the catalyst under test conditions. The stability of the catalyst is important due to the desire to recycle polymers, and so if the catalyst remains active this could aid recyclability.

Based on the results of this testing ceria was considered the best catalyst for this reaction and was the strongest candidate for effective catalytic removal of AA from PET.

### 4.3 Testing with 1000 ppm AA

Due to the conversion of the AA being so close to 100% when using the ceria catalyst ( $\text{CeO}_2$  U1 in table 4.1), the starting concentration of AA was increased from 500 ppm to 1000 ppm. This meant moving further away from the concentrations found in PET (< 10 ppm), however it was considered more important to have a robust and rigorous catalyst testing protocol. It was more critical to have an effective model reaction whereby catalyst efficacy could be accurately measured, rather than to mimic reactions in molten PET (as was attempted in chapter 3). The other parameters in the testing protocol remained the same, with a gas flow of 50 ml/min and a catalyst loading of 50 mg. The testing was still conducted for three hours and so the average conversion, selectivities and carbon balance were measured over that period. The initial conversion is taken from the first measurement recorded by the online GC analysis.

#### 4.3.1 Testing of Ceria Catalysts Prepared by Urea Precipitation

Before carrying out extensive catalyst screening it is important to establish the margin of error within the testing. To be able to compare the performance of different

samples accurately, any variation within repeat experiments needs to be accounted for. Therefore, the CeO<sub>2</sub> U1 catalyst was tested in triplicate to determine the experimental error associated with this screening methodology. In table 4.2 the results for this triplicate testing can be found, and the mean initial AA conversion for these tests was found to be 94% with a standard deviation of  $\pm 4\%$ . This indicates that if a catalyst outperforms another sample by  $> 4\%$  conversion, then one can have confidence that that catalyst is more effective for AA conversion catalysis under the conditions of this test. When the concentration of AA was increased to 1000 ppm the ceria catalysts were also found to deactivate during the course of a three-hour reaction. This indicates that the testing at 500 ppm (see table 4.1) was limited due to the low concentration of AA, and so the results are not a true reflection of the activity or stability of the catalysts. However, the selectivities and carbon balance remained very similar when the AA concentration was increased to 1000 ppm, which indicates that the same reaction mechanism was responsible.

Table 4.3 Repeated experiments using U1 catalyst. Selectivities and carbon balance are average of 3 hours of testing, initial conversion is taken from first injection. Conditions: 1000 ppm AA in He at 50 ml/min, catalyst loading of 50 mg, 300 °C for 3 hours.

Sample	Initial AA Conversion (%)	CO <sub>2</sub> Selectivity (%)	Acetone Selectivity (%)	Carbon Balance (%)
CeO <sub>2</sub> U1 (1)	99	57	39	63
CeO <sub>2</sub> U1 (2)	93	60	35	66
CeO <sub>2</sub> U1 (3)	91	55	35	61
Average	94 ( $\pm 4$ )	57 ( $\pm 3$ )	36 ( $\pm 2$ )	63 ( $\pm 3$ )

When small data sets are analysed the standard deviation for a sample should be used to calculate the deviation from the mean.<sup>9</sup> The error in the table 4.2 was calculated using the formula for the standard deviation ( $\sigma$ ) of a sample, as follows:

$$\sigma = \sqrt{\frac{\sum(x - \bar{x})^2}{(n - 1)}}$$

Equation 4.1 Standard deviation ( $\sigma$ ) of a sample.  $x$  = observed value,  $\bar{x}$  = mean value,  $n$  = number of values in sample

Further samples of ceria were prepared using urea precipitation and were screened in the gas phase AA test. In table 4.3 the activities of U2, U3, and U4 were compared to the activity of the U1 catalyst. All four samples were prepared using the same method except that U4 was prepared using a greater volume of water. U4 was prepared in 200 ml, whereas the other catalysts were prepared using 100 ml of deionised water. The activities of the U2 and U4 were found to be comparable to that of the U1 material, however the activity of U3 was found to be significantly lower with an initial AA conversion of 76%. The activity of a commercial ceria nanopowder (Cerium(IV) oxide nanopowder, < 25 nm particle size, purchased from Sigma-Aldrich) was also measured, however it was found to be far less effective for AA conversion than all the samples prepared in the laboratory by urea precipitation, with an initial conversion of 40%.

Table 4.4 Testing data for ceria catalysts prepared with 3:1 urea to nitrate precursor molar ratio.

Sample	Initial AA Conversion (%)	CO <sub>2</sub> Selectivity (%)	Acetone Selectivity (%)	Carbon Balance (%)
CeO <sub>2</sub> U1	94	57	38	63
CeO <sub>2</sub> U2	92	58	35	67
CeO <sub>2</sub> U3	76	76	15	78
CeO <sub>2</sub> U4	92	72	20	68
Nano	40	80	9	78

To this point the catalysts that had been tested were prepared using a 3:1 urea to cerium nitrate molar ratio. In a study conducted by Taylor and co-workers the effect of altering the urea to metal nitrate precursor molar ratio upon ceria catalysts for the total oxidation of naphthalene was examined.<sup>10</sup> In the study it was found that the most active ceria catalysts for naphthalene oxidation were prepared using either 1:1 or 1:2 urea to cerium nitrate molar ratios. It was also found that using an even greater excess of urea than a 3:1 ratio yielded higher activity catalysts. Therefore, ceria catalysts were prepared using different urea ratios to determine whether this adjustment to the preparation of the catalyst could lead to greater AA conversion (for experimental details see section 2.2.1). U7 was prepared using a 1:1 urea to nitrate molar ratio, U8

was prepared using a 1:2 ratio, and U9 was prepared using a 5:1 ratio. The testing results for these samples is presented in table 4.4 and none of these materials were found to outperform the U1 catalyst. The activities of U7 and U8 were only slightly less than that of the U1, U2, and U3, however the changes in urea ratio were certainly not found to generate catalysts with improved performance. The activity of the U9 catalyst prepared with greatest urea excess was found to be comparable to that of the U3 catalyst. In this case changing the urea ratio in the preparation of the ceria catalysts was not found to improve the catalyst performance for AA conversion.

Table 4.5 Testing data for ceria catalysts prepared with different urea to nitrate precursor molar ratios. U7 = 1:1 urea to nitrate ratio, U8 = 1:2 urea to nitrate ratio, U9 = 5:1 urea to nitrate ratio.

Sample	Urea:metal nitrate ratio	Initial AA Conversion (%)	CO <sub>2</sub> Selectivity (%)	Acetone Selectivity (%)	Carbon Balance (%)
CeO <sub>2</sub> U7	1:1	90	45	43	59
CeO <sub>2</sub> U8	1:2	86	46	42	60
CeO <sub>2</sub> U9	5:1	75	77	13	78
CeO <sub>2</sub> U1	3:1	94	57	38	63

#### 4.3.2 Testing of Ceria Catalysts Prepared with Structure Directing Agents

To improve the physical properties and enhance the catalytic performance of the ceria materials, preparation methods involving the use of structure directing agents were investigated (for experimental details see sections 2.2.2 and 2.2.3). Templatting agents such as tetradecyltrimethylammonium bromide (TTAB) and Pluronic P123 can be used to increase the surface area and control the porous structure of a material. The preparation of ceria using TTAB was adopted from a study by Yuejuan *et al.*<sup>11</sup>, and the method for preparing ceria using Pluronic P123 was based on research by Yoshikawa *et al.*<sup>12</sup>

Table 4.6 BET surface area data for ceria catalysts prepared with structure directing agents. T1, T2 = TTAB, P1 = Pluronic P123 aged overnight at 60 °C, P2 = Pluronic P123 aged for 7 days at 40°C. CeO<sub>2</sub> U1 is included as a standard reference for a ceria catalyst prepared without a structure directing agent.

Sample	BET Surface Area (m <sup>2</sup> /g)
CeO <sub>2</sub> T1	310
CeO <sub>2</sub> T2	230
CeO <sub>2</sub> P1	50
CeO <sub>2</sub> P2	30
CeO <sub>2</sub> U1	140

The T1 and T2 catalysts prepared using TTAB were found to have very high surface areas from BET analysis (see table 4.5). The surface areas of both the T1 and T2 catalysts were far higher than the ceria samples prepared by standard urea precipitation. However, the activity of the T1 and T2 catalysts was lower than that of the U1 sample (see table 4.6). This could indicate that the BET surface area values for the T1 and T2 catalysts are inaccurate. If they have a microporous structure this can cause discrepancies within BET theory which leads to false results.<sup>13</sup> Also these catalysts were prepared using NaOH as a base and so the catalytic activity of these samples could be dampened by Na<sup>+</sup> poisoning.<sup>14</sup>

The P1 catalyst was aged overnight at 60 °C, whereas the P2 catalyst was aged for 7 days at 40 °C. When using Pluronic P123 long aging times are used to generate the porous structure within the metal oxide being prepared. However, these preparations generated materials with surface areas of 50 and 30 m<sup>2</sup>/g, whereas urea precipitation yielded a material with a surface area of 140 m<sup>2</sup>/g. In the catalyst testing the P1 catalyst was found to convert 69% AA, which was significantly more active than the P2 catalyst which only converted 19% AA. The commercial nanopowder catalyst was also more active than the P2 catalyst with an initial AA conversion of 40%. Raman spectroscopy showed the P2 catalyst to be highly crystalline and to have a very low concentration of defects (see figure 4.12). Defect sites are very important for the catalytic activity of ceria-based catalysts and the lack of defects could help to explain the low activity of the P2 catalyst.<sup>6,15,16</sup> None of the materials generated using

structure directing agents were found to be more active for AA conversion in the gas phase test than the catalysts prepared with urea precipitation.

Table 4.7 Testing data for ceria catalysts prepared with structure directing agents. T1, T2 = TTAB, P1 = Pluronic P123 aged overnight at 60 °C, P2 = Pluronic P123 aged for 7 days at 40°C. CeO<sub>2</sub> U1 is included as a standard reference for a ceria catalyst prepared without a structure directing agent.

Sample	Initial AA Conversion (%)	CO <sub>2</sub> Selectivity (%)	Acetone Selectivity (%)	Carbon Balance (%)
CeO <sub>2</sub> T1	77	63	6	57
CeO <sub>2</sub> T2	87	72	2	57
CeO <sub>2</sub> P1	69	58	38	78
CeO <sub>2</sub> P2	19	76	9	92
CeO <sub>2</sub> U1	94	57	38	63

#### 4.4 Effect of Space Velocity on Activity

It was deemed necessary to increase the space velocity of testing as it is not optimal to study catalysts at such high conversions. At the lower space velocities many of the catalysts were achieving initial activities of > 90%, which can be problematic due to mass transfer limitations. It could be the case that catalysts were more active than the test was able to reveal, and that the activity of the test was limited by mass transfer. This means that the conversion can be limited by the rate at which the reactant reaches the catalyst surface, not by the properties of the catalyst itself. Conversion measurements do not give much insight into diffusion limitations affecting the reaction. Diffusion limitations can be identified using activation energies (derived from the Arrhenius equation) or by measuring the effect of catalyst particle size or flow rate. According to Bond diffusion limitations can begin to play a part at conversions of 50% and often become dominant once conversion is above 75%.<sup>17</sup> Therefore, Bond recommends testing catalysts in a regime where conversion will be less than 30%, to ensure that the observed activity is within the kinetic regime. Catalyst activities are most often compared using reaction rate rather than conversion. However, if the reaction is taking place within the kinetic regime then the conversion is directly proportional to the reaction rate.

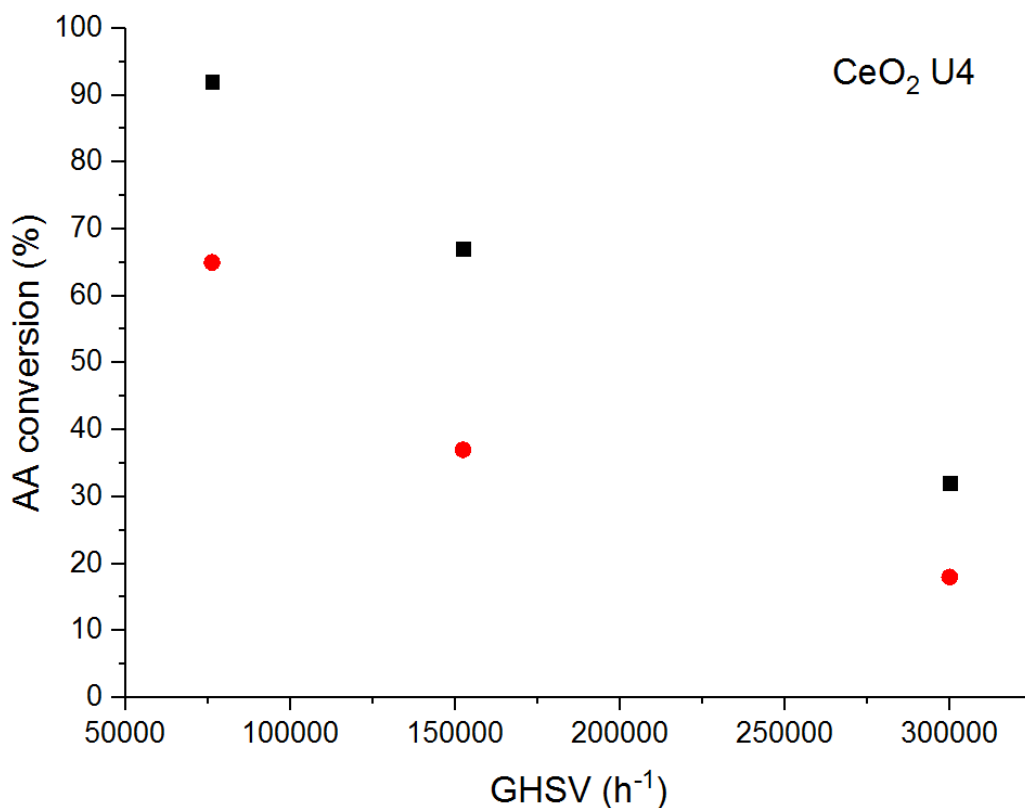


Figure 4.2 Effect of increasing GHSV on activity of CeO<sub>2</sub> U4 for AA conversion. Black squares = initial activity, red circles = average activity. Conditions: 1000 ppm AA/He flowed over a CeO<sub>2</sub> catalyst bed at increasing space velocity at 300 °C for 3 hours.

To test the effect of increasing the space velocity upon the activity of catalysts in this reaction, the U4 catalyst was tested at three different space velocities (see figure 4.1). The first result is taken from the testing using a 50 ml/min flow rate and a 50 mg catalyst loading which corresponds to a GHSV of 76,200 h<sup>-1</sup> due to the density of U4 being 1.27 g/ml (for details on GHSV calculations see section 2.3.1). When the gas flow was increased to 100 ml/min this yielded a space velocity of 152,400 h<sup>-1</sup>, and when the flow was further increased to 200 ml/min and the catalyst loading was slightly increased to 51 mg a space velocity of 300,000 h<sup>-1</sup> was the result. A space velocity of 300,000 h<sup>-1</sup> corresponds to a residence time of 0.012 s, whereas a space velocity of 76,200 h<sup>-1</sup> is equal to a residence time of 0.047 s. At the lowest space velocity the initial AA conversion was 92%. When the space velocity was doubled the initial conversion was reduced to 67%, and when the highest space velocity was used the conversion was equal to 32%. An activity of 32% is much closer to regime within which Bond proposes catalyst testing should be undertaken, so these conditions are

more suitable for measuring the effectiveness of the ceria catalysts for AA conversion. When the space velocity was increased by a factor of 2 the conversion only decreased by less than a factor of 1.5, this suggests that at a space velocity of  $76,200\text{ h}^{-1}$  there were some mass transfer limitations. However, when the space velocity was further increased by close to a factor of 2, the decrease in conversion was much closer to a factor of 2. This suggests that mass transfer is playing a much less significant role at the reactions run at higher space velocities.

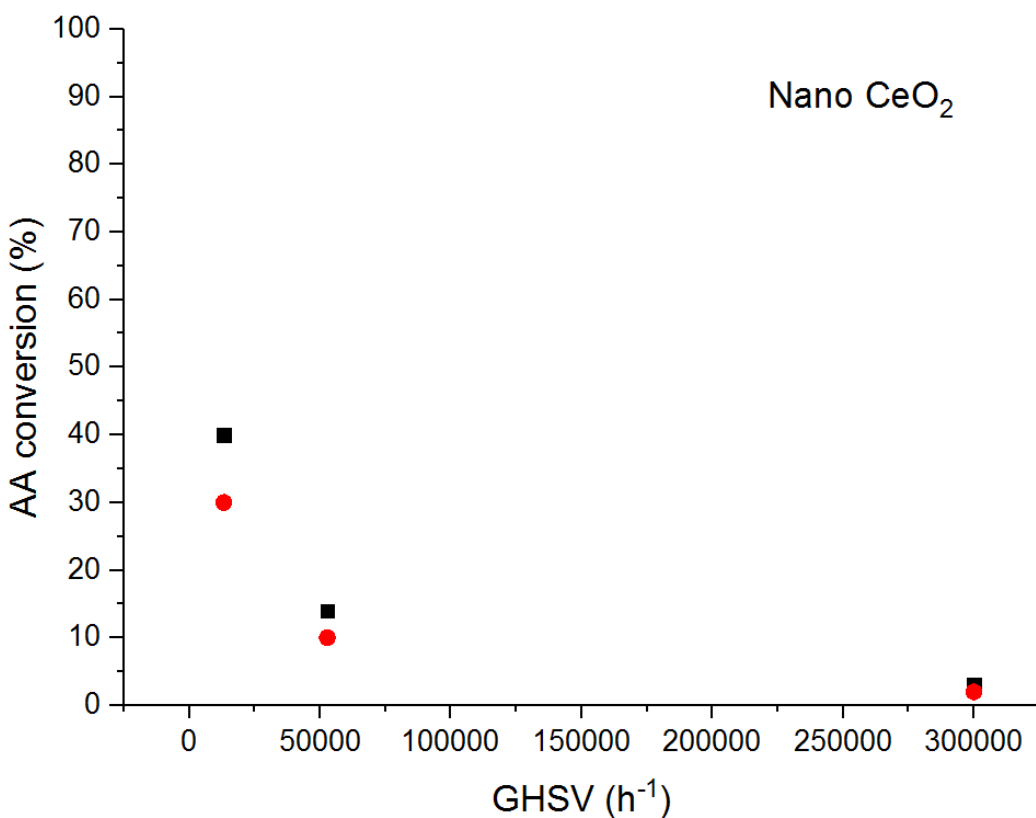


Figure 4.3 Effect of increasing GHSV on activity of Nano CeO<sub>2</sub> for AA conversion. Circles = initial activity, squares = average activity. Conditions: 1000 ppm AA/He flowed over a CeO<sub>2</sub> catalyst bed at increasing space velocity at 300 °C for 3 hours.

A similar study was also conducted using the less active commercial nano ceria catalyst (see figure 4.2). Due to the density of this material being only 0.22 g/ml the original space velocities that it was tested at were far lower than for the U4 catalyst. The initial test was conducted at a space velocity of  $13,200\text{ h}^{-1}$  and the initial conversion of AA under these conditions was 40%. When the flow was increased to 200 ml/min the velocity was increased to  $52,800\text{ h}^{-1}$  the initial AA conversion

decreased to 14%. To test at a space velocity of  $300,000\text{ h}^{-1}$  the catalyst loading was reduced from 50 mg to 9 mg, and as result of this the conversion was further reduced to 3%. Due to the conversion of AA nearing 0% at  $300,000\text{ h}^{-1}$  it is more difficult to directly compare the activity at the different space velocities, however the conversion of AA is clearly reduced by increasing the space velocity of the reaction.

## 4.5 Testing at a GHSV of $300,000\text{ h}^{-1}$

For testing at higher space velocities, the reaction time was reduced as only the initial activity is of relevance for the end process. The process under which these catalysts were tested for their performance in PET, involved a reaction window of 285 °C for roughly 1 minute (see chapter 5). Therefore, the selectivities quoted in the following datasets are not average values but the values associated with the initial activity. A selection of catalysts were retested at an increased space velocity of  $300,000\text{ h}^{-1}$  which involved using a 200 ml/min flow of gas and a particular volume of catalyst dependent upon the density of the material. In the previous testing the catalysts were compared using the same mass, whereas under this testing regime the catalysts were compared using the same volume.

### 4.5.1 Testing of Ceria Catalysts Prepared by Urea Precipitation

In the same way that the experimental error was established under the previous testing conditions, the U1 catalyst was tested in triplicate to identify the level of variation between tests (see table 4.7). The mean initial conversion for the three tests was found to be 31% with a standard deviation of  $\pm 3\%$ , therefore the margin of error is very similar at higher space velocities as it was previously. One difference under the new testing conditions is that there is far less selectivity towards CO and CH<sub>4</sub>, which suggests that those products are only formed when there is a longer contact time between the AA and the catalyst. At the shorter residence times there is either very little formation of CO and CH<sub>4</sub> observed or none at all. Also, the carbon balance is significantly higher than at lower space velocities, and this could indicate that less high molecular weight products are able to form during the shorter residence times. Although, carbon balance can also be affected by discrepancies in response factors for the reactants versus the products. For instance, if the response factor for the reactant

is more accurate than for the reaction products, then a lower conversion will lead to a more accurate carbon balance.

Table 4.8 Repeated experiments using U1 catalyst. All values are taken from the first injection. Conditions: 1000 ppm AA in He at 200 ml/min, catalyst loading of 61 mg, GHSV = 300,000 h<sup>-1</sup>, 300 °C for 1 hour.

<b>Sample</b>	<b>Initial AA Conversion (%)</b>	<b>CO<sub>2</sub> Selectivity (%)</b>	<b>Acetone Selectivity (%)</b>	<b>Carbon Balance (%)</b>
CeO <sub>2</sub> U1 (1)	34	71	25	81
CeO <sub>2</sub> U1 (2)	32	74	26	80
CeO <sub>2</sub> U1 (3)	28	74	26	82
Average	31 (± 3)	73 (± 2)	26 (± 1)	81 (± 1)

The ceria catalysts prepared *via* urea precipitation with a 3:1 urea ratio were retested at a space velocity of 300,000 h<sup>-1</sup> (see table 4.8). The same trend is observed for these catalysts as was seen previously, whereby U1, U2, and U4 all have comparable activities while U3 is less active. The difference in activity between U3 and the most active sample in table 4.3 was 19% (76:94), and the discrepancy between U3 and the highest conversion in this case was also 19% (26:32). This gives good confirmation that the data is reproducible across the different testing regimes. And in general, suggests that the urea precipitation method for preparing ceria catalysts is reproducible.

Table 4.9 Testing data for ceria catalysts prepared using a 3:1 urea to nitrate precursor molar ratio. Conditions: 1000 ppm AA in He at 200 ml/min, GHSV = 300,000 h<sup>-1</sup>, 300 °C for 1 hour.

<b>Sample</b>	<b>Initial AA Conversion (%)</b>	<b>CO<sub>2</sub> Selectivity (%)</b>	<b>Acetone Selectivity (%)</b>	<b>Carbon Balance (%)</b>
CeO <sub>2</sub> U1	31	73	26	81
CeO <sub>2</sub> U2	30	76	22	81
CeO <sub>2</sub> U3	26	76	24	85
CeO <sub>2</sub> U4	32	75	19	80

#### 4.5.2 Effect of Ball Milling on Activity of Ceria Catalysts

Catalyst samples were milled in a planetary ball mill for 3 hours at 300 rpm. This was done to reduce the particle size of the catalyst which could later aid dispersion when adding it to PET. However, the greatest effect upon the material caused by the milling was to increase the density of the powder. The average crystallite size of the milled materials was calculated from XRD analysis using the Scherrer equation (see equation 2.7). The average crystallite size of the nano CeO<sub>2</sub> was found to decrease from 315 to 270 Å due to the milling, and the average crystallite size of the U6 catalyst was reduced from 81 to 79 Å. These changes in crystallite size are small and insignificant, and the Scherrer equation is not accurate enough to quantify such small changes in average crystallite size. Whereas, the density of the nano CeO<sub>2</sub> catalyst increased from 0.22 g/ml to 2.25 g/ml and the density of the U6 material increased from 1.70 g/ml to 2.28 g/ml. In terms of both crystallite size and density, the effect of milling upon the nano CeO<sub>2</sub> was more significant than its impact upon U6. This enabled the nano catalyst to achieve a far greater AA conversion, which increased from 3% to 23% (see table 4.9). However, the activity of the U6 catalyst was only slightly improved, increasing from 31% to 36%. Increasing the density of a material means more mass can be packed into a smaller volume, and this could account for why the catalysts with increased density achieve a greater conversion.

Table 4.10 Testing data for ceria catalysts milled in planetary ball mill at 300 rpm for 3 hours. Conditions: 1000 ppm AA in He at 200 ml/min, GHSV = 300,000 h<sup>-1</sup>, 300 °C for 1 hour.

Sample	Density (g/ml)	Initial AA Conversion (%)	CO <sub>2</sub> Selectivity (%)	Acetone Selectivity (%)	Carbon Balance (%)
Nano CeO <sub>2</sub>	0.22	3	100	0	98
Nano CeO <sub>2</sub> ball milled	2.25	23	75	25	88
CeO <sub>2</sub> U6	1.70	31	76	23	81
CeO <sub>2</sub> U6 ball milled	2.28	36	71	25	78

### 4.5.3 Effect of Drying on Activity of Ceria Catalysts

To identify the effect of moisture in the catalyst material upon the activity of the materials, samples were dried overnight in a vacuum oven at 120 °C. The TGA data in figure 4.4 shows that the dried material showed much less mass loss below 150 °C than the materials which were not dried. The TGA data indicates that between 3-4% of the mass of the non-dried materials was moisture, and in the dried material this moisture has been removed. From the data in table 4.10, the initial AA conversion achieved by these materials is far less than that achieved by the undried samples. Drying reduced the activity of the U6 catalyst from 31% to 14% and the ball milled U6 catalyst was reduced from 36% to 19%. This suggests that surface hydroxides play a large role in the reaction mechanism for conversion of AA on a ceria surface. When these surface species are removed by drying, the catalyst becomes less effective for the conversion AA. This offers support as to why Rule specifies that the AA removal catalyst is a hydrous zirconium oxide, and these results indicate that the presence of the hydration is crucial for the catalyst performance.<sup>4</sup>

Table 4.11. Testing data for dried and undried catalysts, samples dried overnight in vacuum oven at 120 °C. Conditions: 1000 ppm AA in He at 200 ml/min, GHSV = 300,000 h<sup>-1</sup>, 300 °C for 1 hour.

Sample	Initial AA Conversion (%)	CO <sub>2</sub> Selectivity (%)	Acetone Selectivity (%)	Carbon Balance (%)
CeO <sub>2</sub> U6	31	76	23	81
CeO <sub>2</sub> U6 dried	14	80	20	90
CeO <sub>2</sub> U6 ball milled	36	71	25	78
CeO <sub>2</sub> U6 ball milled dried	19	77	23	89

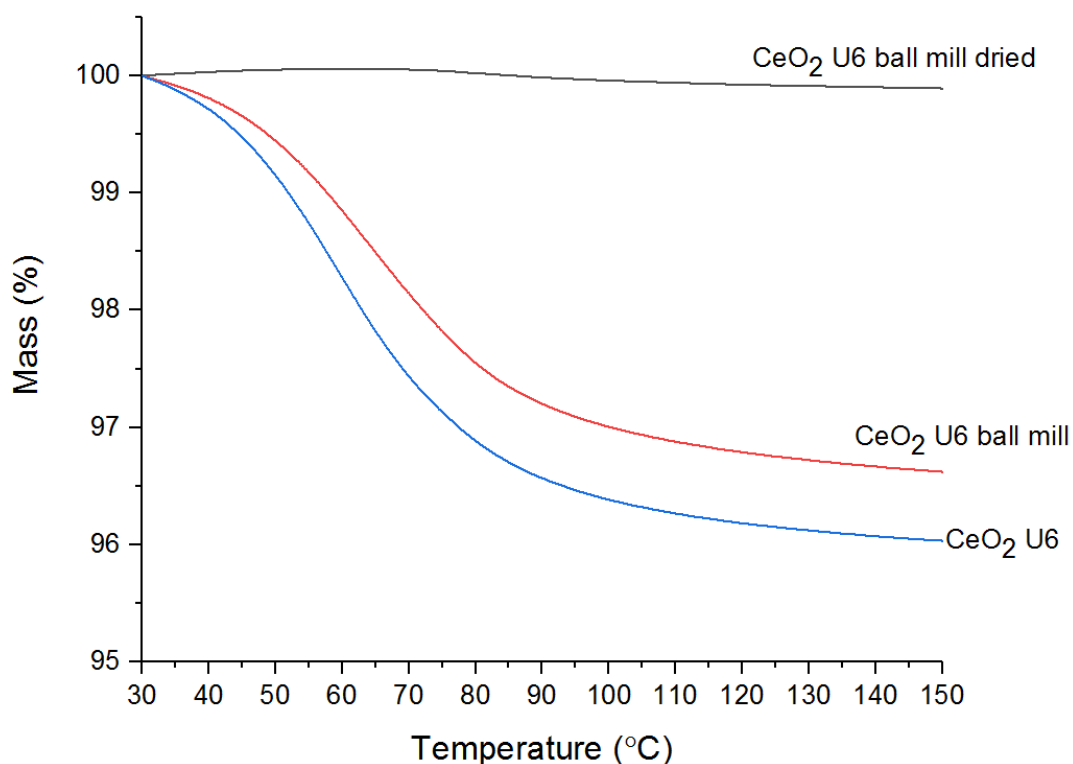


Figure 4.4 TGA data up to 150  $^{\circ}\text{C}$  for the dried and the non-dried materials. Black line =  $\text{CeO}_2$  U6 ball mill dried, red line =  $\text{CeO}_2$  U6 ball mill, blue line =  $\text{CeO}_2$  U6

#### 4.5.4 Testing of Doped Ceria Catalysts

Another technique for the enhancement of ceria as a catalytic material is through the addition of dopants. Doping with zirconia has been shown to increase the OSC of ceria and has been studied extensively for use in automotive catalysis in three-way catalysts.<sup>18–20</sup> The addition of copper oxide to ceria has been shown to increase the concentration of lattice defects in the material and hence offer greater catalytic performance for oxidation reactions, such as the total oxidation of naphthalene and carbon monoxide oxidation.<sup>16,21</sup>

Table 4.12 BET and Raman spectroscopy analysis data for ceria catalysts doped with a 5% loading of other metal oxides. CeO<sub>2</sub> U1 is included as a standard reference for a ceria catalyst prepared without a dopant.

Sample	BET Surface Area (m <sup>2</sup> /g)	Raman Defect Ratio (I <sub>600</sub> /I <sub>460</sub> )
5%ZrO <sub>x</sub> -CeO <sub>2</sub>	170	0.03
5%MnO <sub>x</sub> -CeO <sub>2</sub>	95	0.006
5%CuO <sub>x</sub> -CeO <sub>2</sub>	105	0.1
CeO <sub>2</sub> U1	140	0.02

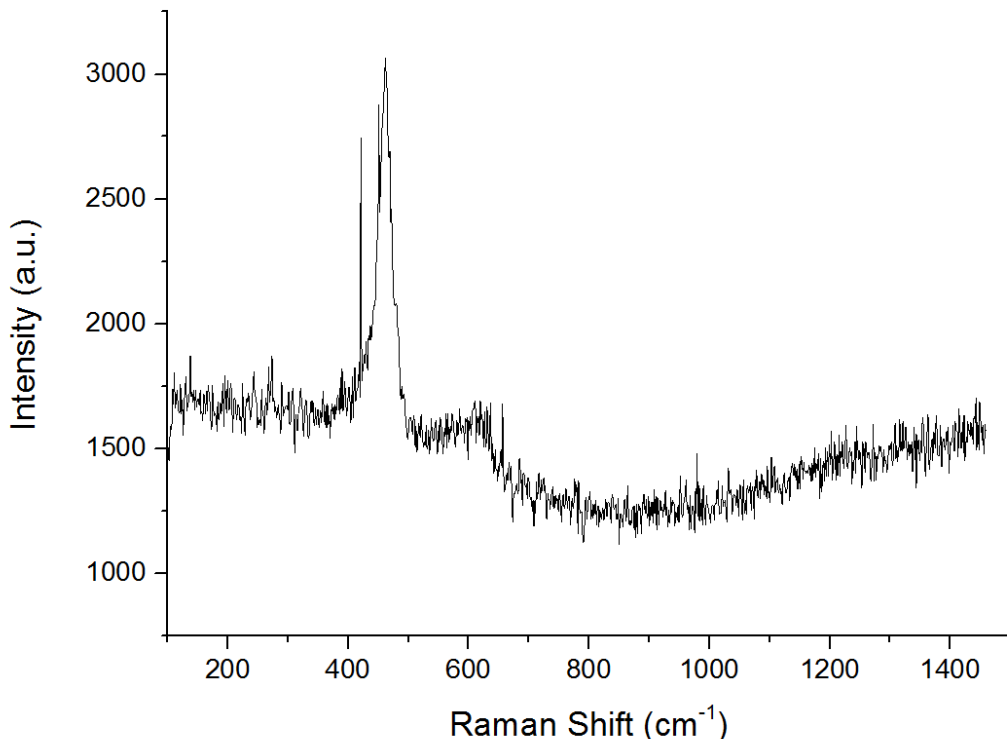


Figure 4.5 Raman spectrum of 5%CuOx-CeO<sub>2</sub>

The testing data for the doped ceria catalysts is presented in table 4.12, and it was found that the zirconia and copper doped materials were more effective, 29% and 27% respectively, than the ceria doped with manganese, 17%. However, the doped catalysts were still slightly less active than the urea precipitation catalysts that were able to achieve a reduction in AA of >30%. Raman spectroscopy was able to confirm that doping the ceria with copper oxide does indeed increase the concentration of defects. The Raman defect ratio increased by a factor of 10 in comparison to the U1

catalyst (see table 4.11). The Raman defect ratio is calculated by taking the ratio between the  $F_{2g}$  band at about  $460\text{ cm}^{-1}$  and the “defect” band at around  $600\text{ cm}^{-1}$ . The larger the ratio, the higher the concentration of defects in the lattice of the ceria-based material.<sup>22</sup> In this case the increase in defects does not lead to an increase in AA conversion which could indicate that, although increased defect concentration leads to greater activity in oxidation reactions, it is not such an important parameter for the system being studied here. The surface area seems to have a larger influence on the catalyst activity as the two higher surface area materials achieve the greatest AA conversion. However, the zirconia doped sample has a slightly lower initial conversion than the U1 catalyst despite having a higher BET surface area. This suggests that the addition of the zirconia is not enhancing the properties of the catalyst, because the conversion is comparable to the undoped ceria.

Table 4.13 Testing data for ceria catalysts doped with a 5% loading of other metal oxides.  $\text{CeO}_2$  U1 is included as a standard reference for a ceria catalyst prepared without a dopant. Conditions: 1000 ppm AA in He at 200 ml/min, GHSV = 300,000  $\text{h}^{-1}$ , 300 °C for 1 hour.

Sample	Initial AA Conversion (%)	$\text{CO}_2$ Selectivity (%)	Acetone Selectivity (%)	Carbon Balance (%)
5% $\text{ZrO}_x$ - $\text{CeO}_2$	29	78	19	81
5% $\text{MnO}_x$ - $\text{CeO}_2$	17	80	20	89
5% $\text{CuO}_x$ - $\text{CeO}_2$	27	71	24	84
$\text{CeO}_2$ U1	31	73	26	81

In a study conducted by Kydd *et al.* it was found that loading ceria and other metal oxides with copper did increase conversion of AA.<sup>5</sup> However, in that research they were not using mixed metal oxides, the copper was added as metal nanoparticles and the ceria was used as a catalyst support. Also, the catalyst testing was carried out in the presence of air (200 ppm AA in air) so that the AA was totally oxidised to  $\text{CO}_2$ . The different conditions used meant that 100% AA conversion was observed at below

200 °C with a 4wt% Cu/CeO<sub>2</sub> catalyst. The system under investigation in this thesis is very different and so different outcomes have been observed.

## 4.6 Structure-Activity Relationship

It has been demonstrated that CeO<sub>2</sub> is more effective than ZrO<sub>2</sub> and Mn<sub>2</sub>O<sub>3</sub> for converting AA at 300 °C. Consequently, CeO<sub>2</sub> was prepared *via* a variety of methods to attempt to improve upon the urea precipitation catalysts. However, the urea precipitation material remained the benchmark material. The characterisation of the CeO<sub>2</sub> catalysts will be examined to attempt to determine what properties are important for an effective AA conversion catalyst. The catalysts underwent extensive characterisation including BET surface area analysis, Raman spectroscopy, powder XRD, and XPS in order to identify any correlations between physicochemical properties and catalyst activity. This can help to establish a structure-activity relationship which can then guide future catalyst development in this area. One of the most important characteristics for the effectiveness of ceria in catalysis is its ability to form oxygen defect sites. Many studies have been written on the influence of oxygen defects upon the catalytic performance of ceria-containing materials.<sup>6,15,16</sup> The majority agree that the ability of ceria to generate and degenerate oxygen vacancy sites is fundamental to the activity of the catalyst, especially for oxidation reactions.

### 4.6.1 Influence of Surface Area

Surface area is an important parameter for the effectiveness of a heterogeneous catalyst. The surface area of a material can be calculated by adsorbing N<sub>2</sub> onto a material at cryogenic temperatures and through the processing of the isotherm data using the BET equation (see section 2.4.4). One factor that is worth bearing in mind when using BET surface area is that the error in the measurement can be as high as 20%.<sup>23</sup> Therefore, similar BET surface area values cannot be distinguished from each other.

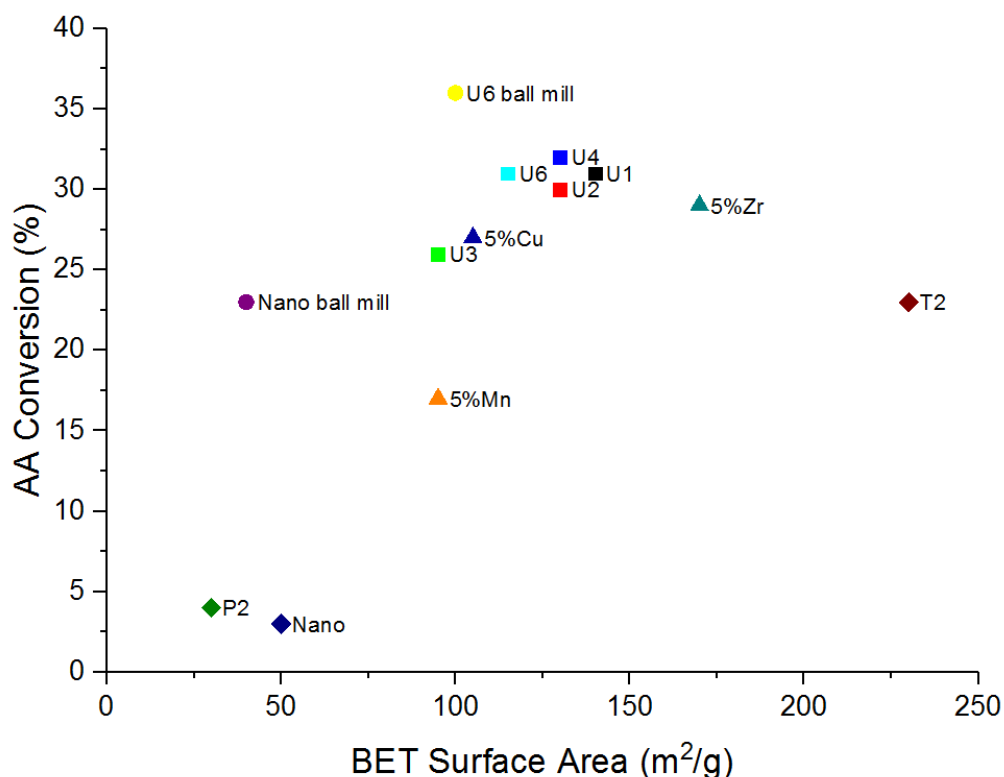


Figure 4.6 Correlation between BET surface area and AA conversion at  $300,000\text{ h}^{-1}$  at  $300\text{ }^\circ\text{C}$  for various ceria catalysts. Black square = U1, red square = U2, green square = U3, blue square = U4, light blue square = U6, yellow circle = U6 ball mill, purple circle = nano ball mill, brown diamond = T2, green diamond = P2, blue diamond = nano, green triangle = 5%Zr, blue triangle = 5%Cu, orange triangle = 5%Mn

There is a general trend within the data showing that increased surface area leads to increased conversion of AA. It is likely that the T2 material is an outlier in this case due to micropores in its structure, as T2 was prepared using the surfactant TTAB to introduce greater porosity into the material. It is well established that BET theory cannot be accurately applied to microporous materials, so this value could be inflated due to these limitations.<sup>13</sup> The T2 was able to adsorb 46 cc/g of  $\text{N}_2$  at a  $\text{P}/\text{P}_0$  ratio of 0.05 which is the lowest pressure value obtained in a standard five point BET experiment. This large uptake of  $\text{N}_2$  at low pressure does indicate that this is a microporous material, which supports the hypothesis that the high BET surface area of the T2 material is erroneous. Microporous materials are generally incompatible with BET theory because monolayer coverage is so ill-defined for materials containing micropores.<sup>13</sup> To overcome this, it is advised that the following criteria should be met: C should be positive, only use the range where  $n(1-\text{P}/\text{P}_0)$  continuously increases with  $\text{P}/\text{P}_0$ , and the value of  $\text{P}/\text{P}_0$  that corresponds with  $V_m$  should be within the BET range.<sup>24</sup>

The P2 and nano catalysts show that low surface area materials are not as effective as catalysts for this reaction. The ball milled nano material is most likely more active than the other catalysts with similar surface areas due to its increased density, as previously discussed. The most effective catalysts in the gas phase reaction were found to have a BET surface of  $> 100 \text{ m}^2/\text{g}$  which is considered to be a high surface area for ceria materials. Ceria with a surface area of  $88 \text{ m}^2/\text{g}$  is referred to as a high surface area material in the scientific literature.<sup>25</sup> This elucidates how the urea precipitation method is a very good technique for preparing high surface area ceria.

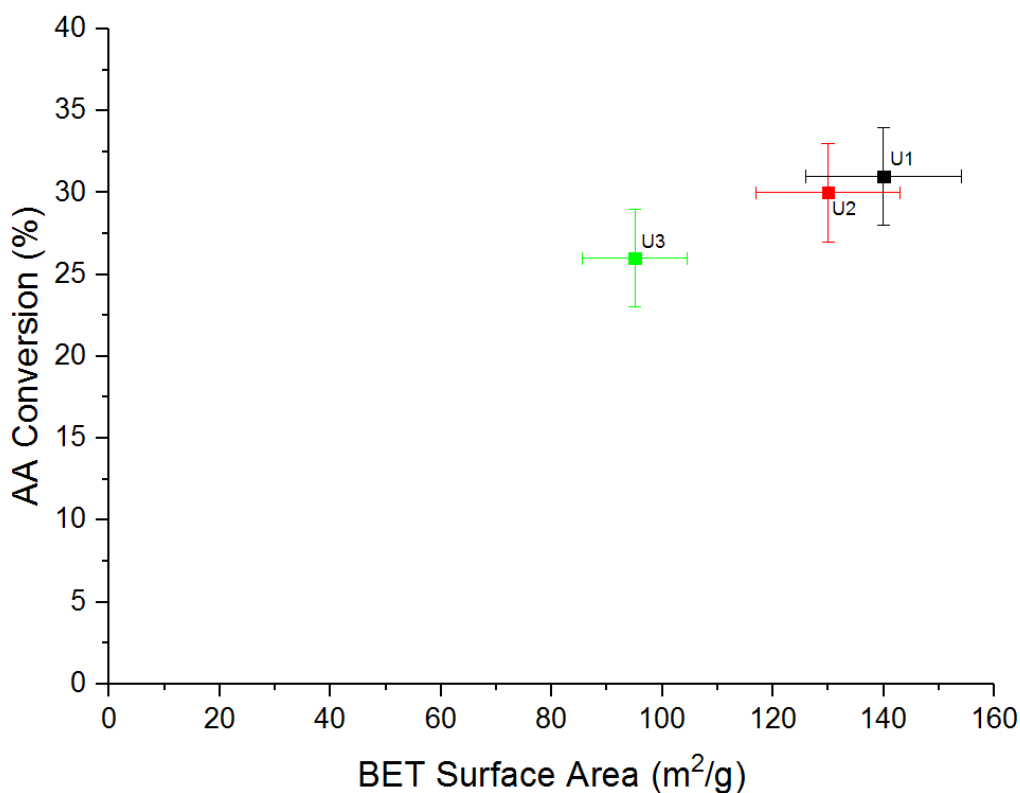


Figure 4.7 Correlation between BET surface area and AA conversion at  $300,000 \text{ h}^{-1}$  at  $300^\circ\text{C}$  for ceria catalysts U1, U2, U3. Black square = U1, red square = U2, green square = U3 (with error bars)

If catalysts prepared using the same preparation method are compared such as the U1, U2, and U3 catalysts, the relationship between AA conversion and BET surface area is close to linear. The U1 and U2 catalysts have similar surface areas and their activity is comparable. However, the U3 catalyst has a lower BET surface area and this is reflected in its lower performance for the conversion of AA.

These three materials were also subjected to full N<sub>2</sub> adsorption/desorption isotherms using a Micromeritics 3flex. It was found that the U1 and U2 had similar N<sub>2</sub> uptakes at low relative pressure (up to 0.1 P/P<sub>0</sub>), while the U3 was able to adsorb less than both of those materials. This indicates that the U1 and U2 catalysts have greater microporosity than the U3 material which could act as an indicator for effectiveness in AA conversion catalysis. The total porosity of the U3 catalyst is comparable to that of the U1 material yet its catalytic performance is less. This suggests that the microporosity could be a more important parameter for catalytic activity in this system than the total porosity. The BET surface areas measured using the 3flex apparatus were 151, 133, and 102 m<sup>2</sup>/g for the U1, U2 and U3 materials respectively which offer good confirmation of the values measured on the Quantachrome.

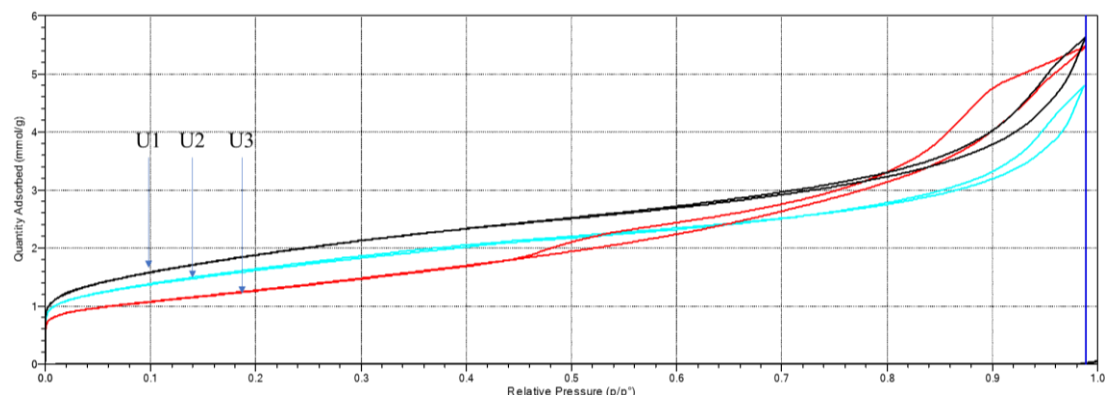


Figure 4.8 Full N<sub>2</sub> adsorption and desorption isotherms for U1, U2 and U3 catalysts. Black = U1, blue = U2, red = U3.

#### 4.6.2 Influence of Crystallite Size

The average crystallite size of a material can be measured using the Scherrer equation (see equation 2.7) in conjunction with powder XRD data. The four major reflections of the ceria diffraction pattern (111, 200, 220, 311) were used to calculate the crystallite size of the material. Smaller crystallite sizes often lead to increased catalytic activity due to the greater surface area of the materials.

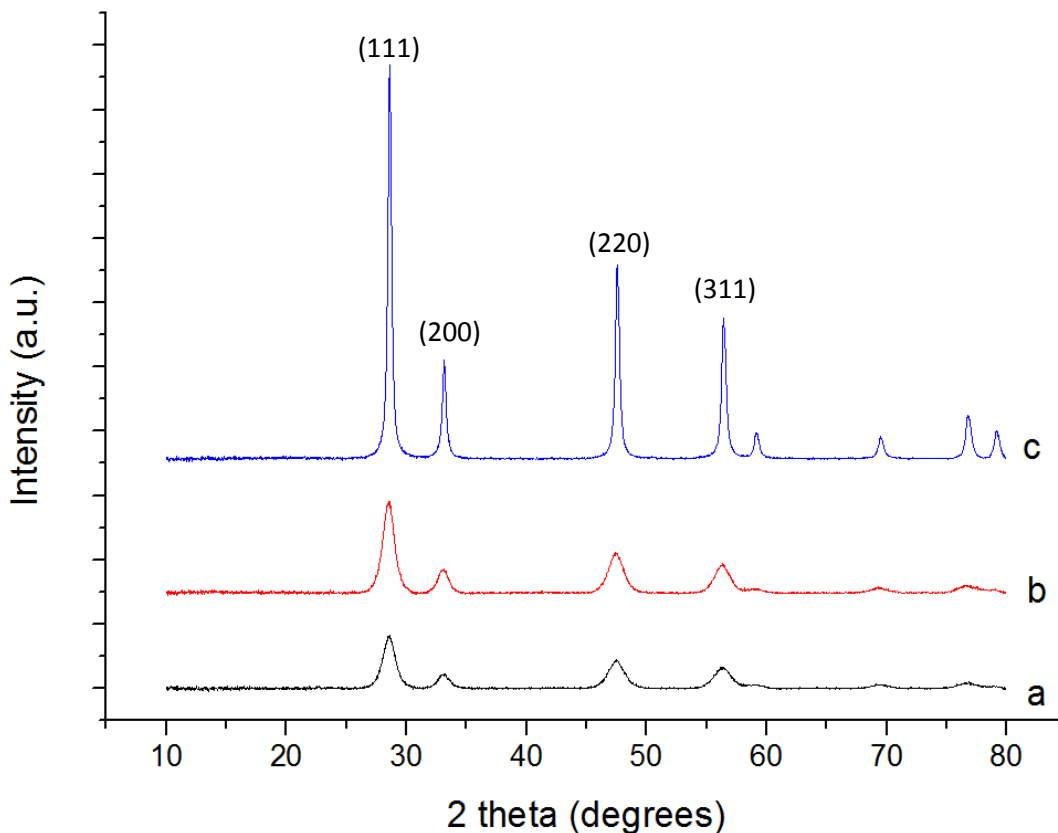


Figure 4.9 PXRD patterns for different CeO<sub>2</sub> catalysts. a = U1, b = U2, c = commercial nano powder

In figure 4.7 PXRD patterns for ceria are displayed which show the major reflections of (111) at around 28 °, (200) at around 33 °, (220) at around 47 °, and (311) at around 56 °. This diffraction pattern is indicative of a cubic fluorite structure which is the most common crystal structure for CeO<sub>2</sub>.<sup>26</sup> The diffraction patterns in figure 4.7 show the greater crystallinity of the commercial ceria in comparison to the lab prepared U1 and U2 samples. The commercial ceria is shown to be more crystalline due to the greater intensity and resolution of the reflections. However, the testing data suggests that the more amorphous U1 and U2 are more active for AA conversion. Whilst the surface areas of U1 and U2 are also greater than the commercial sample, the more defective crystal structures of U1 and U2 could also contribute to their enhanced activities.

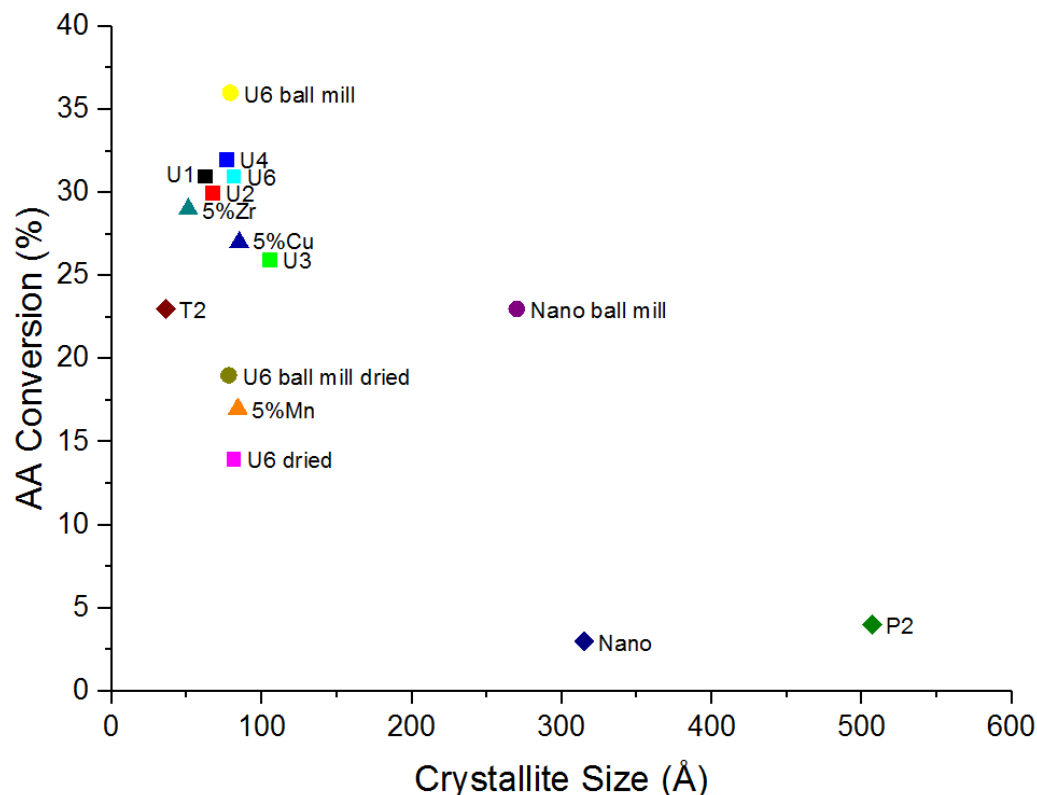


Figure 4.10 Correlation between crystallite size and AA conversion at  $300,000 \text{ h}^{-1}$  at  $300^\circ\text{C}$  for various ceria catalysts. Black square = U1, red square = U2, green square = U3, blue square = U4, light blue square = U6, pink square = U6 dried, yellow circle = U6 ball mill, purple circle = nano ball mill, green circle = U6 ball mill dried, brown diamond = T2, green diamond = P2, blue diamond = nano, green triangle = 5%Zr, blue triangle = 5%Cu, orange triangle = 5%Mn

As anticipated the catalysts with smaller crystallite sizes tend to achieve greater AA conversions. The nano and P2 samples have the largest crystallite sizes which are consistent with the low BET surface areas from figure 4.4. The T2 catalyst has the smallest crystallite size which is again consistent with the high surface area measured using BET. Most of the catalysts have an average crystallite size of below 100 Å (10 nm) which confirms the nanocrystalline nature of these materials. And the catalysts with an average crystallite size less than 100 Å are found to be more active for the conversion of AA.

In figure 4.9 the catalysts prepared using urea precipitation are compared and the U3 catalyst which has the highest average crystallite size is the least active. This is in agreement with figure 4.4, where increasing BET surface area was shown to lead to increased catalytic activity.

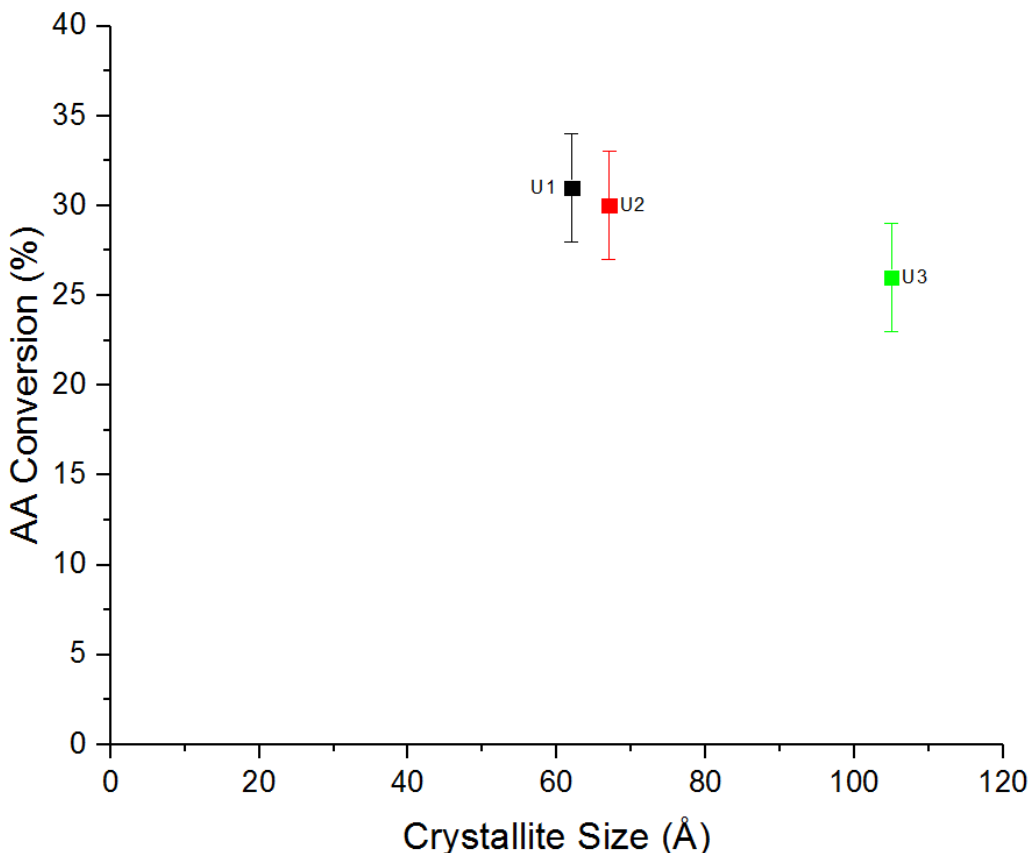


Figure 4.11 Correlation between crystallite size and AA conversion at  $300,000\text{ h}^{-1}$  at  $300\text{ }^\circ\text{C}$  for ceria catalysts U1, U2, U3. Black square = U1, red square = U2, green square = U3 (with error bars)

#### 4.6.3 Influence of Raman FWHM

$\text{CeO}_2$  has a characteristic  $\text{F}_{2g}$  band found at around  $460\text{ cm}^{-1}$  in its Raman spectrum, the FWHM of which is related to the crystallite size of the material.<sup>27</sup> The FWHM has an inverse relationship to the crystallite size, therefore as the FWHM value increases the crystallite size decreases. This means that a larger FWHM should be indicative of a catalyst with greater activity, in the same way that greater BET surface and smaller average crystallite size are.

In figure 4.10, the Raman FWHM of the ceria catalysts is plotted against the AA conversion achieved by the catalysts in the gas phase reactor. A general trend between increasing FWHM and increasing AA conversion can be observed. In agreement with the BET and XRD data, the P2 and nano catalysts are shown to have the lowest FWHM values. The catalysts with a FWHM greater than  $20\text{ cm}^{-1}$  are generally found to convert more AA at  $300\text{ }^\circ\text{C}$ .

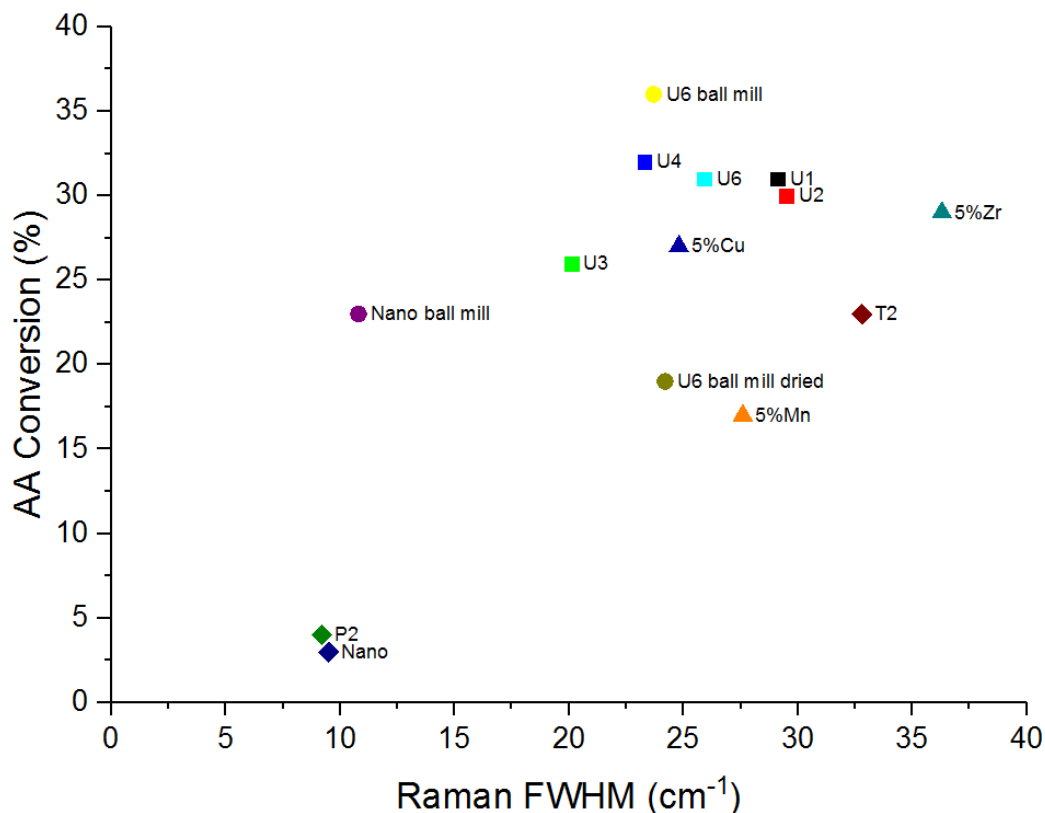


Figure 4.12 Correlation between  $F_{2g}$  Raman band FWHM and AA conversion at  $300,000\text{ h}^{-1}$  at  $300\text{ }^{\circ}\text{C}$  for various ceria catalysts. Black square = U1, red square = U2, green square = U3, blue square = U4, light blue square = U6, yellow circle = U6 ball mill, purple circle = nano ball mill, green circle = U6 ball mill dried, brown diamond = T2, green diamond = P2, blue diamond = nano, green triangle = 5%Zr, blue triangle = 5%Cu, orange triangle = 5%Mn

When the urea precipitation catalysts U1, U2, and U3 are compared the activity of the catalysts is found to increase with greater FWHM values. U1 and U2 have comparable FWHM values and comparable activity, whereas U3 has a lower FWHM value and is found to be less active for AA conversion in the gas phase reactor.

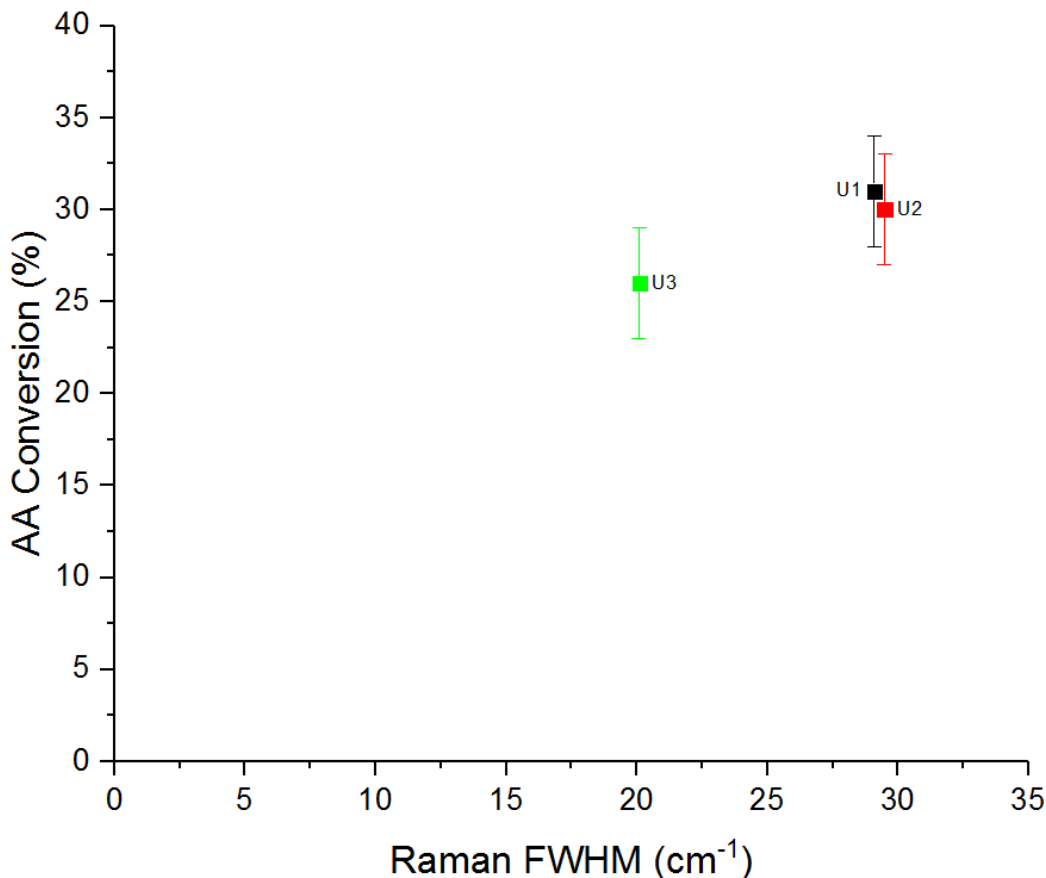


Figure 4.13 Correlation between crystallite size and AA conversion at 300,000 h<sup>-1</sup> at 300 °C for ceria catalysts U1, U2, U3. Black square = U1, red square = U2, green square = U3 (with error bars)

#### 4.6.4 Influence of Oxygen Defects

Raman spectroscopy can also be used to give an indication of the oxygen defect concentration of ceria by calculating the ratio between the  $F_{2g}$  band and the “defect” band. The “defect” band is a signal found at a higher Raman shift than the  $F_{2g}$  band at around 600 cm<sup>-1</sup>.<sup>22</sup> As previously mentioned, oxygen defects are very important for the catalytic activity of ceria so this feature of Raman spectroscopy makes it a very powerful tool for studying ceria-based catalysts. In figures 4.12 and 4.13 Raman spectra for two ceria catalysts are shown. Figure 4.12 contains the spectrum for a ceria catalyst prepared using urea precipitation and a small signal can be seen at around 600 cm<sup>-1</sup> which represents the defect band. The area of this signal is divided by the area of  $F_{2g}$  band at around 460 cm<sup>-1</sup> to give a ratio which is indicative of the prevalence of oxygen defect sites in the material. Figure 4.13 displays the spectrum for a ceria catalyst prepared using Pluronic P123 and shows that the defect band for this material

is much smaller than for the U1 catalyst, indicating that the ceria contains fewer defect sites.

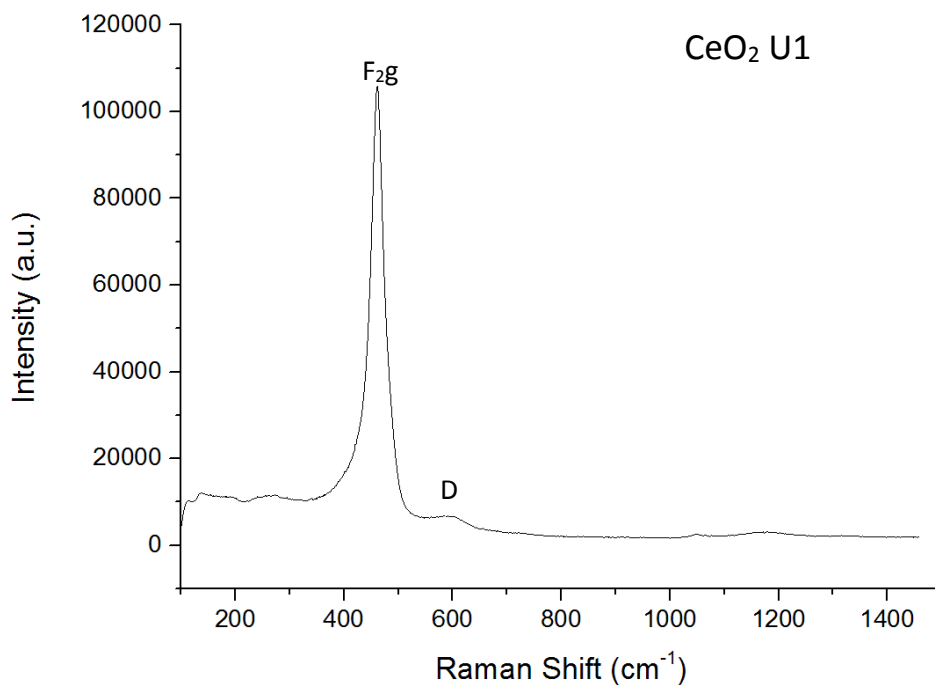


Figure 4.14 Laser Raman spectrum for U1 catalyst (with F<sub>2g</sub> and defect (D) bands labelled). Laser  $\lambda = 514 \text{ cm}^{-1}$

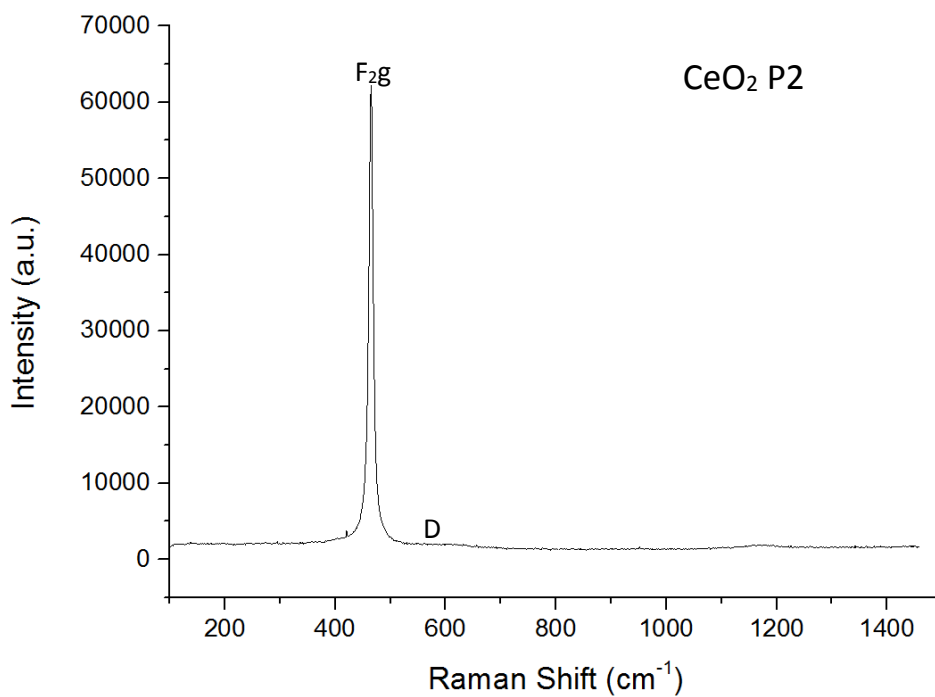


Figure 4.15 Laser Raman spectrum for P2 catalyst (with F<sub>2g</sub> and defect (D) bands labelled). Laser  $\lambda = 514 \text{ cm}^{-1}$

The catalysts were compared for their activity relative to their Raman defect ratio value and the data is plotted in figure 4.14. The P2 and nano catalysts have ratios very close to 0 and this is reflected in their poor activity for AA conversion. The most active catalysts have a ratio of around 0.02 and the catalyst doped with 5% CuO is an outlying result with a ratio of 0.14 but an AA conversion of 27%. As previously mentioned, doping with CuO causes an increase in defect concentration in CeO<sub>2</sub> and that is shown to be the case here also, however this has not led to an increase in catalytic activity. This seems to indicate that the defect concentration in the ceria lattice is not the most important parameter for the conversion of AA at 300 °C in an anaerobic atmosphere.

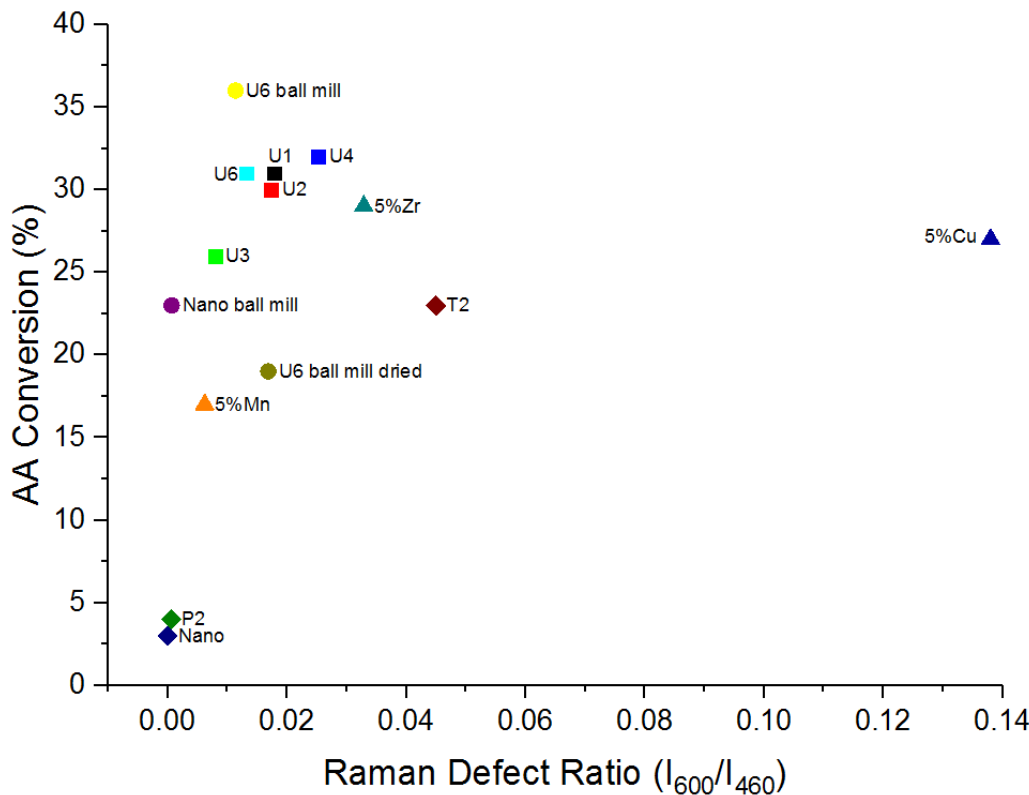


Figure 4.16 Correlation between ratio of the peak areas of Raman bands at 600 and 460 cm<sup>-1</sup> and AA conversion at 300,000 h<sup>-1</sup> at 300 °C for various ceria catalysts. Black square = U1, red square = U2, green square = U3, blue square = U4, light blue square = U6, yellow circle = U6 ball mill, purple circle = nano ball mill, green circle = U6 ball mill dried, brown diamond = T2, green diamond = P2, blue diamond = nano, green triangle = 5%Zr, blue triangle = 5%Cu, orange triangle = 5%Mn

For all the physicochemical properties that have been measured to this point the milling of the U6 and nano catalysts has had very little effect, and the surface area

of the materials was slightly reduced. This suggests that the increase in density of the materials is the most likely cause of the greater catalytic performance. The same can be said also of the dried catalyst samples, the physicochemical properties are largely unchanged. Therefore, it is most likely the removal of the surface hydroxyl groups that has caused the reduction in catalyst activity for AA conversion.

When the urea precipitation catalysts are compared for their activity in relation to the Raman defect ratio a similar trend is seen as with previous characteristics. The U1 and U2 catalysts have similar activities and this is reflected by similar defect ratio values. Whereas the U3 catalyst is less active and has a lower concentration of defect sites according to the Raman spectroscopy analysis.

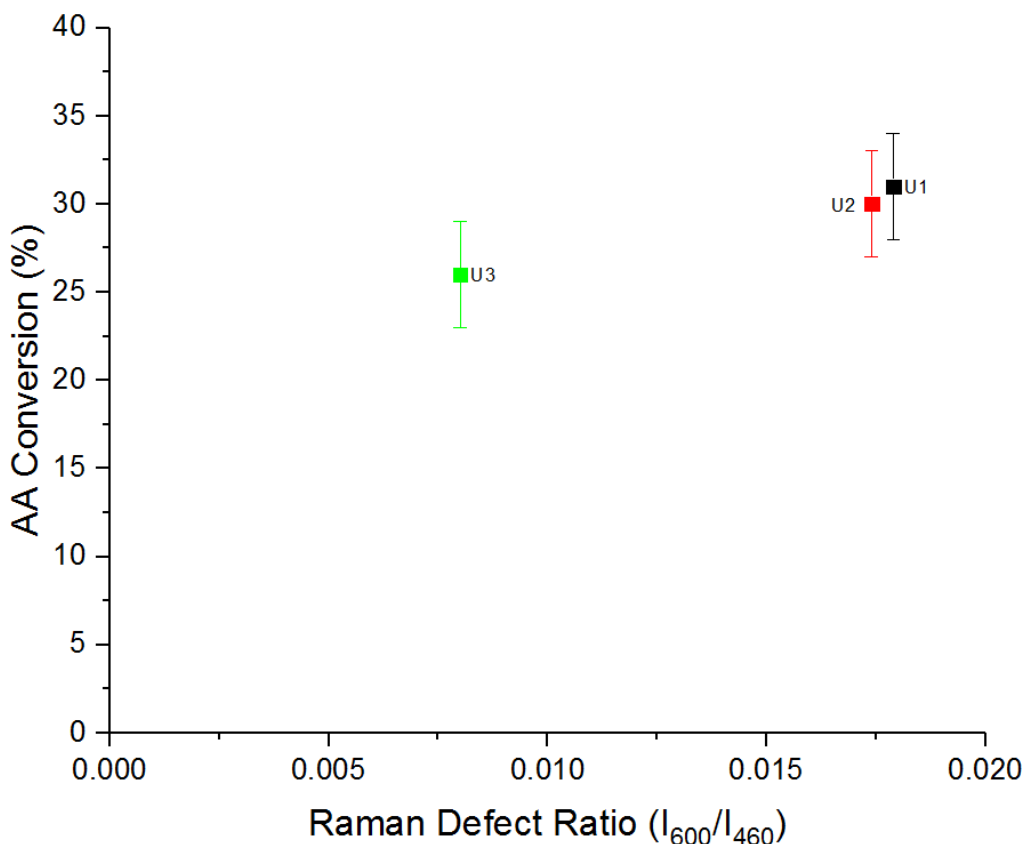


Figure 4.17 Correlation between Raman defect ratio and AA conversion at  $300,000\text{ h}^{-1}$  at  $300\text{ }^{\circ}\text{C}$  for ceria catalysts U1, U2, U3. Black square = U1, red square = U2, green square = U3 (with error bars)

Oxygen defects can also be measured using XPS analysis and comparing the values for alpha and beta oxygen concentrations. Different oxygen states within the

ceria lattice can be detected due to their characteristic binding energies. In CeO<sub>2</sub>, alpha oxygen has a binding energy of 529-530 eV, and this represents the lattice or bulk oxygen. The beta oxygen has a binding energy of 531-533 eV and this represents the defect or surface oxygen, which is generally considered to be the more reactive oxygen.<sup>28</sup> The surface oxygen can also be contributed to by hydroxyl or carbonate groups on the surface of the oxide.<sup>29</sup> An example of a fitted XPS spectrum of the oxygen 1s peaks of ceria can be found in figure 4.16. In the figure the alpha oxygen peak is the larger signal at about 529 eV, whilst the beta oxygen peak is a shoulder of the larger signal at around 532 eV.

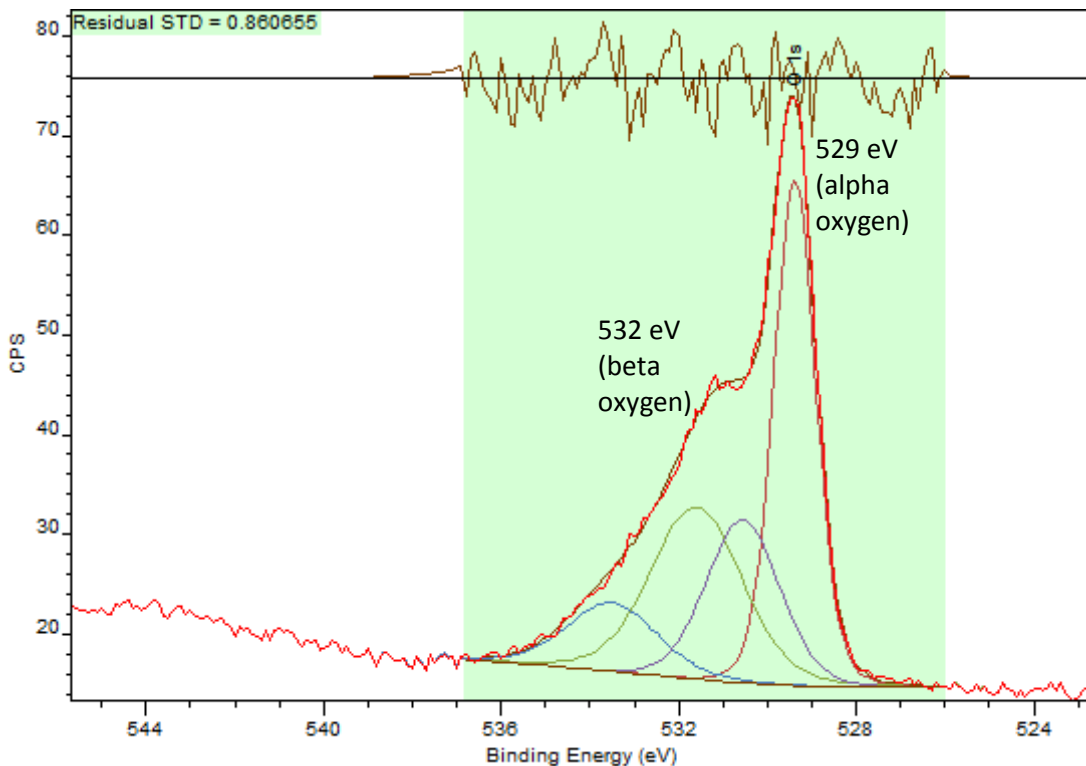


Figure 4.18 XPS spectrum of oxygen 1s peaks of the U1 catalyst

Unlike previous parameters where there has been a general trend between the physicochemical characteristic and catalyst activity this is not the case with relative beta oxygen concentration. The P2 and nano catalysts have comparable levels of beta oxygen to the other catalysts, but their activities are far lower. There is also no obvious trend between activity and beta oxygen concentration for the more active samples. This would indicate that physical factors such as low surface area and large crystallite

size are predominant and able to prevent these catalysts from achieving higher conversions despite the concentration of beta oxygen that is present.

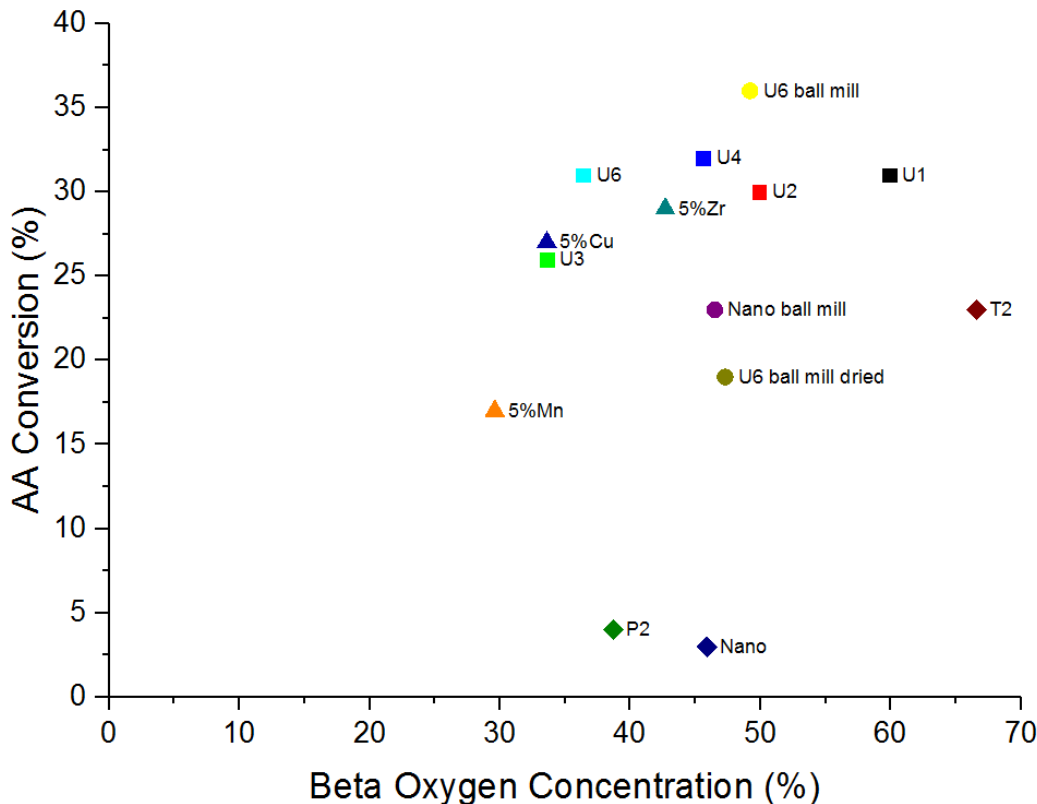


Figure 4.19 Correlation between relative beta oxygen concentration and AA conversion at  $300,000 \text{ h}^{-1}$  at  $300^\circ\text{C}$  for various ceria catalysts. Black square = U1, red square = U2, green square = U3, blue square = U4, light blue square = U6, yellow circle = U6 ball mill, purple circle = nano ball mill, green circle = U6 ball mill dried, brown diamond = T2, green diamond = P2, blue diamond = nano, green triangle = 5%Zr, blue triangle = 5%Cu, orange triangle = 5%Mn

The oxygen defect analysis of the urea precipitation catalysts conducted by Raman spectroscopy and XPS are in general agreement. The U3 has the lowest concentration of defects, whereas the U1 and U2 catalysts have similar defect concentration and similar AA conversion activities. This provides good confirmation that both Raman and XPS techniques are effective for evaluating the concentration of oxygen defects within a ceria sample.

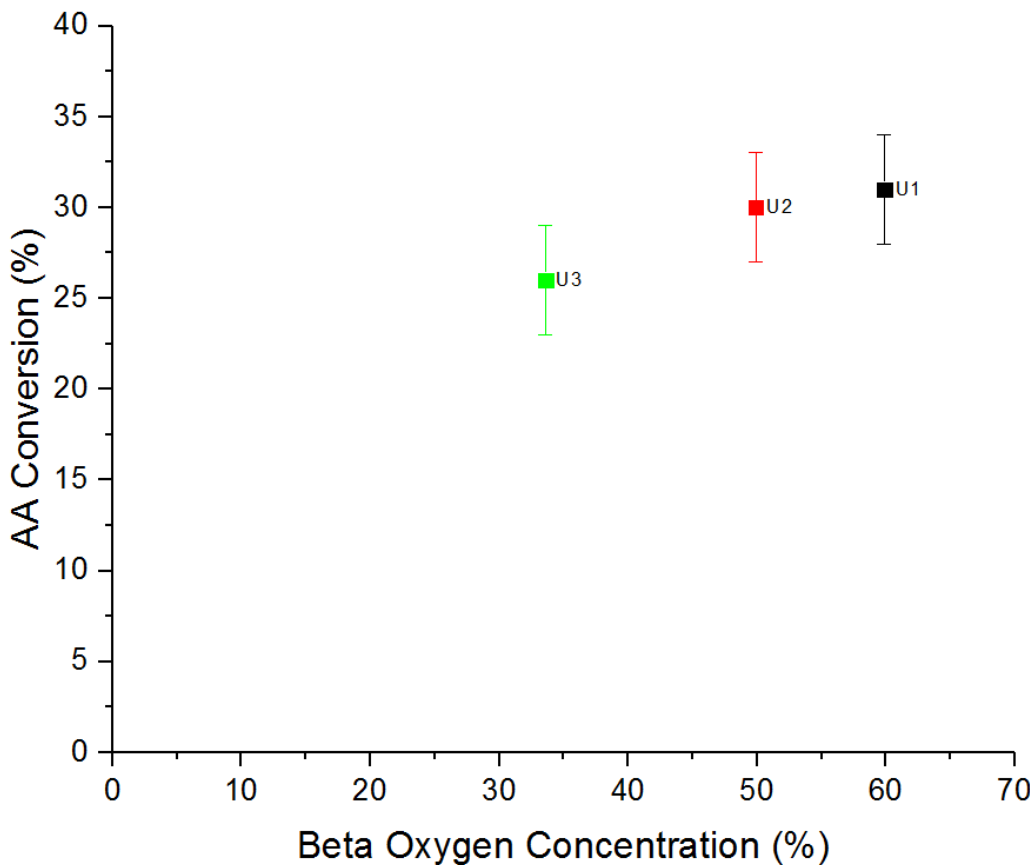


Figure 4.20 Correlation between beta oxygen concentration and AA conversion at  $300,000\text{ h}^{-1}$  at  $300\text{ }^{\circ}\text{C}$  for ceria catalysts U1, U2, U3. Black square = U1, red square = U2, green square = U3 (with error bars)

#### 4.6.5 Influence of Oxidation State

Another characteristic that can be determined using XPS analysis is the ratio between the 3+ and 4+ oxidation states of the cerium in the metal oxide catalyst. The different cerium oxidation states have different binding energies and so give rise to distinctive signals in the XPS spectrum. A fitted XPS spectrum of cerium 3d peaks from a ceria catalyst can be seen in figure 4.19.  $\text{Ce}^{3+}$  gives rise to doublet peaks at 881 and 886 eV, and 899 and 904 eV, whereas  $\text{Ce}^{4+}$  gives rise to signals at 883, 889, 898, 901, 907 and 917 eV.<sup>30</sup> The Ce3d peaks of  $\text{Ce}^{4+}$  can be categorised into two groups, the 901, 907, and 917 eV peaks correspond to  $\text{Ce3d}_{3/2}$ , whilst the 883, 889, and 898 eV peaks correspond to  $\text{Ce3d}_{5/2}$ . The most distinguishing factor between the Ce3d spectra of the two cerium oxidation states is the peak at 917 eV which is only present in the  $\text{Ce}^{4+}$  spectrum. The  $\text{Ce}^{3+}$  peaks cannot be seen in the spectrum of U1 in figure 4.19, because there is so little 3+ present and it is obscured by the much larger signal for the 4+ oxidation state.

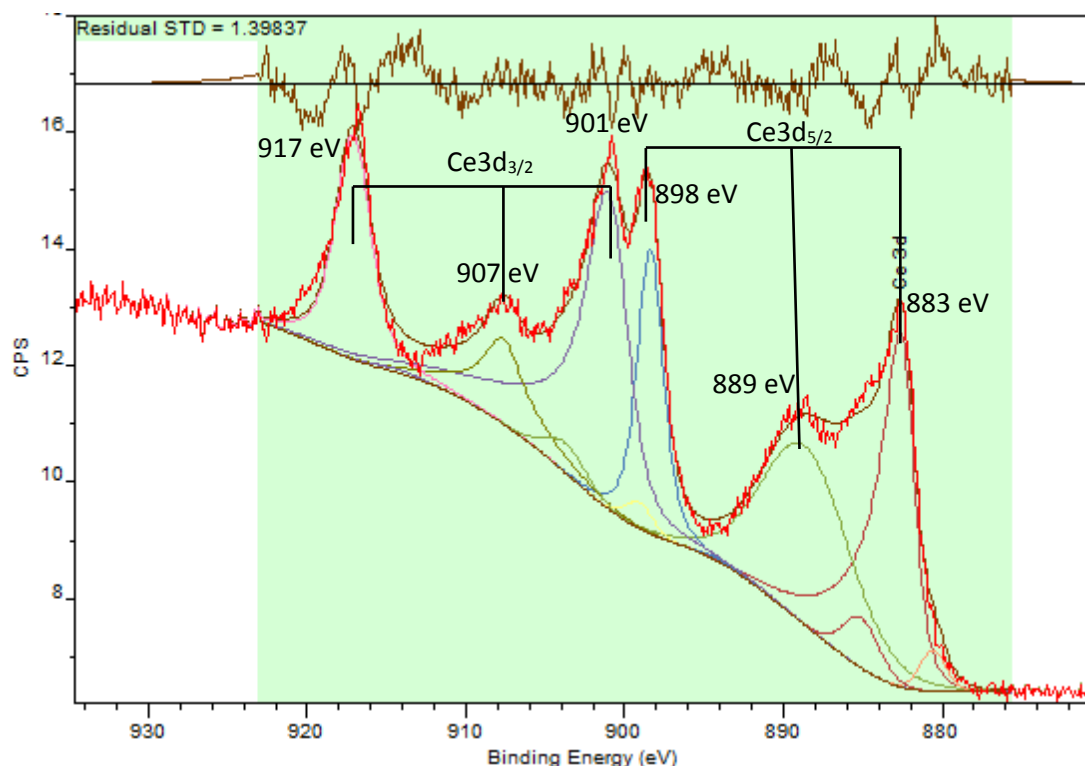


Figure 4.21 XPS spectrum of cerium 3d peaks of the  $\text{CeO}_2$  U1 catalyst with  $\text{Ce}3\text{d}_{3/2}$  and  $\text{Ce}3\text{d}_{5/2}$  peaks labelled.<sup>31</sup>

The redox properties of ceria, its ability to accept and donate electrons by transitioning between the 3+ and 4+ oxidation states, are crucial for its catalytic activity. The 3+/4+ ratio of the material can give an indication of the resting oxidation state of the catalyst and give an indication as to whether the catalyst is in a more oxidised or reduced state. It may be the case that the catalyst is more active in a particular system when it is in a reduced or oxidised form, and this can be tailored by pre-treating the catalyst with  $\text{H}_2$  or air.

In figure 4.20 the ceria catalysts have been compared for their AA conversion activity in relation to their 3+/4+ ratio as determined by XPS. The correlation is similar to the relationship between activity and beta oxygen concentration in figure 4.16. The P2 and nano catalysts have comparable oxidation state ratios to much more active samples. There is also no correlation between the oxidation state ratio and activity of the more active catalysts. Therefore, the Ce 3+/4+ ratios as determined by XPS analysis is not suitable as a predictive tool for the activity of ceria samples for AA conversion.

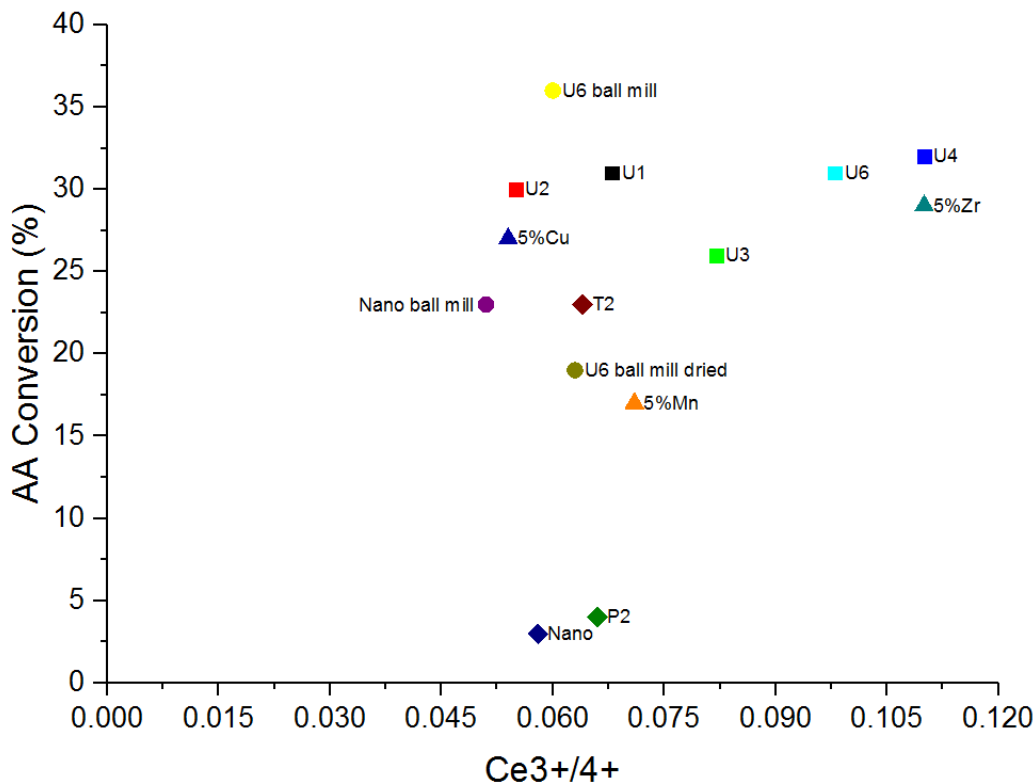


Figure 4.22 Correlation between cerium oxidation state ratio and AA conversion at  $300,000 \text{ h}^{-1}$  at  $300^\circ\text{C}$  for various ceria catalysts. Black square = U1, red square = U2, green square = U3, blue square = U4, light blue square = U6, yellow circle = U6 ball mill, purple circle = nano ball mill, green circle = U6 ball mill dried, brown diamond = T2, green diamond = P2, blue diamond = nano, green triangle = 5%Zr, blue triangle = 5%Cu, orange triangle = 5%Mn

In figure 4.21 the urea precipitation catalysts are compared for their activity in relation the oxidation state of the cerium. The data indicates that a lower 3+/4+ ratio could lead to greater activity between the least active sample, U3, has a higher 3+/4+ ratio than the U1 and U2 samples. However, the U1 sample is slightly more active and has a higher 3+/4+ ratio than U2, so there is no obvious trend between activity and this particular parameter.

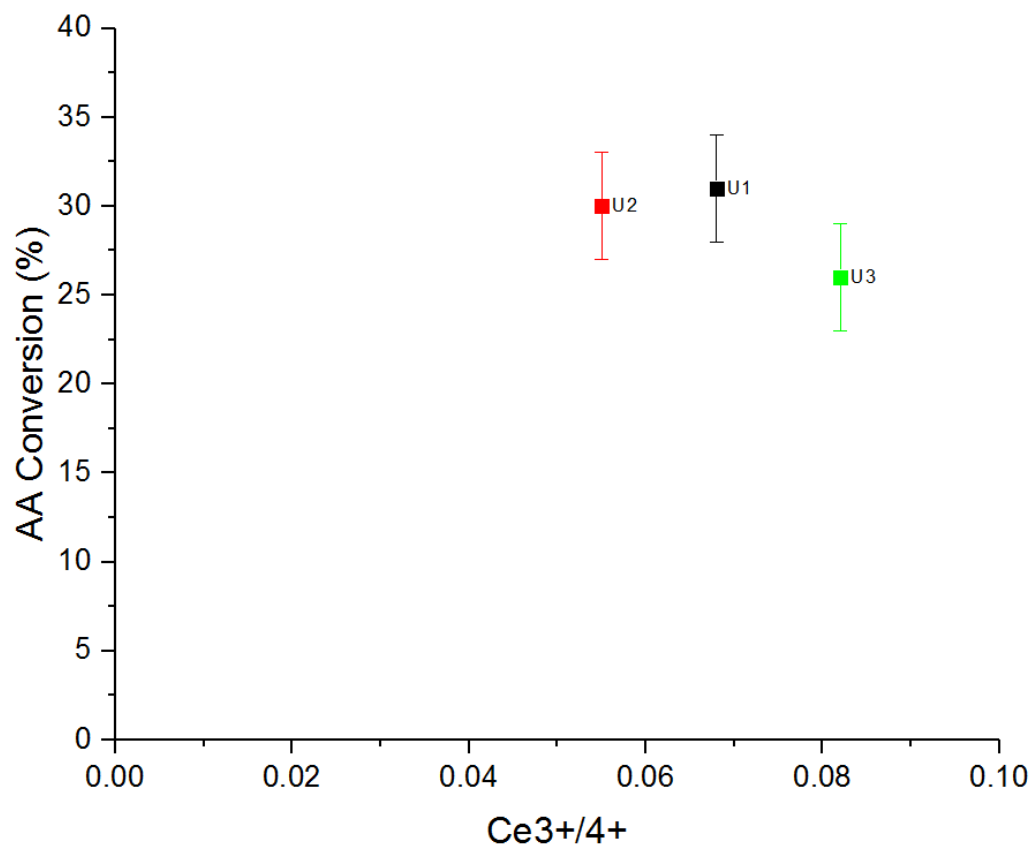


Figure 4.23 Correlation between cerium oxidation state ratio and AA conversion at  $300,000 \text{ h}^{-1}$  at  $300^\circ\text{C}$  for ceria catalysts U1, U2, U3. Black square = U1, red square = U2, green square = U3 (with error bars)

In many catalytic reactions that utilise ceria as a catalyst, parameters such as beta oxygen concentration and cerium oxidation state ratio often provide very powerful indicators for catalyst performance. However, for the system under investigation here this is not found to be the case. This could be because most often, ceria is used to catalyse oxidation reactions, whilst the reaction of AA on ceria in this study has been conducted in the absence of oxygen. Therefore, the reaction mechanism requires further investigation to gain a greater understanding of the system and the action of the catalyst within it. The structure-activity investigation has highlighted that the physical properties (e.g. surface area, crystallite size) are able to give a far greater indication of the activity of a material for AA conversion than the chemical properties determined by XPS analysis (e.g. beta oxygen concentration, Ce 3+/4+ ratio).

## 4.7 Mechanistic Investigation

To probe the mechanism of the interactions between AA and a ceria catalyst surface Diffuse Reflectance Infrared Fourier Transform Spectroscopy (DRIFTS) was utilised. Due to the strong IR signal of aldehydes at around 1700-1800 cm<sup>-1</sup> infrared spectroscopy can be a powerful tool for studying molecules like AA. In DRIFTS analysis, diffuse reflectance of an IR beam is measured following its interaction with a reflective surface (for more details see section 2.5.1). Surface bound species give rise to signals in the resulting spectrum, and this can give an indication as to the nature of surface bound intermediates through which a reaction mechanism progresses.<sup>32,33</sup>

### 4.7.1 AA DRIFTS Studies

In the reactions at 300 °C the two major products observed are CO<sub>2</sub> and acetone, whereas at 175 °C the formation of ethanol is observed (see section 3.4). AA DRIFTS was conducted upon a selection of the catalyst samples at room temperature, 175 °C, and 300 °C to gain insight into the mechanism of the reaction.

Assignment of the peaks was carried out aided by information found in studies by Overbury and co-workers (see table 4.13).<sup>34,35</sup> Many of the signals associated with interactions between AA and ceria have been assigned to the appropriate functionalities in this very helpful research.

Table 4.14 Vibrational assignments for peaks observed in DRIFTS spectra of AA adsorption on CeO<sub>2</sub> surface. Reproduced from refs 34 and 35.

Vibrational mode	Vibrational assignments (cm <sup>-1</sup> )
v <sub>as</sub> (CH <sub>3</sub> )	3002, 2969, 2965
v <sub>as</sub> (CH <sub>2</sub> )	2964, 2925
v <sub>s</sub> (CH <sub>3</sub> )	2918, 2864
v <sub>s</sub> (CH <sub>2</sub> )	2836
v(CH) η <sup>1</sup> -acetaldehyde	2760-2746, 2759
v(C=O) η <sup>1</sup> -acetaldehyde	1723
v(C=O) and (C=C) coupling products	1656, 1642, 1630
v <sub>as</sub> (OCO) acetate / bidentate carbonate	1584, 1611, 1565
v(C=C) enolate	1600
v <sub>s</sub> (OCO) acetate	1443, 1429, 1406, 1422
δ <sub>s</sub> (CH <sub>3</sub> )	1380, 1365
δ(CH <sub>2</sub> ) enolate	1317
δ(OH) ethanol	1269
v <sub>s</sub> (OCO) bidentate carbonate	1269, 1260
v(C-O) monodentate ethoxide	1134, 1120, 1096
v(C-O) bidentate ethoxide	1050, 1028

#### 4.7.2 AA DRIFTS with Nano CeO<sub>2</sub>

As previously mentioned, each sample was analysed at room temperature, 175 °C, and 300 °C under a flow of AA(2000 ppm)/He to probe the different observed reaction mechanisms. Firstly, the commercial ceria nano powder was examined, and the spectra taken at each temperature are presented in figure 4.22. At room temperature (spectrum a) the signal for the carbonyl stretch of AA at 1710 cm<sup>-1</sup> can be clearly identified. There is also a large signal at 1120 cm<sup>-1</sup> which is most likely a monodentate interaction with the C-O of an ethoxide species. A small signal can be seen at 2975 cm<sup>-1</sup> which is indicative of the asymmetric stretch of a CH<sub>3</sub> group. As is expected at this temperature there is no indication of the formation of any reaction products in this spectrum.

As the temperature is increased to 175 °C (spectrum b) the signals at 1710 and 1120 cm<sup>-1</sup> have reduced in intensity and signals at 1660 and 1630 cm<sup>-1</sup> have emerged.

These signals could indicate the formation of C=C and C=O coupling products, which would suggest the occurrence of a condensation reaction leading to formation to products such as crotonaldehyde. The signal at  $2975\text{ cm}^{-1}$  has also become less prominent and a signal at  $2820\text{ cm}^{-1}$  can now be seen. This is most likely due to symmetric stretch the of a  $\text{CH}_2$  moiety.

Finally, the temperature was increased to  $300\text{ }^{\circ}\text{C}$  (spectrum c) to gain insight into the mechanism at work during the gas phase testing. At this temperature a signal at  $1710\text{ cm}^{-1}$  for AA can no longer be identified. A broad signal at around  $2350\text{ cm}^{-1}$ , is one obvious difference between this spectrum and the previous two. This signal indicates the formation of  $\text{CO}_2$  which is good confirmation for what has been observed using the GC-FID analysis in the gas phase test. There is also the presence of large signals at  $1550$  and  $1420\text{ cm}^{-1}$  which could indicate the formation of acetates on the surface of the catalyst. This helps to explain how the AA is converted to acetone on the catalyst surface, and again offers strong confirmation for what has been previously observed in the reactor. Another signal that can be identified is found at  $2830\text{ cm}^{-1}$  which suggests the presence of  $\text{CH}_2$ , as was observed at  $175\text{ }^{\circ}\text{C}$ .

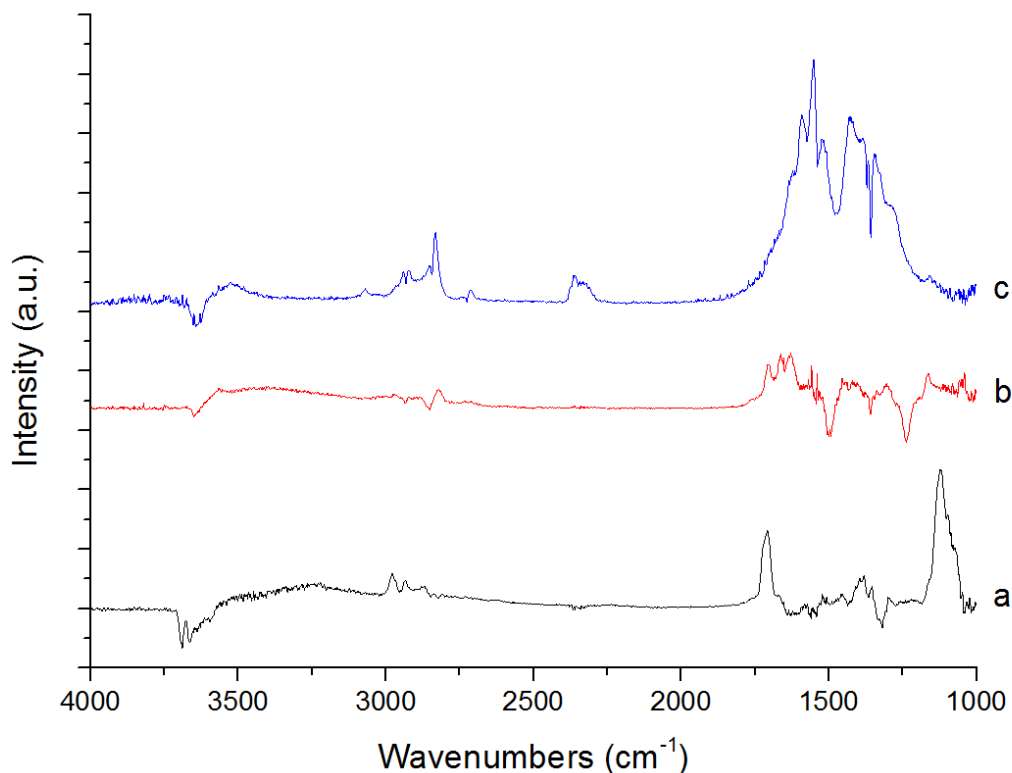


Figure 4.24 DRIFTS spectra of AA(2000ppm)/He flowed (30 ml/min) over Nano  $\text{CeO}_2$  at different temperatures.  
a = room temperature, b =  $175\text{ }^{\circ}\text{C}$ , c =  $300\text{ }^{\circ}\text{C}$

#### 4.7.3 AA DRIFTS with CeO<sub>2</sub> U1

The same experiment was carried out using the U1 catalyst to analyse a material that has been found to be effective for converting AA. The spectra for this analysis can be found in figure 4.23 and at room temperature (spectrum a) the data looks very similar to that of the nano ceria in figure 4.22. The two most prominent signals are found at 1720 and 1120 cm<sup>-1</sup> and these indicate the presence of AA and monodentate C=O respectively. Therefore, interaction between the ceria and AA is observed but no transformation of the AA is taking place.

As the temperature is increased to 175 °C (spectrum b) signals at 1660, 1600, 1100, and 1060 cm<sup>-1</sup> become evident. The peak at 1660 cm<sup>-1</sup> likely indicates the formation of C=C and C=O coupling products as was seen previously, while the signal at 1600 cm<sup>-1</sup> could indicate the presence of an enolate species. The signal for AA is only just visible as a shoulder to the signal at 1660 cm<sup>-1</sup>. The signals at 1100 and 1060 cm<sup>-1</sup> are caused by the vibrational modes of monodentate and bidentate ethoxides respectively. These ethoxide signals could be an indication that some of the AA is being converted into ethanol which was observed in the gas phase reactor. Signals at 2830 and 2970 cm<sup>-1</sup> are also observed due to the symmetric and asymmetric vibrational modes of CH<sub>2</sub>.

When the temperature is increased further to 300 °C (spectrum c) the formation of CO<sub>2</sub> as a signal 2350 cm<sup>-1</sup> is again observed. Signals at 1575 and 1430 cm<sup>-1</sup> are observed which indicate the presence of acetate species which could act as intermediate species for the conversion of AA to acetone. The DRIFTS spectra would suggest that both the U1 and nano catalysts convert AA to acetone *via* the same reaction mechanism.

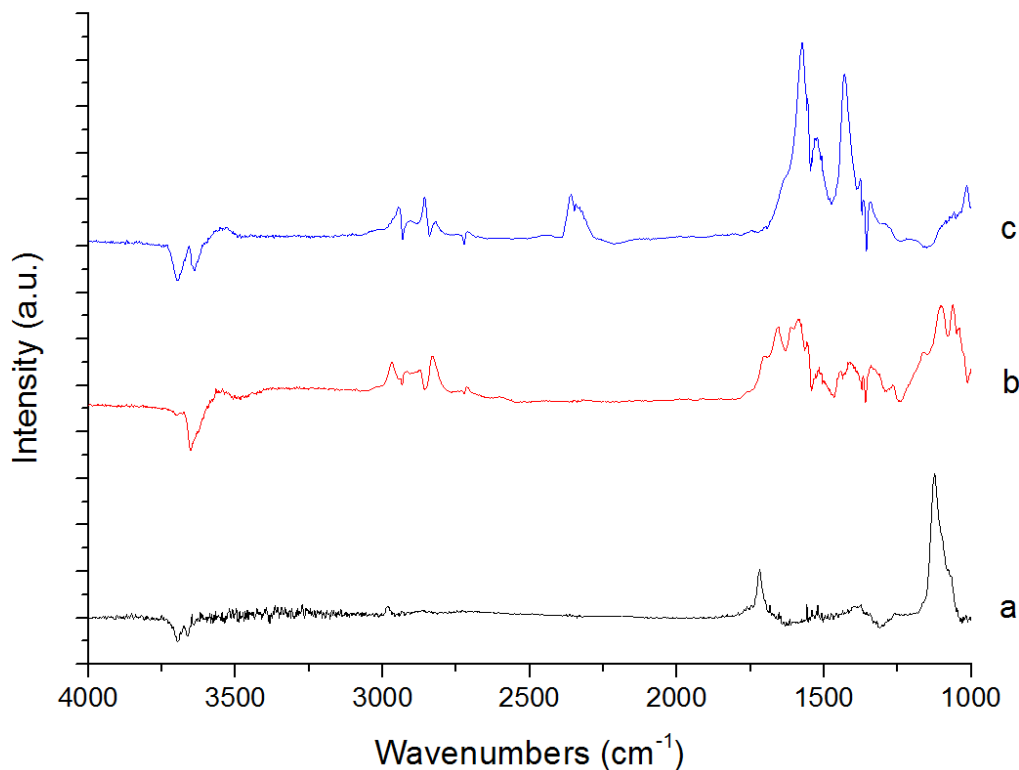


Figure 4.25 DRIFTS spectra of AA(2000ppm)/He flowed (30 ml/min) over CeO<sub>2</sub> U1 at different temperatures. a = room temperature, b = 175 °C, c = 300 °C

#### 4.7.4 AA DRIFTS with 5%CuOx-CeO<sub>2</sub>

A doped ceria catalyst was also subjected to AA DRIFTS analysis and the 5%CuO<sub>x</sub> was selected for this (figure 4.24). At room temperature (spectrum a) the same signals are observed as with the previous samples.

At 175 °C the spectrum is more similar to the spectrum observed with nano CeO<sub>2</sub> than the spectrum observed with the U1 catalyst. There is a broad signal at 1620 cm<sup>-1</sup> which could again indicate the formation of coupling products *via* condensation type reactions. However, we do not observe any ethoxide species in this case, similar to the nano ceria spectrum. It may be the case that only the U1 catalyst is active enough to form ethanol at 175 °C and, therefore it is only with that catalyst that the ethoxide signals are observed. The nano and copper doped catalysts may require a slightly higher reaction temperature in order to convert AA to ethanol.

When the temperature of the experiment was increased to 300 °C the resulting spectrum is very similar to the previously analysed samples. Signals at 1570 cm<sup>-1</sup> and 1440 cm<sup>-1</sup> are indicative of acetate intermediates and the formation of CO<sub>2</sub> is indicated

by a signal at  $2350\text{ cm}^{-1}$ . All three catalyst samples appear to exhibit the same reaction mechanism at  $300\text{ }^{\circ}\text{C}$ .

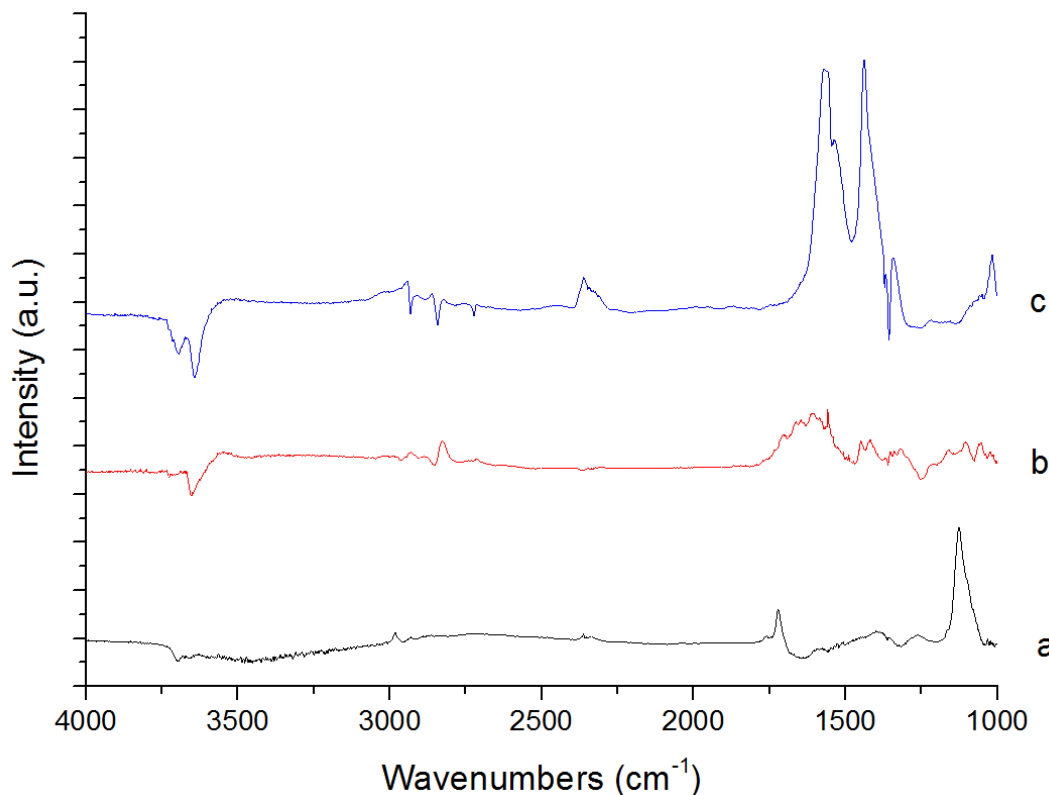
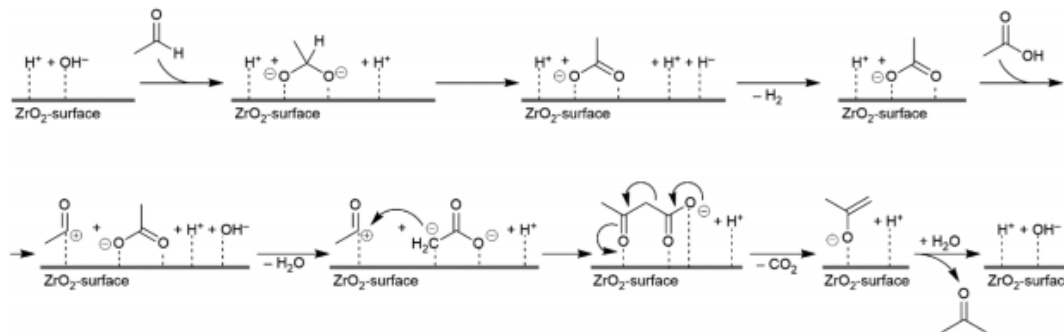


Figure 4.26 DRIFTS spectra of AA(2000ppm)/He flowed (30 ml/min) over 5%CuOx-CeO<sub>2</sub> at different temperatures. a = room temperature, b =  $175\text{ }^{\circ}\text{C}$ , c =  $300\text{ }^{\circ}\text{C}$

## 4.8 Reaction Mechanism

The observations that have been made regarding the mechanism of the reaction between AA and a CeO<sub>2</sub> surface are supported by reports in the scientific literature. For example, in a study by Corma and co-workers, a mechanism for the ketonisation of AA to form acetone on a ZrO<sub>2</sub> surface is outlined (scheme 4.1)<sup>36</sup>, which is in general agreement with the data generated by this DRIFTS study. Even though the mechanism is depicted as taking place on a ZrO<sub>2</sub> surface, investigations have confirmed that the same mechanism is operative on a ceria surface also. These reactions were conducted by flowing heptanal and water in N<sub>2</sub> over a metal oxide catalyst diluted with silicon carbide at temperatures between  $300\text{-}450\text{ }^{\circ}\text{C}$ .<sup>37</sup> This mechanism agrees with the DRIFTS analysis as the major intermediate species suggested by Corma is a surface-

bound acetate. Acetate formation has been observed with each of the ceria samples analysed by DRIFTS at 300 °C as indicated by signals at 1550-1575 and 1420-1440 cm<sup>-1</sup>.

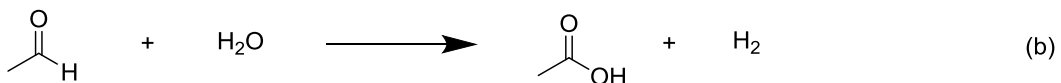


Scheme 4.1 Literature mechanism for reaction of AA on zirconia catalyst. Reproduced from ref 36.

The mechanism is comprised of two major reaction steps; the first of which is aldehyde oxidation, which is then followed by ketonic decarboxylation. Firstly, the aldehyde is oxidised to the carboxylic acid, after which two carboxylic acids can react together to form the ketone along with the evolution of CO<sub>2</sub>. It has been found that ZrO<sub>2</sub> is more active for aldol condensation reactions in the presence of AA, whereas CeO<sub>2</sub> is more active for ketonisation.<sup>37</sup> This would help to explain why the CeO<sub>2</sub> catalyst was found to be more selective towards acetone than either of the ZrO<sub>2</sub> catalysts in the gas phase testing. This may also help to elucidate as to why the carbon balance was found to be lower for the ZrO<sub>2</sub> materials. If larger molecular weight products were being formed due to condensation reactions these would likely not be observed in the GC analysis.

This mechanism shows water being used to replenish hydroxides on the catalyst surface following the conversion of AA to acetone and CO<sub>2</sub>. Often water is co-fed into these reactions to increase the catalyst performance due to this effect. This offers a good explanation as to why the dried catalysts were found to be far less active for AA conversions than their undried counterparts. This could also begin to explain why the catalysts have been found to deactivate so rapidly. Once the surface hydroxides have been used to convert AA then they need to be replenished by water or an alternative source, or the catalyst will lose activity. In the reactions conducted in

in the gas phase testing of this study the only gas fed into the reactor was AA(1000 ppm)/He, so no sacrificial oxidant or water is present to regenerate the surface hydroxide groups.



Scheme 4.2 a = Overall reaction equation for ketonisation of AA, b = oxidation of aldehyde using water, c = ketonic decarboxylation of two carboxylic acids to form a ketone and CO<sub>2</sub>.<sup>36</sup>

The reaction equation for the ketonisation of AA to acetone (scheme 4.2) reinforces the need for water or surface hydroxyl groups in this reaction. The oxidation of the aldehyde requires an oxygen and a proton, and this is supplied from the water or surface hydroxyl groups. It was for this reason that in the research conducted by Corma and co-workers that water is co-fed into the reactor. However, if too much water is added to the reaction the catalytic activity begins to decrease, and this is most likely due to competition between the water and aldehyde for adsorption to sites on the catalyst surface.

However, this mechanism does not explain how the ethanol is formed at the lower reaction temperature, and it also does not correlate with the selectivities observed in the gas phase reactions. The ethanol formation at 175 °C could be due to disproportionation of the AA via a Cannizzaro reaction. The Cannizzaro reaction describes how two aldehyde molecules can disproportionate to yield an alcohol and carboxylic acid in the presence of a base.<sup>38,39</sup> In the case of AA this will lead to the formation of ethanol and acetic acid from two AA molecules. The acetic acid product could stay bound to the catalyst surface as acetate groups, which then undergo ketonisation at 300 °C to form acetone and CO<sub>2</sub> (as shown in (c) in scheme 4.2). The

Cannizzaro reaction was also suggested as a possible mechanism by Mark Rule in the ColorMatrix patent.<sup>4</sup>

Further issues with the Corma mechanism are that it suggests that one CO<sub>2</sub> molecule is formed for each acetone molecule, whereas in the testing carried out in this study it was observed that more CO<sub>2</sub> is formed than acetone. Also, there is no oxygen in the reaction system which could be used to oxidise the aldehyde. Therefore, it is more likely that the acetate formation would likely occur *via* disproportionation than an oxidation process.



Scheme 4.3 Cannizzaro disproportionation of two AA molecules to form ethanol and acetic acid in the presence of a base

#### 4.9 Conclusions

In conclusion gas phase testing at 300,000 h<sup>-1</sup> was found to be an effective and reliable method for catalyst screening and for measuring the activity of catalysts for AA conversion at 300 °C within the kinetic regime. Catalysts prepared *via* urea precipitation with a 3:1 urea to metal nitrate ratio were found to be the most effective AA conversion catalysts. Preparation methods involving structure directing agents such Pluronic P123 and TTAB were not able to improve catalyst performance. However, this is a positive result due to the fact that the urea precipitation method is cheaper and easier to scale up than the more elaborate preparations. Milling of ceria catalysts was found to increase activity but this is most likely due to an increase in density of the material.

It was also found that the catalysts deactivated rapidly during the course of a reaction, and this is most likely due to the depletion of surface hydroxides that could not be regenerated. Another factor that could contribute to the loss of catalyst activity is the accumulation of carbonaceous deposits on the catalyst surface that could block access to active sites.

Characterisation of the ceria catalysts was not able to provide a clear relationship between the structure of the catalyst and its activity for AA conversion at 300 °C. It was found that there is a complex relationship between the physicochemical characteristics of the ceria and its catalytic activity, and that no single characteristic had a significant effect that could be used as a single focus for future catalyst design. Whilst increased surface area and decreased crystallite size were found to enhance catalyst performance, it was also found that properties such as oxygen defect ratio and Ce 3+/4+ ratio had no correlation with catalyst activity for this system. These findings match closely with a previous study that stated,

*“the catalytic chemistry in vapor phase aldolization of acetaldehyde under the steady-state condition was complicated and multifariously controlled”<sup>7</sup>*

Based on the data collected in this chapter, the same can be said of the catalytic chemistry of the vapour phase ketonisation of AA.

AA DRIFTS analysis has confirmed that the conversion of AA to acetone and CO<sub>2</sub> at 300 °C occurs *via* the ketonisation of acetate groups, and this has strong precedent in the academic literature.<sup>36,37</sup> The literature mechanism for ketonic decarboxylation on a metal oxide surface also offers support for the hypothesis that depletion of surface hydroxides can cause catalyst deactivation, which was observed when dried catalysts were found to be less active. This could be further tested by examining the FTIR spectra of fresh and spent catalysts and comparing the strength of the -OH signal at 3500 cm<sup>-1</sup>. Often water is co-fed into these systems to provide a source for the regeneration of surface hydroxide groups.

The acid-base properties of the catalysts should be investigated because Lewis acidic and basic sites are thought to be involved in ketonisation reactions. Acidic sites could be probed using ammonia chemisorption, and basic sites could be probed using carbon dioxide chemisorption.<sup>40</sup> Further study should be conducted into the reaction mechanism to determine whether the reaction proceeds via the mechanism suggested by Corma or via a disproportionation route. The disproportionation route is the more likely mechanism based on the data collected in this chapter. Further investigation into the mechanism of the reaction could be carried out by measuring the amount of H<sub>2</sub> generated. This could be done by using argon as the GC carrier gas instead of helium, and then using the TCD to quantify the H<sub>2</sub>. This would help to establish whether any

dehydrogenation steps were involved in the reaction. If dehydrogenation is observed, then this would offer support to the Corma mechanism.

#### 4.10 Chapter 4 - References

1. S. R. Shukla, E. A. Lofgren and S. A. Jabarin, *Polym. Int.*, 2005, **54**, 946–955.
2. R. Di Felice, D. Cazzola, S. Cobrini and L. Oriani, *Packag. Technol. Sci.*, 2008, **21**, 405–415.
3. M. Frounchi and A. Dourdash, *Macromol. Mater. Eng.*, 2009, **294**, 68–74.
4. WO2005010088 A1, 2005.
5. R. Kydd, W. Y. Teoh, J. Scott, D. Ferri and R. Amal, *ChemCatChem*, 2009, **1**, 286–294.
6. C. T. Campbell and C. H. F. Peden, *Science*, 2005, **309**, 713–714.
7. W. Ji, Y. Chen and H. H. Kung, *Appl. Catal. Gen.*, 1997, **161**, 93–104.
8. H. Idriss, C. Diagne, J. P. Hindermann, A. Kiennemann and M. A. Barteau, *J. Catal.*, 1995, **155**, 219–237.
9. E. Bauer, *A Statistical Manual for Chemists*, Elsevier, 2012.
10. E. Ntanjua N., T. Garcia, B. Solsona and S. H. Taylor, *Catal. Today*, 2008, **137**, 373–378.
11. W. Yuejuan, M. Jingmeng, L. Mengfei, F. Ping and H. Mai, *J. Rare Earths*, 2007, **25**, 58–62.
12. K. Yoshikawa, H. Sato, M. Kaneeda and J. N. Kondo, *J. CO<sub>2</sub> Util.*, 2014, **8**, 34–38.
13. J. Rouquerol, P. Llewellyn and F. Rouquerol, in *Characterization of Porous Solids VII*, Elsevier, 1st edn., 2007, vol. 160, pp. 49–56.
14. H. Wang, X. Chen, S. Gao, Z. Wu, Y. Liu and X. Weng, *Catal. Sci. Technol.*, 2013, **3**, 715–722.
15. E. Mamontov, T. Egami, R. Brezny, M. Koranne and S. Tyagi, *J. Phys. Chem. B*, 2000, **104**, 11110–11116.
16. A. Aranda, S. Agouram, J. M. López, A. M. Mastral, D. R. Sellick, B. Solsona, S. H. Taylor and T. García, *Appl. Catal. B Environ.*, 2012, **127**, 77–88.

17. G. C. Bond, *Catal. Rev.*, 2008, **50**, 532–567.
18. D. R. Sellick, A. Aranda, T. García, J. M. López, B. Solsona, A. M. Mastral, D. J. Morgan, A. F. Carley and S. H. Taylor, *Appl. Catal. B Environ.*, 2013, **132–133**, 98–106.
19. R. Ramdas, E. Nowicka, R. Jenkins, D. Sellick, C. Davies and S. Golunski, *Appl. Catal. B Environ.*, 2015, **176–177**, 436–443.
20. S. Bedrane, C. Descorme and D. Duprez, *Catal. Today*, 2002, **75**, 401–405.
21. W. Zhan, S. Yang, P. Zhang, Y. Guo, G. Lu, M. F. Chisholm and S. Dai, *Chem. Mater.*, 2017, **29**, 7323–7329.
22. Z. Wu, M. Li, J. Howe, H. M. Meyer and S. H. Overbury, *Langmuir*, 2010, **26**, 16595–16606.
23. K. S. W. Sing, in *Adsorption by Powders and Porous Solids*, Elsevier, 2nd edn., 2013, pp. 237–268.
24. M. Thommes, K. Kaneko, A. V. Neimark, J. P. Olivier, F. Rodriguez-Reinoso, J. Rouquerol and K. S. W. Sing, *Pure Appl. Chem.*, 2015, **87**, 1051–1069.
25. W. Kang, D. O. Ozgur and A. Varma, *ACS Appl. Nano Mater.*, 2018, **1**, 675–685.
26. V. Sánchez Escribano, E. Fernández López, M. Panizza, C. Resini, J. M. Gallardo Amores and G. Busca, *Solid State Sci.*, 2003, **5**, 1369–1376.
27. D. Mukherjee, B. G. Rao and B. M. Reddy, *Top. Catal.*, 2017, **60**, 1673–1681.
28. C. Hardacre, G. M. Roe and R. M. Lambert, *Surf. Sci.*, 1995, **326**, 1–10.
29. J. Wang, M. Shen, J. Wang, M. Yang, W. Wang, J. Ma and L. Jia, *Catal. Lett.*, 2010, **140**, 38–48.
30. E. Bêche, P. Charvin, D. Perarnau, S. Abanades and G. Flamant, *Surf. Interface Anal.*, 2008, **40**, 264–267.
31. Thermo Scientific XPS: Knowledge Base,  
<https://xpssimplified.com/elements/cerium.php>, (accessed 27 May 2020).

32. J. Velasquez Ochoa, E. Farci, F. Cavani, F. Sinisi, L. Artiglia, S. Agnoli, G. Granozzi, M. C. Paganini and L. Malfatti, *ACS Appl. Nano Mater.*, 2019, **2**, 3434–3443.
33. G. Jacobs, L. Williams, U. Graham, G. A. Thomas, D. E. Sparks and B. H. Davis, *Appl. Catal. Gen.*, 2003, **252**, 107–118.
34. A. K. P. Mann, Z. Wu, F. C. Calaza and S. H. Overbury, *ACS Catal.*, 2014, **4**, 2437–2448.
35. M. Li, Z. Wu and S. H. Overbury, *J. Catal.*, 2013, **306**, 164–176.
36. L. M. Orozco, M. Renz and A. Corma, *Green Chem.*, 2017, **19**, 1555–1569.
37. L. M. Orozco, M. Renz and A. Corma, *ChemSusChem*, 2016, **9**, 2430–2442.
38. S. Cannizzaro, *Justus Liebigs Ann. Chem.*, 1853, **88**, 129–130.
39. T. A. Geissman, in *Organic Reactions*, John Wiley & Sons, Ltd, New York, 1944, pp. 94–113.
40. K. Tanabe, M. Misono, Y. Ono and H. Hattori, Eds., in *Studies in Surface Science and Catalysis*, Elsevier, 1989, vol. 51, pp. 5–25.

## 5 Application Testing of Metal Oxide Catalysts for AA Removal in PET

### 5.1 Introduction

In the previous chapter catalysts have been prepared, tested for AA conversion in a gas phase test, and then characterised to understand which physical and chemical properties are most crucial for an effective AA removal catalyst. The next important step was to take the catalysts, and all the information that had been gathered about them, from the labs in Cardiff and test them in PET under more representative conditions at ColorMatrix in Knowsley. This will help to confirm whether the Cardiff testing was a good model that could make accurate predictions as to which catalysts would be best for removal of AA in PET. It would also help to confirm whether these catalysts could function effectively in the industrial process and whether they could potentially ever have a commercial application.

To test the catalysts in PET a twin-screw extruder was used to add the catalyst to the polymer and mimic the processing conditions that PET undergoes in the polymer industry. The extruder temperature was set to 285 °C and the screw speed was set to 150 rpm for the testing of these metal oxide catalysts (see section 2.3.2 for full experimental details). This screw speed results in a residence time of around 70 seconds, meaning that the catalyst has a reaction window of just over a minute at 285 °C. The extruded PET pellets were analysed using headspace GC-FID to determine the AA concentration<sup>1–3</sup> and were also analysed for any changes in intrinsic viscosity (IV) that could indicate degradation of the polymer chains.

PET loaded with metal oxide nanoparticles is referred to as a PET nanocomposite in the scientific literature.<sup>4,5</sup> The addition of materials such as silica or layered clays to PET is carried out to improve certain properties of the polymer. These properties include stiffness, strength, flame retardancy, and barrier performance to name just a few. Therefore, there is a precedent for adding metal oxides to PET to correct deficiencies associated with the polymer.

## 5.2 AA Levels in Blank PET

The typical concentration of AA in PET is often quoted as being between 6-8 ppm,<sup>6</sup> however with highly efficient modern processing the level of AA in bottle grade PET is often around 4 ppm.<sup>7</sup> Testing conducted on a lab scale twin screw extruder determined that the concentration of AA in blank PET samples in some experiments was between 7.5-9 ppm, whilst in other experiments it was found to be between 9-11 ppm (see figure 5.1). During some tests it was observed as being as high as 13 ppm, and the average blank value for all of the tests that were conducted throughout this project was 10.2 ppm. It is to be expected that the AA levels would be slightly higher using small laboratory scale equipment, which has only been given an hour to reach a steady state, than under industrial conditions where apparatus are able to run under steady state conditions for up to two weeks. It is very important to avoid line shutdowns in order to keep AA levels to a minimum and maximise the quality of the PET being produced. After restarting an injection moulding machine the first preforms produced can contain AA concentrations as high as 50 ppm.<sup>7</sup>

The AA concentration in blank PET was found to fluctuate over the course of a day, starting with a lower concentration at the beginning of the day and rising to a higher concentration by the time testing was concluded. This could be due to an increase in moisture in the system (see sections 1.4.42 and 1.4.7.3), the presence of moisture can lead to degradation of the polymer and formation of AA. Although the PET is dried at 150 °C prior to use, the capacity of the drier is most likely the biggest contributing factor to this observation. The PET that is removed from the drier at the start of the day will have been drying overnight, whereas PET removed from the drier later in the day will not have been dried so thoroughly. The PET drier was automatically refilled with fresh PET once the amount of PET stored in the drier went below a certain level. Moisture can also be absorbed by the PET while it is being weighed out and transported to the extruder. The time between the PET being removed from the drier and added to the extruder can be up to around 5 minutes, and there is also the time that the PET is sat in the hopper as the material is fed into the extruder. In typical equipment configurations PET is transferred directly from the drier into the extruder or moulder, so that the levels of moisture are kept down to a minimum. This could be another reason why the AA levels we observe are slightly higher than those quoted in the literature.

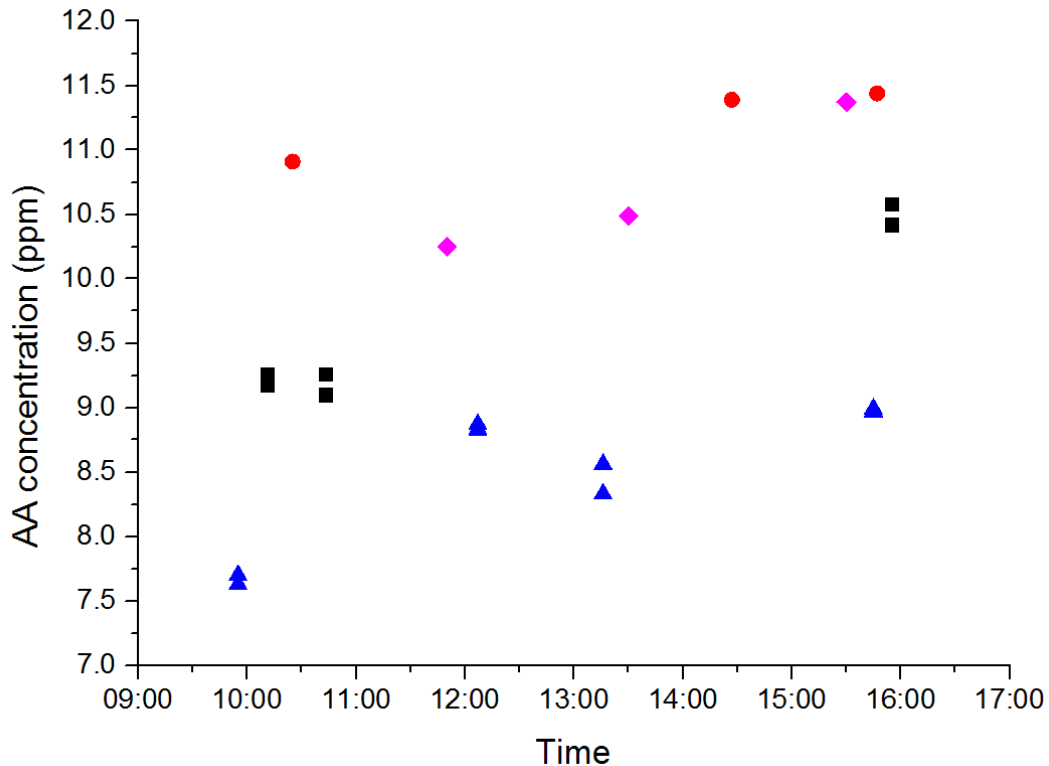


Figure 5.1 AA levels in PET extruded using Rondol twin screw extruder measured in various experiments without carrier, under the same conditions on different days. Blue triangles = experiments 12 & 13, black squares = experiment 5, pink diamonds = experiment 15, red circles = experiment 6

### 5.3 Calculation of Error

Measuring AA levels in blank samples is very important for establishing a baseline for the testing of the catalysts. It is necessary for identifying when a catalyst offers a genuine reduction in the AA concentration and for when a result falls within the error of the test. Once the degree of fluctuation in the blank samples has been measured then it is possible to ascertain the efficacy of the catalyst samples and compare their activities. If all the results for the catalyst testing fall within the error of the experiment, then that data cannot be used as evidence of AA removal performance. As previously mentioned, the mean AA value in blank PET throughout all the testing that was carried out was equal to 10.2 ppm. When the standard deviation is calculated for all the blank samples the deviation from the mean was found to be 1.3 ppm. Using equations 5.1 and 5.2 this standard deviation corresponds to a standard error of 0.21 ppm which is equal to a 95% confidence interval of 0.43 ppm. This means that 95% of the time the blank AA value will not deviate by more than 4.2% or 0.43 ppm. If the

change in AA concentration in the PET is greater than  $\pm 4.2\%$  one can be 95% certain that it is not due to experimental error.

$$\text{Standard error of the mean} = s/\sqrt{n}$$

Equation 5.1 Equation for calculation of standard error.  $s$  = standard deviation,  $n$  = number of measurements ( $n = 40$ )<sup>8</sup>

$$95\% \text{ confidence interval} = \bar{x} \pm t_{n-1}s/\sqrt{n}$$

Equation 5.2 Equation for the calculation of a 95% confidence interval.  $\bar{x}$  = mean,  $t$  = t value (for a 95% confidence interval and  $n = 40$ ,  $t = 2.023$ )<sup>8</sup>

However, for each experiment where more than one blank sample was measured the standard deviation in the blank values for that particular experiment will be quoted. This will help to give an idea as to the error for that specific instance, as the blank values varied quite significantly between the experiments (as highlighted by the data presented in figure 5.1).

In most cases a blank test was run as the first test and the final test of the day so the increase in the baseline AA level would be known, and the deviation between those two values can give a measure of the deviation throughout the entire period of testing. In a few experiments more blank tests were run to give a more detailed baseline and a greater understanding as to how the levels of AA fluctuated over time. It was found that the increase in AA was not always linear but moved in a general upward trend as the day progressed.

#### 5.4 Testing of Metal Oxide Catalysts using Extruder

An initial selection of metal oxide catalysts were tested in the extruder test at a 100 ppm loading, in the same way as a variety of metal oxides were initially tested in the gas phase reactor. The catalysts were added to the PET along with a triglyceride carrier material at a loading of 900 ppm, which ColorMatrix use to disperse their additives within PET. All of the samples used in this test were prepared using the urea precipitation method and calcined at 400 °C, except for the m-ZrO<sub>2</sub> which was

prepared by calcining Zr(OH)<sub>4</sub> at 400 °C. In preparation for the extruder test each sample was sieved and the sieve fraction between 25-75 µm was used in the testing. It was considered necessary to have a known and well-defined particle size range to ensure that the testing was reproducible and offered a fair comparison between samples.

On this occasion a blank sample was only run as the first experiment, hence the error quoted for the blank is only the error associated with the GC-FID analysis. The 0 error refers to the duplicate samples taken for that test giving the same AA concentration not that the blank AA level was constant throughout the testing. The number of blank samples that were extruded is indicated in brackets next to the sample name. It is also the case that the error associated with the catalyst tests is the error between the duplicate analyses. This error is related to the duplicate headspace GC-FID analysis, it is not caused by multiple experiments on the extruder.

Table 5.1 Extruder Experiment 1 - AA concentration data for PET loaded with various catalyst samples and triglyceride carrier (900 ppm). Analysis was conducted in duplicate.

<b>Sample (loading)</b>	<b>AA Concentration / ppm (error)</b>	<b>AA Reduction / ppm</b>	<b>AA Reduction / %</b>
Blank with carrier (x1)	6.8 ( $\pm 0$ )	n/a	n/a
m-ZrO <sub>2</sub> (100 ppm)	8.5 ( $\pm 0.021$ )	-1.7	-25
t-ZrO <sub>2</sub> (100 ppm)	8.1 ( $\pm 0.042$ )	-1.3	-19
Mn <sub>2</sub> O <sub>3</sub> (100 ppm)	7.8 ( $\pm 0.17$ )	-1.0	-15
CeO <sub>2</sub> U1 (100 ppm)	7.5 ( $\pm 0.014$ )	-0.7	-10
ATA (500 ppm)	1.7 ( $\pm 0.057$ )	5.1	75

It can be seen from experiment 1 (see table 5.1) that all the catalysts tested in this set of experiments caused the level of AA to increase compared to the blank sample. This leads to a negative reduction of AA, and is certainly not an ideal result as the intention is to reduce the concentration of AA in the PET. The final sample that was tested was the industrial standard AA scavenger, anthranilamide (ATA), and offered a control test that could confirm that the test was functioning properly. ColorMatrix claim that ATA can reduce AA levels by up to 80%,<sup>9</sup> so a reduction of 75% is a reasonable result. Therefore, the results from this testing can be considered reliable and the test and the apparatus used to conduct the experiment were functional. An ATA test was often used during experiments to act as a control measurement.

Table 5.2 Extruder Experiment 2 - AA concentration data for PET loaded with various catalyst samples at higher and lower loadings and triglyceride carrier (900 ppm). Analysis was conducted in duplicate.

<b>Sample (loading)</b>	<b>AA Concentration / ppm (error)</b>	<b>AA Reduction / ppm</b>	<b>AA Reduction / %</b>
Blank with carrier (x1)	7.1 ( $\pm 0.19$ )	n/a	n/a
CeO <sub>2</sub> U1 (30 ppm)	8.0 ( $\pm 0.28$ )	-0.9	-13
CeO <sub>2</sub> U1 (300 ppm)	6.4 ( $\pm 0.18$ )	0.7	10
m-ZrO <sub>2</sub> (30 ppm)	8.0 ( $\pm 0.02$ )	-0.9	-13
m-ZrO <sub>2</sub> (300 ppm)	8.5 ( $\pm 0.55$ )	-1.4	-20
t-ZrO <sub>2</sub> (30 ppm)	7.7 ( $\pm 0.18$ )	-0.6	-8
t-ZrO <sub>2</sub> (200 ppm)	8.3 ( $\pm 0.044$ )	-1.2	-17
ATA (500 ppm)	2.1 ( $\pm 0.057$ )	5.0	70

Based on the data collected in experiment 1, it was decided that for experiment 2 the same catalysts should be retested at different loadings. The metal oxides were tested at a higher loading of 300 ppm (except for  $\text{ZrO}_2$  which was added at 200 ppm), and a lower loading of 30 ppm. The data for this round of testing can be found in table 5.2, and it was observed that the catalysts performed similarly to the previous experiments at 100 ppm. However, the  $\text{CeO}_2$  catalyst at a loading of 300 ppm did achieve a reduction in AA concentration. It was only a very slight reduction of 0.7 ppm, which could be considered within the error of the experiment (although it is greater than the 95% confidence interval of 0.43 ppm), and a reduction of greater than 1 ppm is desired to be fully convinced of a genuine result. However, it is still significant that it was the only result which did not show an increase in AA, and therefore showed the most potential as an AA scavenger and required further study.

One reason why the metal oxides may cause an increase in AA in the PET could be due to the presence of moisture in the material. As previously mentioned, any moisture introduced to the system could cause hydrolytic degradation of the polymer leading to an increase in AA. Based on this possibility the catalysts were subjected to TGA to determine the level of moisture in the materials. The TGA data (displayed in figure 5.2) shows that the t- $\text{ZrO}_2$  contained the most moisture followed by the  $\text{CeO}_2$ , the m- $\text{ZrO}_2$ , and the  $\text{Mn}_2\text{O}_3$  contained the least. If the level of moisture, as determined by TGA, is compared with the increase in AA observed in the extruder test it is found that there is no correlation between the two (see table 5.3). However, if the AA data is compared with literature enthalpies of water adsorption for these materials then a trend can be observed (also found in table 5.3).<sup>10-12</sup> As the enthalpy of water adsorption decreases, the increase of AA concentration in PET is found to increase. This suggests that the enthalpy of water adsorption of a catalyst could be used to indicate which materials lead to greater hydrolytic degradation of PET. However, the literature values may not be representative of the materials used in this study, so it would be preferable to measure the enthalpies of the prepared catalysts to identify any correlation. This could be the subject of future research that could help to increase the efficiency of AA removal catalysts.

In the previous chapter, in section 4.5.3, it was observed that drying the catalysts made them less active and the literature also supports this claim.<sup>13,14</sup> This is significant because the catalysts need to be hydrated in order to be active, and this

finding indicates that the level of moisture in the catalyst doesn't necessarily correlate with greater degradation of the PET.

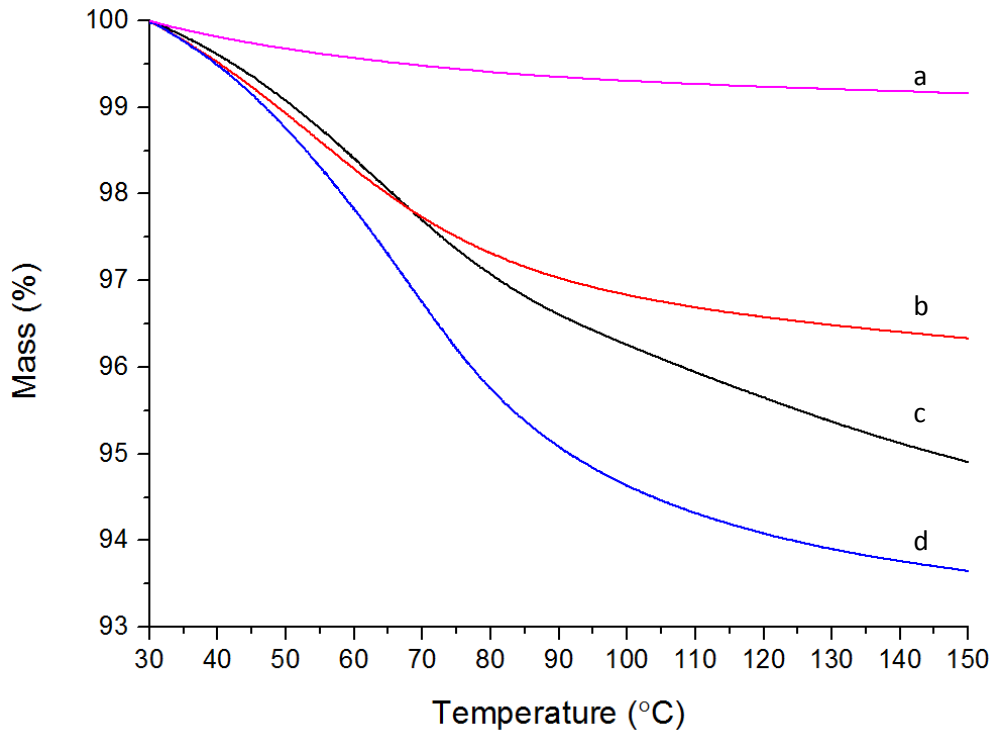


Figure 5.2 TGA of catalysts used in extruder test showing mass loss up to 150 °C; a = Mn<sub>2</sub>O<sub>3</sub>, b = m-ZrO<sub>2</sub>, c = CeO<sub>2</sub> U1, d = t-ZrO<sub>2</sub>

Table 5.3 A comparison between the level of moisture in the catalyst sample and the increase in AA concentration in the extruder test

Sample	Average Increase in AA (%)	TGA Mass loss up to 150 °C (%)	Enthalpy of water adsorption (kJ/mol)	Reference
Mn <sub>2</sub> O <sub>3</sub>	15	0.8	-107	10
m-ZrO <sub>2</sub>	19	3.7	-110 to -170	11
CeO <sub>2</sub> U1	4	5.1	-60	12
t-ZrO <sub>2</sub>	15	6.3	-90	11

Another important factor to note is that experiments 1 and 2 were both conducted using a carrier material. This means that the catalysts were added to the PET along with an oil to aid dispersion and mixing with the polymer. This oil is a triglyceride that ColorMatrix use as a vehicle to add ATA to PET in commercial applications. Whilst this oily carrier might be helpful when using ATA as a scavenger, it could be hindering the activity of the metal oxide catalysts and could be a contributing factor to the poor performance observed by the metal oxides to this point. Therefore, for the next round of experiments the catalysts would be tested in the presence and the absence of the carrier to identify if it was adversely affecting the activity (see section 5.6). The chemical structure of the carrier is presented in figure 5.3, and the material is composed of two major compounds (labelled A and B).

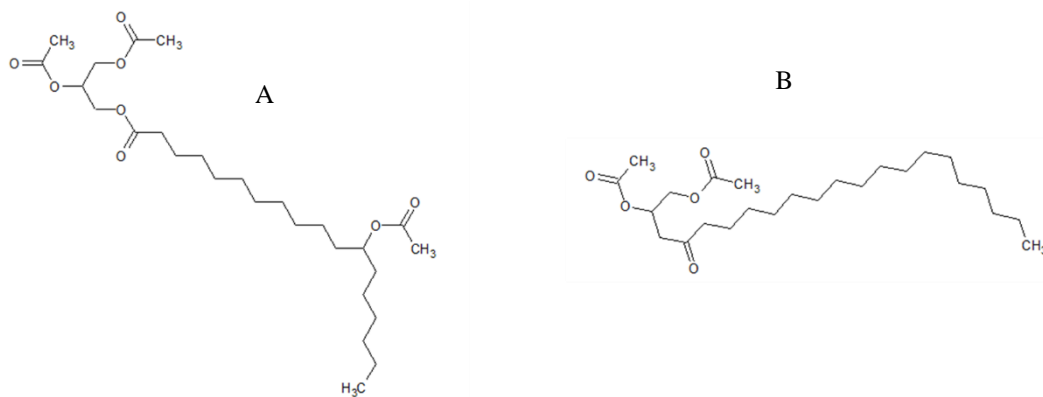


Figure 5.3 Chemical structure of triglyceride carrier oil.

## 5.5 Colour Testing of PET loaded with metal oxide catalysts

The metal oxides also had varying effects upon the aesthetics of the PET, causing alterations to the colour and optical clarity of the polymer (see figure 5.4). To measure the colour properties of the PET loaded with catalyst the PET was moulded into plaques using an injection moulder. The plaques were tested for their colour and haze properties using a spectrophotometer (see section 2.3.7 for details), the data from which can be found in table 5.4.  $L^*$ ,  $a^*$ , and  $b^*$  all refer to the colour of the material according to CIELAB colour space, whilst the haze is measured as a comparison with a standard.  $L^*$  is a measure of the lightness with black = 0 and white = 100,  $a^*$  is a measure of green (-) and red (+), and  $b^*$  is a measure of blue (-) and yellow (+). The

$L^*$  values aren't changed very much by the catalysts except for the  $Mn_2O_3$  which darkened the plastic significantly as shown by the reduction in  $L^*$ . All the catalysts caused an increase in  $b^*$  while ATA causes the greatest yellowing of the PET, with a  $b^*$  value of 3.9. The largest effect of the catalyst samples was in the level of haze, which was significantly higher than the blank and the ATA samples. This poses a problem for potential commercial applications as haze in the PET is highly undesirable as it will not offer a crystal-clear bottle for displaying mineral water. Haze is also more difficult to correct than discrepancies in colour. When ATA is used commercially the discolouration it causes is corrected using toners and dyes. However, it could be possible to minimize the haze by reducing the particle size of the catalyst or by using a lower loading of catalyst. For a lower loading to be effective the catalyst would have to be highly active or better dispersed, and so for that to be a viable option the catalysts would require significant development.

Table 5.4 Colour and haze data for PET loaded with different metal oxide catalysts

Sample (loading)	$L^*$	$a^*$	$b^*$	Haze
Blank	95.462	-0.072	0.996	0.398
$CeO_2$ U1 (100 ppm)	92.356	0.066	3.004	18.432
$t-ZrO_2$ (100 ppm)	94.806	0	1.14	6.242
$m-ZrO_2$ (100 ppm)	92.462	0.144	2.07	29.156
$Mn_2O_3$ (100 ppm)	82.562	1.802	3.324	19.462
ATA (500 ppm)	95.416	-1.27	3.912	0.32

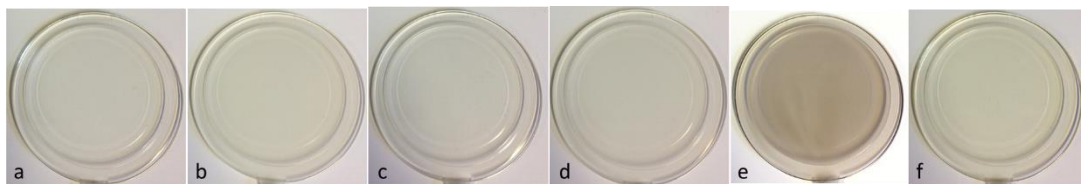


Figure 5.4 Photographs of PET plaques loaded with 100 ppm of different metal oxide catalysts. a = blank, b =  $\text{CeO}_2$ , c =  $\text{t-ZrO}_2$ , d =  $\text{m-ZrO}_2$ , e =  $\text{Mn}_2\text{O}_3$ , f = ATA (500 ppm). Each sample also contained triglyceride carrier (900 ppm).

## 5.6 Testing of $\text{CeO}_2$ Catalysts using Extruder

Due to the  $\text{CeO}_2$  catalyst showing the greatest potential for AA sequestration and based on its activity in gas phase testing (see chapter 4), it was chosen to be the subject of further testing. A new batch of ceria,  $\text{CeO}_2$  U2, was prepared using the urea precipitation method, and this new sample was tested to confirm the validity of the previous positive result. The  $\text{CeO}_2$  U2 catalyst was tested with and without the triglyceride carrier, and the blank samples were also tested with and without the vehicle to provide a more accurate baseline for the measurements. Also, the loading of the catalyst was again increased, this time to 500 ppm, to ascertain whether increasing the loading results in a higher degree of AA removal. The data obtained from these experiments can be found in tables 5.5 and 5.6. The results demonstrate that the presence of the carrier dampens the activity of the  $\text{CeO}_2$  for AA conversion. In both cases the AA reduction achieved in the presence of the carrier is roughly half that of the levels achieved in its absence (12% vs 24% in table 5.5, and 8% vs 14% in table 5.6).

The results from these tests in the presence of the carrier match up well with the previous testing. The  $\text{CeO}_2$  U1 achieved a 10% AA reduction at a loading of 300 ppm in the presence of carrier (table 5.2), whilst  $\text{CeO}_2$  U2 achieved reductions of 12% and 8% in the presence of the carrier at a loading of 500 ppm (table 5.5). This indicates that while there is an increase in activity from a loading of 100 ppm to a loading of 300 ppm, there is a little effect when increase the loading from 300 to 500 ppm. It could alternatively be the case that the U2 catalyst is less active than the U1 catalyst, and so by increasing the loading that gap in activity has been bridged. It was found in the gas phase testing conducted in Cardiff that the U1 catalyst was slightly more active than the U2 catalyst (see table 4.8 in the previous chapter).

Table 5.5 Extruder Experiment 3 - AA concentration for PET loaded with CeO<sub>2</sub> catalyst with and without triglyceride carrier. The samples run with carrier use the triglyceride at a loading of 1000 ppm. Analysis was conducted in duplicate.

<b>Sample (loading)</b>	<b>AA Concentration / ppm (error)</b>	<b>AA Reduction / ppm</b>	<b>AA Reduction / %</b>
Blank with carrier (x1)	10.3 ( $\pm 0.15$ )	n/a	n/a
CeO <sub>2</sub> U2 with carrier (500 ppm)	9.1 ( $\pm 0.099$ )	1.2	12
Blank without carrier (x1)	10.6 ( $\pm 0.32$ )	n/a	n/a
CeO <sub>2</sub> U2 without carrier (500 ppm)	8.1 ( $\pm 0.15$ )	2.5	24

Table 5.6 Extruder Experiment 4 - AA concentration for PET loaded with CeO<sub>2</sub> catalyst with and without triglyceride carrier. The samples run with carrier use the triglyceride at a loading of 1000 ppm. Analysis was conducted in duplicate. Rerun of testing in table 4 one week later.

<b>Sample (loading)</b>	<b>AA Concentration / ppm (error)</b>	<b>AA Reduction / ppm</b>	<b>AA Reduction / %</b>
Blank with carrier (x1)	9.9 ( $\pm 0.14$ )	n/a	n/a
CeO <sub>2</sub> U2 with carrier (500 ppm)	9.1 ( $\pm 0.099$ )	0.8	8
Blank without carrier (x1)	10.3 ( $\pm 0.22$ )	n/a	n/a
CeO <sub>2</sub> U2 without carrier (500 ppm)	8.9 ( $\pm 0.13$ )	1.4	14

The AA reductions achieved by the U2 catalyst in the absence of carrier were more positive than any previous results and showed that a metal oxide catalyst could be effective for removing AA from PET. The 2.5 ppm reduction of AA is also the first result that has been without doubt beyond the margin of error for the extruder test, and so offers strong confirmation that the reduction in AA observed is due to the action of the catalyst. Therefore, from this point on, the standard conditions that were used to test CeO<sub>2</sub> catalysts in the extruder were a 500 ppm loading without carrier.

From experiments 3 and 4 (tables 5.5 and 5.6 respectively) it was demonstrated that the presence of the triglyceride carrier causes a lower AA concentration in the blank samples. In both cases the reduction in AA caused by the carrier is about 0.3 ppm. This effect is caused by the way that the carrier can lubricate the extrusion process. Due to the lubrication the polymer undergoes less sheer stress and therefore undergoes less degradation leading to a lower concentration of AA. It is not a large effect however these experiments indicate that it is fairly reproducible, and this is why it is important to run blank tests with and without carrier to obtain a true comparison of the catalysts when in the presence or the absence of carrier. If the blank had only been measured without the carrier, then the activity of catalyst in the presence of the carrier would have been exaggerated.

Following this confirmation, that CeO<sub>2</sub> could act as an effective AA removal catalyst in PET, an investigation was begun into alternative preparation methods. Could the performance of the ceria catalysts be improved by using more elaborate methods of preparation that could provide improvements in the physicochemical properties of the material? Of particular interest was whether through the use of structure directing agents, aimed at increasing the porosity of the ceria, could the activity of the catalyst could be enhanced. Therefore, CeO<sub>2</sub> was prepared using Pluronic P123, and TTAB as structure directing agents by adapting preparation methods laid out in the scientific literature (see sections 2.2.2, 2.2.3, and 4.3.2).<sup>15,16</sup>

Table 5.7 Extruder Experiment 5 - AA concentration data for PET loaded with CeO<sub>2</sub> catalysts prepared by various methods. No triglyceride carrier was used in these experiments. Blank is an average of two samples. Analysis was conducted in duplicate.

<b>Sample (loading)</b>	<b>AA Concentration / ppm (error)</b>	<b>AA Reduction / ppm</b>	<b>AA Reduction / %</b>
Blank (x3)	9.6 ( $\pm 0.68$ )	n/a	n/a
CeO <sub>2</sub> U1 (500 ppm)	6.5 ( $\pm 0.085$ )	3.1	32
CeO <sub>2</sub> P2 (500 ppm)	10.4 ( $\pm 0.099$ )	-0.8	-8
CeO <sub>2</sub> T1 (500 ppm)	8.9 ( $\pm 0.042$ )	0.7	7
CeO <sub>2</sub> P1 (500 ppm)	9.9 ( $\pm 0.13$ )	-0.3	-3
Nano CeO <sub>2</sub> (500 ppm)	10.1 ( $\pm 0.028$ )	-0.5	-5

P1 and P2 refer to materials prepared with Pluronic P123, the difference between the two materials was the aging process during the preparation. P1 was aged at 60 °C overnight, whereas P2 was aged at 40 °C for 7 days. The T1 material was prepared using TTAB as a structure directing agent. TTAB (tetradecyltrimethylammonium bromide) is a quaternary ammonium surfactant that can be used to tailor the porosity of a catalyst. It is very similar in structure to the more commonly used CTAB (cetyltrimethylammonium bromide), but TTAB has a slightly shorter carbon chain length containing two fewer carbons. The U1 catalyst is the same material used in previous experiments, and the Nano CeO<sub>2</sub> was a commercial material purchased from Sigma-Aldrich. All these materials were tested for their ability to reduce AA levels in PET in the extruder test. All the samples were sieved to a particle size between 25-75 µm and tested at a loading at 500 ppm without carrier.

From experiment 5 (see table 5.7) it can be clearly seen that the U1 offers by far the best performance in terms of reducing the concentration of AA in the PET. A reduction in the AA of 32% also indicates that the U1 catalyst is more active than the

U2 catalyst, which was also observed in the gas phase testing. All the results for the other materials that were tested gave an increase in AA concentration except for T1 which achieved a slight reduction in AA, but it falls within the error of experiment. Apart from U1 all the other materials altered the AA concentration by less than 1 ppm and so are best considered as being within the natural variation of the test. Therefore, none of the preparation methods that incorporated structure directing agents offered any improvement over the urea precipitation preparation. In fact, they generate materials which are significantly less active for removing AA from PET. The materials prepared by these alternative routes are essentially inactive in the extruder test, whereas the U1 catalyst was able to reduce the AA by more than 30%. This is also supported by the data from the gas phase testing where the U1 catalyst outperformed the other catalysts in table 4.6 (see previous chapter). As discussed in section 4.3.2, the discrepancies in activity could be due to the low surface areas of the P1 and P2 catalysts, and the use of NaOH in the preparation of the T1 catalyst could cause poisoning of the catalyst.

Experiment 5 (table 5.7) also highlights that the U1 material is a far better catalyst than commercially available CeO<sub>2</sub> nanopowder. Again, this is supported by the gas phase testing data and characterisation from the previous chapter. Where it was found that due to factors such as lower surface area and lower lattice defect concentration that the commercial nanopowder was a less active catalyst than the catalysts prepared *via* urea precipitation.

Table 5.8 Extruder Experiment 6 - AA concentration data for PET data loaded with ceria catalysts at different loadings. No triglyceride carrier was used. A 25-75 µm sieve fraction was used. Blank is an average three samples. Analysis was conducted in duplicate

<b>Sample (loading)</b>	<b>AA Concentration / ppm (error)</b>	<b>AA Reduction / ppm</b>	<b>AA Reduction / %</b>
Blank (x3)	11.2 ( $\pm 0.30$ )	n/a	n/a
CeO <sub>2</sub> U1 (50 ppm)	12.5	-1.3	-12
CeO <sub>2</sub> U1 (250 ppm)	11.0	0.2	2
CeO <sub>2</sub> U1 (500 ppm)	7.6	3.6	32
CeO <sub>2</sub> U2 (50 ppm)	11.6	-0.4	-4
CeO <sub>2</sub> U2 (250 ppm)	10.3	0.9	8
CeO <sub>2</sub> U2 (500 ppm)	8.0	3.2	29

In experiment 6 the U1 and U2 catalysts were investigated further by testing at different loadings without carrier. The data collected in experiment 6 (table 5.8) supports previous findings that at lower loading loadings of < 100 ppm the catalysts have very little effect upon the AA concentration in the PET. In fact, the AA is slightly increased by the presence of the ceria catalysts at these lower loadings. When the loading is increased to 250 ppm the catalysts again have a very small effect, however this time the AA levels are slightly decreased. The changes in AA concentration at these loadings is so small that they are best considered as being with the margin of error for the experiment. However, when the loading of catalyst is increased to 500 ppm, significant reduction in AA is observed. The U1 catalyst matched its previous performance of 32% reduction in AA concentration and the U2 gave a slightly greater reduction than previous tests achieving an AA reduction of 29%. This small difference

in activities, between the U1 and U2 catalysts, is very similar to what was observed in the gas phase testing.

Table 5.9 Extruder experiment 7 – AA concentration data for PET loaded with ceria catalyst at 500 ppm loading and no triglyceride carrier. A 25-75 µm sieve fraction was used. Blanks are an average of two samples. Analysis was conducted in duplicate.

<b>Sample (loading)</b>	<b>AA Concentration / ppm (error)</b>	<b>AA Reduction / ppm</b>	<b>AA Reduction / %</b>
Blank (x2)	9.8 ( $\pm$ 1.15)	n/a	n/a
CeO <sub>2</sub> U3 (500 ppm)	10.1 ( $\pm$ 0.064)	-0.3	-4
Blank (x2)	12.8 ( $\pm$ 0.55)	n/a	n/a
CeO <sub>2</sub> U3 (500 ppm)	12.2 ( $\pm$ 0.03)	0.6	5

A third batch of ceria was prepared using the same urea precipitation method and was tested at a 500 ppm loading in the extruder test. In the gas phase testing this catalyst was found to be less active than the U1 and U2 catalysts (see table 4.8), where the U3 catalyst achieved an initial activity of 26% whereas the U1 and U2 were able to achieve an initial AA conversion of 31% and 30% respectively. This same trend in activity is observed in the extruder test also. The U1 and U2 catalysts have achieved AA conversions of up to around 30% at a loading of 500 ppm, the U3 catalyst is not able to reduce the AA concentration beyond the error of the experiment and so is found to be essentially inactive in this test (see table 5.9). This offers good confirmation that the gas phase laboratory test has some predictive power as to which materials will perform better in PET in the extruder test. However, the discrepancy in activity between the U3 catalyst and the U1 and U2 catalysts in the extruder test is far greater in the extruder test than the gas phase testing. This may indicate that the extruder test is more sensitive to certain parameters which are as yet unknown.

## 5.7 Intrinsic Viscosity of PET Loaded with Ceria Catalysts

Samples from experiment 6 were examined for their intrinsic viscosity (IV) to gain information as to whether the catalysts were causing degradation of the polymer. If the IV of the PET is significantly reduced in the presence of the catalysts, this would indicate that the polymer chains were being broken down into shorter chains through interactions with the ceria. If this were the case it would help to explain why some of the metal oxides have caused the levels of AA to increase in the PET.

Table 5.10 IV data for PET loaded with ceria catalysts at different concentrations

Sample	IV / dL/g
C93 (control)	0.78
Blank (x2)	0.69
U1 (50 ppm)	0.68
U1 (250 ppm)	0.68
U1 (500 ppm)	0.67
U2 (50 ppm)	0.69
U2 (250 ppm)	0.68
U2 (500 ppm)	0.66
ATA (500 ppm)	0.66

From the results in table 5.10, there is little evidence to suggest that the catalysts are reducing the chain lengths of the PET. The PET loaded with catalyst has the same IV as the blank PET which suggests that the catalyst samples have no effect upon the IV of the polymer. The C93 PET is a bottle grade polymer that was run as a control experiment to verify the accuracy of the analysis. C93 is expected to have an IV of 0.80 dl/g with an error of  $\pm 0.02$  dl/g so a result of 0.78 dl/g is good evidence that the test is working well. The IV of the polymer is unchanged by the presence of the catalysts which indicates that the  $\text{CeO}_2$  is not causing scission of the PET chains. However, these results do not confirm or disconfirm whether the catalysts are degrading the end groups of the polymer (e.g. vinyl esters) as this would not have much of an impact upon the IV. Therefore, the catalysts could be causing the formation of AA by degrading the polymer end groups, whilst also reacting with AA that is

generated to yield a net reduction in AA concentration. An alternative test would need to be developed in order to examine whether the ceria catalysts are active for degrading end groups in PET. Using headspace GC-MS one could attempt to quantify all of the organic products that are evolved from the PET.

### 5.8 Effect of Carrier on Catalyst Activity

A comparison could now be made using all the data collected using the U1 and U2 catalysts in the extruder test in the presence and absence of the carrier. This data clarified that the triglyceride carrier has a negative effect upon the activity of these catalyst samples. In figure 5.5 the catalyst activity of CeO<sub>2</sub> U1 and U2 is plotted against the catalyst loading, and the open and filled symbols indicate whether carrier was used or not.

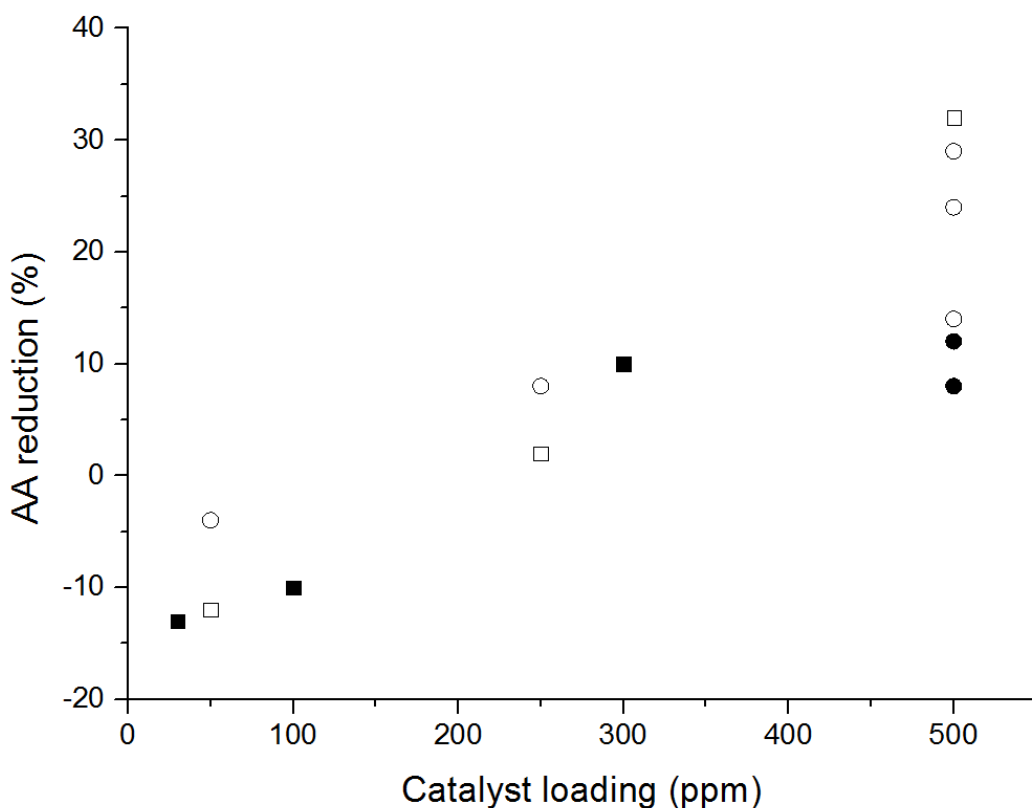


Figure 5.5 Effect of carrier on the activity of CeO<sub>2</sub> catalysts (CeO<sub>2</sub> U1 & U2) for AA reduction in PET. Squares = U1, circles = U2, filled symbols = with carrier, open symbols = without carrier

At 500 ppm loading, five tests without carrier can be compared with two tests with carrier, and the performance of the catalysts is clearly better in the absence of the triglyceride. The detrimental effect of the carrier is less clear at lower loadings, and under those regimes the catalyst has a similar effect upon the AA concentration whether the carrier is present or not. However, at lower loadings the results are close to the experimental error of  $\pm 4.2\%$ . It is hypothesised that the reduction in activity is caused by the oil coating the surface of the  $\text{CeO}_2$  and blocking the porous structure of the catalyst, thereby preventing the AA from interacting with the  $\text{CeO}_2$  as effectively.

Due to the observations that were made in the extruder test regarding the effect of the carrier on the activity of the catalysts, it was also examined in the gas phase test. A ceria catalyst was dosed with carrier before being tested for AA conversion in the gas phase reactor under the standard testing conditions.

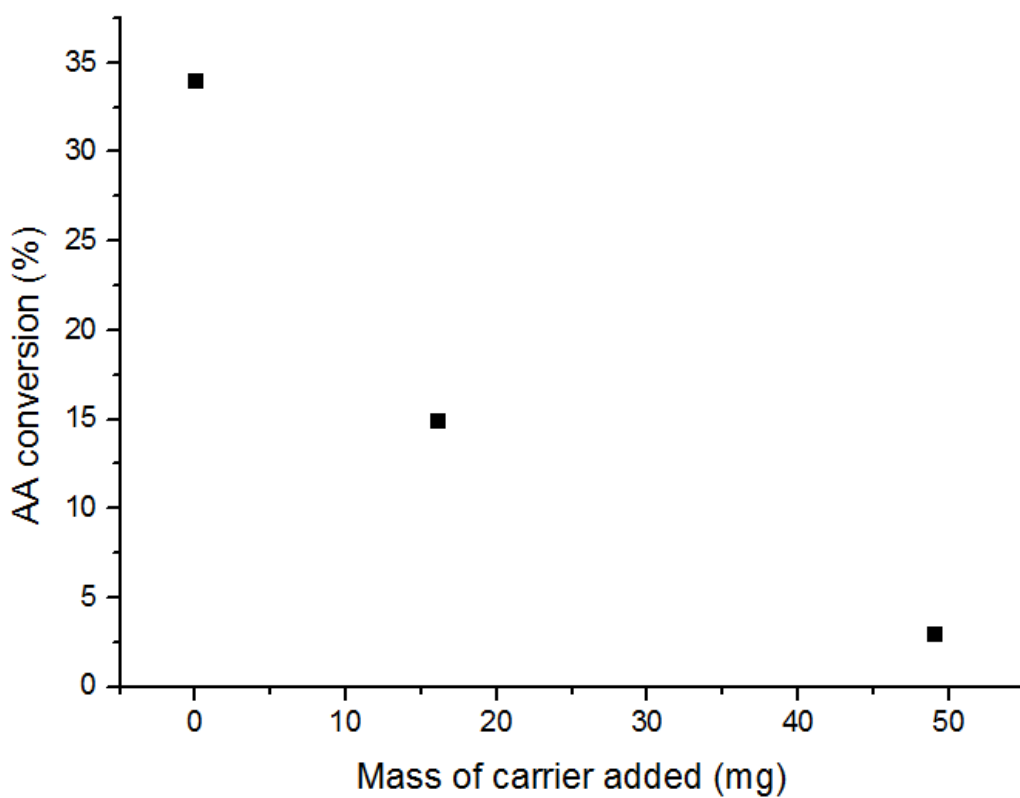


Figure 5.6 Effect of carrier on activity of U1 catalyst (61 mg) for conversion of AA in gas phase test at 300 °C and a GHSV of 300,000 h<sup>-1</sup>

When carrier was added to the catalyst it was found to also reduce the activity in the gas phase test (see figure 5.6). Under the normal testing conditions (61 mg catalyst bed in 200 ml/min flow of AA(1000 ppm)/He, GHSV = 300,000 h<sup>-1</sup>) with no carrier present the U1 catalyst achieved a reduction in AA of 34%. When one drop of carrier (16 mg) was added to the catalyst the AA conversion dropped by more than half, down to 15%. When more carrier was added (3 drops, 49 mg) the AA conversion dropped even further, down to 3%. This offers further confirmation that the presence of the carrier material has a detrimental effect on the catalyst, and this is most likely due to pore blockage. Although the loadings used in the experiments are high, with 3.8:1 and 1.2:1 catalyst to carrier ratios. The catalyst to carrier ratio used in the extruder test for a catalyst loading of 500 ppm is 1:1.8, where the carrier is in excess relative to the catalyst.

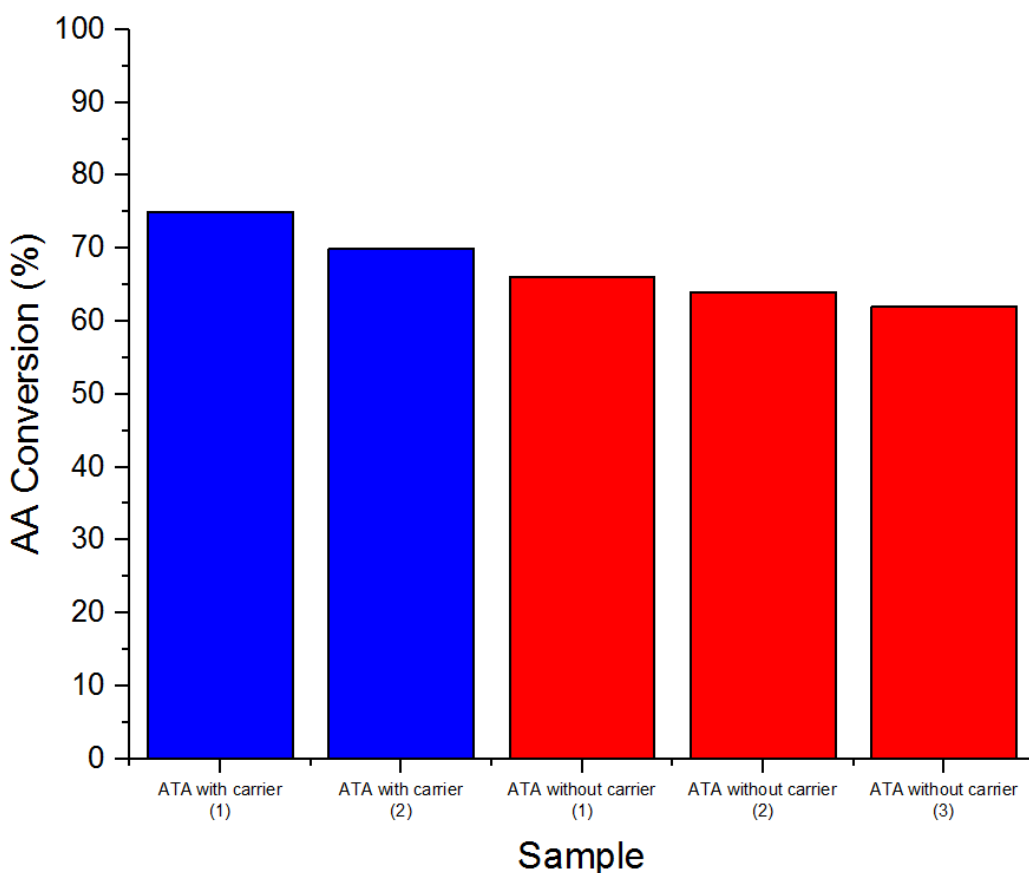


Figure 5.7 Effect of carrier on activity of ATA at 500 ppm loading with and without triglyceride carrier in extruder test.

In the case of ATA, it was found that the presence of the carrier does improve the performance of the additive for conversion of AA in PET. For the two experiments that were conducted in the presence of the carrier the average AA conversion was 73%, whereas in the absence of the carrier the average conversion was only 64% (see figure 5.7). ATA is not a porous solid like a metal oxide and so the pore blockage that is observed with the ceria catalysts is not an issue. The carrier aids the dispersion of the ATA within the PET enabling more of the additive to come into contact with the AA. Part of the increase in activity could also be due to the lubricating effect of the carrier which causes the degradation of the PET during extrusion to be less severe. However, this effect should be accounted for as, the blanks for the experiments with carrier were also conducted with carrier.

## 5.9 Testing of milled CeO<sub>2</sub> catalysts

Hitherto an AA reduction of around 30% has been achieved and attempts to improve upon this result with the use of more sophisticated and elaborate catalyst preparations have been unsuccessful. Also, all the testing had been performed using the 25-75 µm sieve fraction of the catalyst samples. Therefore, it was hypothesised that a major factor limiting the activity of the catalysts could be the particle size. Is a particle size of 25-75 µm just too large to achieve greater reductions in AA concentration in PET? Would a smaller particle size allow for a greater dispersion of the catalyst within the PET and therefore, enable it to interact with more of the AA present in the polymer?

To investigate this hypothesis a large amount of ceria was prepared by doubling the scale of the urea precipitation method and by repeating it 5 times. This generated over 60 g of material and 50 g of it was milled at ColorMatrix in a wet mill process (see section 2.2.4). For this milling process the ceria (50 g) was added to the triglyceride (350 g) and circulated through the mill (7:1 carrier to catalyst ratio). When the ceria and carrier were added together there was a noticeable temperature increase of the mixture. This suggests that the interaction between the carrier and the metal oxide is exothermic. This could be due to interactions between the ceria and ester groups in the carrier structure. Ceria has been shown to be an effective transesterification catalyst at temperatures of around 160 °C, and so is known for

effectively interacting with ester moieties.<sup>17</sup> Ceria is also known to be able to convert triglycerides to fatty ketones at 300-400 °C.<sup>18</sup> This indicates that the triglyceride cannot be considered an entirely inert carrier material for the ceria catalysts. Samples were removed from the mill at different intervals (2, 10, and 20 minutes) to give variation to the degree in which they were milled.

However, as was observed with catalysts previously tested in the presence of carrier, the catalyst activity is essentially null. For all three of the samples tested in experiment 8 (see table 5.11) the change in AA with respect to the blank samples is very small and falls within the margin of error. This offers further confirmation to the claim that has already been made, that the carrier causes pore blockage and reduces catalyst activity. The wet milled samples were taken back to the laboratories in Cardiff and washed thoroughly with hexane to remove the carrier. The excess 10 g of ceria from the upscaled catalyst preparations was milled in a planetary ball mill to offer a comparison between a wet milling process and a dry milling process.

Table 5.11 Extruder Experiment 8 - AA concentration for PET loaded with CeO<sub>2</sub> catalysts milled for differing durations with triglyceride carrier. Catalysts were loaded as part of dispersion made with 1:7 CeO<sub>2</sub>:carrier ratio. 4 g of dispersion to give 500 ppm catalyst loading. Blank is an average value of two samples. Analysis was conducted in duplicate.

<b>Sample</b>	<b>AA Concentration / ppm (error)</b>	<b>AA Reduction / ppm</b>	<b>AA Reduction / %</b>
Blank with carrier (x2)	13.0 ( $\pm 0.90$ )	n/a	n/a
CeO <sub>2</sub> U5 milled 2 mins	12.4 ( $\pm 0.14$ )	0.6	5
CeO <sub>2</sub> U5 milled 10 mins	12.7 ( $\pm 0.12$ )	0.3	2
CeO <sub>2</sub> U5 milled 20 mins	13.3 ( $\pm 0.014$ )	-0.3	-2

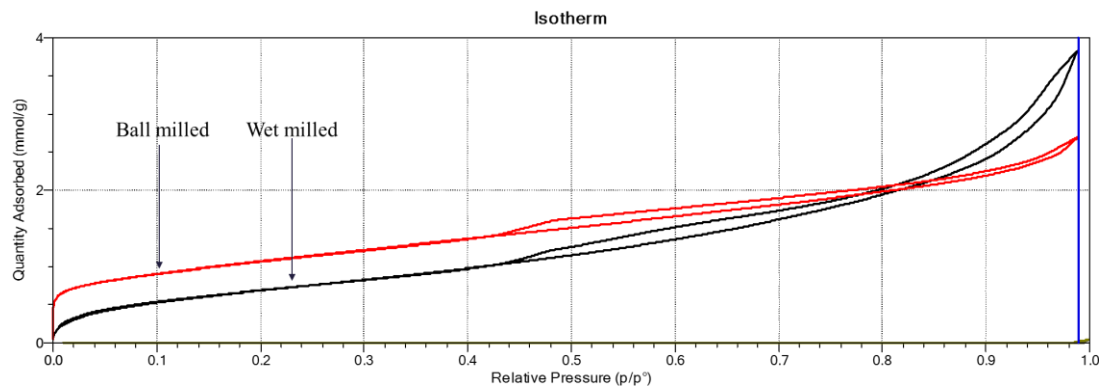


Figure 5.8 Full N<sub>2</sub> adsorption/desorption isotherms for ball milled catalyst (red) and wet milled catalyst (black)

From the isotherms in figure 5.8, measured using a Micromeritics 3flex, it can be seen that the carrier has affected the N<sub>2</sub> adsorption properties of the wet milled material. There is far less adsorption at low pressure for the wet milled sample compared to the quantity of N<sub>2</sub> adsorbed by the ball milled material. This indicates that there is more adsorption into small pores for the ball milled ceria, which suggests that this material is more microporous than the wet milled version. This is also supported by data measured using a Quantachrome Nova that shows the ball milled catalyst was able to adsorb 22 cc/g of N<sub>2</sub> at 0.05 P/P<sub>0</sub>, whereas the wet milled sample only adsorbed 8 cc/g. 0.05 P/P<sub>0</sub> is the lowest pressure measurement in the 5 point BET surface area analysis that was conducted, and so that point gives the strongest indication as to the level of N<sub>2</sub> adsorption at low relative pressures from a 5 point BET measurement. However, at higher relative pressure the wet milled sample is able to adsorb more N<sub>2</sub> than the ball milled sample. The BET surface areas measured from these analyses gave a value of 85 m<sup>2</sup>/g for the ball milled material, and a value of 60 m<sup>2</sup>/g for the wet milled material. This data may not be truly representative of how the ceria is affected by the carrier in the extruder process due to all of the washing and treatment that the sample had to undergo to make it suitable for analysis in the 3flex apparatus. This treatment included thorough washing with hexane and centrifugation to remove the triglyceride oil. The sample was also degassed offline at 250 °C prior to porosity analysis to ensure that the 3flex apparatus was not damaged by the expulsion of organic moieties from the surface of the ceria.

These samples were tested in the gas phase reactor at 300 °C and a GHSV of 300,000 h<sup>-1</sup> to see how their activities compared in that test (see table 5.12). From the

results of the gas phase testing it can be clearly seen that the ball milled material is a far more active catalyst than the material that was milled in oil. The activity of the wet milled catalyst is 18% conversion, which is close to half that of the ball milled catalyst at 35%. The selectivities are very similar for both materials which indicates that both react with the AA *via* the same mechanism.

Table 5.12 Gas phase testing data. Conditions: 1000 ppm AA in He at 200 ml/min, GHSV = 300,000 h<sup>-1</sup>, 300 °C for 1 hour.

Sample	AA conversion (%)	CO <sub>2</sub> selectivity (%)	Acetone selectivity (%)	Carbon balance (%)
U5 ball mill	35	74	26	81
U5 wet mill	18	76	24	88

Following analysis in Cardiff the ball milled and wet milled catalysts were tested in the extruder to compare their activities (see table 5.13). In the extruder test both catalysts were found to have low activity for removal of AA from PET. The wet milled catalyst only reduced the AA concentration by 4% and so is within the experimental error. The ball milled material achieved a greater reduction in AA of 8%, however this is still less than the 10% reduction in AA required to be certain of a genuine result. The difference in performance between the two catalysts is far greater in the gas phase test than in the extruder test. This could be due to the fact that for the gas phase test the catalysts were loaded in terms of volume, whereas for the extruder test the catalysts were added in terms of mass. The ball milled material has a density of 2.2 g/ml, whilst the wet milled material has a lower density of 1.5 g/ml. This significant difference in density of the two materials could be a factor behind the discrepancies between the testing protocols.

Table 5.13 Extruder Experiment 9 - AA concentration for PET loaded with CeO<sub>2</sub> that has been milled and sieved. Catalysts were loaded without triglyceride carrier. Blank is an average of two samples. Analysis was conducted in duplicate.

<b>Sample (loading)</b>	<b>AA concentration / ppm (error)</b>	<b>AA Reduction / ppm</b>	<b>AA reduction / %</b>
Blank (x2)	11.0 ( $\pm 0.35$ )	n/a	n/a
U5 ball milled  $< 25 \mu\text{m}$  (300 ppm)	10.0 ( $\pm 0.21$ )	1.0	8
U5 wet milled  $< 25 \mu\text{m}$  (300 ppm)	10.5 ( $\pm 0.18$ )	0.5	4

Due to the good performance of the U5 ball mill in the gas phase testing it was used to study a wide range of catalyst loadings in the extruder test. To this point catalysts had been tested from 30-500 ppm loadings, so the U5 ball mill catalyst was used to investigate if the activity would continue to increase as the catalyst loading becomes even greater. In table 5.14 the results from using the U5 ball mill in loadings from 50-1000 ppm show that the activity of the catalyst does not plateau at 500 ppm but continues to increase up to 1000 ppm where the greatest AA reduction of 20% was achieved. The activity of this catalyst was found to be less than both the U1 and U2 catalysts even though it slightly outperformed those two catalysts in the gas phase testing. The U5 ball mill catalyst converted 35% of the AA in the gas phase test, whereas the U1 and U2 catalysts removed 31% and 30% respectively. However, in the extrusion test the U5 ball mill catalyst was only able to convert 20% of the AA at a loading 1000 ppm, whilst the U1 and U2 catalysts outperformed that result at half the catalyst loading. The densities of the materials could be playing a large part in the disagreement between the two tests. The U1 catalyst has a density of 1.5 g/ml, and the U2 catalyst has a density of 1.4 g/ml, so the ball milled material is far more dense. This allows for more material to be packed into the volume required to pack the reactor tube for the gas phase test. If the catalyst was added in terms of volume to extruder

test also, maybe there would be more agreement between the tests when using these materials. Although, the more dense material may not be able to disperse as effectively within the PET, which could contribute to the lesser activity of the ball milled catalyst in the extruder test.

Table 5.14 Extruder experiment 10 - AA concentration data for PET loaded with catalysts. Catalysts were loaded without triglyceride carrier. Blank is an average of two samples. Analysis was conducted in duplicate.

<b>Sample (loading)</b>	<b>AA Concentration / ppm (error)</b>	<b>AA Reduction / ppm</b>	<b>AA Reduction / %</b>
Blank (x2)	12.8 ( $\pm 0.55$ )	n/a	n/a
U5 ball mill (50 ppm)	12.7 ( $\pm 0.30$ )	0.1	1
U5 ball mill (250 ppm)	11.9 ( $\pm 0.09$ )	0.9	7
U5 ball mill (500 ppm)	12.9 ( $\pm 1.26$ )	-0.1	-1
U5 ball mill (750 ppm)	11.4 ( $\pm 0.66$ )	1.4	11
U5 ball mill (1000 ppm)	10.2 ( $\pm 0.16$ )	2.6	20
ATA (500 ppm)	4.9 ( $\pm 0.13$ )	7.9	62

In figure 5.9 a linear trend can be seen between AA conversion and catalyst loading, with higher conversions observed with increased catalyst loadings. Higher loadings of catalyst in PET are undesired, however, because as more catalyst is added the hazier the polymer becomes. Crystal-clear PET is preferred to make mineral water most appealing to customers.

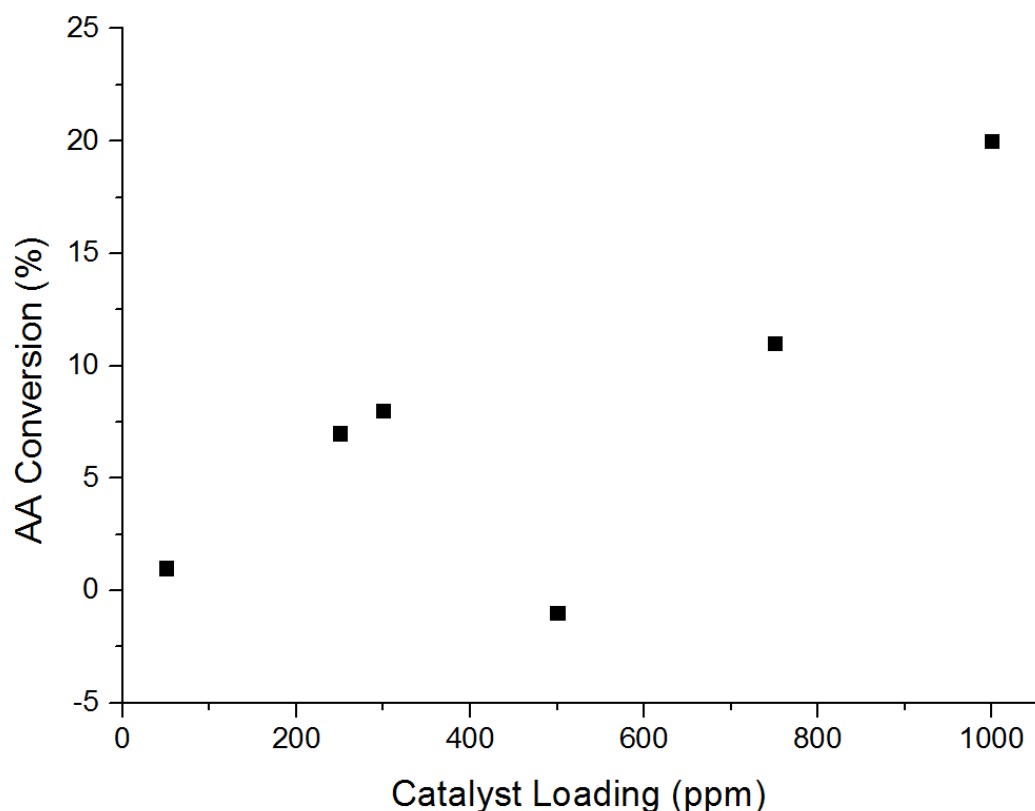


Figure 5.9 Effect of catalyst loading upon AA conversion in extruder test using U5 ball mill catalyst without carrier. All experiments used a 25-75 µm sieve fraction, except for the 300 ppm loading which used a < 25 µm sieve fraction.

To further examine the effect of ball milling upon the activity of ceria catalysts, a U6 catalyst was prepared using the same method as U5 to offer a comparison between a ball milled and an unmilled sample. Also, the commercial ceria nanopowder was subjected to milling in the planetary ball mill to determine if the activity, of this previously poor catalyst, could be improved by milling. The results for the testing of these catalysts in the extruder can be found in table 5.15. The nano catalyst gave a similar result to the previous test (-5% in experiment 5, see table 5.7), and on both occasions it essentially had no effect upon the AA concentration in the PET. After milling, the nano ceria achieved a reduction in AA of 11% which places it right on the cusp of what can be confidently considered a genuine result beyond the margin of experimental error. However, the standard deviation for the blank samples in that experiment was only 0.35 ppm which makes it more likely that the catalyst did indeed cause a reduction in AA.

For the U6 catalyst, the unmilled sample reduced the AA concentration by 10% but the deviation of the blank samples for that experiment was greater than 10%. Therefore, that result cannot be attributed to the action of the catalyst as it falls within the error of the test. When the ball milled sample was tested, the error in the blanks was far lower and the reduction in AA was almost doubled to 19%. In this case there can be confidence that this alteration in AA concentration is due to the activity of the catalyst. In both cases, the use of milling and a smaller particle size sieve fraction increases the efficacy of the catalyst for removal of AA from PET. This suggests that particle size and catalyst dispersion throughout the polymer are likely to be major factors upon the efficacy of the catalyst in the PET. Also, the increase in density caused by the milling cannot be discounted as a major contributing factor.

Table 5.15 Extruder Experiment 11 - AA concentration for PET loaded with CeO<sub>2</sub> prepared via various methods. Catalysts were loaded without triglyceride carrier. Blank is an average of two samples. Analysis was conducted in duplicate.

<b>Sample (loading)</b>	<b>AA concentration / ppm (error)</b>	<b>AA Reduction / ppm</b>	<b>AA reduction / %</b>
Blank (x2)	9.8 ( $\pm 1.15$ )	n/a	n/a
Nano 25-75 $\mu\text{m}$ (500 ppm)	9.9 ( $\pm 0.17$ )	-0.1	-1
U6 25-75 $\mu\text{m}$ (500 ppm)	8.8 ( $\pm 0.11$ )	1.0	10
Blank (x2)	11.0 ( $\pm 0.35$ )	n/a	n/a
Nano ball mill $< 25 \mu\text{m}$ (500 ppm)	9.7 ( $\pm 0.00$ )	1.3	11
U6 ball mill $< 25 \mu\text{m}$ (500 ppm)	8.8 ( $\pm 0.25$ )	2.2	19

## 5.10 Testing of dried CeO<sub>2</sub> catalysts

In section 5.4 it was noted that the presence of moisture in the catalysts could play a part in the generation of AA *via* hydrolytic degradation of the PET. However, TGA showed that the level of moisture in the catalyst sample could not be correlated to the observed increase in AA concentration. To further examine the effect of moisture in the catalyst samples, the materials were dried overnight in a vacuum oven at 120 °C prior to testing in the extruder, and this was compared with a catalyst that had not been dried. The U3 catalyst was tested for the effect of drying and for the effect of using a smaller particle size sieve fraction. The results for these tests can be found in table 5.16, and in both cases the catalyst was unable to achieve an AA reduction of greater than 10%. When these results are compared to the data acquired in experiment 7 (table 5.9) no noticeable improvement in catalytic performance is attained by drying or using a smaller particle size.

Table 5.16 Extruder experiment 12 – AA concentration data for PET loaded with catalysts that had been dried overnight in a vacuum oven at 120 °C or not dried. Catalysts were loaded without carrier. Blank is an average of two samples. Analysis was conducted in duplicate.

<b>Sample (loading)</b>	<b>AA Concentration / ppm (error)</b>	<b>AA Reduction / ppm</b>	<b>AA Reduction / %</b>
Blank (x2)	8.3 ( $\pm 0.68$ )	n/a	n/a
U3 25-75 µm dried (500 ppm)	8.1 ( $\pm 0.12$ )	0.2	2
Blank (x2)	8.7 ( $\pm 0.32$ )	n/a	n/a
U3 < 25 µm not dried (500 ppm)	8.1 ( $\pm 0.14$ )	0.6	7

Table 5.17. Extruder Experiment 13 - AA concentration data for PET loaded with catalysts that had been dried overnight in a vacuum oven at 120 °C or not dried. Catalysts were loaded without carrier. Blank is an average of two samples. Analysis was conducted in duplicate.

<b>Sample (loading)</b>	<b>AA Concentration / ppm (error)</b>	<b>AA Reduction / ppm</b>	<b>AA Reduction / %</b>
Blank (x2)	8.3 ( $\pm 0.68$ )	n/a	n/a
U6 ball mill < 25 µm dried (500 ppm)	7.2 ( $\pm 0.0070$ )	1.1	13
U6 ball mill 25-75 µm dried (500 ppm)	7.5 ( $\pm 0.16$ )	0.8	10
U6 25-75 µm dried (500 ppm)	7.4 ( $\pm 0.014$ )	0.9	11
Blank (x2)	8.7 ( $\pm 0.32$ )	n/a	n/a
U6 < 25 µm (500 ppm)	7.7 ( $\pm 0.11$ )	1.0	11
U6 ball mill < 25 µm (500 ppm)	7.5 ( $\pm 0.035$ )	1.2	14
U6 ball mill 25-75 µm (500 ppm)	7.5 ( $\pm 0.23$ )	1.2	14
ATA (500 ppm)	3.0 ( $\pm 0.092$ )	5.7	66

The U6 catalysts were also subjected to further analysis to determine the effect of drying upon them. In each case the AA concentration was slightly reduced with the levels decreasing by 10-14%, showing that these catalysts have similar levels of activity to the U5 material. These results indicate that drying or milling the catalysts have very little effect upon the effectiveness of these materials for removing AA from PET. Even if these preparations do slightly increase the catalyst activity, they do not increase it beyond the error of the experiment and so cannot be considered to have any clear positive effect. These catalysts also fail to match the performance of the U1 and U2 catalysts where about 30% of the AA was converted. As previously noted, it has already been demonstrated that the catalysts are more active when they are hydrated (see section 4.5.3) and there is literature precedent for this conclusion.<sup>13,14</sup>

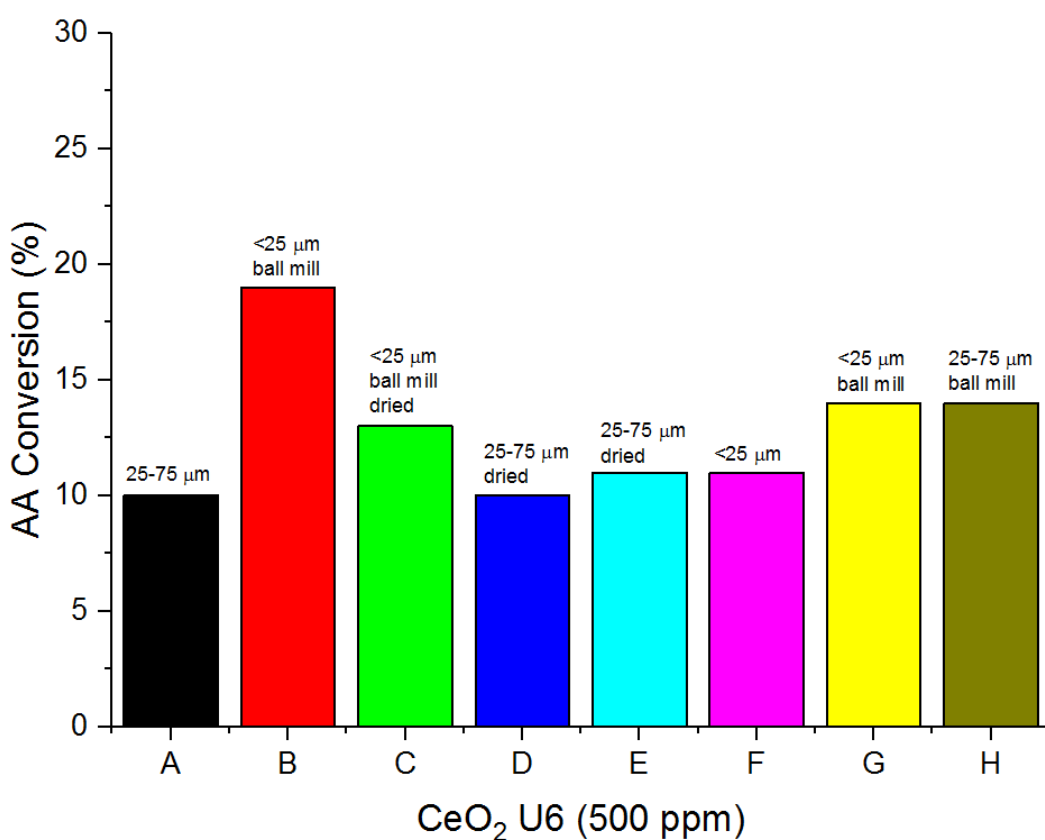


Figure 5.10 Extruder test data for CeO<sub>2</sub> U6 samples prepared in different ways at a 500 ppm loading. A = 25-75 µm, B = < 25 µm ball mill, C = < 25 µm ball mill dried, D = 25-75 µm dried, E = 25-75 µm dried, F = < 25 µm, G = < 25 µm ball mill, H = 25-75 µm ball mill.

## 5.11 Testing of Doped Ceria Catalysts

The results in experiment 14 (table 5.18) show that the ceria doped with copper oxide and manganese oxide have very little activity for removal of AA from PET. Both catalysts achieved an AA reduction of less than 10% and so neither can be considered to have any significant impact upon the levels of AA in PET. The ceria doped with zirconia however, attained a reduction in AA of 24%, and so achieved the largest conversion of AA behind the benchmark U1 and U2 catalysts. These results indicate that to improve these catalysts for performance in converting AA in PET is not as simple as enhancing one characteristic of the material. Zr is known to increase the OSC (oxygen storage capacity) of ceria, yet does not improve catalyst performance beyond the 30% reduction in AA that has been previously achieved.<sup>19-21</sup> Similarly, Cu is known to increase the number of defects in the ceria, yet the catalytic performance in this particular process was not improved.<sup>22,23</sup> These findings are also supported by testing in the gas phase where the doped catalysts were all found to convert less AA than the U1 and U2 catalysts.

Table 5.18 Extruder Experiment 14 - AA concentration data for PET loaded with doped ceria catalysts. No carrier was used. A 25-75 µm sieve fraction was used for each catalyst sample. Blank is an average three samples. Analysis was conducted in duplicate

Sample (loading)	AA Concentration / ppm (error)	AA Reduction / ppm	AA Reduction / %
Blank (x3)	10.7 ( $\pm 0.59$ )	n/a	n/a
5%ZrO <sub>x</sub> -CeO <sub>2</sub> (500 ppm)	8.1	2.6	24
5%CuO <sub>x</sub> -CeO <sub>2</sub> (500 ppm)	9.9	0.8	7
5%MnO <sub>x</sub> -CeO <sub>2</sub> (500 ppm)	9.7	1.0	9
ATA (500 ppm)	3.8	6.9	64

## 5.12 IV of PET Loaded with Doped Ceria Catalysts

The samples in experiment 14 (table 5.18) were subjected to IV analysis in the same manner as the samples in experiment 6. The results obtained in this testing (see table 5.19) were very similar to the previous results with the ceria catalysts, as the IV of the PET was unaffected by the presence of the catalyst samples. This offers further evidence that the catalysts are not causing the degradation of the polymer chains. However, as aforementioned this does not offer much insight into the interactions between the catalysts and the polymer end groups which could be degraded without much change to the IV.

Table 5.19 IV data for PET loaded with doped ceria catalysts

Sample	IV dL/g
C93 (control)	0.78
Blank	0.67
5%ZrO <sub>x</sub> -CeO <sub>2</sub> (500 ppm)	0.67
5%CuO <sub>x</sub> -CeO <sub>2</sub> (500 ppm)	0.67
5%MnO <sub>x</sub> -CeO <sub>2</sub> (500 ppm)	0.67
ATA (500 ppm)	0.66

## 5.13 SEM of PET loaded with CeO<sub>2</sub>

In order to analyse the dispersion of the catalysts within PET, SEM was used to examine the particles embedded in the polymer matrix. PET was loaded with CeO<sub>2</sub> U3 (500 ppm, 25-75 µm sieve fraction) and injection moulded to form a preform (this can be seen on the left side of images a and b in figure 5.11). The preform was then blow moulded to form a bottle (this can be seen on the right images a and b in figure 5.11). A bottle is suitable for providing samples that can be analysed using electron microscopy as they have a wall thickness of around 300 µm. As was observed in the data when analysing the PET plaques loaded with catalyst (see figure 5.4 and table 5.4), the presence of the ceria causes haze within the polymer (see figure 5.11 image b). The blank PET bottle has far greater clarity (see figure 5.11 image a) than the bottle containing 500 ppm of ceria. The haze is less severe in the bottle than the preform as the polymer is expanded and the wall thickness is reduced, however there is still an

obvious hazing effect upon the bottle also. As mentioned in section 5.5, haze is more problematic than discolouration in the PET because colour can be corrected by dyes and toners whereas haze can not. The two best routes to reduce the level of haze in the PET would be to either reduce the loading of catalyst or to reduce the particle size of the catalyst.



Figure 5.11 PET preform (left) and bottle (right): a = blank PET, b = PET loaded with 500 ppm CeO<sub>2</sub> U3 (25-75  $\mu\text{m}$  sieve fraction)

For use in the SEM small segments of PET were cut out from the bottles and were sonicated in ethanol for 10 mins to remove any surface debris. The cleaned PET was stuck onto SEM holders using silver DAG (a silver-based paint used in SEM for its conductive properties). The sample was then sputter coated with Au/Pd to a thickness of 10  $\mu\text{m}$ .

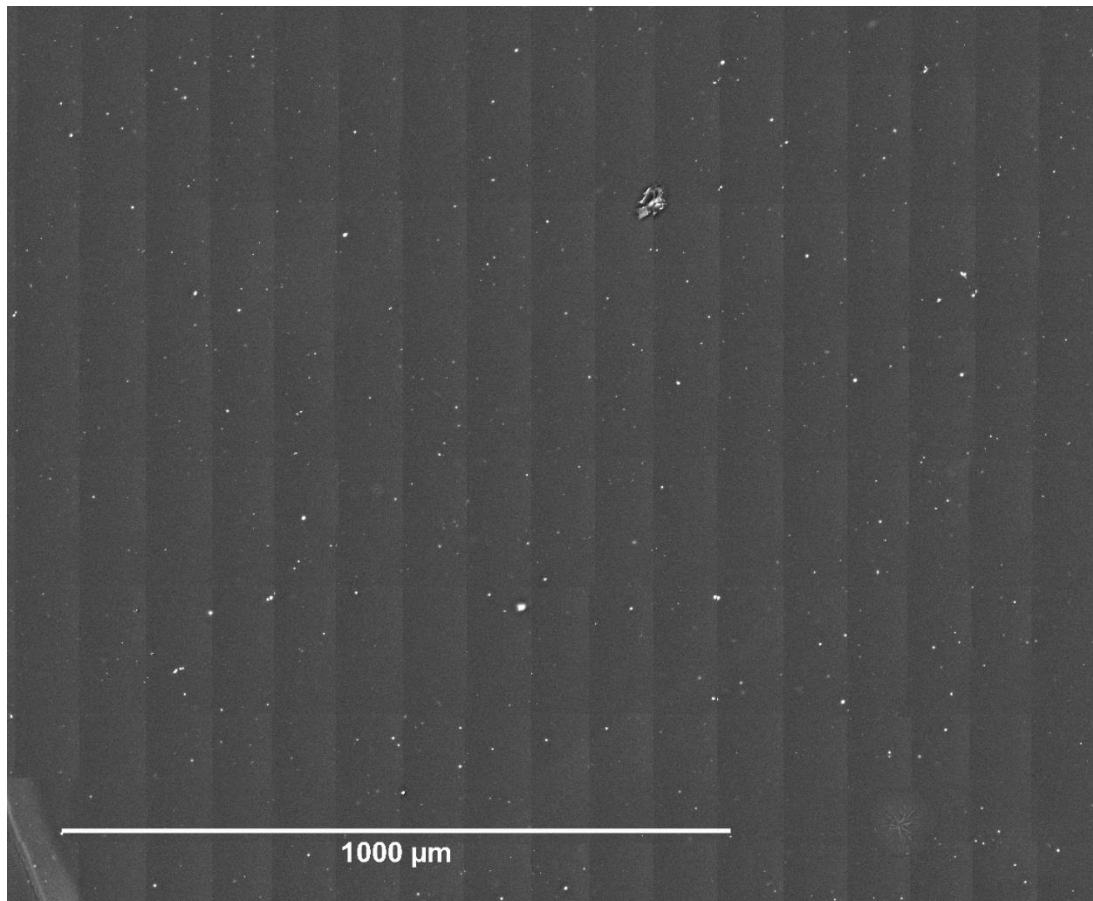


Figure 5.12 Montage of SEM images of PET loaded with CeO<sub>2</sub> U3

In order to gain an insight into the level of catalyst dispersion within the PET bottle wall, an image of a large section of the sample was generated by creating a montage of 252 images (see figure 5.12). From this more global perspective it can be observed that the ceria is dispersed throughout the PET although some particles are quite large, i.e. > 5  $\mu\text{m}$ . From the individual images the length of the particles can be measured using software such as ImageJ (see figure 5.13). In order to conduct a statistical analysis, it is important to gather a large enough dataset, therefore a few hundred datapoints should be collected before the analysis can be applied.

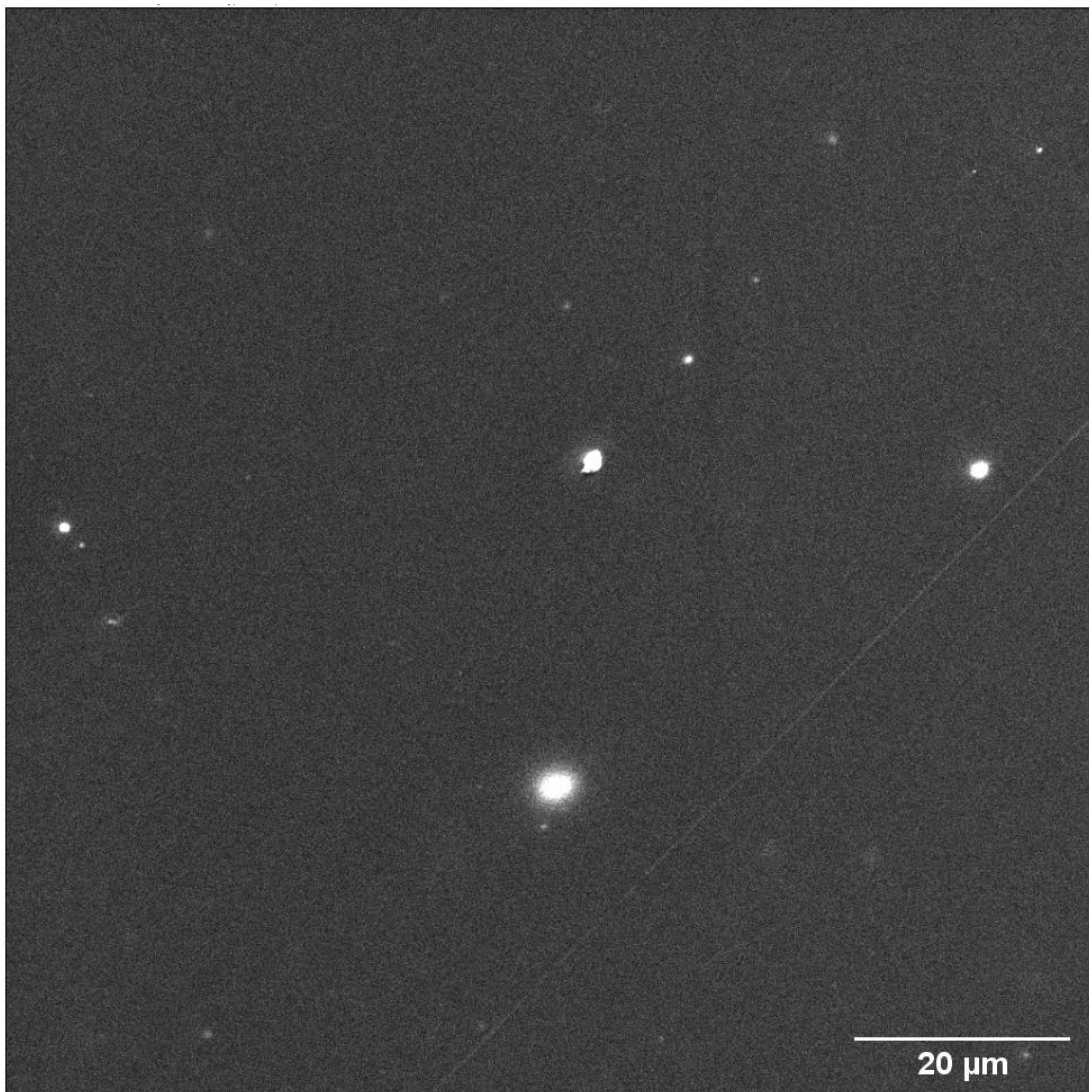


Figure 5.13 Example of a single 100x100  $\mu\text{m}$  image with 20  $\mu\text{m}$  scale bar

Once 350 particles had been measured, which involved measuring particles from 61 of the 252 images, statistical analysis was conducted to give a particle size distribution for the ceria particles observed in the PET. In each 100x100  $\mu\text{m}$  image there were on average 5-6 ceria particles that were observable and measurable. The particle size distribution histogram for the 350 particles can be found in figure 5.14 and shows that the majority of the ceria particles are between 0.5 – 1.5  $\mu\text{m}$  in length. The mean particle size is also found in this range at 1.20  $\mu\text{m}$ . The standard deviation for the particle size of the 350 measured particles is 0.77  $\mu\text{m}$ . The catalyst that was added to this PET sample was a 25-75  $\mu\text{m}$  sieve fraction, which suggests that during the process of adding it to the PET the particles were further broken down to a smaller

size. However, these particle sizes of around  $1\text{ }\mu\text{m}$  are still quite large for the desired interaction with AA throughout the polymer and is most likely the source of the haze that the catalyst causes within the bottle wall. A nanoparticle dispersion would likely be more effective for scavenging AA and could reduce the level of haze within the polymer. This could suggest that for a heterogenous catalyst to be suitable for this application it would have to have much smaller particulates, or that a homogeneous catalyst approach could potentially be more applicable.

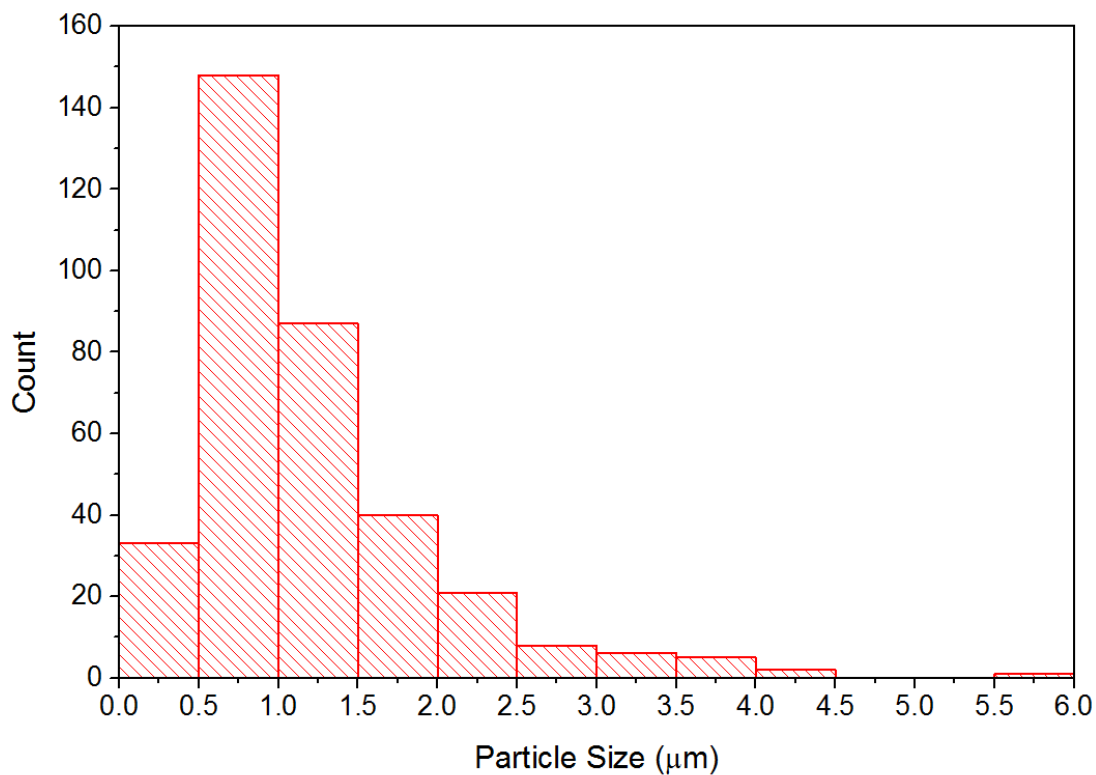


Figure 5.14 Histogram for the ceria particle sizes in PET observed in SEM

The SEM images in figure 5.15 offer good confirmation that the ceria is embedded within the polymer and is not protruding from the surface. Figure 5.15a was taken using an accelerated voltage of 5 kV and in this instance no ceria can be identified. However, it does appear as though something is buried beneath the surface of the polymer, as the surface looks slightly perturbed. When the accelerated voltage was increased to 30 kV the ceria can then be seen glowing within the image (figure 5.15b). This elucidates that the ceria is embedded within the polymer below the surface

of the bottle, and that increased accelerated voltages are required for electrons to penetrate far enough into the polymer substrate to interact with the metal oxide.

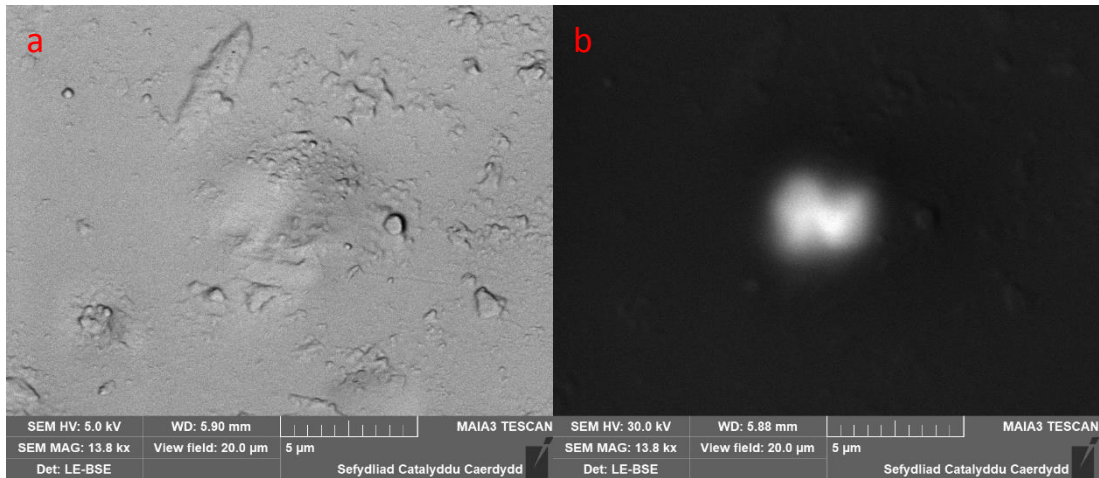


Figure 5.15 SEM images of PET loaded with CeO<sub>2</sub>: left image was taken using accelerated voltage of 5 kV, right image was taken using accelerated voltage of 30 kV.

To determine the different levels of electron penetration achieved at the different voltages, Monte Carlo simulations were conducted using a software package called Monte Carlo Simulation of Electron Trajectory in Solids (CASINO)<sup>24</sup> (see section 2.4.9). PET has a density of 1.38 g/ml and a composition of (C<sub>10</sub>H<sub>8</sub>O<sub>4</sub>) and using this information, the CASINO software can simulate the trajectory of electrons within that solid matrix. In figure 5.16 the simulation for electrons at 5 kV in PET is displayed and shows that the electrons can penetrate to a depth of around 400 nm at this voltage. Figure 5.17 contains the simulation for the penetration of electrons into PET at 30 kV, and at this voltage the electrons can penetrate up to around 8000 nm into the solid.

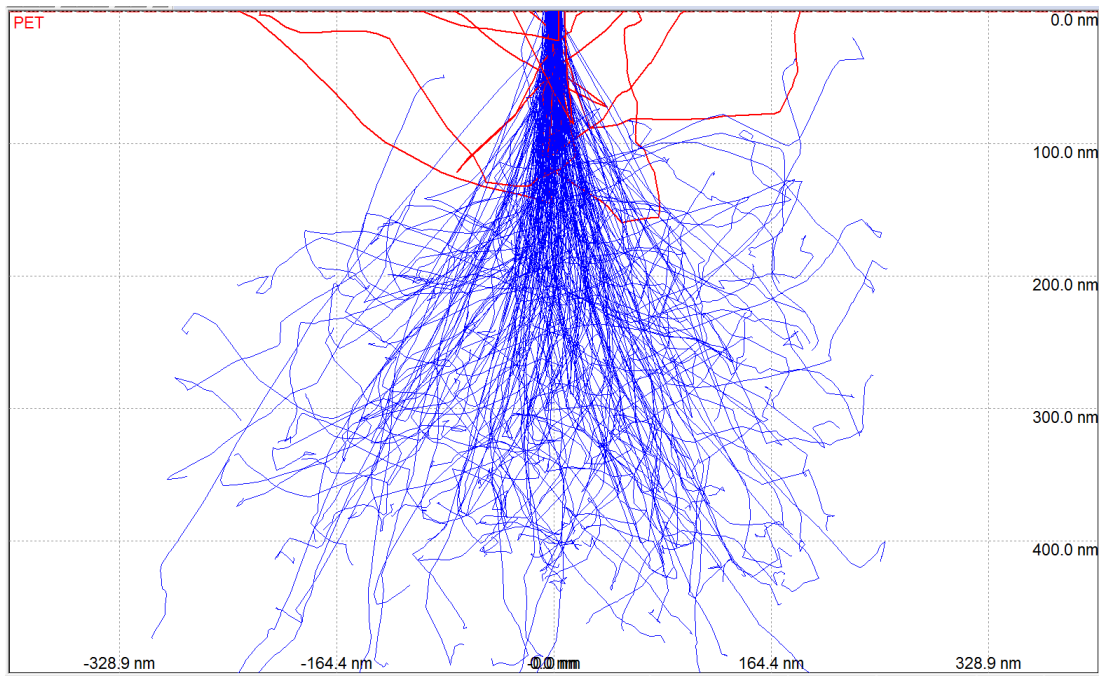


Figure 5.16 Monte Carlo simulation for penetration of electron into PET at an accelerated voltage of 5 kV

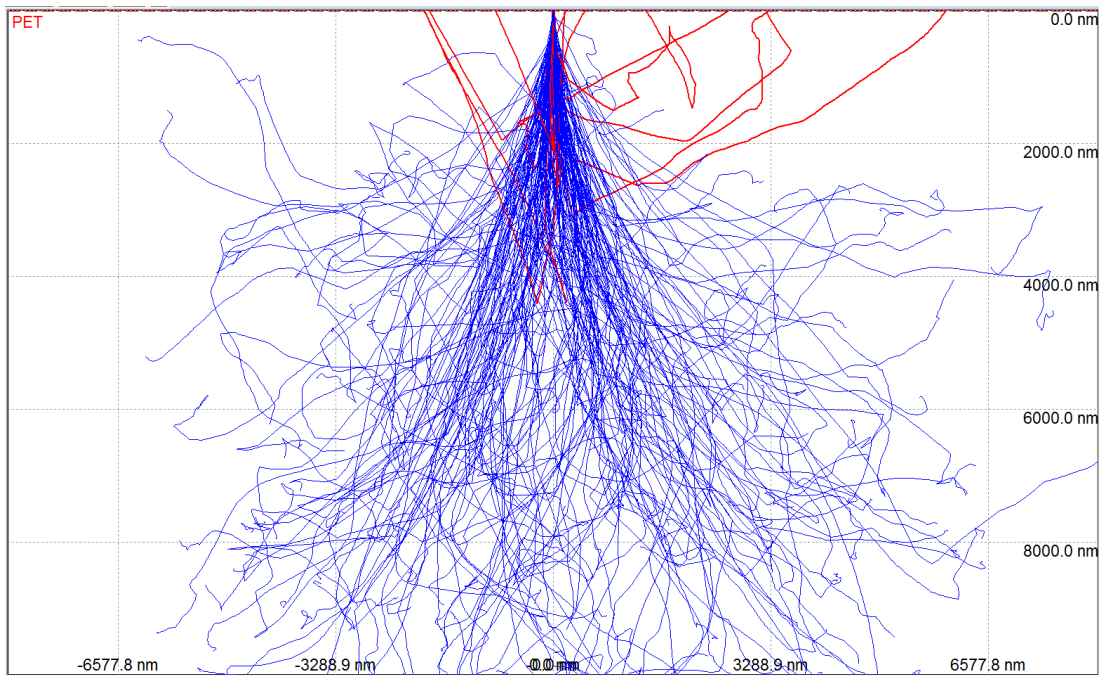


Figure 5.17 Monte Carlo simulation for penetration of an electron into PET at an accelerated voltage of 30 kV

These simulations indicate that the ceria observed in the image in figure 5.15 is most likely to be between 400 – 8000 nm beneath the surface of the PET. However, these simulations are also helpful for exposing the limitations of SEM for examining

catalysts loaded into PET. The bottle wall thickness, and hence the thickness of the samples that were investigated was 300 µm, and even at an accelerated voltage of 30 kV the electrons are only able to penetrate about 8 µm into the sample. Therefore, what is observable *via* SEM is only a very shallow snapshot of the entire bulk of the sample. Therefore, it is likely that in the images in figures 5.12 and 5.13 the ceria that can be observed is only that which can be found in top 8 µm of sample.

### 5.14 Generation of CeO<sub>2</sub> *in-situ*

SEM analysis has highlighted that the average particle size of the CeO<sub>2</sub> catalyst was found to be around 1 µm. Milling of the materials did not provide the desired reduction in particle size and those materials still required sieving. Milling the catalysts caused the density of the materials to increase but did not reduce the particle size. It was hypothesised that an alternative sample preparation could be used for the extruder testing, whereby the ceria would be generated in the extruder process by adding ceria precursors to the PET. By generating the ceria *in-situ* a material with a smaller particle size could be formed that would be able interact with the AA more effectively.

There are large range of cerium precursors available, however, certain parameters needed to be considered for this particular application. The toxicity of the precursor must be considered because it would need to be safe for food contact if it were to be added to a plastic bottle. Also, the precursor must not be too expensive if it is to be used within an industrial context where the financial bottom line is a crucial consideration. The five precursors that were examined using TGA were cerium(IV) hydroxide (Ce(OH)<sub>4</sub>), cerium(III) carbonate (Ce<sub>2</sub>(CO<sub>3</sub>)<sub>3</sub>.xH<sub>2</sub>O), cerium(III) acetate (Ce(CH<sub>3</sub>CO<sub>2</sub>)<sub>3</sub>.xH<sub>2</sub>O), cerium(III) oxalate (Ce<sub>2</sub>(C<sub>2</sub>O<sub>4</sub>)<sub>3</sub>.xH<sub>2</sub>O), cerium(III) acetylacetone (acac) (Ce(C<sub>5</sub>H<sub>7</sub>O<sub>2</sub>)<sub>3</sub>.xH<sub>2</sub>O).

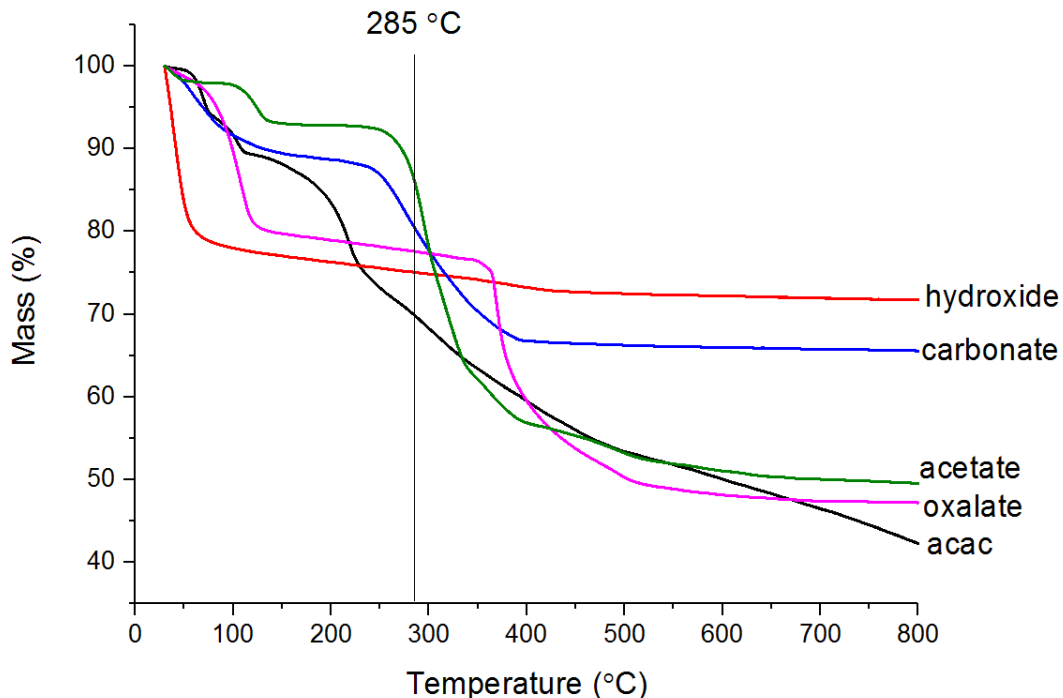


Figure 5.18 TGA of different ceria precursors conducted from room temperature to 800 °C at 1 °C/min in an atmosphere of N<sub>2</sub>. Red = cerium hydroxide, blue = cerium carbonate, green = cerium acetate, pink = cerium oxalate, black = cerium acac

To determine which precursors would be the best for use in the extruder test each one was subjected to TGA (see figure 5.18). The extruder temperature is set to 285 °C for the AA experiments so the precursor would need to be converted to ceria below that temperature. From the results of the TGA the cerium hydroxide was shown to decompose at the lowest temperature, and the majority of the mass loss for this material occurred below 100 °C. This means that the hydroxide would most likely begin to decompose when added to the dried PET, which is about 150 °C, before it is even added to the extruder. This makes it more likely that ceria will be generated because the exposure to 285 °C in the extruder is for such a short period of time (about 1 minute). Also, Ce(OH)<sub>4</sub> has no related hazards and its price is comparable with the other precursors, apart from the acac material which is far more expensive than all of the others (according to Sigma Aldrich prices for 99.9% metal basis materials), so the Ce(OH)<sub>4</sub> is very good candidate.

Table 5.20 Extruder experiment 15 - AA concentration data for PET loaded with metal hydroxides. Catalysts were loaded without carrier. Blank is an average of two or three samples. Analysis was conducted in duplicate.

<b>Sample (loading)</b>	<b>AA Concentration / ppm (error)</b>	<b>AA Reduction / ppm</b>	<b>AA Reduction / %</b>
Blank (x3)	11.2 ( $\pm 0.30$ )	n/a	n/a
Ce(OH) <sub>4</sub> (100 ppm)	11.0	0.2	2
Blank (x2)	12.8 ( $\pm 0.55$ )	n/a	n/a
Ce(OH) <sub>4</sub> (500 ppm)	9.9 ( $\pm 0.16$ )	2.9	23
Zr(OH) <sub>4</sub> (500 ppm)	11.0 ( $\pm 0.00$ )	1.8	14

Initially the cerium hydroxide was tested at a low loading of 100 ppm and unsurprisingly had very little affect upon the AA concentration. As has been previously shown with ceria catalysts at similar loadings, the additives have had very little impact upon the AA concentration in the PET and are indistinguishable from blank experiments. However, when the loading was increased to 500 ppm a significant reduction in AA concentration was observed, which also matches previous observations from the testing with ceria catalysts. The loading of the hydroxide is not directly comparable to the loading of the oxide, because according to the TGA the hydroxide has lost around 25% of its mass at 285 °C. This would mean that 500 ppm would generate about 375 ppm of cerium oxide, and the 23% AA reduction is about 72% of the 32% AA reduction achieved by the CeO<sub>2</sub> U1 catalyst, which would indicate that the activity is comparable on a per ceria loading basis.

Zirconium hydroxide was also tested by way of comparison and to link this testing back to the ColorMatrix patent for a hydrous zirconium oxide catalyst. In this experiment the cerium-based catalyst was again shown to be more effective for removing AA than its zirconium-based counterpart.

### 5.15 Comparison between Testing in Gas Phase and Testing in PET

To determine the relationship between the gas phase testing conducted in Cardiff and extruder testing in ColorMatrix the two sets of data were compared in a single plot.

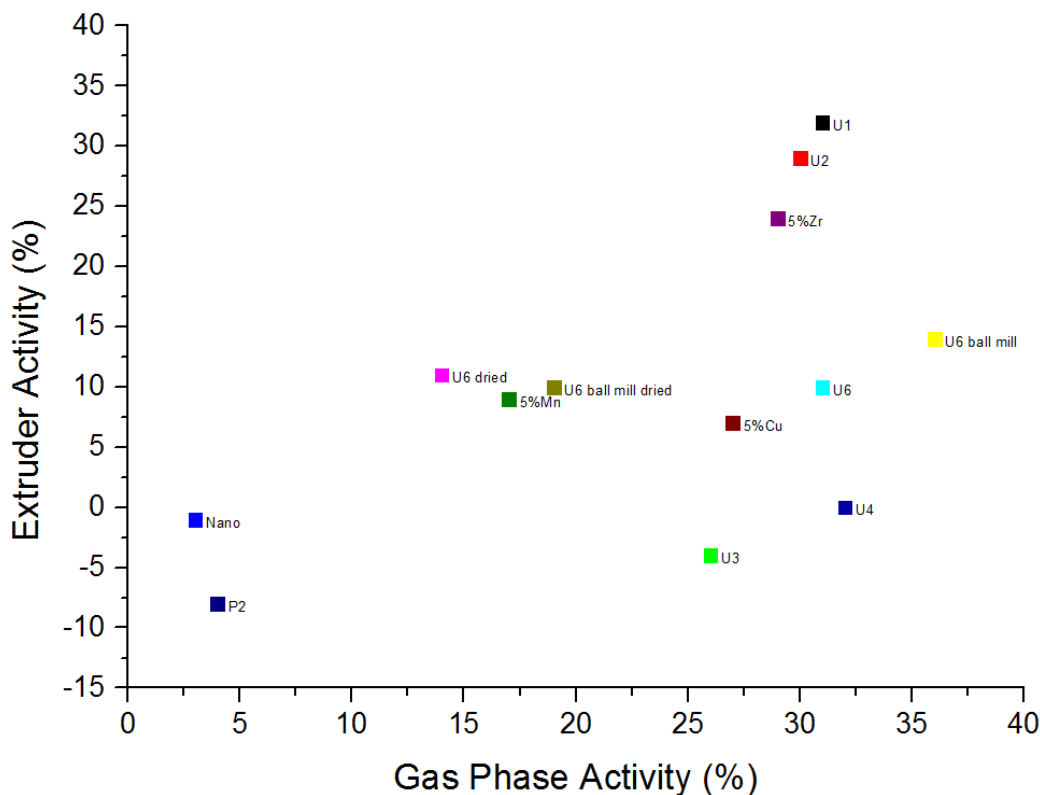


Figure 5.19 Comparison between catalytic activity for AA conversion in the gas phase and extruder tests. The data for the gas phase activity is catalysts tested at  $300000\text{ h}^{-1}$ , and the extruder activity is for catalysts tested at a 500 ppm loading without carrier using a 25-75  $\mu\text{m}$  sieve fraction.

From the data in figure 5.19 a general correlation can be seen between the observed catalytic activities for each material in the two different testing protocols. This means that the gas phase testing cannot be wholly relied upon to provide the basis for which ceria catalyst will be most effective for removing AA from PET, but it can help to give an indication as to which catalysts will perform better than others. This correlation offers confirmation that the gas phase testing can be used within further study to screen catalysts that could potentially be utilised to scavenge AA within PET bottles.

## 5.16 Conclusions

In conclusion, CeO<sub>2</sub> has been shown to effectively reduce the concentration of AA in PET. Other metal oxides such as ZrO<sub>2</sub> and Mn<sub>2</sub>O<sub>3</sub> were found to be less effective than ceria, and the doping of ceria with other metal oxides was also found not to improve the catalyst activity. The greatest reduction in AA, of 32%, was achieved using a ceria catalyst (U1) prepared *via* urea precipitation, which was also found to be the best method for preparing the most active catalysts in the gas phase testing. Pre-test conditioning of the ceria catalysts (e.g. drying and/or milling) and alternative preparation methods (e.g. use of structure directing agents) were not found to improve the AA removal activity of the ceria samples. This is in general agreement with the testing data discussed in chapter 4, where the urea precipitation catalysts were also found to be the most active. However, Ce(OH)<sub>4</sub> was found to have comparable activity to the CeO<sub>2</sub> U1 if the results are weighted to reflect the actual loading of cerium oxide catalyst. This offers an alternative pathway of future study whereby the metal oxide catalysts are generated *in-situ* during the PET extrusion process.

SEM analysis was able to establish that the ceria was incorporated and embedded into the wall of a PET bottle. It was found that the average particle size of the CeO<sub>2</sub> U3 catalyst in the PET was around 1 µm, but by generating the ceria *in-situ* smaller particle sizes could be attained. Making ceria with a smaller average particle size could also help to reduce the haze in the PET which has been observed when adding ceria catalysts to PET. Consideration of aesthetic factors upon the PET will become more prominent as the AA removal catalyst product gets closer to potential commercialisation. It is not known at this stage whether the *in-situ* formation of ceria aided dispersion and had a lower effect upon aesthetics, and this would be the subject of future study.

The addition of triglyceride carrier to act as a vehicle for the dispersion of the additive within the PET was found to dampen the catalytic activity of the ceria samples. This is most likely due to the carrier coating the surface of the ceria and blocking access to the active sites of the catalyst. This was supported by results from adding the triglyceride carrier to the laboratory gas-phase testing, where it was also found to reduce the catalyst activity. The best results for the conversion of AA within PET were achieved when the triglyceride carrier was not added to the system.

The current industrial standard, anthranilamide (ATA), was found to remove more than 70% of the AA from the PET, and so there is still some way to go before the catalyst system can outperform the ATA. However, it has been confirmed that metal oxide catalysts can be used to remove AA in PET and further study and optimisation could enable a catalyst system to offer comparable performance to scavengers like ATA.

### 5.17 Chapter 5 - References

1. M. Dong, A. H. DiEdwardo and F. Zitomer, *J. Chromatogr. Sci.*, 1980, **18**, 242–246.
2. N. H. Snow and G. C. Slack, *TrAC Trends Anal. Chem.*, 2002, **21**, 608–617.
3. J. Linssen, H. Reitsma and J. Cozijnsen, *Z. Für Lebensm.-Unters. Forsch.*, 1995, **201**, 253–255.
4. M. Parvinzadeh, S. Moradian, A. Rashidi and M.-E. Yazdanshenas, *Appl. Surf. Sci.*, 2010, **256**, 2792–2802.
5. S. Sinha Ray and M. Okamoto, *Prog. Polym. Sci.*, 2003, **28**, 1539–1641.
6. US7041350 B1, 2006.
7. A. Dąrowska, A. Borcz and J. Nawrocki, *Food Addit. Contam.*, 2003, **20**, 1170–1177.
8. J. N. Miller and J. C. Miller, *Statistics and Chemometrics for Analytical Chemistry*, 6th Edition, Pearson Education, 2010.
9. ColorMatrix Triple A Acetaldehyde Scavenger for PET | PolyOne, <https://www.polyone.com/products/polymer-additives/acetaldehyde-scavengers-pet/colormatrix-triple-aa-scavenger-pet>, (accessed 2 August 2019).
10. N. Birkner and A. Navrotsky, *Am. Mineral.*, 2012, **97**, 1291–1298.
11. S. V. Ushakov and A. Navrotsky, *Appl. Phys. Lett.*, 2005, **87**, 164103.
12. S. Hayun, T. Y. Shvareva and A. Navrotsky, *J. Am. Ceram. Soc.*, 2011, **94**, 3992–3999.
13. L. M. Orozco, M. Renz and A. Corma, *ChemSusChem*, 2016, **9**, 2430–2442.
14. L. M. Orozco, M. Renz and A. Corma, *Green Chem.*, 2017, **19**, 1555–1569.
15. W. Yuejuan, M. Jingmeng, L. Mengfei, F. Ping and H. Mai, *J. Rare Earths*, 2007, **25**, 58–62.
16. K. Yoshikawa, H. Sato, M. Kaneeda and J. N. Kondo, *J. CO<sub>2</sub> Util.*, 2014, **8**, 34–38.

17. M. Tamura, S. M. A. H. Siddiki and K. Shimizu, *Green Chem.*, 2013, **15**, 1641–1646.
18. US9574138B2, 2017.
19. D. R. Sellick, A. Aranda, T. García, J. M. López, B. Solsona, A. M. Mastral, D. J. Morgan, A. F. Carley and S. H. Taylor, *Appl. Catal. B Environ.*, 2013, **132–133**, 98–106.
20. R. Ramdas, E. Nowicka, R. Jenkins, D. Sellick, C. Davies and S. Golunski, *Appl. Catal. B Environ.*, 2015, **176–177**, 436–443.
21. S. Bedrane, C. Descorme and D. Duprez, *Catal. Today*, 2002, **75**, 401–405.
22. A. Aranda, S. Agouram, J. M. López, A. M. Mastral, D. R. Sellick, B. Solsona, S. H. Taylor and T. García, *Appl. Catal. B Environ.*, 2012, **127**, 77–88.
23. W. Zhan, S. Yang, P. Zhang, Y. Guo, G. Lu, M. F. Chisholm and S. Dai, *Chem. Mater.*, 2017, **29**, 7323–7329.
24. Casino, <https://www.gel.usherbrooke.ca/casino/What.html>, (accessed 26 June 2020).

## 6 Conclusions and Future Work

In conclusion, ceria catalysts have been shown to effectively reduce the concentration of AA in PET under processing conditions. The greatest AA removal achieved in this project of 32% is not as effective as the industrial benchmark, anthranilamide, so further development is required to usurp the incumbent technology. However, the research undertaken in this project was able to confirm that metal oxides, such as ceria, do have potential for application as catalytic AA scavengers in PET.

In the gas phase studies conducted in the CCI, a ketonisation reaction mechanism was observed to yield acetone and CO<sub>2</sub> as the major reaction products. However, it seems unlikely that such a bimolecular reaction mechanism would be feasible in a molten polymer matrix with such a low AA concentration (around 10 ppm). Therefore, more understanding needs to be gained as to how the ceria catalysts convert the AA within the PET. It may be the case that during PET processing the catalysts are only able to oxidise the AA to acetic acid, as observed in the first step of the AA ketonisation mechanism. A headspace GC-MS method could be developed to identify other organic products trapped in the PET that would give insight into the reactions that take place between the AA and the metal oxide catalyst during PET processing. This analysis could also help to indicate whether the catalysts cause degradation of the PET end-groups during extrusion of the polymer. ColorMatrix have headspace GC-MS apparatus, so this testing could be carried out in their laboratory in Knowsley.

In attempting to understand what physicochemical properties yield an effective catalyst for AA conversion, it was found to be a complex picture. No single parameter had a direct relationship with catalyst activity at 300 °C and 300000 h<sup>-1</sup> for all the samples that were prepared and tested. BET surface area had the most linear relationship with AA conversion of all the parameters that were measured in this study. However, when only U1, U2, and U3 were compared, as three catalysts which had been prepared using the same method, the correlations were stronger. Also, when comparing the AA conversion achieved in the two different testing protocols, there is a good correlation between the activity in the two tests. This suggests that the test that was developed in Cardiff is able to indicate which catalysts will be more effective for AA conversion in PET.

Further experimentation should be conducted to determine the effect of the ceria catalysts upon the polymer chain of PET. It is known that oxidation catalysts based on Co and Mn are active for the degradation of PET and hence cause the generation of AA.<sup>1</sup> IV testing indicated that the polymer chain lengths were not affected by the catalysts but the interaction between the catalysts and the polymer end groups requires further study. A model laboratory test could be designed whereby a molecule could be used to mimic the vinyl ester end groups of PET and could be reacted with ceria. An example of a compound that could be used to mimic the PET vinyl ester end groups is vinyl benzoate (see figure 6.1). If it is found that ceria is active for converting the vinyl group to AA, this could give insight into the way in which ceria interacts with vinyl ester groups within PET.

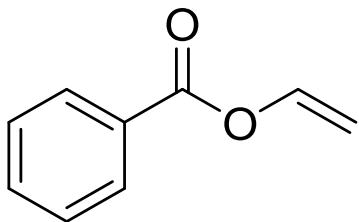


Figure 6.1 Chemical structure of vinyl benzoate

Another test that could be carried out to model interaction between catalysts and PET in the laboratory is to use benzyl benzoate.<sup>2</sup> Vinyl benzoate could be reacted with ceria in the gas phase due its boiling point being 95 °C. However, benzyl benzoate has a much higher boiling point of 324 °C and so could be used in the liquid phase at PET processing temperatures at around 300 °C to mimic a molten PET reaction matrix. This would require a very different reaction setup to the gas phase reactor used in this project, but could offer very helpful insights into the nature of interactions between ceria catalysts and PET.

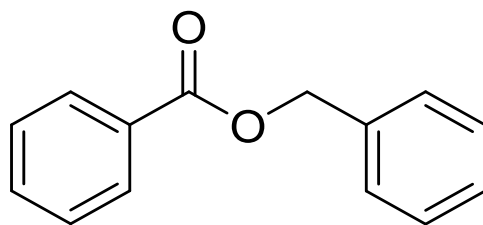


Figure 6.2 Chemical structure of benzyl benzoate

A final candidate for mimicking reactions between PET and ceria catalysts is BHET, which is the monomer that PET is constructed from. This would most likely have to be handled in a similar fashion to the benzyl benzoate. BHET melts at temperatures between 106-109 °C and has a boiling point of 446 °C, so could be tested in the liquid phase at PET melt-processing temperatures.

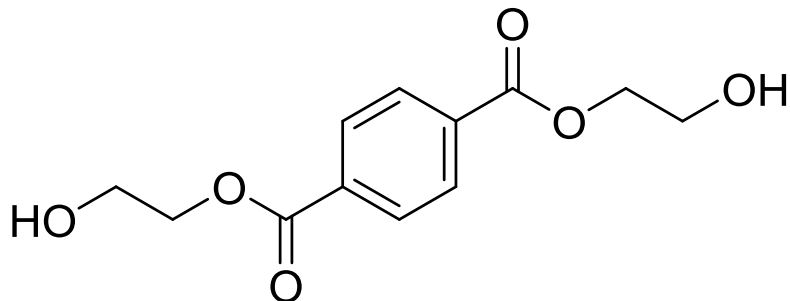


Figure 6.3 Chemical structure of BHET

It is claimed that doping metal oxide catalysts with alkaline metals such Na or K can increase the performance of the catalyst for the ketonisation of aldehydes or carboxylic acids.<sup>3,4</sup> The effect of group I metal dopants could be investigated to determine if it increases the efficacy of the catalysts for AA conversion.

As mentioned in section 5.4, measuring the enthalpies of water adsorption of the catalyst materials could be used to identify which catalysts cause more hydrolytic degradation of PET, and therefore lead to the formation of AA. It is counterproductive for additives designed to remove AA to cause the generation of more AA, so it is very likely that catalysts that do not degrade PET will be more efficient for the reduction of AA concentration. Enthalpies of water adsorption can be measured according to the

water adsorption calorimetry methodology developed by Ushakov and Navrotsky, whereby a volumetric dosing system is used to accurately dose gases onto a metal oxide sample placed in a Calvet-type microcalorimeter.<sup>5</sup> Once the enthalpies of the catalysts have been determined, the catalysts would undergo testing in PET to identify if there is any correlation between the enthalpy of water adsorption and generation of AA within PET.

Amphoteric reducible metal oxides (e.g. ceria) have been found to be the most active ketonisation catalysts in this study and in the scientific literature.<sup>6</sup> The acid-base properties of such materials have been suggested to play a major role in their activity for ketonisation. Therefore, future study could focus on gaining a greater understanding of the effect of the acidity/basicity of the metal oxide catalyst for effectiveness in the ketonisation reaction.

In terms of the future direction for this project, as was mentioned in the previous chapter, it could be that a heterogeneous metal oxide catalyst is not an optimal solution to the problem posed in this project. A homogeneous catalyst system that could be dissolved into the polymer matrix may be more effective for converting for AA and may also have a less negative impact upon the aesthetics of the polymer. Alternatively, a nano dispersion could be developed to incorporate very small catalyst particles into the polymer, and potentially improve upon the results that have been achieved thus far.

Further study should be conducted into looking at the *in-situ* generation of the catalysts (see section 5.14) to determine whether a greater dispersion of catalyst with a smaller particle size is achieved, and if this leads to greater activity. The particle size distribution could be analysed using SEM in the same way that the urea precipitation ceria catalyst dispersed within a PET bottle wall was analysed in section 5.13.

Another potential direction that could be taken, which is hinted at in the ColorMatrix patent,<sup>7</sup> is instead of using a catalyst to react with AA during injection moulding at high temperature, use a catalyst to react with the AA in the bottle walls at low temperature. The AA can migrate from the bottle wall into a beverage so it must have a certain mobility within a polymer matrix. This mobility could enable the AA to interact with catalysts embedded within the catalyst walls. A low temperature AA oxidation catalyst could then be used to reduce the AA concentration of the PET bottle

throughout its shelf-life. The ceria catalysts examined in this research could be active for AA conversion in PET bottle walls at low temperature, but this would require further investigation.

## 6.1 Chapter 6 – References

1. US20020136808 A1, 2002.
2. I. Marshall and A. Todd, *Trans. Faraday Soc.*, 1953, **49**, 67–78.
3. A. V. Ignatchenko, *Catal. Today*, 2019, **338**, 3–17.
4. K. Parida and H. K. Mishra, *J. Mol. Catal. Chem.*, 1999, **139**, 73–80.
5. S. V. Ushakov and A. Navrotsky, *Appl. Phys. Lett.*, 2005, **87**, 164103.
6. T. N. Pham, T. Sooknoi, S. P. Crossley and D. E. Resasco, *ACS Catal.*, 2013, **3**, 2456–2473.
7. WO2005010088 A1, 2005.